NUMERICAL INVESTIGATION OF VIBRATION IN A STEAM TURBINE CONTROL VALVE

A Thesis
Submitted to the Graduate Faculty
of the
North Dakota State University
of Agriculture and Applied Science

By

Luke Michael Novak

In Partial Fulfillment of the Requirements
for the Degree of
MASTER OF SCIENCE

Major Department:
Mechanical Engineering

December 2016

Fargo, North Dakota

North Dakota State University
Graduate School

Title

Numerical Investigation of Vibration in a Steam Turbine Control Valve

By

Luke Novak

The Supervisory Committee certifies that this ***disquisition*** complies with North Dakota State University's regulations and meets the accepted standards for the degree of

MASTER OF SCIENCE

SUPERVISORY COMMITTEE:

Dr. Bora Suzen
Chair

Dr. Ghodrat Karami

Dr. Om Yadav

Dr. Forrest Ames

Approved:

12/20/2016
Date

Dr. Alan R. Kallmeyer
Department Chair

ABSTRACT

A numerical analysis is performed at North Dakota State University to investigate and resolve steam inlet control valve vibration in a Minnkota Power Cooperative turbine. Pressure fluctuations resulting from an unstable flow pattern are found to cause vibration. Multiple valve disc and seat design modifications to stabilize the flow are made and tested. The full scale geometry is used with steam as the working material. Both steady-state and transient analyses are completed. Analytical calculations are used for verification. Investigation of all modifications is discussed. Results from the original valve configuration show vortex shedding off of the disc. A currently installed cutoff disc has not removed flow-induced vibration. Flow expansion generates unstable flow, creating an unsteady separation bubble on the valve seat at the throat exit. Changing the throat from a converging-diverging to a purely converging nozzle stabilizes the flow, removing the flow-induced pressure forces causing disc vibration.

ACKNOWLEDGEMENTS

Foremost, I would like to extend my gratitude to Dr. Bora Suzen for his assistance and guidance on this project. His understanding of the subject has been invaluable. It has been a privilege to work under him.

Many thanks to the staff at the Minnkota Power Plant, especially Roger Gazur, Lucas Schaaf, and Dylan Wolf. They have been extremely helpful in providing me with information related to the project, as well as offering constructive suggestions.

I would also like to thank my colleague Alan Perrault. His suggestions and assistance with data processing were very helpful.

Finally, I would like to express my sincere thanks to my family and friends for providing me with support throughout graduate school.

TABLE OF CONTENTS

LIST OF TABLES

LIST OF FIGURES

LIST OF SYMBOLS

a ..... speed of sound, ft/s

A ..... cross-sectional area, ft^2

c_p ..... specific heat constant for constant pressure, Btu/lbm·°R

c_v ..... specific heat constant for constant volume, Btu/lbm·°R

D ..... valve disc/seat sealing diameter, in

h ..... valve disc lift, in

$\dot{m}$ ..... mass flow rate, lbm/s

M ..... Mach number

OR ..... opening ratio, h/D

P ..... pressure, psf or psi

P_c ..... critical pressure, psf or psi

P_i ..... valve inlet pressure, psf or psi

P_e ..... valve exit pressure, psf or psi

P_t ..... total pressure, psf or psi

PR ..... pressure ratio, P_e/P_i

q ..... proportional mass flow rate, $\dot{m}/\dot{m}_{max}$

R ..... gas constant, Pa

R_s ..... specific gas constant for steam, ft·lbf/lbm·°R

Re ..... Reynolds number, $\frac{\rho V L_{ref}}{\mu}$

T ..... temperature, °R

T_c ..... critical temperature, °R

T_t ..... total temperature, °R

V ..... flow velocity, ft/s

γ ..... specific heat ratio

ρ ..... fluid density, lbm/ft^3

μ ..... dynamic viscosity, lbf·s/ft^2

v ..... specific density, $\frac{1}{\rho}$, ft^3/lbm

v_k ..... kinematic viscosity, $\frac{\mu}{\rho}$, ft^2/s

τ_w ..... wall shear stress

1. INTRODUCTION

When steam turbines were first built for power generation, they were built robustly, with moderate performance requirements. Under these conditions, flow-induced vibrations were not common. As the demand for increased efficiency and performance rose, along with the technology to make it possible, steam turbine systems were subjected to more extreme conditions. Higher system temperatures, pressures, and flow rates led to a greater number of flow-induced vibrations, which then increased the number of related component failures. [1]

In the steam turbine system, steam is created in the steam generator. After it forms, it is sent to the steam chest, where it is held at temperatures and pressures reaching 900 °F and 2900 psi, respectively. It enters the turbine at a rate that is controlled by a series of valves. Venturi valves are used extensively throughout the steam turbine industry as a means to regulate the flow of steam as it moves from the steam chest to the turbine. The pressure drop across a fully open control valve can reach 200 psi [2]. At these conditions, supersonic, asymmetric, and unstable flow conditions can cause flow-induced vibrations within the valve [3]. These can cause serious damage to the valve components, leading to valve failure [4].

This particular investigation involves the Unit 1 main steam turbine installed in 1970 at the Minnkota Power Cooperative (MPC) Milton R. Young station. As explained in reports provided by MPC [5, 6], the Unit 1 turbine utilizes a set of eight cam-operated, venturi-style, control valves. There are four valves in both an upper and a lower steam chest to control the flow of steam into the turbine. A diagram of one of the valves is shown in figure 1.1.

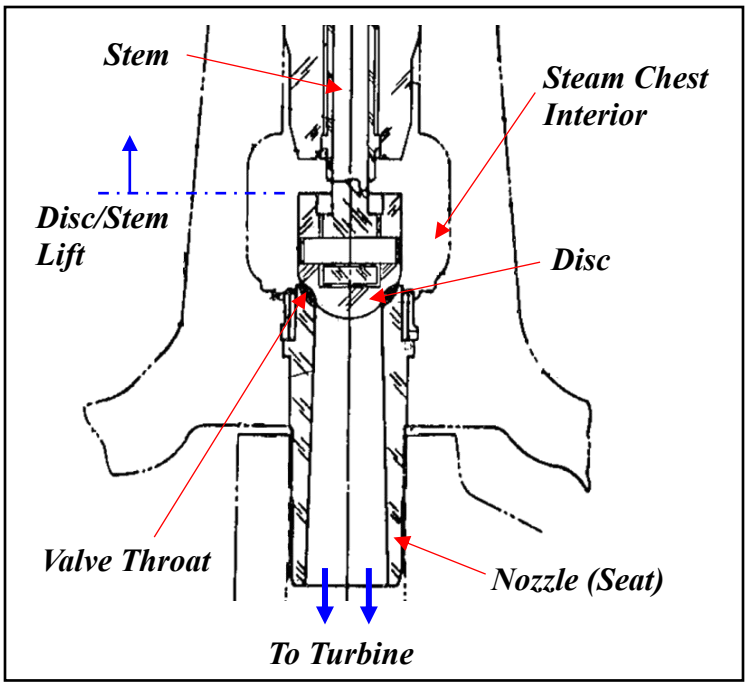

Figure 1.1. Control Valve.

In 2006, a retrofit was installed which changed the opening sequence of the control valves from eight steam admissions to three. The turbine was returned to service and operated without incident until a maintenance shutdown was performed in 2009. Upon inspection of valves 7 and 8, damage to the valve discs and seats and camshaft cam faces was discovered and the crosshead on valve 7 was found to be cracked. The vibration was powerful enough to overcome the valve spring force and cause the cam roller to lift off of the camshaft. This damage can be seen in figures 1.2 and 1.3.

Figure 1.2. Vibration-Induced Damage to Valve 7 [5].

Figure 1.3. Divot in Camshaft Cam due to Valve Vibrations [5].

The valve seats and camshaft cam faces were repaired and the bushings, stems, and discs were replaced following the damage. After the turbine was returned to service, a strong vibration appeared to occur in valves 7 and 8 from what appeared to be the crack point of the valves up to an approximate stem lift of 1/8 inches.

In an effort to rectify the vibration problem and correct the related damage, the valve discs, stems, bushings, and springs on both valves were replaced during a shutdown in 2011. However, replacement of these components did not remove the vibrations. A modified disc,

shown in figure 1.4, was placed into valve 8 in 2013 to attempt to resolve the vibrations; this was also ineffective.

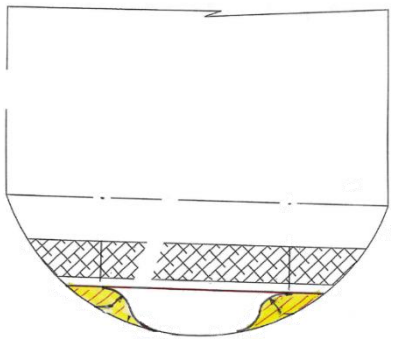

Figure 1.4. MPC Modified Disc [7].

1.1. Research Objective

The objective of this research work is to find and remedy the cause of the vibrations in steam inlet control valves 7 and 8 of the Unit 1 main steam turbine at the Minnkota Power Cooperative Milton R. Young station. A computational fluid dynamics analysis is completed at North Dakota State University to determine the flow characteristics responsible for the valve vibrations. Upon completion of this analysis, design modifications are applied to the valve to stabilize the flow pattern and remove the vibrations. These modifications will be sent to MPC for use in control valves 7 and 8.

Past computational research in this area has focused on the use of air as the simulation fluid, which ignores the effects of steam on the valve vibrations. Much of the research has been completed steady-state, without regard to time-dependent factors. To more accurately depict the flow conditions within the valve, this research work will utilize steam as the operating fluid. A 3D model will be used to capture non-axisymmetric flow phenomena and simulations will be run time-dependent to capture unsteady flow characteristics.

2. PREVIOUS RESEARCH

2.1. Venturi Valve Flow Theory

The flow through a venturi valve can be simplified as flow through a converging-diverging nozzle, as shown in figure 2.1, to obtain an analytical solution.

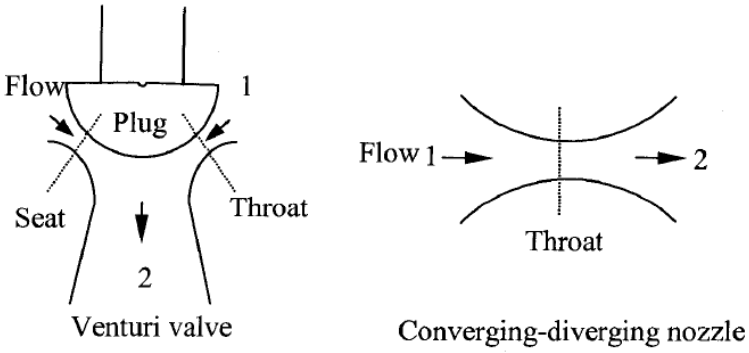

Figure 2.1.Venturi Valve Simplification [8].

At low valve disc lift heights, the pressure differential between the steam chest interior and the valve seat can cause high speed flow through the valve throat. The most useful way to measure this is by use of the Mach number, given in equation (2.1).

$$M = \frac{V}{a} \tag{2.1}$$

Where

$$a = \sqrt{\gamma R_s T} \tag{2.2}$$

And

$$\gamma = c_p / c_v \tag{2.3}$$

At the high temperatures typically seen in steam turbines, steam can be handled as a compressible ideal gas which behaves according to the ideal gas law, shown in equation (2.4). The specific heat ratio is assumed constant for an ideal gas.

$$P = \rho RT \tag{2.4}$$

When a high pressure differential exists across the valve, the flow can become choked, where the Mach number reaches a maximum value of one in the valve throat. Under this condition, the flow can behave a few different ways, as shown in figure 2.2.

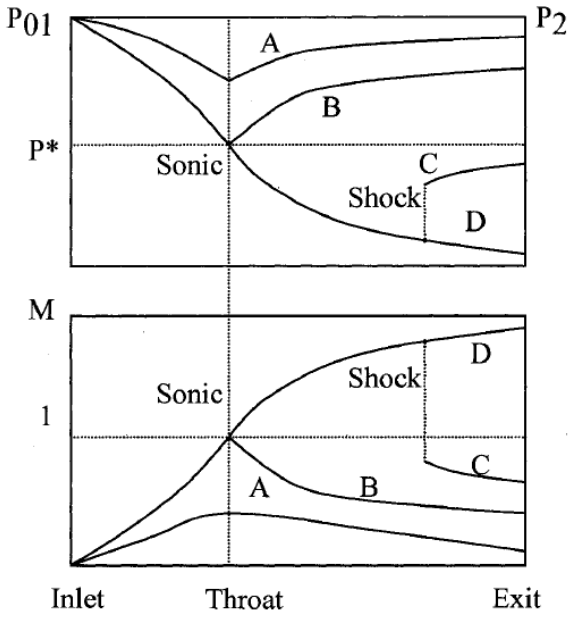

Figure 2.2. Pressure/Mach Number Relation for Choked Flow [8].

As the valve continues to open, the flow transitions out of the high speed flow. When the valve is in the wide-open position, the flow throughout the entire valve is subsonic. If flow is then assumed to be isentropic, the following relations for pressure and temperature can be applied:

$$\frac{P}{P_t} = \left(1 + \frac{\gamma - 1}{2} M^2\right)^{-\frac{\gamma}{\gamma - 1}} \tag{2.5}$$

$$\frac{T}{T_t} = \left(1 + \frac{\gamma - 1}{2} M^2\right)^{-1} \tag{2.6}$$

The general form of the mass flow rate equation is

$$\dot{m} = \rho V A \tag{2.7}$$

A mass flow rate can be developed for an ideal compressible gas by starting with equation (2.7) and first substituting in equations (2.1) and (2.2),

$$\dot{m}_{ideal} = \rho M \sqrt{\gamma R_s T} A \tag{2.8}$$

Then substituting in equation (2.4).

$$\dot{m}_{ideal} = \frac{P}{RT} M \sqrt{\gamma R_s T} A \tag{2.9}$$

Replacing *P* and *T* with equations (2.5) and (2.6), respectively, and simplifying yields the final form of the mass flow rate equation.

$$\dot{m}_{ideal} = \frac{A P_t}{\sqrt{T_t}} \sqrt{\frac{\gamma}{R_s}} M \left(1 + \frac{\gamma - 1}{2} M^2\right)^{-\frac{\gamma + 1}{2(\gamma - 1)}} \tag{2.10}$$

Under choked flow conditions, the Mach number is 1, so the maximum mass flow rate through the valve can be found by reducing equation (2.10) to

$$\dot{m}_{max} = \frac{A P_t}{\sqrt{T_t}} \sqrt{\frac{\gamma}{R_s}} \left(\frac{\gamma + 1}{2}\right)^{-\frac{\gamma + 1}{2(\gamma - 1)}} \tag{2.11}$$

By inserting the maximum mass flow rate back into equation (2.10) and solving numerically, the Mach number at other points in the flow field can be found. This Mach number can then be put into equations (2.5) and (2.6) to find the pressure and temperature, respectively, at those locations.

In the instance where choked flow is present, a normal shock wave can form downstream of the throat as shown in figure 2.2 profile C. The shock wave causes abrupt changes in pressure, temperature, density, and flow velocity. The following equations are used to determine the downstream flow characteristics, where the subscripts 1 and 2 indicate the values upstream and downstream of the shock wave, respectively.

$$M_2 = \sqrt{\frac{(\gamma-1)M_1^2+2}{2\gamma M_1^2-(\gamma-1)}} \tag{2.12}$$

$$T_2 = T_1\left\{\frac{[2\gamma M_1^2-(\gamma-1)][(\gamma-1)M_1^2+2]}{(\gamma+1)^2 M_1^2}\right\} \tag{2.13}$$

$$P_2 = P_1\left[\frac{2\gamma M_1^2-(\gamma-1)}{\gamma+1}\right] \tag{2.14}$$

$$\rho_2 = \rho_1\left[\frac{(\gamma+1)M_1^2}{(\gamma-1)M_1^2+2}\right] \tag{2.15}$$

$$P_{t2} = P_{t1}\left\{\left[\frac{(\gamma+1)M_1^2}{(\gamma-1)M_1^2+2}\right]^{\frac{\gamma}{\gamma-1}}\left[\frac{\gamma+1}{2\gamma M_1^2-(\gamma-1)}\right]^{\frac{1}{\gamma-1}}\right\} \tag{2.16}$$

$$T_{t2} = T_{t1} \tag{2.17}$$

Based on equations (2.12) through (2.17), the velocity decreases after the shock wave and the pressure, temperature, and density increase. The basic flow equations are useful for identifying the flow characteristics of a specific system. When comparing a variety of control valves, non-dimensional terms are required.

2.1.1. Flow Parameters

To allow for comparison between systems and conditions, there are three primary non-dimensional variables used in venturi valve research. The first is the pressure ratio, *PR*, which is the valve outlet pressure divided by the inlet pressure. In a steam turbine control valve, the flow is pressure driven, so the pressure ratio controls the velocity of the flow in conjunction with the

disc lift, *h*. If the disc lift is divided by the disc/seat sealing diameter, *D*, a second variable is obtained. A visual representation of these variables is shown in figure 2.3. The opening ratio, *h/D*, is a non-dimensional measure of the height of the disc above the seat.

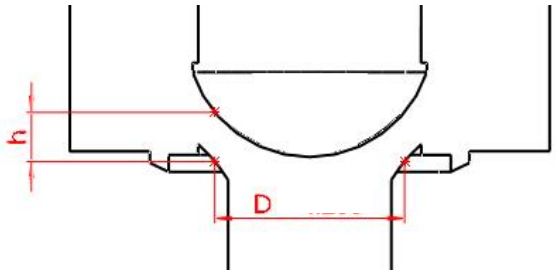

Figure 2.3. Opening Ratio Variables.

The mass flow rate can also be non-dimensionalized by dividing the instantaneous mass flow rate by the maximum mass flow rate to obtain the proportional mass flow rate, *q*. With these variables, the flow across various control valves can be compared.

2.2. Similarity Effects

The flow through steam valves is very complicated. In order to reduce the complexity in experimental testing and numerical simulation, scaling is used. Common scaling found in past research concerns modifying the flow material and reducing the number of valves tested and the size of the valve. These allow for reduced testing equipment, time, and cost.

2.2.1. Physical Scale

Steam turbine systems frequently have multiple steam chests, each containing numerous control valves. This allows for the flow through one valve to affect that through the others. Hardin et al. [3] considered including the entire four valve steam chest into his CFD analysis, but decided it was unnecessary given that past research indicated that the steam chest configuration has minimal effect on the steam flow through individual valves. In addition, CFD simulations were run to evaluate the influence of neighboring valves and the effect of the valve disc being

off-center; these conditions were found to be inconsequential. H. Sam [5] considered the use of a quad-valve experimental arrangement, but decided on a one-valve design; any effects the valves would have on each other was considered less critical than reduced construction time and cost.

Reducing the size of the valve can greatly decrease the size of an experimental test apparatus and considerably improve the solution time of a numerical simulation. H. Graf et al. [9] compared a small scale testing system to a large system. Very good agreement was found, verifying use of scaling for valve design planning and modification.

2.2.2. Flow Medium

Steam is a complex material that requires additional experimental testing infrastructure and causes a less stable computational code. Hence, most of the past research has been completed using air as the working fluid; dimensionless quantities are used relate the two fluids. M. Hajšman et al. [10] used an outlet/inlet pressure ratio and an instantaneous/critical mass flow ratio to non-dimensionalize the flow through the valve. When comparing the numerical results for air and steam, he found that the mass flow rates for the two fluids matched well, but the downstream flow pattern was different. Morita et al. [11] also compared the use of steam to air, both experimentally and numerically, to determine to effects of condensation and the change in the quantity of state between the two materials. The experimental results matched well below a pressure ratio of 0.5; the numerical results for steam agreed with both the numerical results for air and the experimental results. P. Iredale [12] used water as the working fluid because it is more effective for analyzing the flow pattern with Particle Image Velocimetry. He used the Reynolds number as a similarity variable and matched it to air testing. The water pressure loss results agreed excellently with the air for an ‘onion’ disc; a 10% difference was found between the air and water for a ‘cut-off’ disc. The dimensionless steady-state pressure fields are nearly

identical for water and air. The scale difference between steam and air was analyzed by H. Graf et al. [9] to verify the widespread use of air as the test medium in experiments. The two materials were compared experimentally using the pressure ratio, acoustic efficiency, and the Strouhal number as the dimensionless parameters. An excellent correlation was found, validating the use of compressed air for valve noise prediction and reduction.

2.3. Valve Vibration Causes

There are many flow mechanisms that can cause a valve to vibrate, and they can excite vibrations either alone or in combination with each other. According to L. Zeng et al. [13], the source of valve vibrational noise can be caused by shock waves, separation of flow, vortex shedding, mechanical vibrations, acoustic resonance, and turbulence and its interaction with boundaries and shock waves. Vortex shedding is typically coupled with an effect that causes vortex separation [14]. Some of the potential vibration instigators D. Zhang [8] discussed were unstable upstream flow, flow impingement on the upstream portion of the disc, and secondary downstream flows. Two major causes of valve vibrations, as identified by H. Sam [15], are acoustic resonance and flow induced instability. Araki et al. [16] found unstable flow to be the cause of pressure fluctuations on the disc surface, which induced disc vibrations. A few of the more common vibration-causing mechanisms are covered in more depth in the following sections.

2.3.1. Transonic Flow

Instabilities in the flow field as it switches from fully subsonic to subsonic-supersonic are termed transonic flow instabilities. Transonic flow exists at Mach numbers of 0.8 to 1.2 [17] and is characterized by instability, a deep boundary layer, and a wake that is large and violent. As the pressure ratio across the valve increases, the flow changes from subsonic to supersonic. The first

supersonic region to develop is an o-ring shape near the throat wall. This ring grows as the downstream pressure continues to decrease until a complete shock wave forms on the downstream side. The shock wave then grows until a stable subsonic-supersonic relation is formed. Additional flow characteristics such as pressure pulses can occur during transonic flow which can increase the likelihood of vibration occurrence [18]. The work of Liu et al. [19] showed that valve disc vibrations were a result of transonic impinging jet flow and fluctuations in supersonic and transonic flow. These generated an alternative back flow that was greater than the valve damping system, causing axial vibration powerful enough to break the valve stem.

2.3.2. Acoustic Resonance

D. Zhang [8] broke down flow-induced vibrations into two categories: local and system. Local vibration causes the disc to vibrate directly, while system vibrations, such as acoustic resonance, are more indirect. In an investigation by K. Widell [20], acoustic vibration induced oscillations in the valve and related piping system, leading to valve vibrations. Measurements on multiple system components showed a consistent frequency reading around 63 Hz. When analyzing a valve failure, Hardin et al. [4] found that vibrations were present when the natural valve frequency closely matched an acoustic excitation frequency. The pressure pulsations from this were far too low to be considered a source of valve failure, but could have served as a mechanism for activating larger vibration phenomena.

Flow mechanisms such as oblique and normal shocks and unstable jets can excite valves, triggering unwanted acoustic noise. Because of this, acoustic resonance is primarily a concern in convergent-divergent valves; in purely convergent nozzles its effects are greatly reduced [14]. K. Yonezawa et al. [21] reported that an unsteady flow in a valve excited the acoustic resonance mode, damaging the valve from pressure fluctuations. The most effective method for removing

acoustic vibrations is to design the system with a large gap between the natural and acoustic frequencies [8].

2.3.3. Jet Flow

D. Zhang et al. [18] found that due to the large pressure differential across the control valves, the flow can become supersonic. Shock waves form and the subsequent jet causes flow separation from the valve disc and seat. Supersonic jets are complicated and unsteady, leading to large forces acting on the disc that can lead to significant structural vibrations. In research completed by Morita et al. [22] supersonic flow jets struck each other after leaving the valve throat, generating vortices and a high pressure area. This rotated around the disc axis, causing a cyclic load on the disc wall. The case studied by G. Zanazzi et al. [23] showed that valve vibration can be caused by asymmetric supersonic jet interaction. The interaction moved the flow separation point, placing strong radial forces on the disc.

2.3.4. Self-Induced Vibration

Self-excited vibrations, or fluidelastic instability, can cause a system to become unstable, according to D. Weaver et al. [1]. The vibration is initiated when a body immersed in non-periodic fluid flow generates a fluid force in the same direction that the body is moving. In the case of a venturi valve, D. Zhang [8] explains that when the flow separates from both the seat and disc, it can be treated as a free jet. In cases where a normal shock wave is created in the throat, a stable subsonic jet will form downstream. However, it is possible that an oblique shock wave and expansion could form, generating an unstable supersonic jet. This instability can lead to unbalanced pressure forces on the valve disc. If the fluctuations change from one side of the disc to the other at a frequency approaching the disc's natural frequency, then self-induced vibration can occur. If both jets attempt to remain attached to the disc, D. Zhang et al. [18] states

that a constant unstable flow pattern will result at the back of the disc as one jet or the other gains more attachment. The addition of the disc reacting to this aggravates the flow instability. K. Yonezawa [21] also found that disc vibration influences the pressure fluctuations in the flow. At low disc vibration amplitude, forced vibration occurs and random pressure fluctuations drive the vibrations. However, at large amplitudes self-excited vibration is present and the pressure fluctuations in the flow become periodic and act as a damping effect on the disc.

2.3.5. Vortex Shedding

Weaver et al. [1] states that vortex shedding is created by free jet and shear layer instability. These are unstable by nature and only require small disturbances, introduced at the separation location, to develop into vortices structures downstream. If not paired with a mechanism to provide feedback in the flow that allows for oscillations, vortex shedding is typically weak. Structural vibrations, such as the shedding of vortices from a flexible bluff body, can be a feedback mechanism. Other potential mechanisms are impingement and acoustic resonance.

2.3.6. Flow Impingement

As described by S. Ziada et al. [24], flow impingement can cause substantial pressure fluctuations which cause problematic vibrations. When shear layers and free jets, which are fundamentally unstable at certain frequencies, separate, vorticity perturbations are created. These are amplified into full vortical structures with velocity and pressure fluctuations as they travel downstream. At select frequencies, placing an impingement downstream of the separation location for the flow can cause drastic self-enhancement of the fluctuations which then serve as an excitation mechanism for valve vibrations. This cycle is self-sustaining, since impingement-

related vorticity distortions feed upstream to the flow separation point, where new perturbations are introduced.

2.4. Past Research Approaches

Experimental and computational methods have been used, both separately and in conjunction with each other, to determine a solution to valve vibrations. The computational methods vary, encompassing both steady state and time-dependent as well as two and three dimensional simulations and fluid-structure interaction. In most cases, the computational results agree with their experimental counterparts. Completed research in each method is discussed more extensively in the following sections.

2.4.1. Experimental

An experimental valve configuration was used by L. Zeng et al. [13] to investigate the flow patterns present in a control valve. A microphone and pressure sensors were used to collect information about the flow state. L. Zeng concluded that sound mutation can be used to determine a range of potential vibration.

K. Yonezawa et al. [21] used an experimental facility to better understand flow-induced disc vibrations. Two valve disc assembly mounting configurations were used; one flexible and one fixed. Strain gauges were used to measure displacement and pressure sensors on the disc measured pressure fluctuations. By adjusting the flexibility of the disc, the resulting data showed that self-induced vibrations can occur and that their range of influence increases as the stiffness of the disc decreases.

A model valve was used by M. Hajšman et al. [10] as a baseline for CFD comparison and to evaluate the effects of angling the steam inlet. Static taps are used throughout the valve to find the flow characteristics at various lifts.

R. Morita et al. [22, 25, 26, 11] conducted multiple control valve experiments in the mid-opening lift range to determine the flow and vibration characteristics, working fluid effects, and vibration cause. Pressure sensors were placed on the valve seat and disc to identify any fluctuations. The flow was found to have random rotational pressure fluctuations when the opening ratio was between 0.00406 and 0.0325; the fluctuations move outward from the center of the valve and become stronger with increased lift. When a weakly supported valve was used at a lift of 0.024 – 0.031 inches, the fluctuations matched the natural frequency of the valve. Hence, resonance occurred.

Additional experimental research was completed by K. Yonezawa et al. [27] to better understand the flow characteristics of venturi valves across a wide operating range. A test facility was constructed which used pressure sensors mounted to the valve disc and seat to capture pressure fluctuations. Five unsteady flow patterns, based on the pressure fluctuation characteristics and frequency, were observed. Identified as modes, the first two occurred at higher pressure and opening ratios and the others were found at low pressure and opening ratios. The pressure fluctuations in mode 1 were random and pulse-like, with larger pressure fluctuations on the seat than the disc. Mode 2 was similar to mode 1, with larger amplitude fluctuations on the disc. The frequency of mode 3 was very close to that of the acoustic resonance for the system, with periodical fluctuations. Periodic and asymmetric fluctuations are present in modes 4 and 5, with the mode 4 pressure pattern rotating circumferentially.

Based on computational research completed by J. Hardin et al. [4] and D. Zhang et al. [2], D. Zhang et al. [18] determined flow instability and asymmetry to be the cause of the vibrations in control valves. To gain more information about the characteristics of the flow, a valve testing system was built and pressure sensors were placed on the valve disc and seat.

Experiments were run at multiple pressure and opening ratios and compiled to plot the maximum mass flow rate for a range of valve lifts. Figure 2.4 shows that the maximum mass flow rate is constant beyond an opening ratio of 50%. The mass flow rate ratio was also plotted against the pressure ratio at various opening ratios; figure 2.5 indicates the pressure and opening ratio combinations that could result in unstable transonic flow.

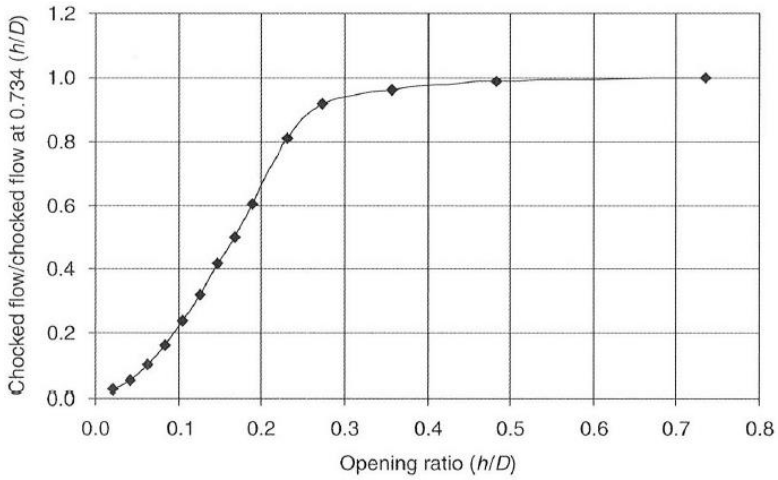

Figure 2.4. Maximum Mass Flow Rate Relation to Opening Ratio [18].

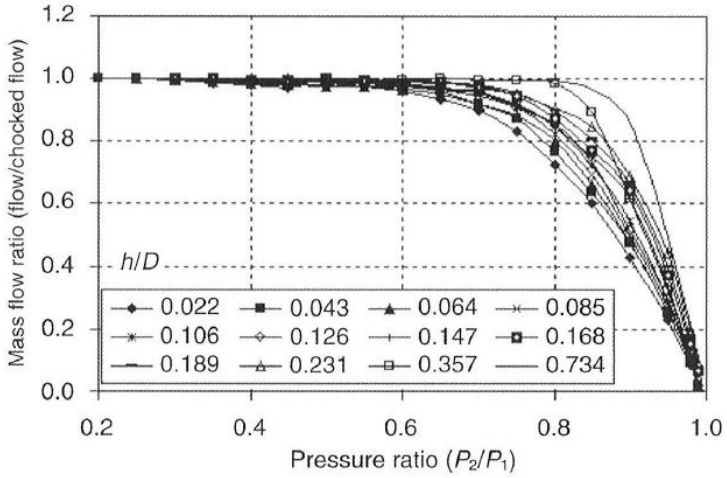

Figure 2.5. Mass Flow Ratio for Given Pressure and Opening Ratios [18].

Taking into consideration the characteristics of the pressure fluctuations in the flow, four different flow pattern regions were found and correlated based on the pressure and opening ratios. These are related in figure 2.6 and shown graphically in figure 2.7.

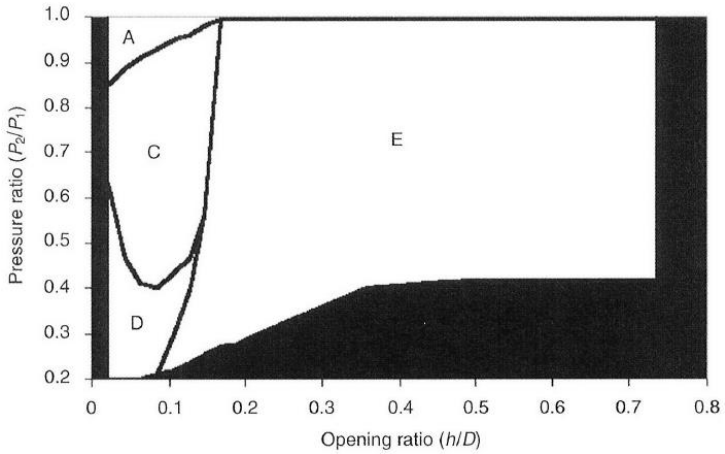

Figure 2.6. Flow Pattern Regions [18].

Patterns A, D, and E only show one type of pressure distribution, and are therefore the most stable. Pattern C shows multiple types of pressure distribution and transitional flows; it is the most unstable region. Because of this, the flow pattern can change between C, C′, C_0, and C_1. A comparison of figures 2.5 and 2.6 indicates that the flow in the upper area of region C is in the transonic flow region.

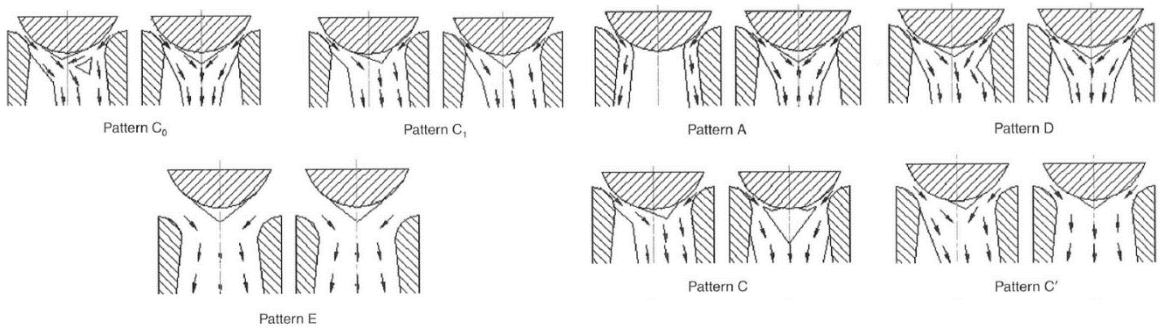

Figure 2.7. Estimated Flow Patterns [18].

Further pressure analysis showed that flow asymmetry and instability due to pressure oscillations was present in the lower portion of region C. Figure 2.8 details which sections of region C are more prone to vibrations; those with darker colors have a higher vibration potential.

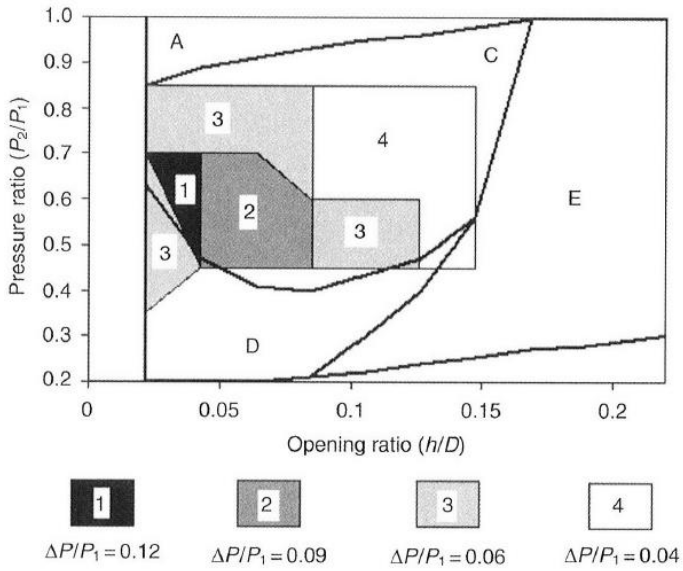

Figure 2.8. Flow Region and Pressure Oscillation Superposition [18].

Continuing the research of D. Zhang et al. [2] and D. Zhang et al. [18], C. Bolin et al. [17] completed testing on the cut off hemispherical disc and short seat used by D. Kim [3] to gain more information on the flow patterns inside the valve. Mass flow rate and pressure ratio data was collected for the entire opening range, and the relation is shown in figure 2.9.

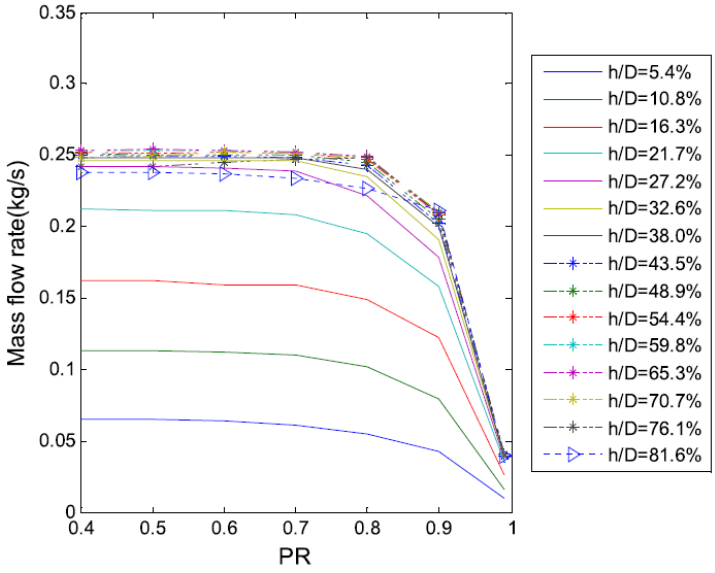

Figure 2.9. Mass Flow Versus Pressure Ratio for Wide Range of Opening Ratios [17].

The mass flow rate and pressure are compared non-dimensionally in figure 2.10. Transonic flow is present in the mass flow ratio range of 0.8 to 1.

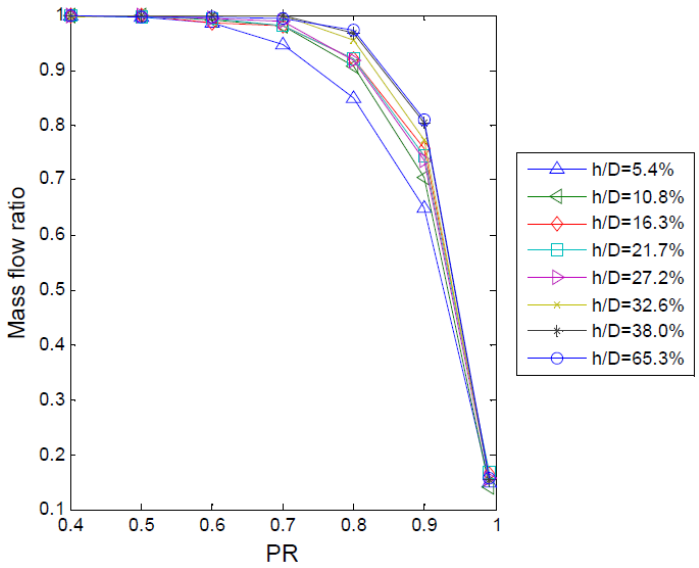

Figure 2.10. Mass Flow Ratio Versus Pressure Ratio for Various Opening Ratios [17].

The difference between pressure taps in a lateral ring was compared to identify and locate pressure fluctuations; a large difference indicates asymmetric flow. Based on the symmetry

results, four different flow patterns were identified and figure 2.11 was created. Region H has symmetric flow, but the flow in regions F, G, and I is asymmetric. The F flow pattern is displayed in figure 2.12.

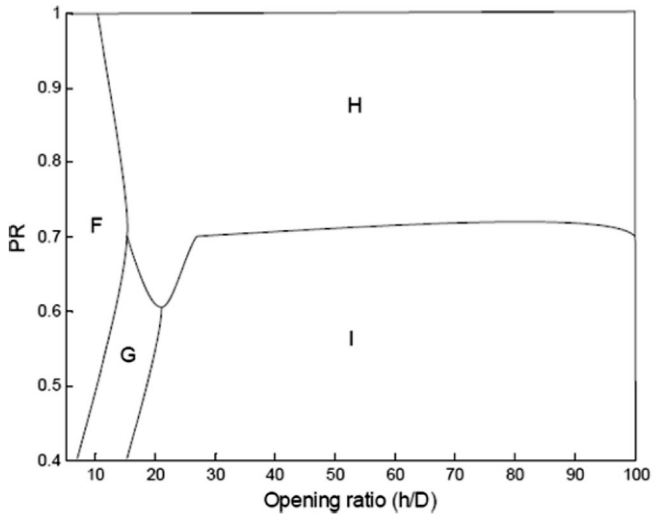

Figure 2.11. Flow Regions Based on Symmetry of Lateral Pressure Data [17].

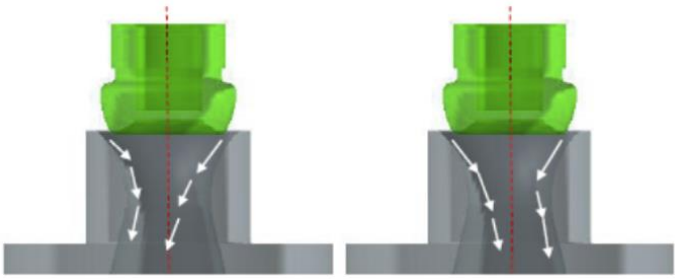

Figure 2.12. Flow Pattern in Region F of Figure 2.11 [17].

Araki et al. [16] experimentally investigated flow variations in control valves. Using a valve model, he found that pressure fluctuations were the cause of valve vibrations. Adjusting the shape of the valve components stabilized the flow so that the vibrations were effectively reduced.

Upon completion of preliminary CFD testing, Hardin et al. [4] conducted experimental testing and verification of CFD results for some modified valve disc designs. Vibration probes

and pressure sensors were used to measure pressure fluctuations and valve vibration. Frequency results for the problematic hemispherical disc showed that the vibrations were entirely flow-induced, and not connected to any structure interaction. Similar to the results of Araki et al. [16], the pressure fluctuations were reduced by completing valve components modifications.

To test the difference between two seat designs, D. Kim [3] used a sound level meter and pressure sensors on the disc and seat of an experimental valve configuration. Accelerometers were used to measure vibrations. The mass flow rate vs. pressure ratio, pressure fluctuation vs. time on the disc surface, and noise level was compared to determine the effectiveness of valve modifications.

P Iredale [12] conducted an experimental investigation to better comprehend the flow phenomena in control valves and test vibration-reduction modifications. By using water as the working fluid and a transparent apparatus, particle image velocimetry and laser light sheet visualization could be used to see the flow patterns. Mercury manometer and pitot rings were used to obtain pressure and loss measurements.

2.4.2. Numerical

The computational fluid dynamics (CFD) work of R. Morita et al. [22, 25, 11] consisted of three dimensional simulations in conjunction with experimental testing to investigate the flow through a control valve in the middle of the opening phase and determine the cause of vibrations. An additional study was completed to asses if the use of air in lieu of steam as the working fluid caused any difference in results. Rotating pressure fluctuations, shown in figure 2.13, were found to generate a large horizontal thrust on the valve disc, causing it to vibrate. The CFD results matched well with the experimental, and the results for air as a working material agreed with those observed using steam.

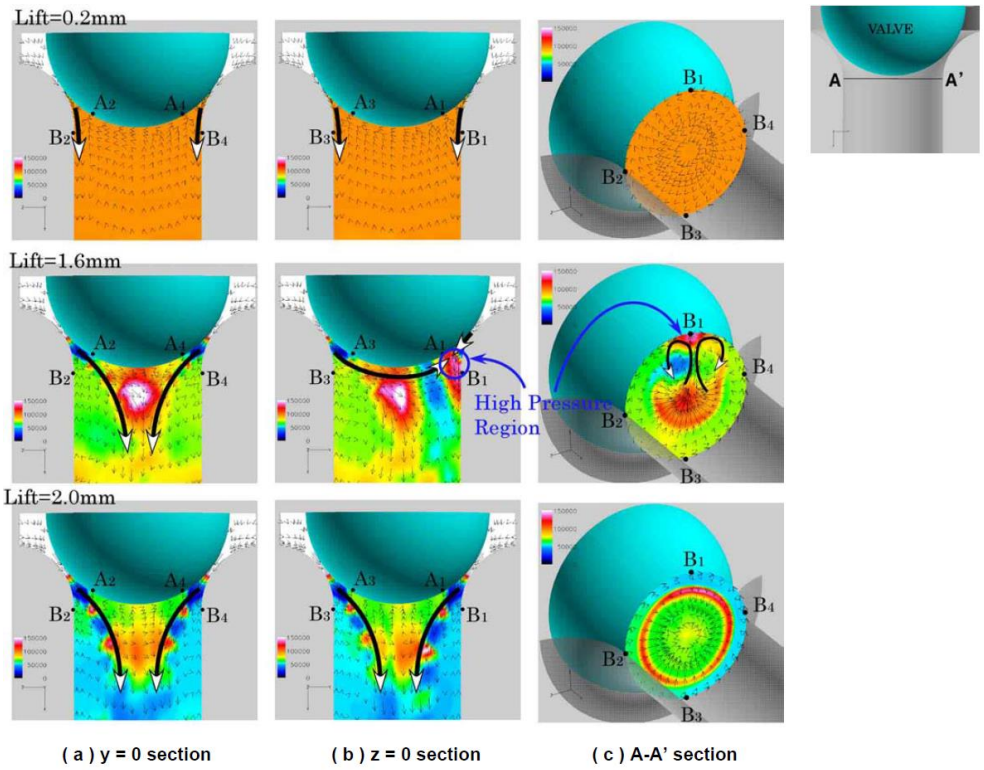

Figure 2.13. Pressure Contour with Velocity Vector [22].

K. Yonezawa et al. [21] completed the numerical portion of his study investigating flow induced vibrations using the finite difference method on a three-dimensional valve model. An O-grid was used to construct the domain and a transforming, moving grid was used to model valve disc vibrations. The flow pattern resulting from the rigid disc simulation was unstable and pressure fluctuations were present in the valve throat and on the disc surface. This is shown in figure 2.14 for a pressure and opening ratio of 0.48 and 0.046, respectively.

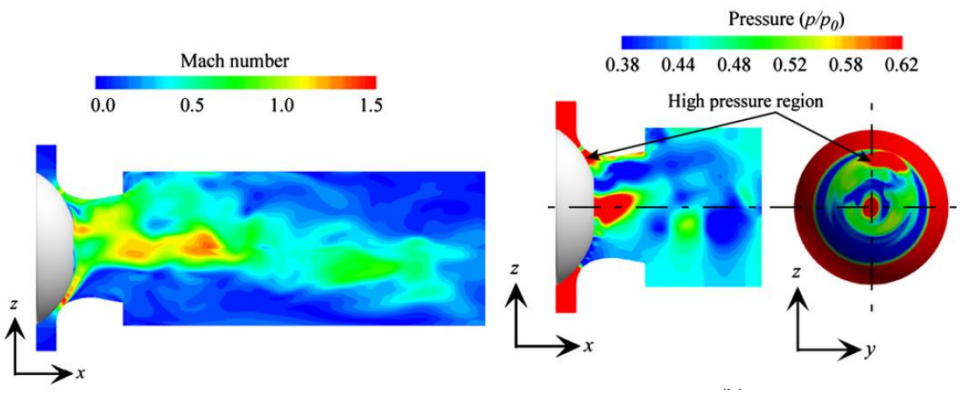

Figure 2.14. Fixed Disc Mach Number (Left) and Pressure Contours (Right) [21].

To model valve disc vibrations numerically, a vibration with a frequency of 32 Hz and a non-dimensional amplitude of 0.016 was applied to the computational grid. The results showed a wave-form pressure fluctuation pattern that matched the experimental results. K. Yonezawa concluded that self-excited vibration was present at a large disc vibration amplitude, and forced vibration existed at a small amplitude.

The experimental work of K. Yonezawa et al. [27] was used as a validation benchmark for the research of G. Zanazzi et al. [23], who completed numerical analysis on a control valve with a hemispherical disc. The numerical results had good quantitative and qualitative correlation with the experimental.

A non-structured three dimensional grid was used by M. Hajšman et al. [10] to obtain control valve data. Experimental testing was used as a verification for the CFD simulations. There is a good correlation between the two; the results are plotted in figure 2.15. The numerical simulations were used to compare inlet flow angles and domain working materials. The resulting plots show that decreasing the valve inlet angle can increase flow while maintaining the flow area. Air and steam were found to behave equivalently.

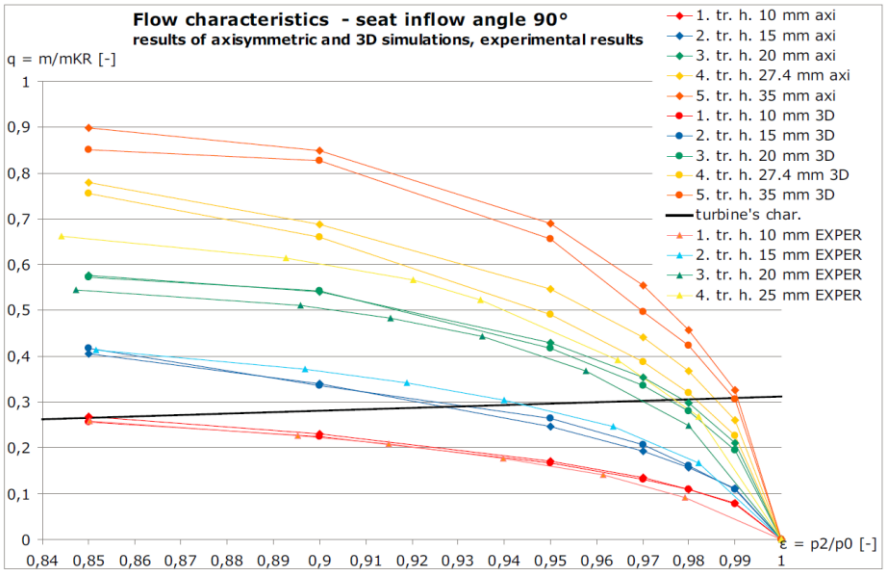

Figure 2.15. Comparison of Numerical and Experimental Methods [10].

The three-dimensional CFD calculations completed by G. Liu et al. [19] highlighted a secondary source of valve vibration. In this case, the steam chest was too small, which caused the flow to travel into the valve in a non-uniform pattern, generating asymmetric flow within the valve.

Computational fluid dynamics was used by C. Domnick et al. [14] to investigate instabilities in the flow through control valves and the resulting vibrations. Steady-state and transient simulations revealed that decreasing the curvature of the seat can decrease pressure fluctuations by increasing flow attachment to the seat.

Hardin et al. [4] used a 90 degree section of a control valve with axisymmetric boundary conditions for computational analysis. Steady-state three dimensional numerical simulations were completed on a problematic valve configuration which had a hemispherical disc. The results showed subsonic flow through the valve throat and strong downstream core flow at the lift where vibration occurred. This disqualified supersonic flow as a vibration cause and indicated that the unstable core flow condition was the culprit for valve vibrations. Further

numerical analysis was concerned with modifying the valve disc to promote the more stable annular flow. The CFD results correlated well with the experimental results, with one exception: the CFD results for a cut off valve disc did not show flow pattern improvement when using a large radius seat versus a smaller radius seat, but the experimental results exhibited a more stable flow structure with the large radius seat. Simulations were also conducted for adjacent valve influence and an off-center valve disc; the effect of these was negligible. A transient model was considered, but avoided due to time constraints and concern that the unstable flow predictions would be inaccurate.

A two dimensional numerical investigation was undertaken by D. Zhang and A. Engeda [2] to better understand the relationship between a valve structure and fluid mechanism. Improved valve designs were then developed from the results. The simulations on the original valve geometry identified five flow patterns that are present in the valve depending on the pressure and opening ratio. These are displayed in figure 2.16 and related to those mentioned in section 2.4.1. The flow in pattern (a) is the stable; it is attached downstream of the throat and has a symmetric distribution of pressure. In pattern (b), the flow is beginning to separate from the valve seat, but is mostly symmetric. Pattern (c) is the least desirable flow condition, and is prevalent at high pressure ratios. The flow is attached to the disc on one side and the seat on the other, causing high pressure forces on the disc. The transient region between patterns (c) and (e) is pattern (d); the pressure is symmetric surrounding the disc, but asymmetric downstream. This pattern mostly occurs at low pressure ratios.

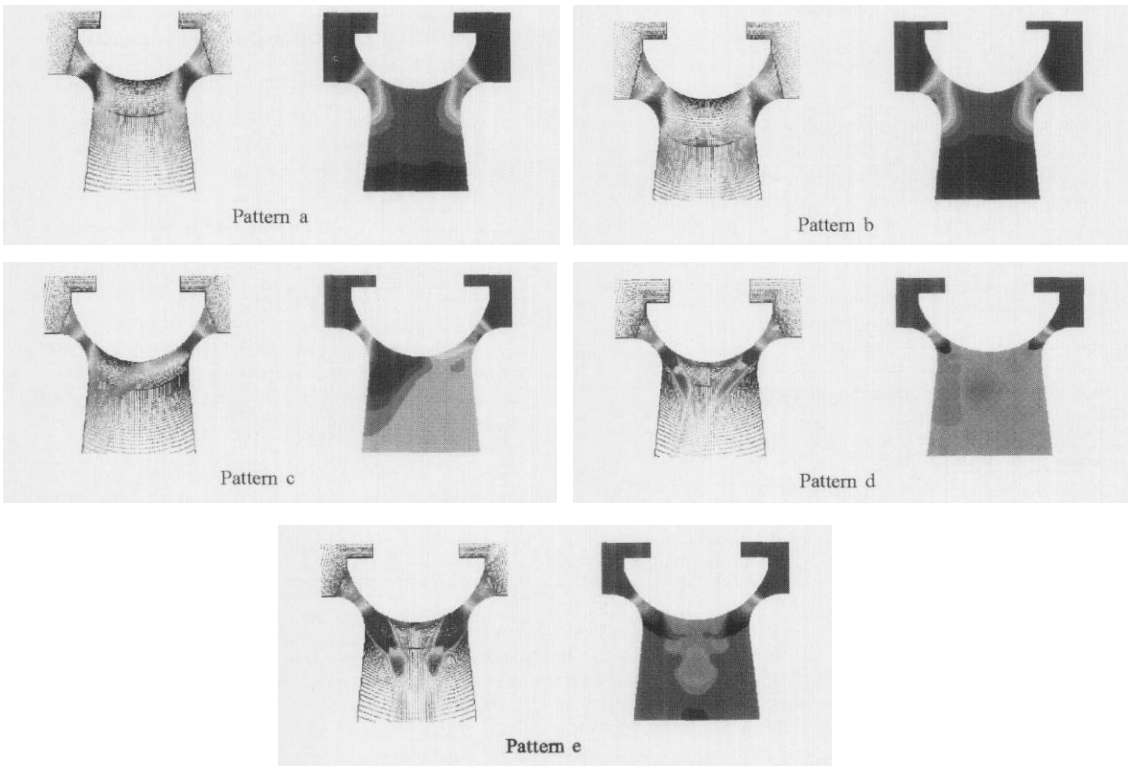

Figure 2.16. Pressure (Left) and Velocity (Right) Flow Patterns Identified by D. Zhang [2].

Changes to the valve design were made with the intent of reducing the excitation mechanism for the vibrations. To make the flow symmetric, the curvature of the disc was decreased. Flow separation from the disc can be forced by using a cut off design, shown for pattern (a) and (d) in figure 2.17. The flow then attaches to the seat, promoting pattern (a) flow at high pressure ratios.

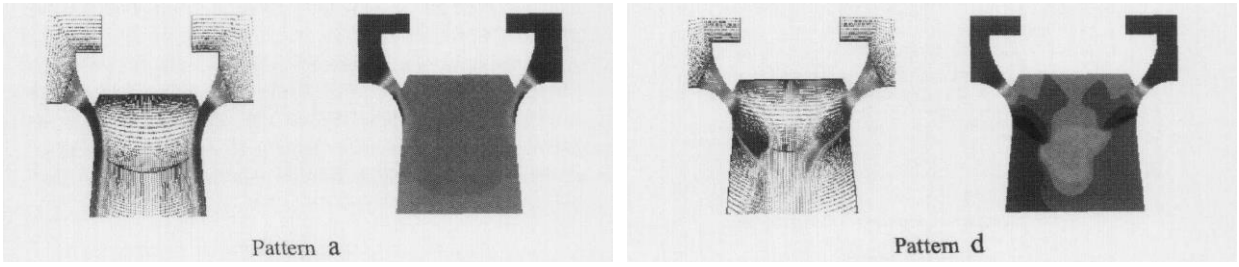

Figure 2.17. Improved Design Flow Patterns [2].

D. Zhang [8] expanded on the two dimensional research completed by himself and A. Engeda [2] by adding a three dimensional numerical analysis and an experimental investigation. This was used to determine the cause of vibrations and the operating regions in which they occur, as well as develop improved valve designs. The flow patterns found in the three dimensional study were similar to those observed in the two dimensional.

2.5. Improved Valve Designs

There is evidence that changing the shape of the valve disc can stabilize the flow through the valve and reduce vibrations. T. Araki et al. [16] obtained significant improvement in flow behavior by modifying the valve disc shape, as shown in figure 2.18.

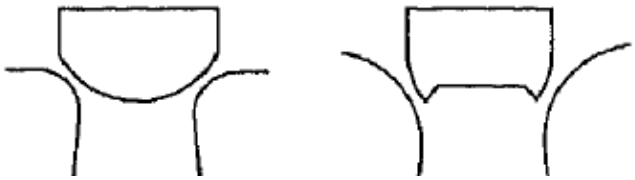

Figure 2.18. Valve Disc Shape Change for Flow Pattern Improvement [16].

D. Zhang [8] identified two methods for improving valve disc design: cutting the nose of a hemispherical disc or extending it, shown in figure 2.19.

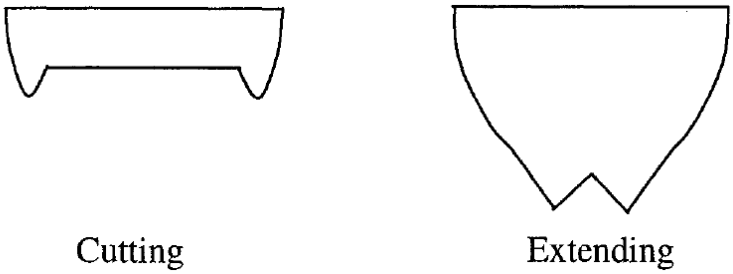

Figure 2.19. Disc Shape Optimization as Defined by D. Zhang [8].

Both have been successfully used to remove vibrations, however, the extended nose may provide increased thermal efficiency. A flat cut off, arc cut, dish bottom, and guiding disc were

also used in numerical simulations by D. Zhang; these are shown in figure 2.20. To determine the effectiveness of the cut height on various discs, the discs were cut off at multiple angles θ (as shown in figure 2.20) and the lateral forces on the disc were compared across a range of pressure ratios.

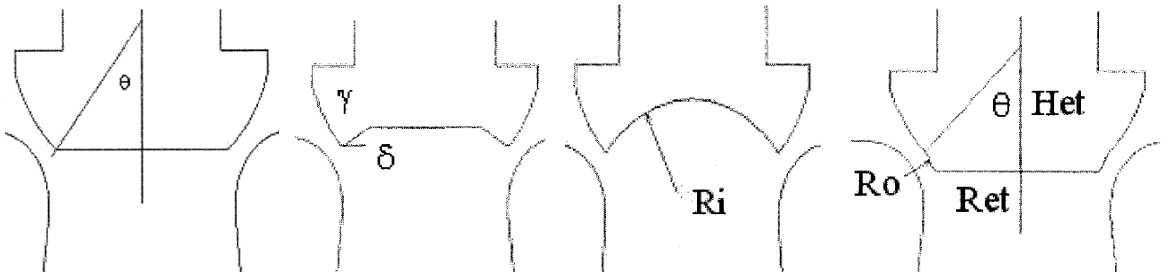

Figure 2.20. L to R: Flat Cut Off, Arc Cut, Dish Bottom, and Guiding Discs by D. Zhang [8].

Additional designs included changing the disc radius. The flat cut off and dish bottom designs performed the best when taking into consideration ease of manufacturing; the guiding design appeared promising, but more research was needed on this design due to the complexity of the curvature. The dish bottom disc with $\theta = 60°$ was selected as the best design.

Further work by D. Zhang et al. [2] identified that valve modifications should be implemented with the intent of reducing the transverse and vertical vibration excitation mechanism. Significant vibration reduction can be completed by adjusting the curvature on a hemispherical disc to make the flow symmetric. The improved dish bottom disc created by D. Zhang is shown in figure 2.21. This modification causes the flow to attach to the seat at high pressure ratios (pattern a) and generate a symmetric core flow at low pressure ratios (pattern d).

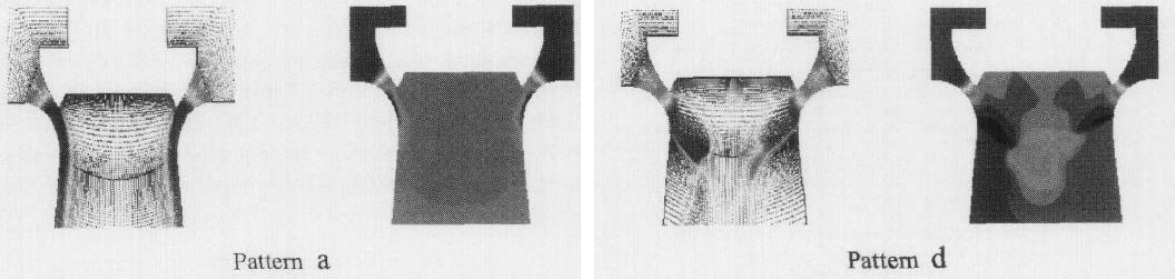

Figure 2.21. CFD Flow Patterns for D. Zhang et al. Improved Disc [2].

The work of J. Hardin et al. [4] focused on altering a control valve to prevent vibrations that were causing valve failure. Three disc modifications were studied: a cutoff disc, which was the original hemispherical disc cut off slightly downstream of the valve throat; a concave disc, which had a concave outer surface that was cut off at the end similar to the onion disc defined by others; and a hybrid disc, which was a combination of the first two. The cutoff disc was designed to cause the flow to adhere to the seat; the CFD results showed strong annular flow at low pressure ratios, but rapid loss of annularity as the pressure ratio increased. The CFD results for the concave disc, designed to cause annular flow at high pressure ratios, were the opposite of the cutoff disc. To obtain strong annular flow at all pressure ratios, the hybrid plug was created; the CFD results showed the flow to behave as predicted. The hybrid disc was installed in two control valves, neither of which were subsequently subject to excessive vibrations.

When vibrations are due to unstable normal shock, C. Domnick et al. [14] reported that changing the geometry of a hemispherical disc to create a purely convergent throat rather than a convergent-divergent geometry can reduce vibrations. Forcing a normal shock out of the valve gap of a convergent-divergent throat, where shock wave instability can apply forces directly to the disc, reduces pressure fluctuations and related forces on the disc.

D. Johns et al. [28] detailed the overhaul of a steam turbine which had issues with governor valve reliability and stability due to vibration at certain lifts. The dome-shaped discs

that were originally installed were replaced with straight discs and seats that had slight taper. Holes were also drilled through the body of the valve to equalize pressure across the valve. These modifications effectively removed the valve vibrations.

Modifications to the disc are the simplest to implement and test, but other components can be modified as well. D. Kim [3] studied a dished cutoff disc with a large outer radius that was paired with both a long and short seat. The disc was found to cause a more asymmetric flow pattern than the hemispherical disc it replaced, but the flow was more stable with no sudden pressure changes. Both the long and short seats created unstable axisymmetric flow that varied based on the pressure and opening ratios.

P. Iredale [12] investigated the effect of modifications to an onion disc and the corresponding valve seat. Examples of the modifications studied are shown in figure 2.22.

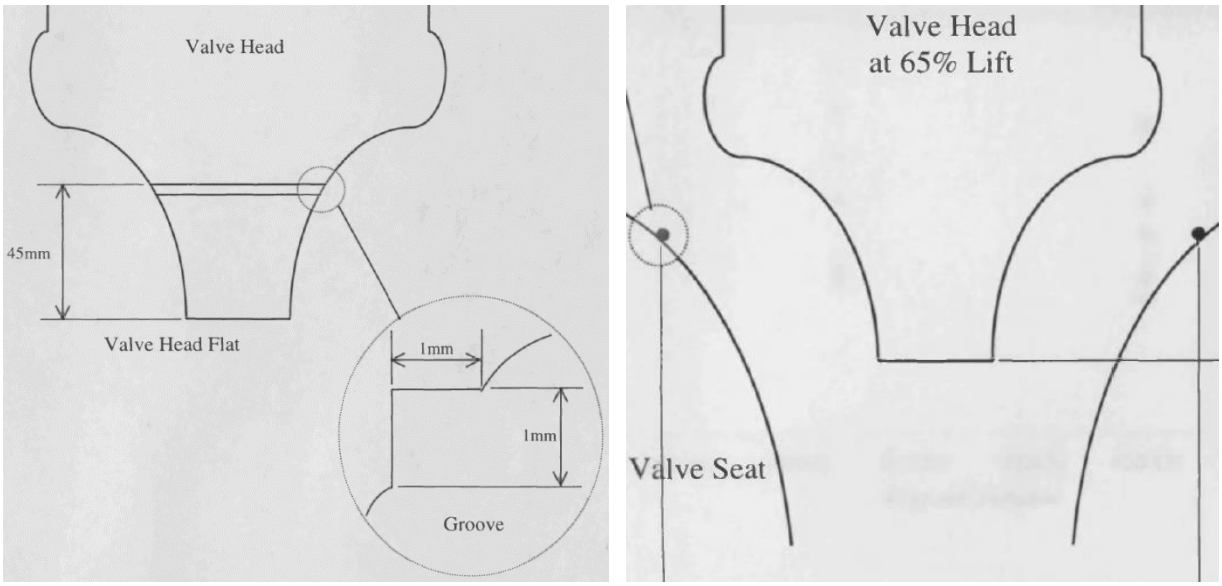

Figure 2.22. Example Modifications Made to Disc (Left) and Seat (Right) by P. Iredale [12].

The disc modifications were made to a) cause the flow to separate off of the disc and remain attached to the valve seat or b) cause early transition to turbulent flow on the disc to encourage flow attachment until the cutoff portion of the disc. Flow disturbance was introduced

by machining grooves around the head as a separation point. For flow adherence to the valve seat, the grooves were placed downstream of the throat where decelerating flow and an adverse pressure gradient are present. Grooves were placed upstream of the throat to initiate flow transition, where laminar accelerating flow and a positive pressure gradient are present. Improvements in flow steadiness were found using both methods; however, they were not consistent across the entire range of the valve lift and further research was considered necessary.

The valve seat modifications were implemented to provide constant flow attachment to the seat. The goal was to remove observed unsteadiness due to flow recirculation. Trip wires of varying thicknesses were placed upstream of the valve throat to initiate flow transition and maintain turbulent flow attachment. A trip wire that was one order of magnitude smaller than the calculated boundary layer thickness was found to improve flow steadiness significantly.

Hardin et al. [4] also conducted a CFD and experimental comparison of an original and large radius seat for a cut off plug. While the CFD results found that a large radius seat did not improve flow stability, the experimental results indicated that increasing the radius of the seat decreases pressure fluctuations.

3. INVESTIGATION APPROACH

After a review of previous work done with control valve vibrations and an analysis of the vibrations that the Minnkota Power Cooperative (MPC) control valves are experiencing, it seems most probable that the control valve vibrations are due to pressure fluctuations in the flow causing irregular forces on the disc surface. These are induced by unstable transonic flow or unsteady downstream jet attachment to the disc rather than acoustic resonance. A computational fluid dynamics (CFD) analysis is used to determine the cause of flow-induced vibrations and test valve design improvements that will resolve them. The use of CFD as a research tool allows for a more rapid and less costly design modification verification process.

3.1. Valve Modifications

When valve modifications are required to remove vibrations, the most preferred solution is to modify the design of the valve disc. The disc is one of the last components put into the valve, and it is easy to remove and replace in comparison to other valve components. This makes the problem solution simpler and more cost-effective. Seat modifications are also considered, but they are set as a secondary option because of the level of effort required to manufacture and replace the valve seat in comparison to the disc.

3.2. Analytical Solution

To determine the flow behavior in the valve, the equations presented in section 2.1 are used with the upstream temperature and pressure provided by MPC. The Matlab code XSteam was used to obtain the steam density and heat capacity ratio from the IAPWS-IF97 steam tables. Dimensions for calculating the throat area were obtained by measuring the narrowest section of the valve throat in the CAD valve assembly, as depicted in figure 3.1.

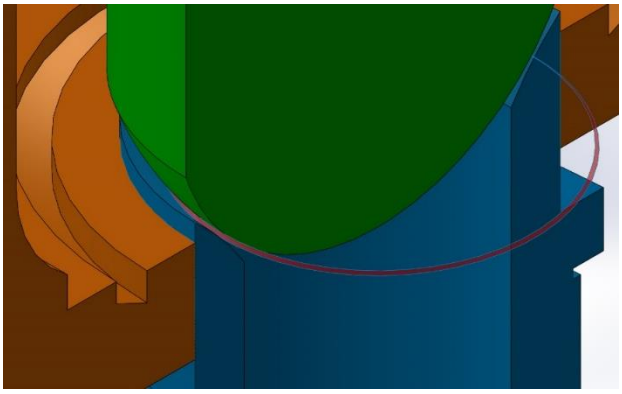

Figure 3.1. Throat Area for *OR* = 0.018, Shown in Red.

Because the pressure in the steam chest is assumed constant and the area at the throat is very small at low opening ratios, the flow velocity in the steam chest is very small. This allows for the static pressure and temperature to be used as the total pressure and total temperature values. Through the use of the section 2.1 equations, the choked (maximum) mass flow rate at the throat and the maximum exit pressure allowed to sustain choked flow are found. This is compared with the numerical results and those calculated by MPC at a set of operation points that span the vibration region of valve opening ratios.

3.3. Operation Point Selection

To verify which flow effects are causing instability and that the simulations are producing the anticipated results, three valve disc lift positions to simulate at steady state were originally established:

1. .030 inches – The crack point of valves 7 and 8.
2. .078 (5/64) inches – In the MPC identified vibration region of the valve.
3. .250 (1/4) inches – Mostly open valve, above the vibration region.

The first two simulation points, or cases, would show the flow structure when vibration is present; the third would serve both to determine which flow effects are causing the vibration and as a validation case. A fourth simulation point was added later in the analysis to confirm that any modifications made to the valve do not affect the maximum mass flow rate through the valve, since emissions conformance testing is required if there is an increase in total steam flow through the steam turbine.

4. 1.092 inches – Valve wide open (VWO), maximum stem lift.

After these operation points were determined, changes and additions were made to the data used to find the valve operating conditions. The increase of available data led to the correction of the first four operation points and the introduction of further points.

3.3.1. Operation Point Adjustment

The initial mass flow rate for the control valve was calculated from the design total steam flow for all eight control valves. To obtain more accurate mass flow rate values, MPC derived a correlation between the control valve opening percentage and the mass flow rate using the measured first stage pressure, throttle flow, and control valve position. The two methods are compared in figure 3.2 using the total percentage of steam flow through the valve system. The control valve percentage shown is for all eight valves; the range for valves 7 and 8 is 83.93 to 100 percent.

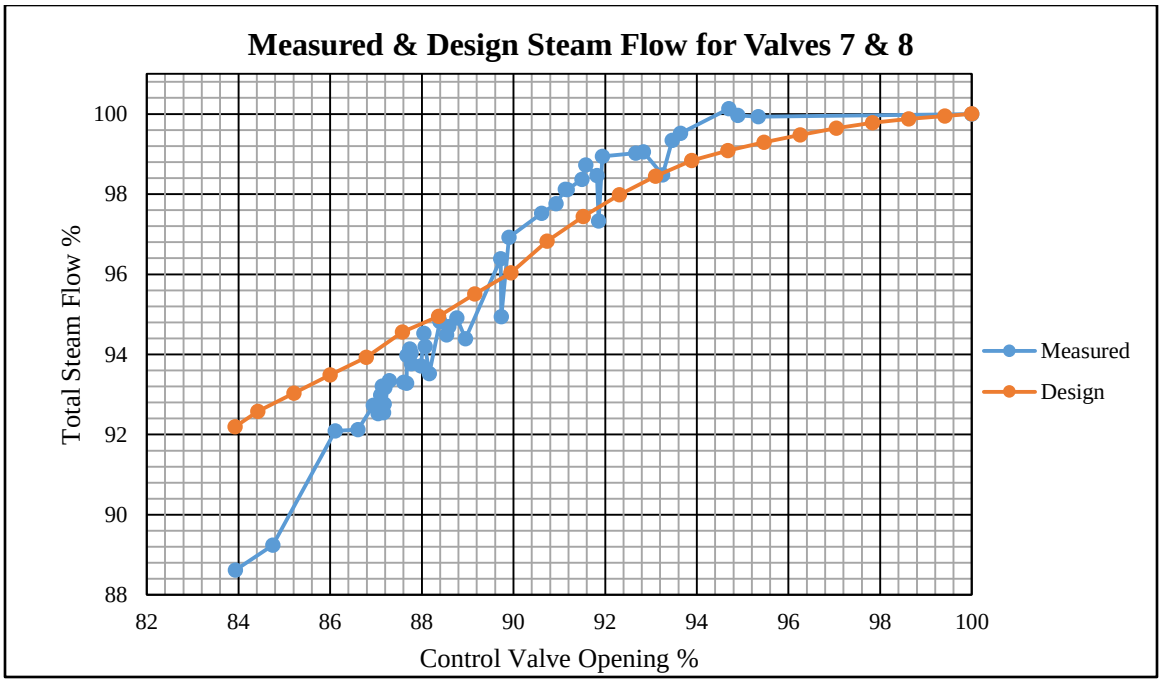

Figure 3.2. Comparison of MPC Derived (Measured) and Design Steam Flow.

The measured values are preferred over the design values for use in numerical analysis because they better capture the vibration conditions. However, the only valve outlet pressure data available was given in the design data, so a trendline was matched to the design steam flow values. The resulting polynomial equation was used to find the outlet pressure based on the measured throttle flow. The outlet pressures for the two methods are compared in figure 3.3; outlet pressure values for the numerical simulations are interpolated from the measured data points.

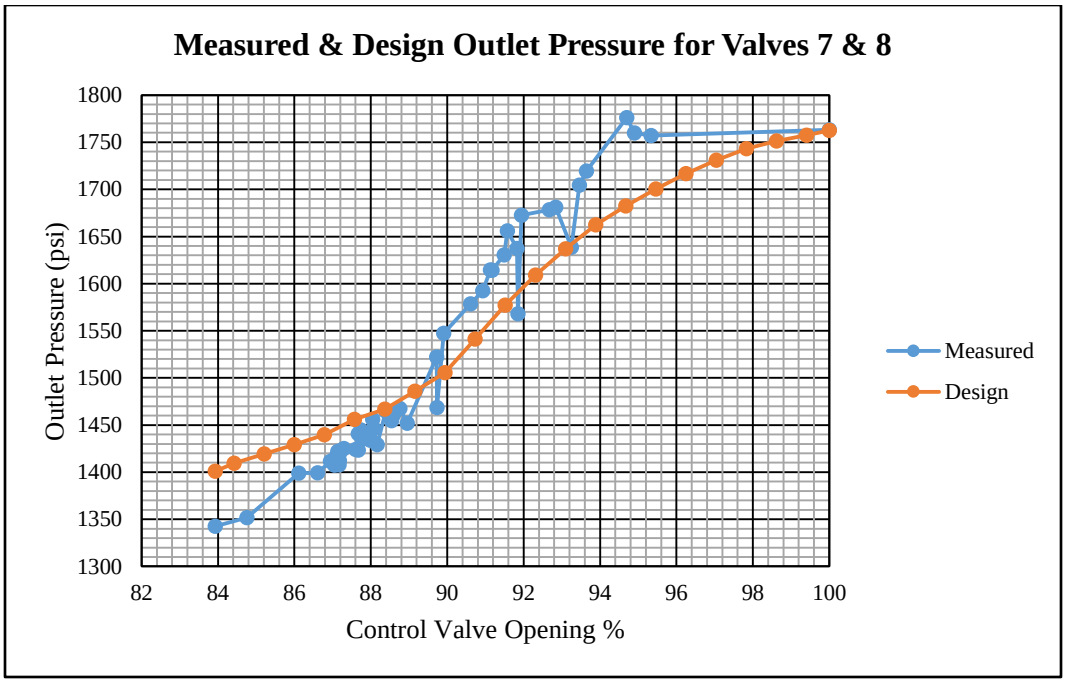

Figure 3.3. Design and Measured Outlet Pressure Comparison.

3.3.2. Minnkota Power Cooperative Test Data Analysis

Minnkota Power Cooperative (MPC) performed testing on multiple occasions to determine the turbine conditions where vibration problems occurred. Test results for three valve configurations are discussed here and compared in figure 3.4:

1. Valve with hemispherical disc installed.
2. Valve with MPC modified disc (Figure 1.4) installed.
3. Valve with NDSU revision 1 disc installed.

The testing data included the control valve opening percentage and the steam chest pressure at the initiation and termination of vibrations; the outlet pressure was not included. The valve lift and subsequent opening ratio was determined from the control valve opening percentage. The outlet pressure was taken from the design outlet pressure data because no measured data was available. All of the test inlet pressures were then set to the design inlet

pressure, although testing was performed at multiple steam chest pressures, to align the inlet pressure to the outlet pressure and provide the correct pressure ratios.

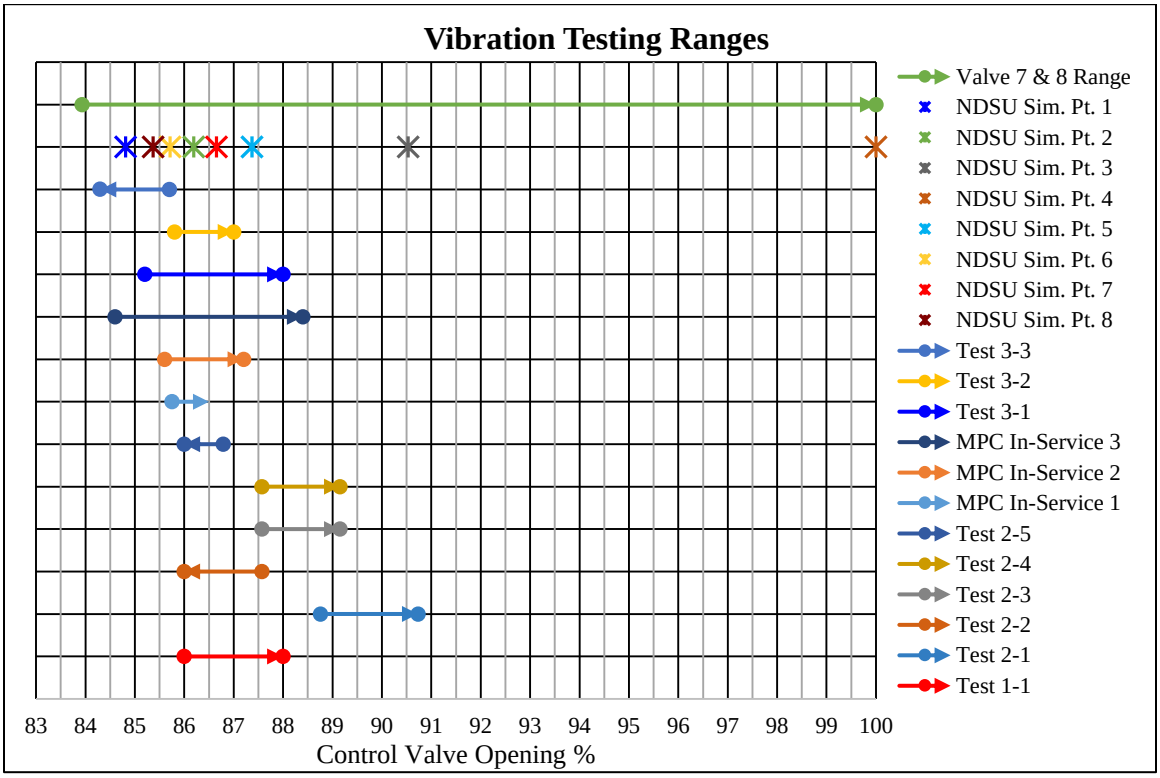

Figure 3.4. MPC Identified Vibration Regions and NDSU Simulation Points.

The test results for the hemispherical disc were conducted prior to any disc modifications. They are shown in figure 3.5 alongside some of the NDSU simulation points. The vibration regions defined by D. Zhang et al. [18] in figure 2.8 are shown in the background for figures 3.5 through 3.7. Valves 7 and 8 began vibrating at 86 percent control valve opening, and ceased at 88 percent. Per figure 2.8, the vibrations are beginning before a defined vibration region, at a very low opening ratio. C Bolin et al. [17] does include the region below an opening ratio of 0.02 into the vibration pattern region, however; this is shown in figure 2.11. Axial movement was present in valve 7 and radial movement was observed in valve 8.

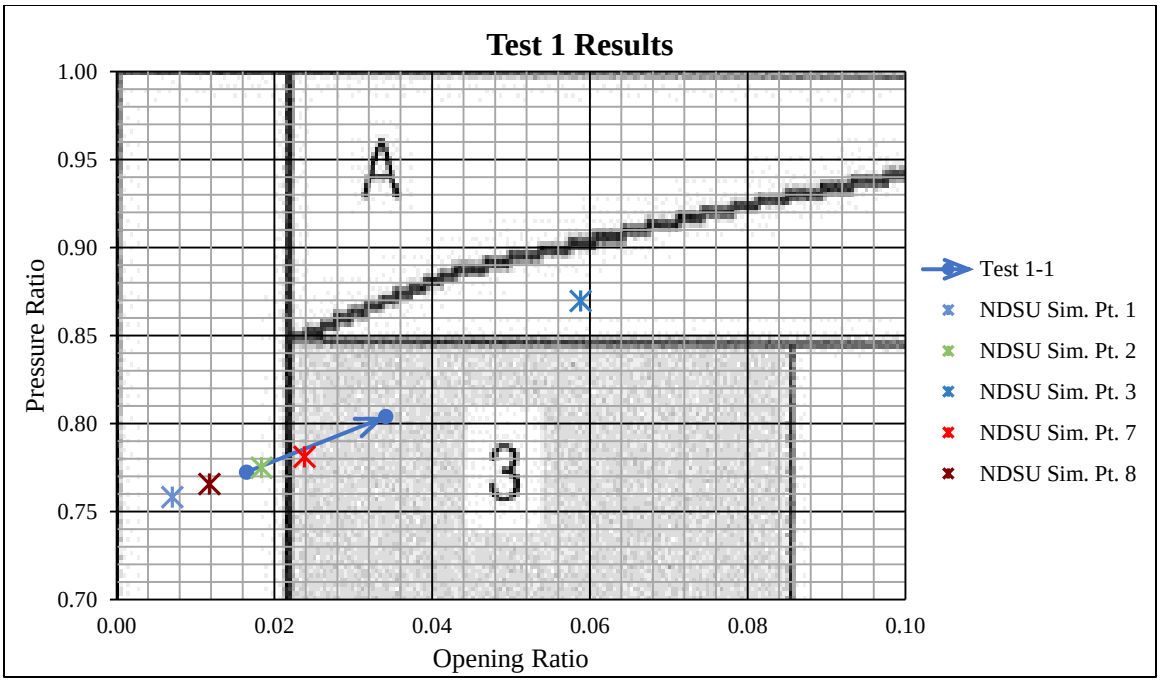

Figure 3.5. MPC Vibration Testing Results for Hemispherical Disc.

Testing for the MPC modified disc, shown in figure 1.4, was completed for a range of steam chest pressures; the results are presented in figure 3.6. The initiation point for all of the vibration test regions shifted into the unstable flow region of figure 2.8. Since the hemispherical disc results are not in a defined region, vibration improvement cannot be determined using the vibration regions. However, the vibration noise level appeared to decrease so this design improved the flow pattern, if only to a limited extent.

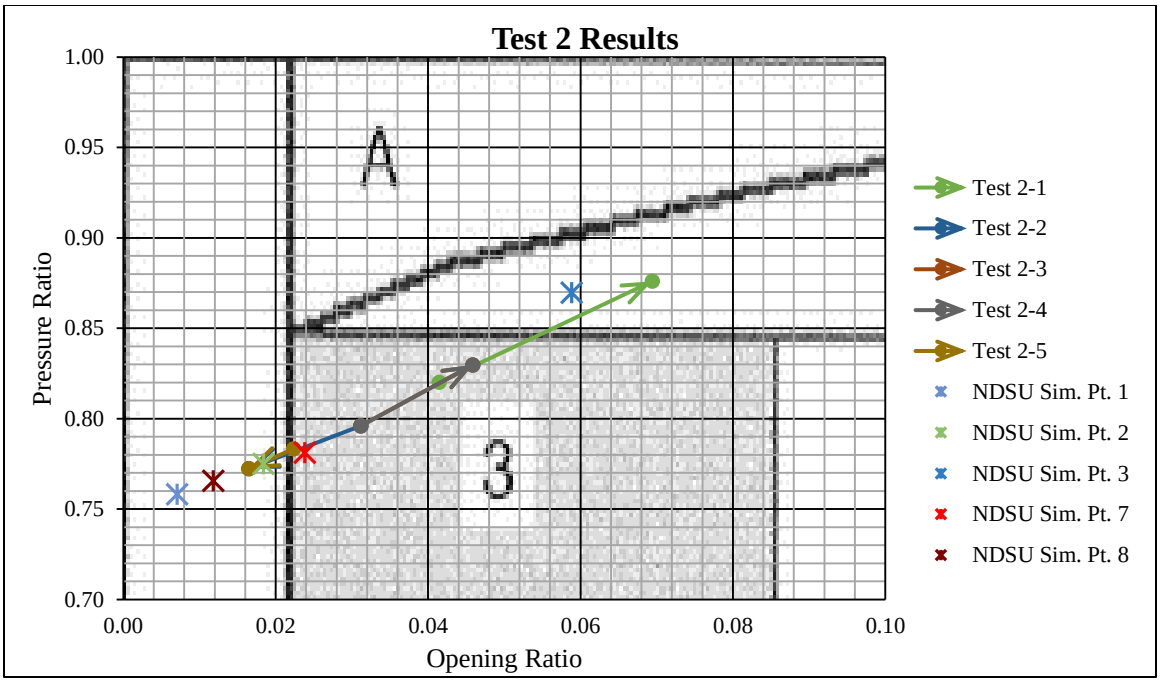

Figure 3.6. MPC Vibration Testing Results for MPC Modified Disc.

The vibration testing results for control valves 7 and 8 with the NDSU revision 1 disc installed are shown in figure 3.7. For tests 3-1 through 3-3, the control valves were opened in 1% control valve opening increments until vibrations were encountered and had ceased. The control valves were then closed in the same manner. The vibrations begin at the same opening and pressure ratios as those for the hemispherical disc, with all beginning as the valve is opening except one.

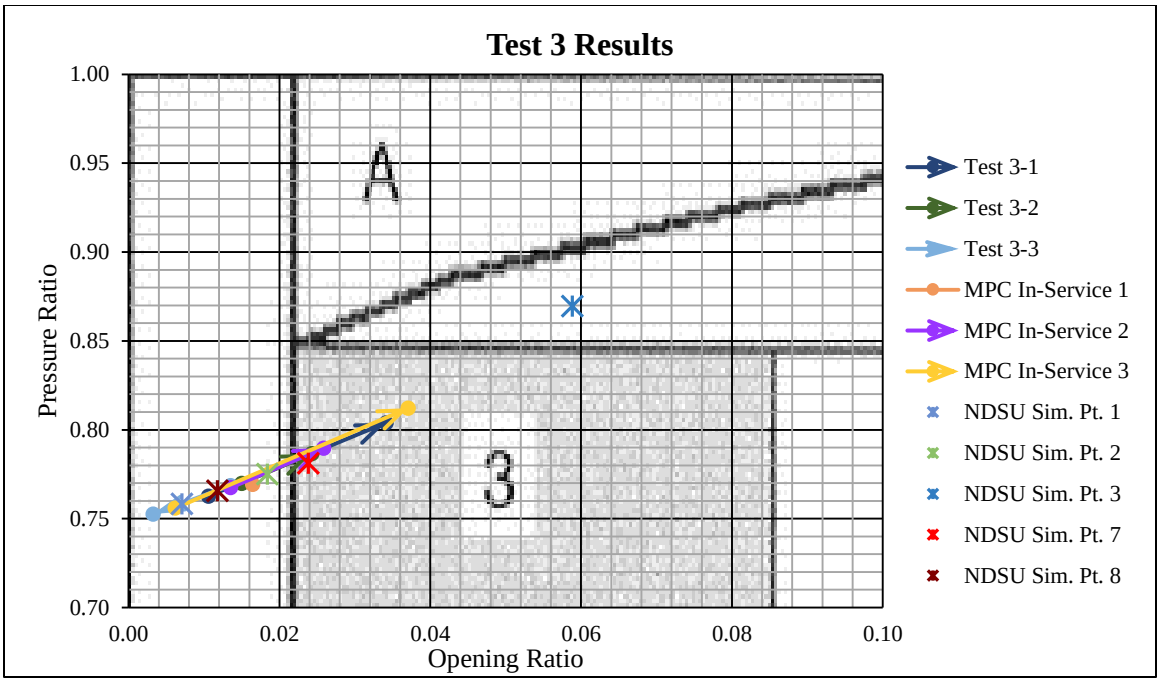

Figure 3.7. In-Service and Scheduled Vibration Testing Results for NDSU Revision 1 Disc.

3.3.3. Additional Operation Points

As a result of the MPC test data analysis, more simulation points were added, as shown and explained below. Because the control valve opening percentage to lift relation can change between valve overhauls, only the most recent (test 3) results were used for determining the lift of the new points.

5. 0.119 inches – Above vibration initiation points.
6. 0.061 inches – At vibration initiation point based on MPC test 3 data.
7. 0.101 inches – Above vibration initiation point.
8. 0.050 inches – At vibration initiation point based on MPC test 3 data.

Simulation point 5 was identified by taking the average pressure differential across the valve at the vibration initiation point for the MPC test 3 results. This was used in conjunction with the design steam chest pressure to find an outlet pressure. The valve lift was found by

correlating the outlet pressure to the control valve opening percentage and translating it to valve lift. Later corrections to the simulation points showed this disc lift to be above the vibration initiation point.

The averaged control valve opening percentage at vibration initiation from the MPC test 3 results was used to determine the disc lift for simulation point 6. The MPC In-Service 3 and 3-1 test results were outliers and thus not included. The design steam chest pressure was used for the inlet pressure and the outlet pressure was found using the design sequence data.

Because the flow through the control valves is pressure driven, the flow mechanisms are dependent on the pressure differential across the valve. The flow transition point from supersonic to subsonic, and vice-versa, is related to the pressure differential across the valve. Based on this understanding, simulation point 5 will capture the flow mechanism that causes the valve to vibrate and design modifications simulated at this point to stabilize the flow will be effective in valves 7 and 8. Thus, all valve modifications tested after the test 3 results were available are conducted at simulation point 5.

When simulation point 5 was established, the outlet pressure for all of the operation points was based on the design valve sequence data. After the adjustment detailed in section 3.3.1 was completed, the average pressure differential across the valve at the vibration starting point for the test 3 results changed noticeably. The procedure to obtain simulation point 5 was repeated for the new average pressure differential, and the resulting operation point was labeled simulation point 7. As with simulation point 5, further simulation point adjustments showed this disc lift to be above the vibration initiation point as well.

Simulation points 5 and 7 were identified prior to the test data inlet pressure adjustment discussed in section 3.3.2. After the pressure and opening ratio analysis was completed for the

test data, the resulting charts clearly showed that the pressure ratio for the test results did not match with the valve opening sequence pressure ratio. This is shown in figure 3.8 for the test 3 results.

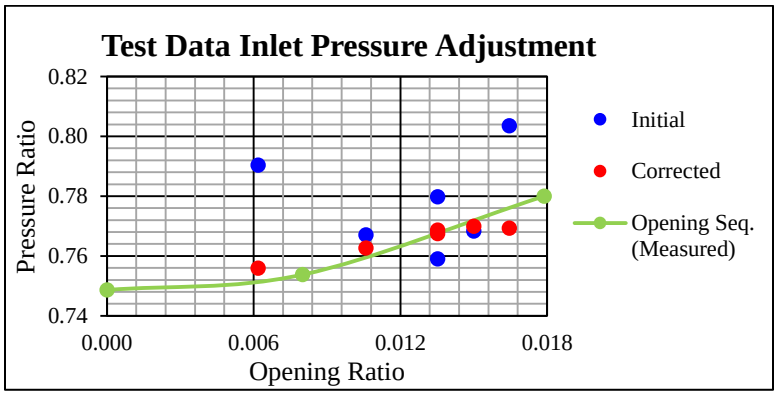

Figure 3.8. MPC Test 3 Inlet Pressure Adjustment.

The inlet pressure for the test results was then adjusted to the design pressure to correctly correlate with the design outlet pressure values that were used. This caused the pressure differential to change across the valve yet again, prompting a repeat of the process used to establish simulation points 5 and 7. Hence, simulation point 8 was created.

3.3.4. Stem/Disc Lift Correction

After some initial simulations were run, a further study of the data correlation between the valve (stem) lift and control valve opening percentage showed that the crack point of all valves is at a valve lift of 0.030 inches. At this point, the disc begins lifting off of the seat. The stem lift was originally interpreted as the disc lift, resulting in the simulation points representing conditions outside of the valve opening sequence. The points were adjusted to match the new conditions.

Cases 1 through 4 were established by setting a specific lift, so the outlet pressure was corrected to the proper value and the disc lift was kept the same. Case 5 is based on the average

valve pressure differential, so the outlet and inlet pressure were maintained and the disc lift was decreased by 0.03 inches. Case 6 was created using the average control valve opening percentage and converting it to valve lift, so the lift was decreased by 0.03 inches. The outlet pressure was retained because the outlet pressure is found by using the valve lift, and is therefore correct. Cases 7 and 8 were not involved in the lift correction.

3.3.5. Final Simulation Point Specifications

The specifications for all established operation points are compiled in table 3.1. These include all of the adjustments discussed in sections 3.3.1 through 3.3.4.

Table 3.1. Simulation Point Specifications.

Simulation Point	Disc Lift (inches)	Opening Ratio	Pressure Ratio	
			Design	Measured
1	0.030	0.007	0.788	0.758
2	0.078	0.018	0.799	0.775
3	0.250	0.059	0.845	0.870
4	1.063	0.250	0.983	0.983
5	0.119	0.028	0.809	—
6	0.061	0.014	0.795	0.769
7	0.101	0.024	—	0.781
8	0.050	0.012	—	0.766

3.4. Simulation Parameters

For the numerical analysis, the steam chest was selected as the inlet and the end of the nozzle was selected as the outlet. The bounded valve is shown in figure 3.9. Because MPC had limited information available on the geometry of the steam chest interior and some of the valve components, the top of the disc is used as the uppermost point in the simulation geometry rather than the top of the steam chest interior. The most complex flow occurs in the valve throat and directly downstream; the steam in the steam chest is assumed to be at a constant temperature and pressure when the valve flow is choked. The upper area of the steam chest, if included, would

then serve as an extended inlet. This is unnecessary, since the lower portion of the steam chest is sufficient to provide even flow distribution through the valve. In addition, placing the simulation inlet at the top of the disc simplifies the mesh and reduces its size.

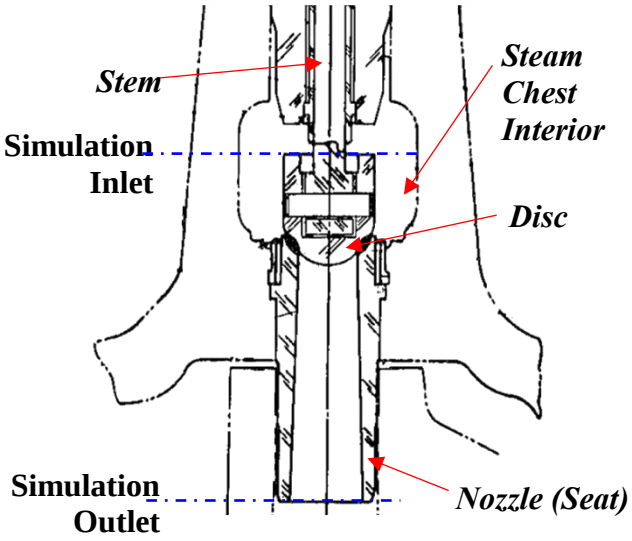

Figure 3.9. Simulation Boundaries.

The cases are initially run steady state to determine the time-independent flow pattern and allow for setup corrections to be made in an expedient manner. Inside the steam chest, at the simulation inlet, the total pressure and total temperature are specified and are the same for all cases with choked flow: 1, 2, 5, 7, and 8. All walls are identified as no-slip walls. The boundary conditions are depicted in figure 3.10. The effects of gravity due to the vertical movement of the steam as it travels through the control valve are assumed negligible.

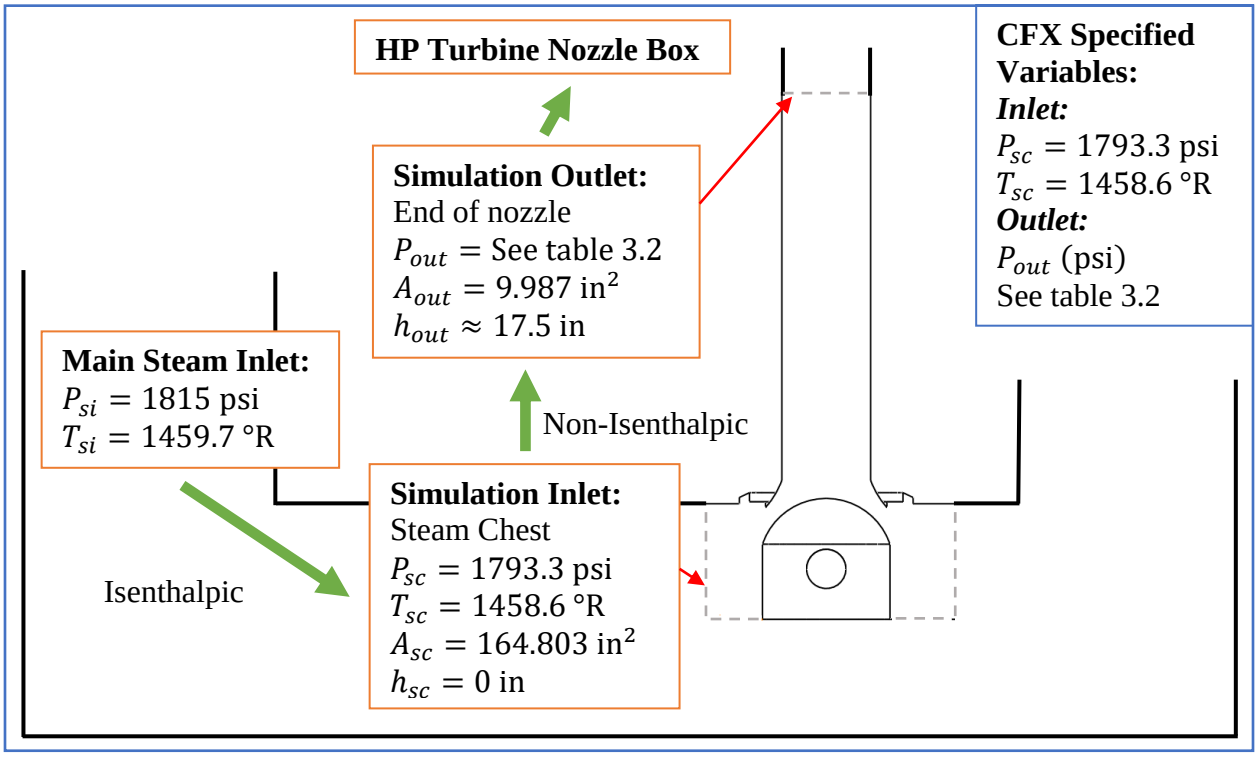

Figure 3.10. CFD Steady State Simulation Inlet/Outlet Boundary Conditions.

3.4.1. Outlet Pressure

The design pressure data for the valve 7 and 8 nozzle box is used for the static pressures at the end of the nozzle, the simulation outlet. As explained in section 3.3.1 and shown in figure 3.3, the outlet pressure was adjusted during the course of the CFD analysis using measured data for the MPC turbine. This was done to more closely match the flow conditions that cause vibrations within the valve. The data adjustment changed the outlet pressure boundary conditions for several simulation cases. The outlet pressures for both design and measured flow data are shown in table 3.2 for cases 1 through 8. The outlet pressures for cases 1 through 4 are given after the lift correction was made.

Table 3.2. Simulation Outlet Pressure Values.

Case	Opening Ratio	Design Static Pressure (psi)	Measured Static Pressure (psi)
1	0.007	1413.4	1359.8
2	0.018	1432.3	1389.8
3	0.059	1514.5	1559.6
4	0.250	1762.5	1763.3
5	0.028	1450.4	1425.5
6	0.014	1425.6	1378.7
7	0.024	—	1400.8
8	0.012	—	1373.0

3.4.2. Working Fluid

Two materials, dry steam based off of the equations developed by Redlich-Kwong and dry steam based off of the International Association for the Properties of Water and Steam (IAPWS) tables were investigated. The dry steam based off of the IAPWS tables is more realistic because it uses experimental data rather than an equation. However, the dry steam based off of the Redlich-Kwong equation of state is more robust within the ANSYS solver. Because of the sensitivity of the flow domain in the area of the valve throat, the increased robustness of the Redlich-Kwong dry steam material allows fewer adjustments to the mesh and setup to be made to achieve a successful simulation run. The slight decrease in accuracy from using the Redlich-Kwong dry steam material is acceptable given its comparative robustness; it is used as the simulation material. To verify that the Redlich-Kwong dry steam model is a suitable approximation for this simulation the Redlich-Kwong equation of state used by the ANSYS solver, found in the ANSYS CFX-Solver Theory Guide [29], was solved for the pressure at the inlet (steam chest) and the outlet for an opening ratio of 0.007.

The Redlich-Kwong equation of state is:

$$P = \frac{R_s T}{\nu - b} - \frac{a}{\nu(\nu + b)} \tag{3.1}$$

where parameters *a* and *b* are set to:

$$a = \frac{0.42747 R_s^2 T_c^2}{P_c}\left(\frac{T}{T_c}\right)^{-0.5}, \qquad b = \frac{0.08664 R_s T_c}{P_c} \tag{3.2}$$

Assuming the inlet temperature as known, solving for the steam chest pressure gives $P_{sc} = 1768.6$ psi. When compared to the actual inlet pressure of 1793.3 psi, the Redlich-Kwong equation of state has a 1.38 % error. Using the same procedure at the outlet for case 1, the calculated outlet pressure was found to be 1345.2 psi, which is a 1.07% error in relation to the measured value of 1359.8 psi. These calculations only cover two points, so there may be higher error in the throat region; however, given the low error at the inlet and outlet, using the Redlich-Kwong dry steam model should provide only a marginal loss in solution accuracy.

3.4.3. Turbulence and Transition Models

The shear stress transport (SST) turbulence model is used in this analysis because it provides very accurate predictions concerning the onset of flow separation. It is a two-equation model with a blending function that was developed to overcome deficiencies in models that were accurate either near the wall or in the freestream region. In order for this model to capture adequate flow detail within the boundary layer, a *y+* value of less than one is required. The variable *y+* is a dimensionless distance from the wall and is used as a parameter to identify the distance of the first node from the wall. The equation is given below:

$$y^+ = \sqrt{\frac{\tau_\omega}{\rho}} * \frac{\Delta n}{\nu_k} \tag{3.3}$$

Where Δn is the distance between the first and second nodes from the wall.

The Gamma Theta (γ-θ) transition model has been developed by ANSYS and uses experimental correlations to relate the momentum thickness Reynolds number to the turbulence intensity in the free stream at transition onset. It is based on an intermittency transport equation and a transition onset criteria transport equation. The intermittency equation is used to activate transition from laminar to turbulent flow. The transition equation identifies onset criteria in terms of the momentum thickness Reynolds number. There has been extensive validation concerning the use of the γ-θ transition model in combination with the SST model for transitional flows.

3.5. Computational Domain

Based on the drawings provided by the Minnkota Power Cooperative, a valve disc, valve nozzle, and steam chest interior wall were modeled using SolidWorks. The individual components were then assembled as shown to the far left in figure 3.11. After the assembly was completed, the valve disc lift positions for all operation points were inputted into the assembly by offsetting the disc from the nozzle the required distance. A mold was then created and the assembly was cut out of it to provide the computational flow domain for both the quarter and full domains. An example of these domains is shown in figure 3.11.

A quarter and full domain were created to maintain an efficient solution process. For the quarter domain, the cross-sectional sides of the domain have a symmetry condition that allows the solver to treat the flow as symmetric around those boundaries. The initial grid was generated and setup was performed on the smaller quarter domain. Once a successful mesh and setup were

in place, the mesh was transferred to the full domain to ensure that the effects of a complete three-dimensional domain are captured.

By using a CAD assembly, new disc and seat designs can be quickly generated and implemented as computational domains. This is done by altering the domain or modifying the components themselves and then creating a new domain. For instance, MPC supplied the drawing for the MPC modified disc that they were testing in valve 8 after the initial domains were created. A new disc was modeled based on this drawing and an additional domain was then created. A cross-section of this domain is shown on the far right in figure 3.11.

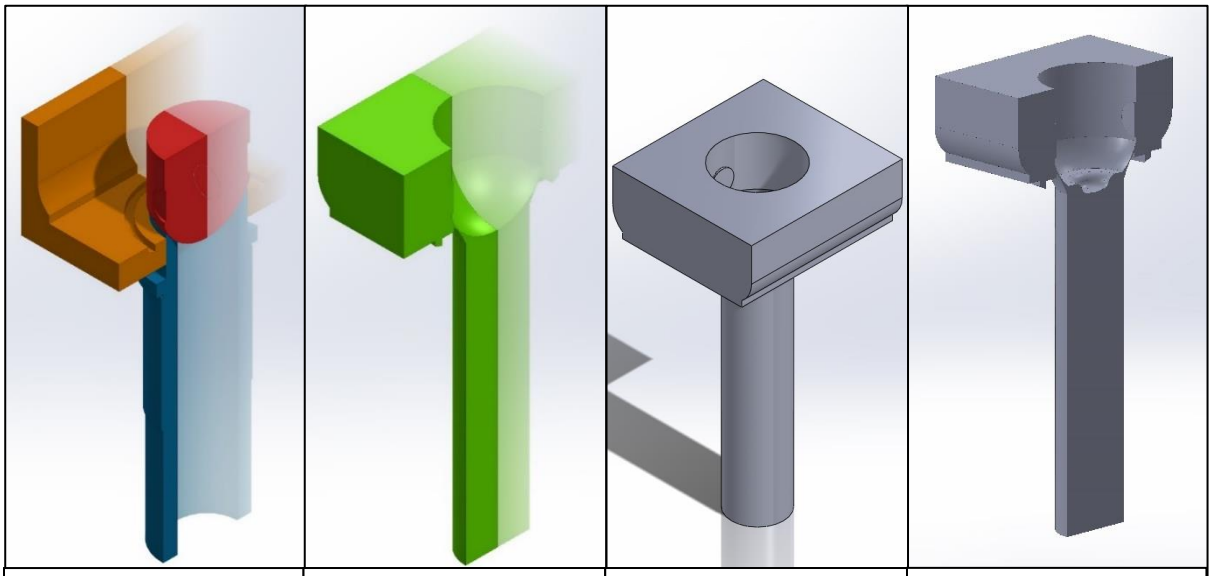

Quarter section of valve assembly.	Quarter flow domain.	Full flow domain.	Cross-section of full flow domain with modified disc.

Figure 3.11. Computational Flow Domains.

The original valve components were modeled independently. Due to the lack of complete dimensions, the modeled valve seat changed the sealing radius from the design dimension stated on the disc drawing. After receiving the revision 1 disc drawing from MPC, this error was realized and the valve seat was remodeled to match the design sealing radius of the disc rather

than the scale of the nozzle drawing. The simulations at an opening ratio of 0.007 and 0.018 were repeated with the new geometry.

3.6. Mesh Generation

After the flow domain was created, the simulation grid used to obtain the flow field information was formed. To create an efficient mesh that will accurately model the flow domain, it is necessary to alter the mesh element size to match the flow geometry and identify the desired flow characteristics. Where the flow structure changes rapidly, a very small element size is required to accurately capture the desired aspects of the flow field. A respectively large element size can be used when there is little to no change in the flow structure; this allows for a reduction in the number of elements, which increases the mesh efficiency. Finding the proper element size for each area within the mesh is done by completing a grid dependence study in which multiple iterations of an adjusted mesh are run and compared to determine which will provide a sufficiently precise simulation at an acceptable efficiency.

A simple mesh consisting of a general element size over the entire domain and one body of influence with a reduced element size near the throat was first generated on the quarter domain to provide a base mesh. Simulations were run on this mesh to show the basic flow pattern and identify that the setup parameters were correct. After the initial simulations were complete, a more complex mesh was generated. This mesh maintains a coarse grid size near the inlet and outlet of the domain, but incrementally increases the grid density into the throat area of the valve, which has the highest grid density. To capture the boundary layer effects on the walls of the disc and seat in the throat, inflation layers were added to the valve disc and nozzle in this region.

Due to the variation in the throat width between the cases, it was not feasible to maintain a constant throat area element size across all cases. For instance, the throat element sizing is required to be much smaller for an opening ratio of 0.007 than 0.028 because the throat width is much narrower; if the element sizing used in the were to be applied to the 0.028 opening ratio throat area, the resulting mesh would be well over 100 million elements. This is very computationally inefficient; therefore, the grid density was not maintained constant in the throat region. The mesh size for every case is between 17 and 26 million nodes, with the majority of the nodes located in the throat region, as shown in figure 3.12.

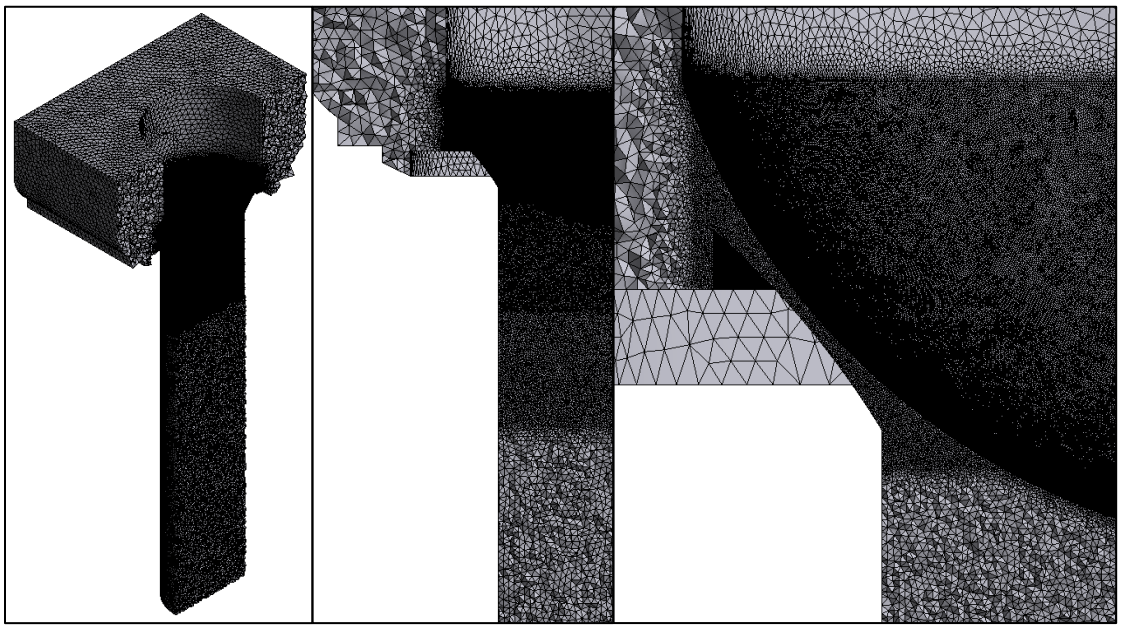

Figure 3.12. Mesh for *OR* = 0.018, Original Disc.

3.7. Computational Software and Hardware

Several software programs were used for this project. The Matlab code XSteam, based on the IAPWS-IF97 steam tables, was used instead of hand tables for finding the values of critical steam variables at various locations throughout the domain. Matlab was also used to solve some

sections of the theoretical solution. The computational domains were generated using the CAD software SolidWorks, and Tecplot 360 was used for post-processing of the results.

The computational components of this project were completed using a combination of a local Windows-based computer and the high-powered computing cluster at NDSU. The domains generated in SolidWorks were imported into ANSYS CFX 14.5 for grid generation and boundary condition establishment. The local machine used initially had 16 GB DDR3 RAM; this was upgraded to 32 GB to decrease the time required for grid generation. The ANSYS CFX simulations were run on the high-powered computing cluster at the NDSU Center for Computationally Assisted Science and Technology (CCAST). At the beginning of the project, simulations were performed on up to 128 processors. This was later increased to 200 processors. The increases in computational power implemented during this project decreased the grid generation and simulation runtime significantly.

4. RESULTS AND DISCUSSION

4.1. Analytical Results

The mass flow rate results of the analytical solution, numerical solution, and MPC calculations are compared in table 4.1. The MPC mass flow rates shown are estimates for the actual mass flow rate through the valves. They are calculated from a combination of measured turbine data, valve sequence calculations, and valve sizing equations. For cases 3 and 4, an analytical solution cannot be obtained without knowing the velocity of the steam flow upstream of the valve. The flow is not choked at these higher opening ratio cases and the flow rate is too high to assume stagnant flow in the steam chest, so the total pressure cannot be found without upstream velocity data. Hence, a mass flow rate cannot be determined at the throat. The two most stable inlet conditions available within ANSYS CFX are mass flow and total pressure because these variables constrain multiple flow properties. Simulations with static pressure and temperature specified as inlet conditions were attempted, but the setup was not robust enough to solve the simulations successfully. Therefore, the high opening ratio cases were abandoned for lack of known flow conditions.

Table 4.1. Analytical Solution Results for Valves 7 and 8.

Opening Ratio	**0.007**	**0.012**	**0.018**	**0.024**	**0.028**
Maximum mass flow rate (lbm/s)	5.00	8.42	13.16	17.11	20.27
Numerical mass flow rate (lbm/s)	5.03	8.50	13.21	17.10	20.30
MPC calculated mass flow rate (lbm/s)	2.60	4.35	6.61	8.39	9.79

The results obtained using the analytical formulas matched very well with those obtained in the simulations where the pressure ratio is large enough and correlates properly with the opening ratio to create choked flow. These values are much greater than the results obtained from MPC; the two are compared in figure 4.1. Given the absence of a direct method to measure

the mass flow rate through valves 7 and 8, the discrepancy is likely due to assumptions required to solve the MPC calculations.

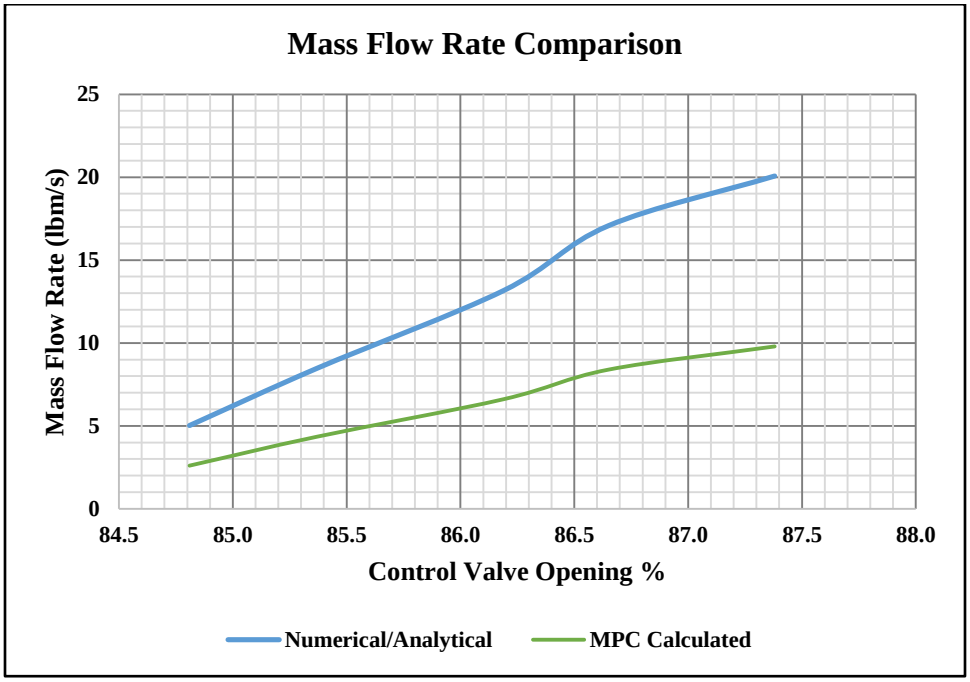

Figure 4.1. MPC and Analytical Mass Flow Rate Comparison.

4.2. Steady State Numerical Results

The original valve design, along with all modifications, was simulated using steady state analysis. The resulting flow velocity and pressure patterns were plotted to determine flow stability and are compared below. The maximum Mach number was recorded for each simulation to monitor the presence of choked flow in the valve throat. Because the vibrations were hypothesized to be due to pressure fluctuations on the valve disc, the pressure forces on the lower portion of the disc, shown in figure 4.2, were used as a gauge of vibration reduction.

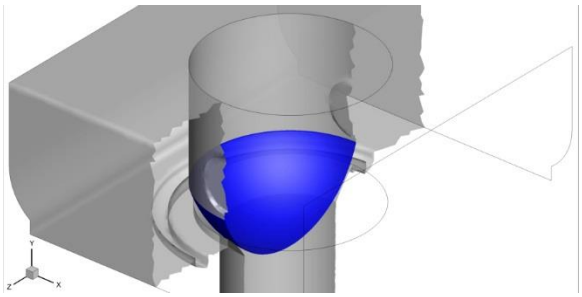

Figure 4.2. Valve Disc Throat Surface.

The valve design modifications are listed in the order they were studied. The original hemispherical disc results are used to show flow pattern changes caused by the operation point and geometry adjustments discussed in section 3.3. Due to the research timeline, some discs do not include any operation point adjustments and are related to later designs through the original disc cases. Some of the revision discs only include some of the adjustments; these are referenced to the revision 1 and original hemispherical discs. The simulation points for each disc are organized in order of increasing opening ratio and the contours are generated on perpendicular planes, displayed in figure 4.3.

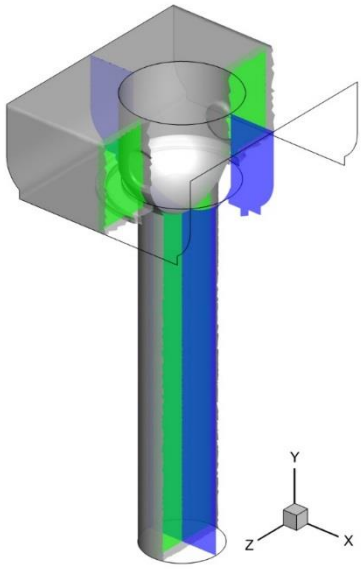

Figure 4.3. Contour Planes for Numerical Results.

4.2.1. Original Valve Configuration

The original hemispherical disc is the original equipment valve disc. It is used at all opening ratios (except 0.014) as a baseline for modified disc design improvements and to determine the existence of a flow structure that would support valve vibration.

4.2.1.1. Opening ratio = 0.007

The case 1 results for the original geometry show that unstable flow patterns exist in the valve at an opening ratio as low as 0.007. Velocity streamlines and contours, given in figures 4.4 and 4.5, respectively, show asymmetric core flow attached to the disc, with irregular reverse flow moving up the seat wall. At a low opening and pressure ratio, high speed flow is present in the valve throat. This is shown in figure 4.6; the maximum Mach number is 1.6, indicating choked flow. The supersonic flow condition displayed on the pressure contours in figure 4.7 matches well with the velocity and Mach contours. The steam chest remains at the inlet pressure and downstream of the shock wave there is little pressure variation from the outlet pressure.

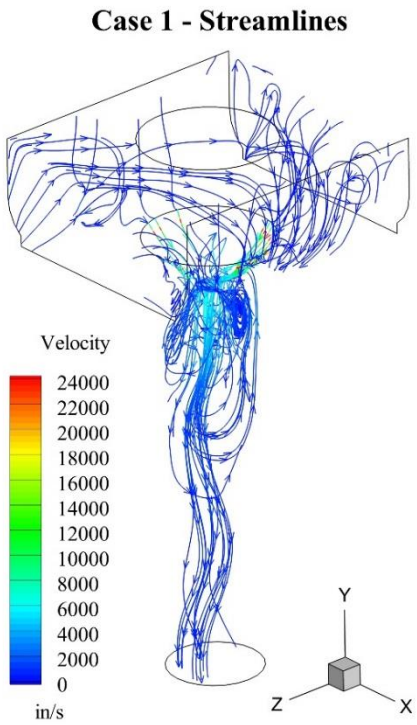

Figure 4.4. Velocity Streamlines at $OR = 0.007$, Original Disc.

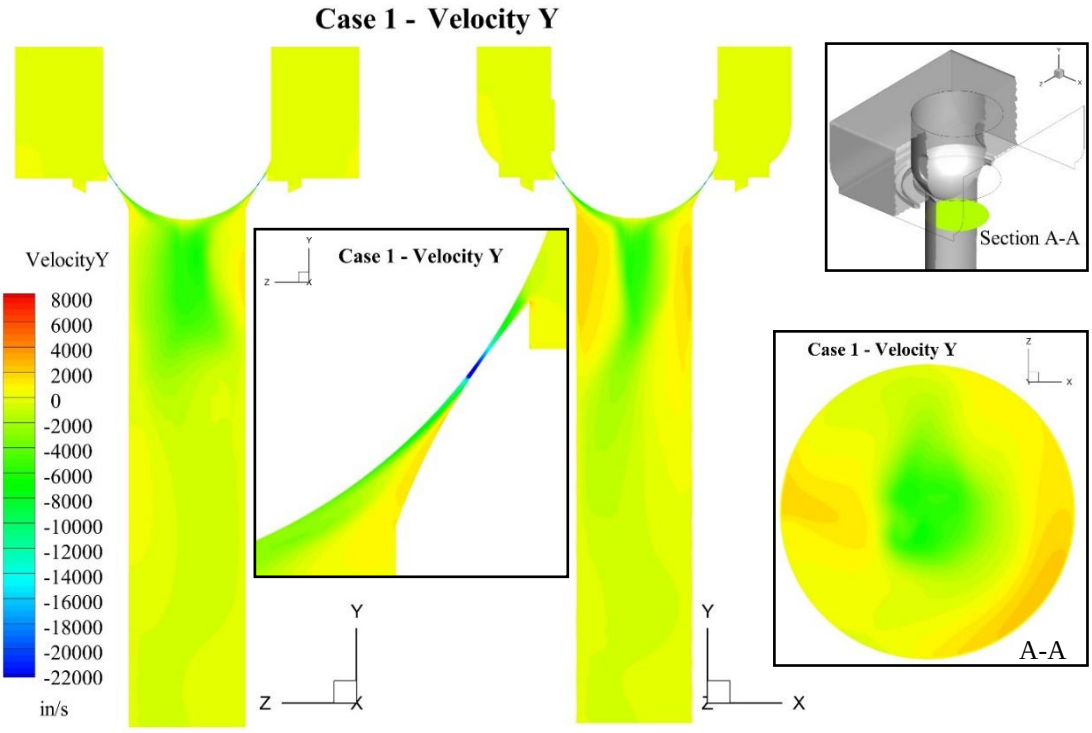

Figure 4.5. Vertical Velocity Contours at $OR = 0.007$, Original Disc.

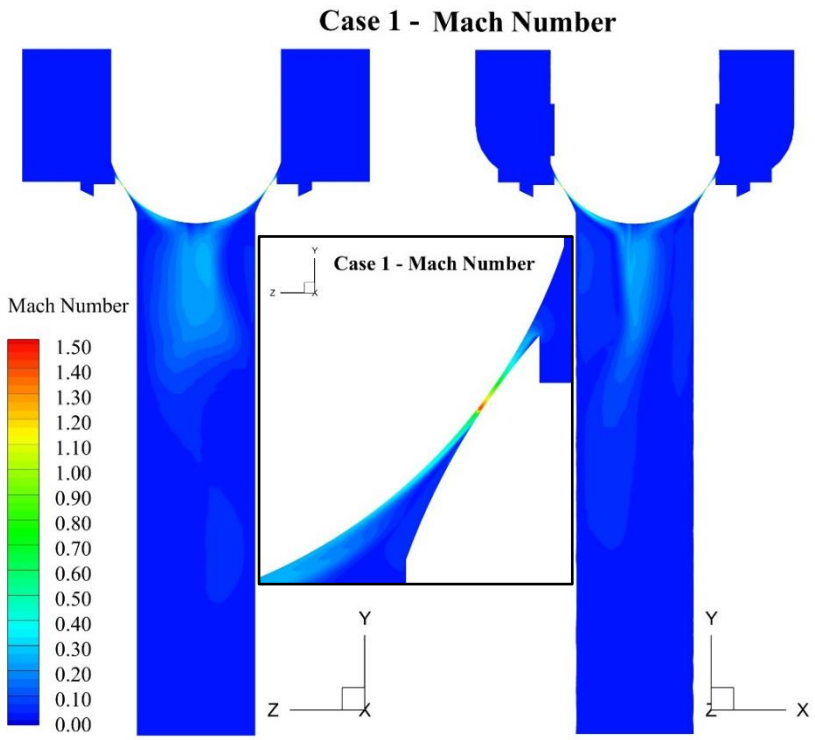

Figure 4.6. Mach Number Contours at $OR = 0.007$, Original Disc.

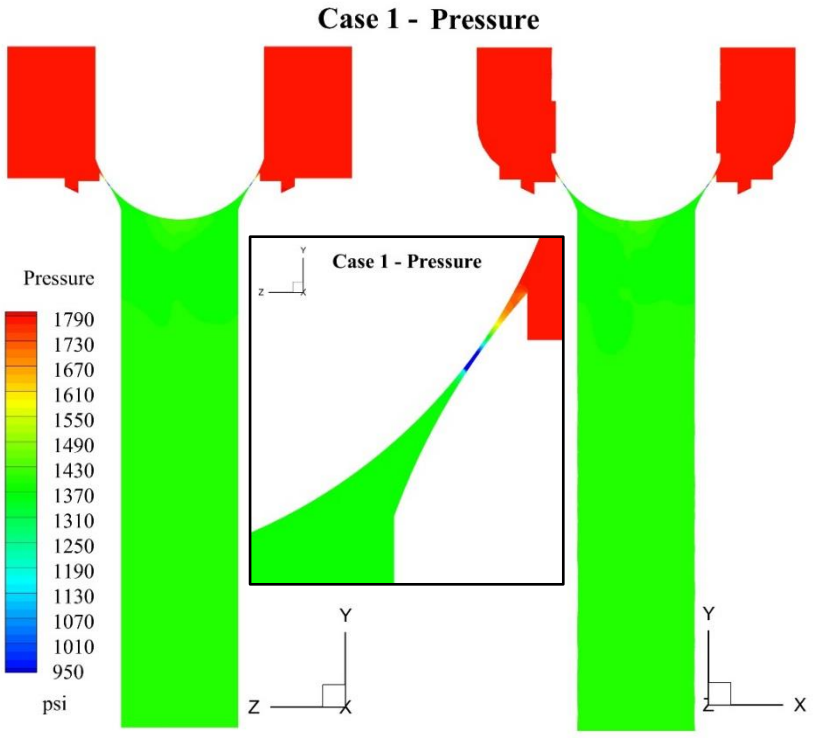

Figure 4.7. Pressure Contours at $OR = 0.007$, Original Disc.

The general flow pattern remains unchanged for the seat geometry correction at case 1, shown in figure 4.8. The reduction in the seat sealing surface angle causes the flow to separate more upon leaving the throat, however. There is less flow attachment to the disc.

The outlet pressure was altered twice after the seat geometry was corrected: once from the design value to the measured and once for the stem/disc lift adjustment. There are no significant flow pattern changes from these adjustments, as indicated in figures 4.9 and 4.10.

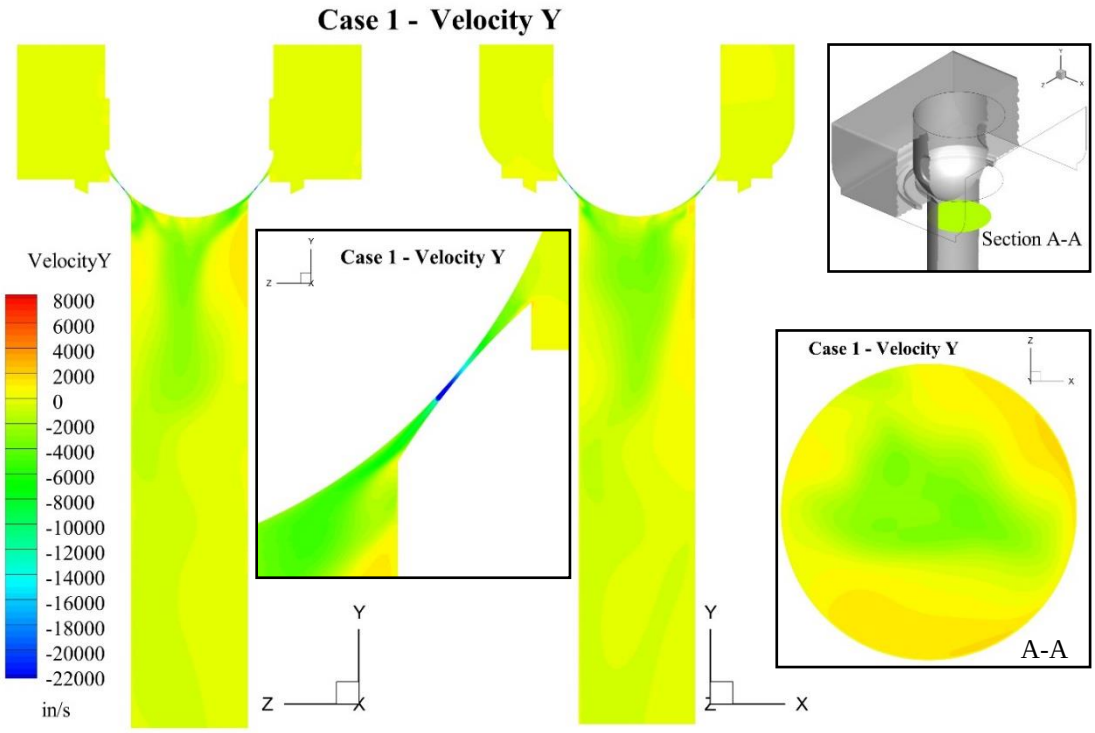

Figure 4.8. Vertical Velocity Contours at $OR = 0.007$, Original Disc, Corrected Seat Geometry.

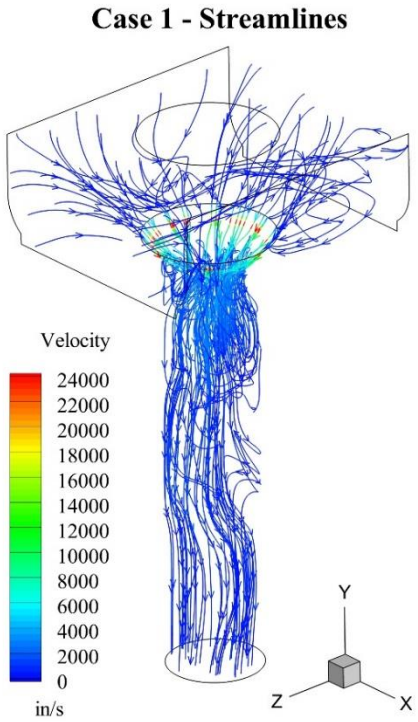

Figure 4.9. Velocity Streamlines at $OR = 0.007$, Original Disc, Corrected Disc Lift.

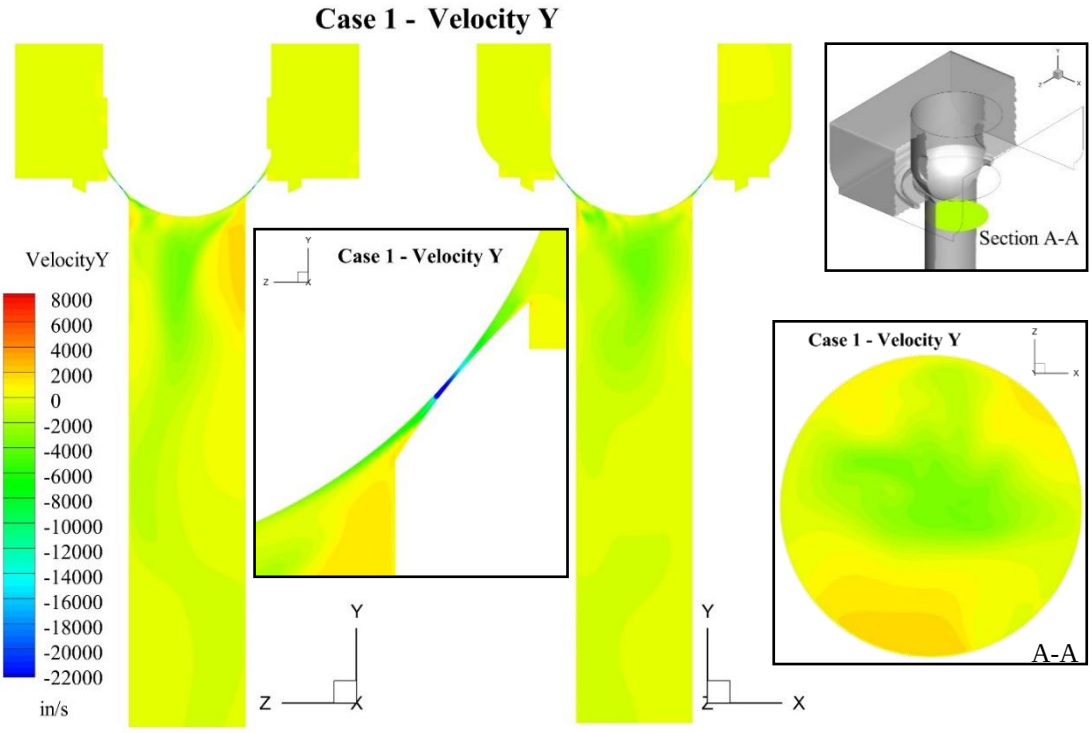

Figure 4.10. Vertical Velocity Contours at $OR = 0.007$, Original Disc, Corrected Disc Lift.

4.2.1.2. Opening ratio = 0.012

The unstable flow pattern increases as the opening ratio rises to 0.012. Figures 4.11 and 4.12 show increased vortex shedding off the disc and irregular reverse wall flow. The flow pattern correlates well with the unstable patterns identified by D. Zhang et al. [18] and T. Araki et al. [16]. The maximum Mach number in the throat is 1.6.

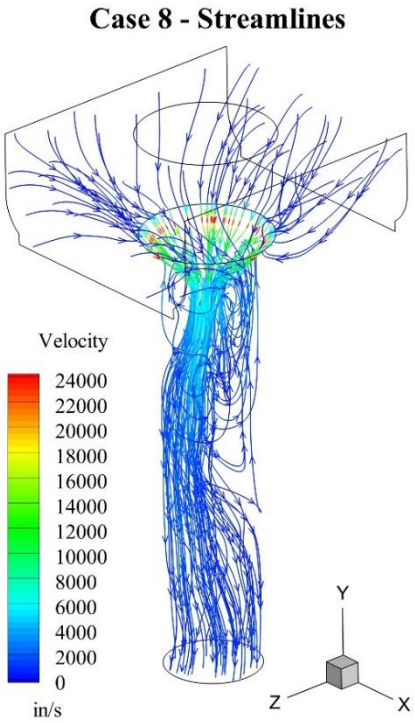

Figure 4.11. Velocity Streamlines at $OR = 0.012$, Original Disc.

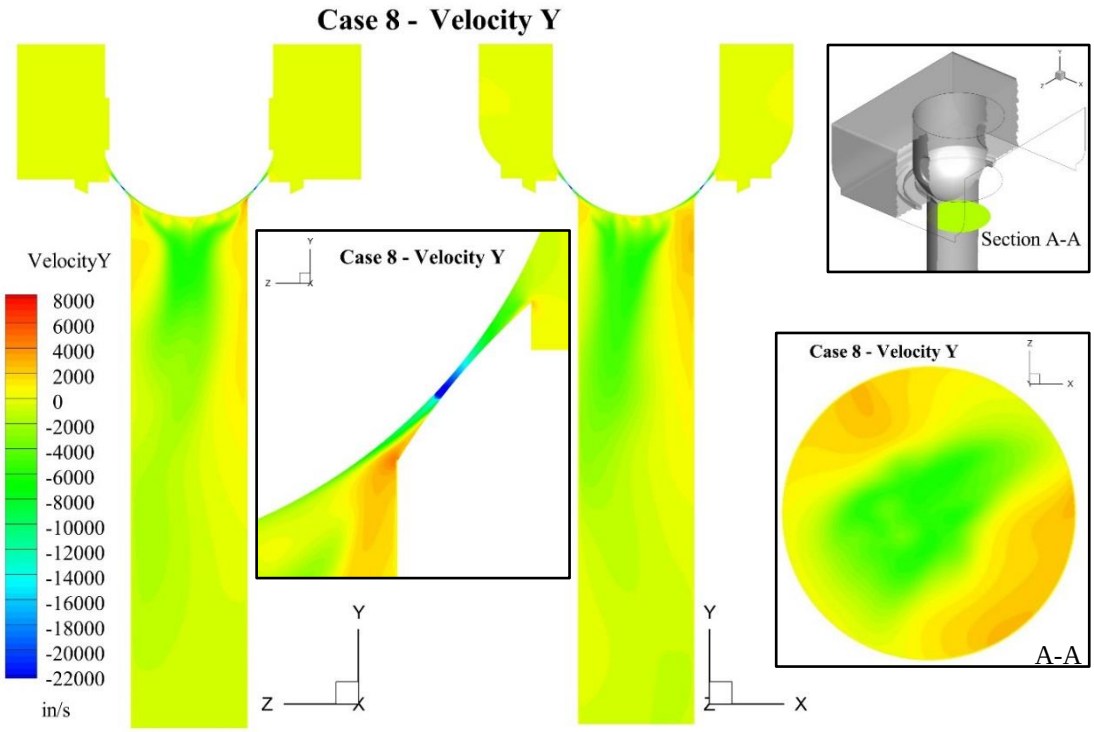

Figure 4.12. Vertical Velocity Contours at $OR = 0.012$, Original Disc.

4.2.1.3. Opening ratio = 0.018

The unstable vortex flow off of the back of the disc strengthens as the opening ratio increases up to 0.018, shown in figures 4.13 and 4.14. The asymmetrical reverse wall flow is more severe as well. The Mach number in the throat reaches 1.3, which is an expected decrease as the valve opens.

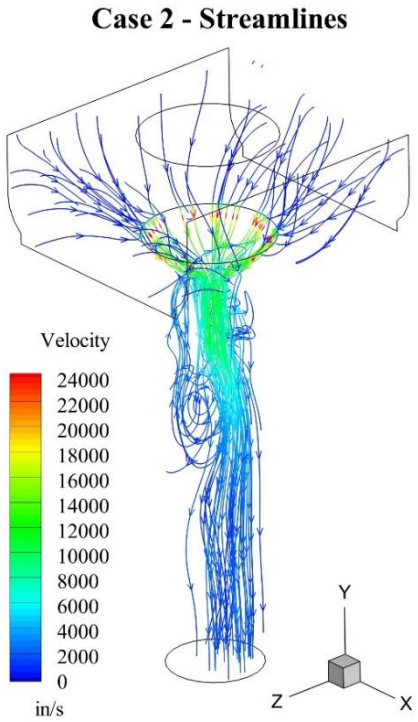

Figure 4.13. Velocity Streamlines at $OR = 0.018$, Original Disc.

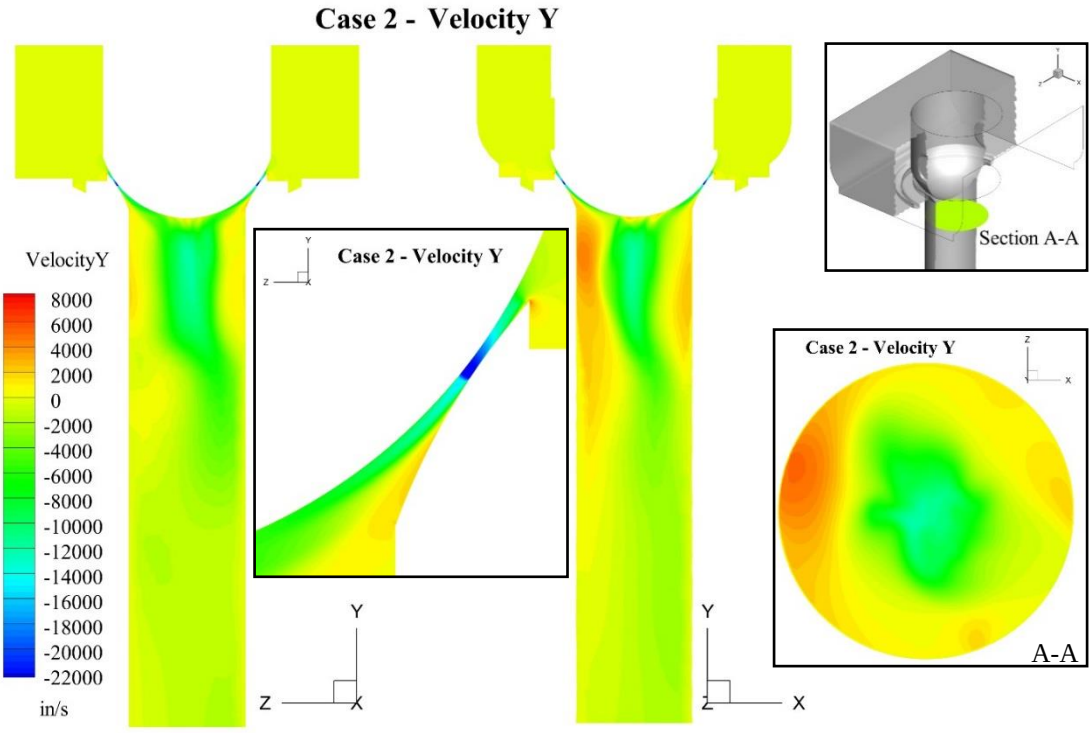

Figure 4.14. Vertical Velocity Contours at $OR = 0.018$, Original Disc.

The changes to the flow pattern due to the seat adjustment are shown in figure 4.15 using velocity contours. There is not a substantial change because the flow is so strongly attached to the disc at this lift.

The result of the outlet pressure adjustments from design to measured values and for stem/disc lift correction is displayed in figures 4.16 and 4.17. The flow pattern does not change significantly, but the velocity streamlines do show slightly more instability due to the decreased pressure differential.

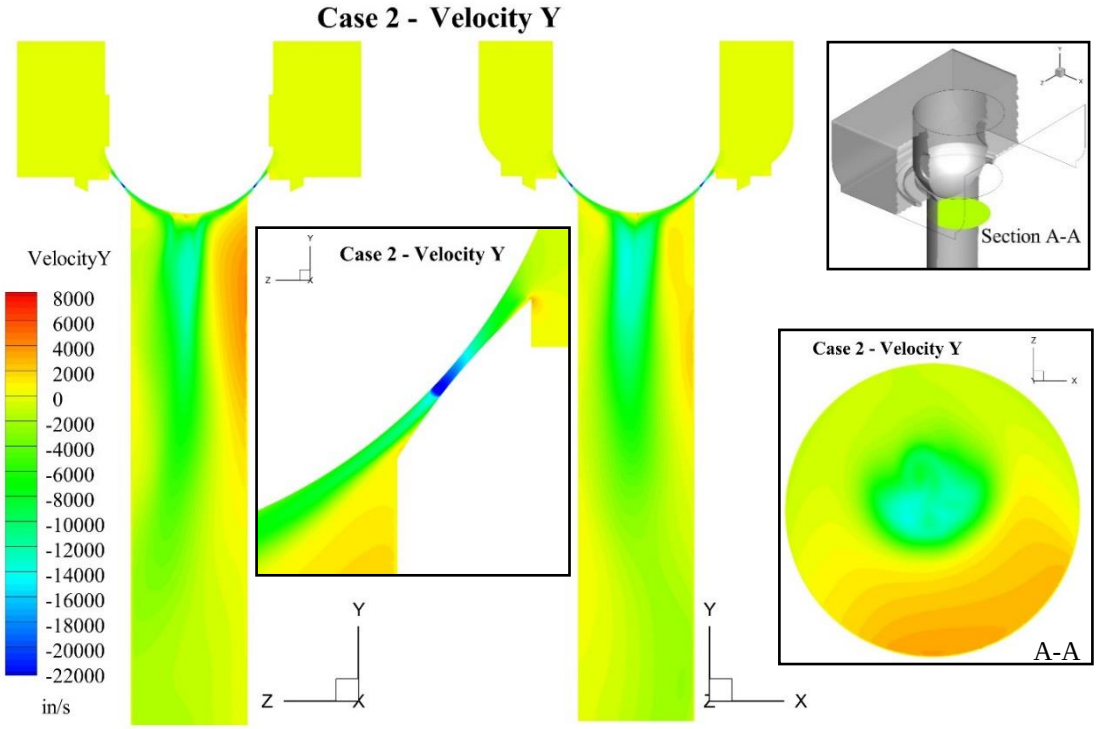

Figure 4.15. Vertical Velocity Contours at $OR = 0.018$, Original Disc, Adjusted Seat Geometry.

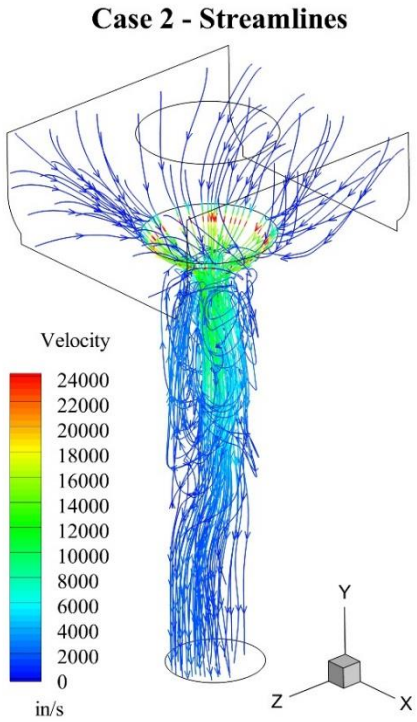

Figure 4.16. Velocity Streamlines at $OR = 0.018$, Original Disc, Corrected Disc Lift.

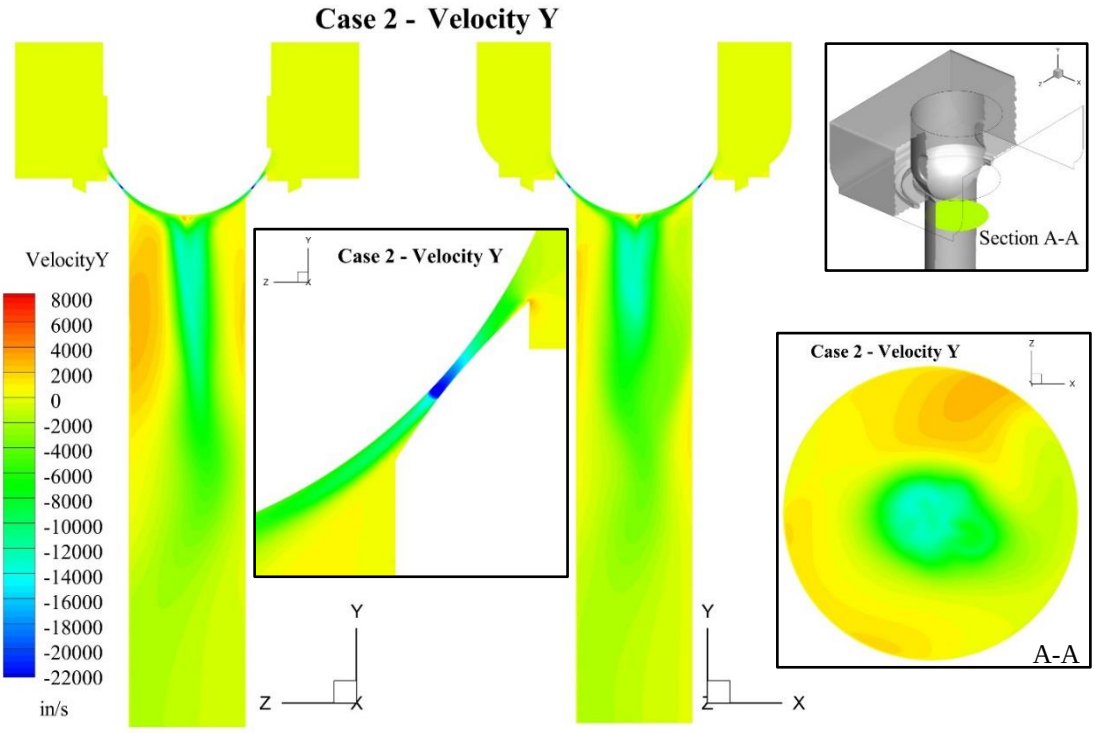

Figure 4.17. Vertical Velocity Contours at $OR = 0.018$, Original Disc, Adjusted Disc Lift.

4.2.1.4. Opening ratio = 0.024

At an opening ratio of 0.024 there is a noticeable increase in the stability of the core flow shedding off of the back of the disc, as indicated in figures 4.18 and 4.19. Irregular reverse wall flow is still present, however, and the flow jets coming out of the throat provide a clear detachment from the seat prior to the end of the sealing face. The maximum Mach number is 1.4.

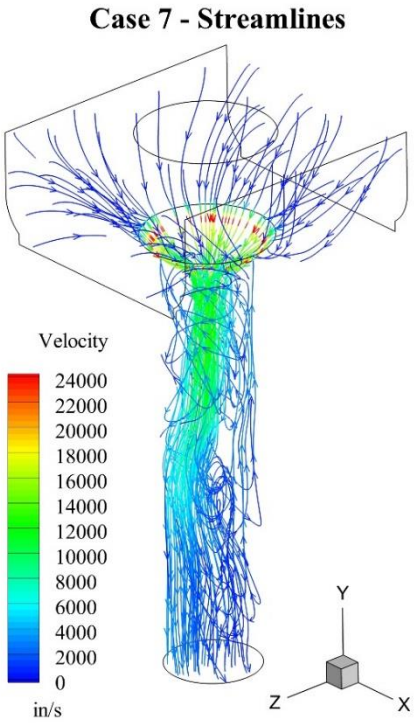

Figure 4.18. Velocity Streamlines at $OR = 0.024$, Original Disc, Corrected Disc Lift.

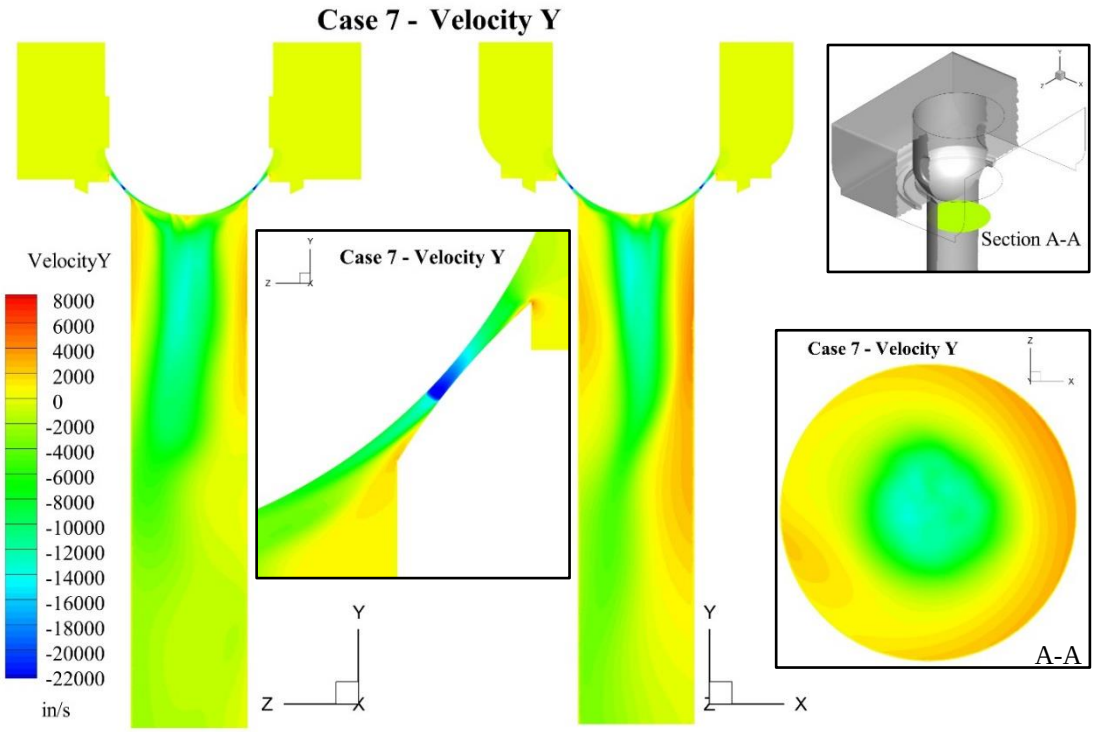

Figure 4.19. Vertical Velocity Contours at $OR = 0.024$, Original Disc.

4.2.1.5. Opening ratio = 0.028

The general flow pattern remains the same at an opening ratio of 0.035, as shown in figures 4.20 and 4.21. The core flow strength has increased from the 0.024 opening ratio and become more unstable, however.

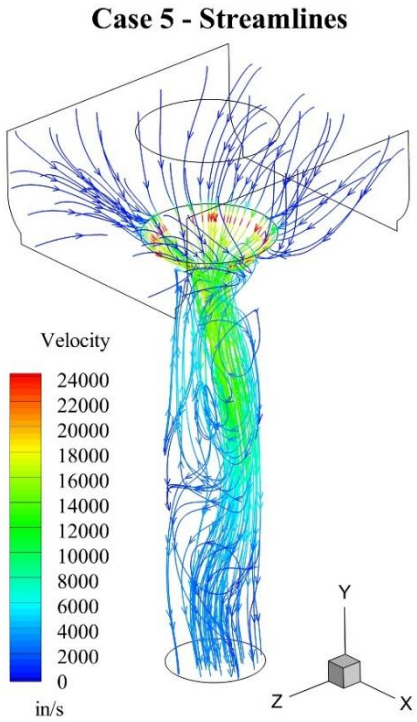

Figure 4.20. Velocity Streamlines at $OR = 0.035$, Original Disc.

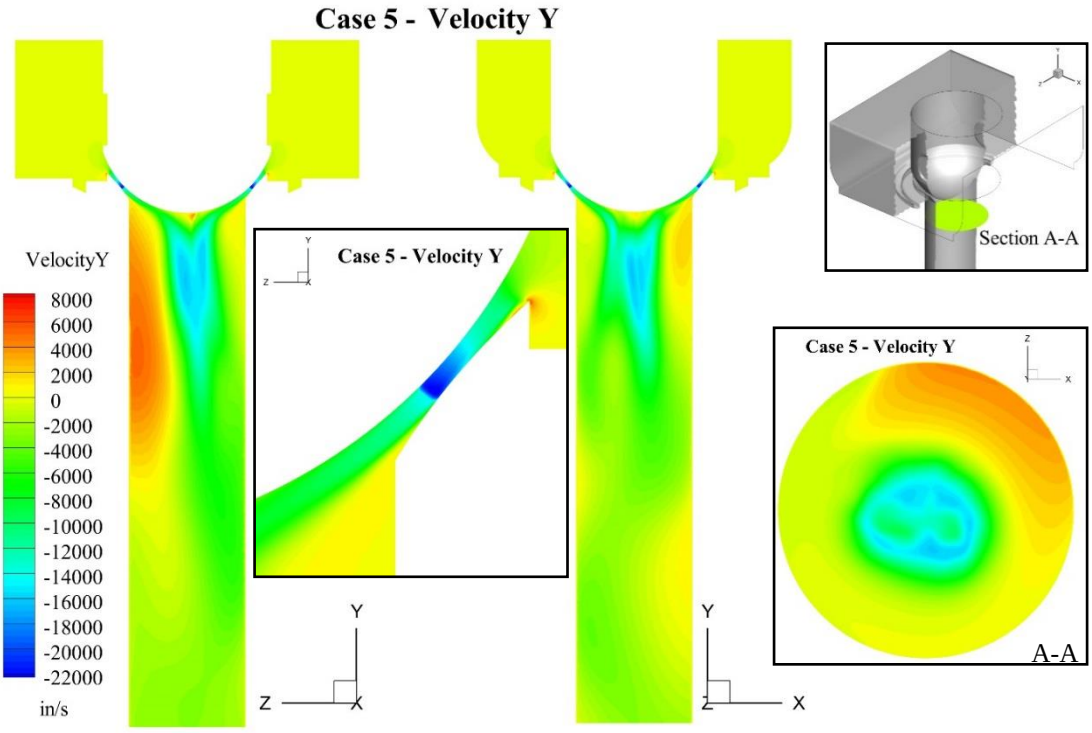

Figure 4.21. Vertical Velocity Contours at $OR = 0.035$, Original Disc.

The opening ratio for the flow condition displayed in figures 4.22 and 4.23 is decreased to 0.028 as result of the stem/disc lift correction. The pressure ratio for this case is unchanged, as is the flow pattern. The maximum Mach number is 1.3.

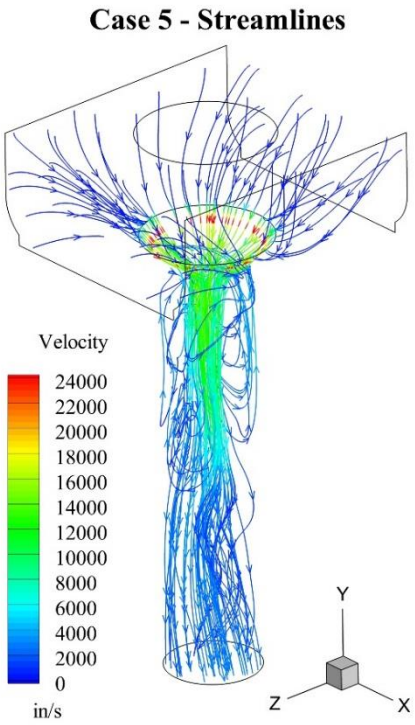

Figure 4.22. Velocity Streamlines at $OR = 0.028$, Original Disc, Corrected Disc Lift.

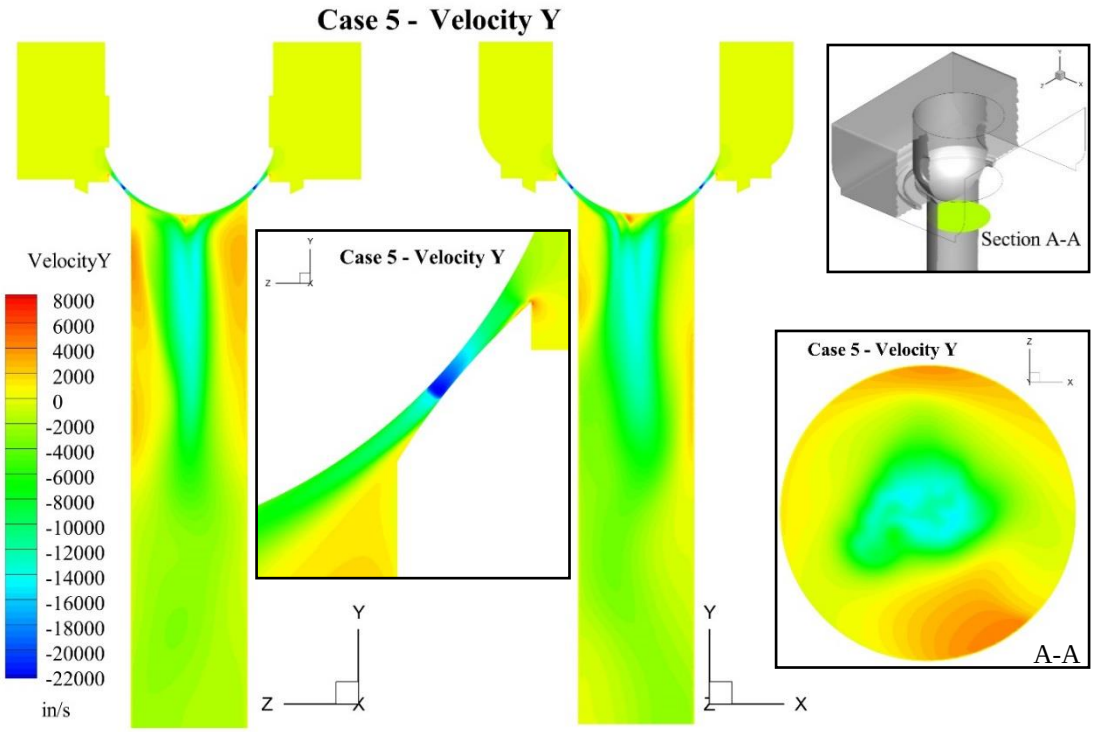

Figure 4.23. Vertical Velocity Contours at $OR = 0.028$, Original Disc, Adjusted Disc Lift.

4.3. Initial Disc Modifications

Several disc modifications were initially considered as a method to remove the flow instability. There are 9 variations total, several of which have the dished or indented geometry used by T. Araki et al. [16], J. Hardin et al. [4], and D. Zhang [8]. The other styles are similar to the onion shape used by P. Iredale [12] and J. Hardin et al. [4]. They were all run using case 2 as the baseline to determine which modifications would prove to be the most beneficial. A description of each modification is given in table 4.2 and the discs are displayed in figures 4.24, 4.25, and 4.26.

Table 4.2. Modified Disc Designs.

Modification	Description
MPC	Modified disc installed by MPC prior to NDSU analysis.
1	Disc cut off flat slightly below design sealing diameter to force flow separation from disc.
2	Disc modified to remove separation of flow off of downstream side of disc. Intended to create stable core flow without random vortex shedding.
3	Indented cutoff disc designed to stabilize the reverse core flow encountered in the modification 1 disc.
4	Extended cutoff disc designed to separate the flow from the disc and direct it downstream.
5	Flat cutoff disc. Cut off lower on disc body than the modification 1 disc to increase the downstream disc-nozzle contact region.
6	Extended cutoff disc with narrower gap in between nozzle wall and disc than modification 4 disc. Intended to remove the flow separation on nozzle wall.
7	Indented cutoff disc. Cut off lower on disc body than the modification 3 disc to increase the downstream disc-nozzle contact region.
8	Indented cutoff disc. Cut off higher on the disc body than the modification 3 disc with wider indentation to improve flow separation on disc wall. Indentation depth decreased to increase wall thickness and decrease amount of flow held in indentation.

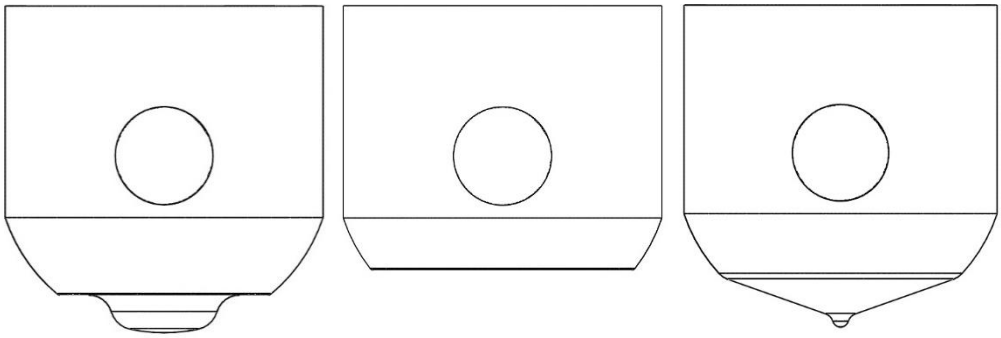

Figure 4.24. From Left to Right: Modification Discs MPC, 1, and 2.

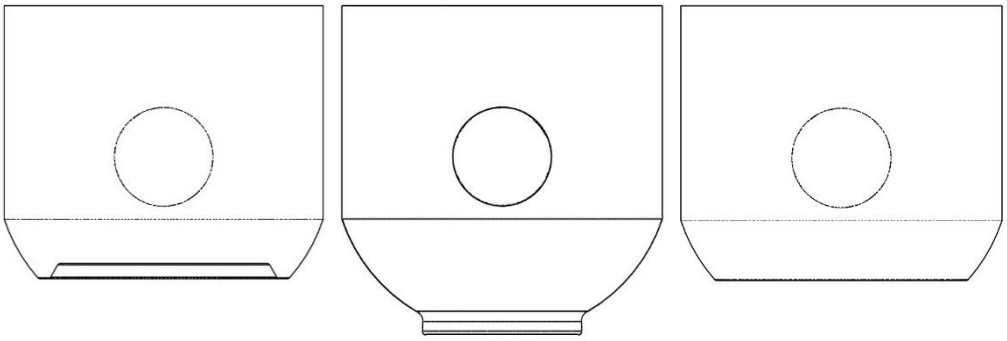

Figure 4.25. From Left to Right: Modification Discs 3, 4, and 5.

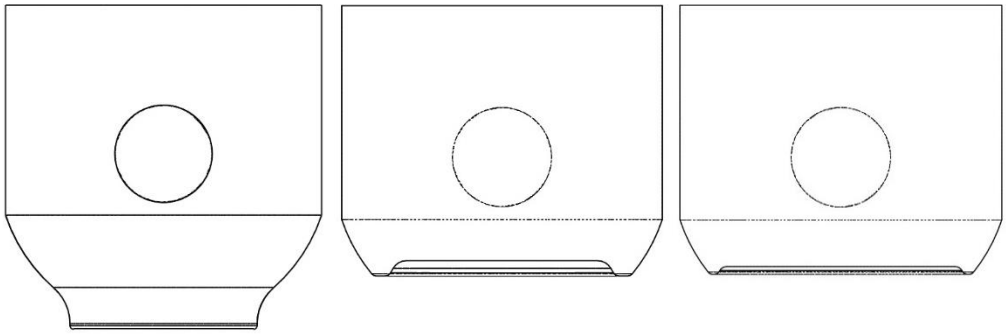

Figure 4.26. From Left to Right: Modification Discs 6, 7, and 8.

4.3.1. Initial Modification Steady State Results

4.3.1.1. Minnkota Power Cooperative disc

The disc modified by MPC was the first modification tested. Because it was unsuccessful in removing vibrations prior to investigation, the MPC disc was a useful tool for gaining insight into disc geometry modifications. The changes in the flow pattern were examined to identify why the modification was ineffective.

Numerical analysis was completed for an opening ratio of 0.018. As shown in figures 4.27 and 4.28, there is a strong core flow condition which is very similar to the original disc in the downstream region. However, the cutoff section does not allow the flow to move around on

the face of the disc; it is fixed at the terminus. There is asymmetric flow separation at the cutoff edge, which could cause pressure fluctuations and vortex shedding off the disc.

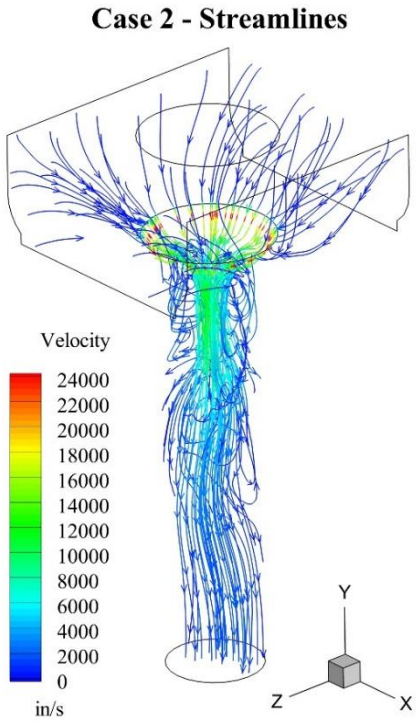

Figure 4.27. Velocity Streamlines at $OR = 0.018$, MPC Disc.

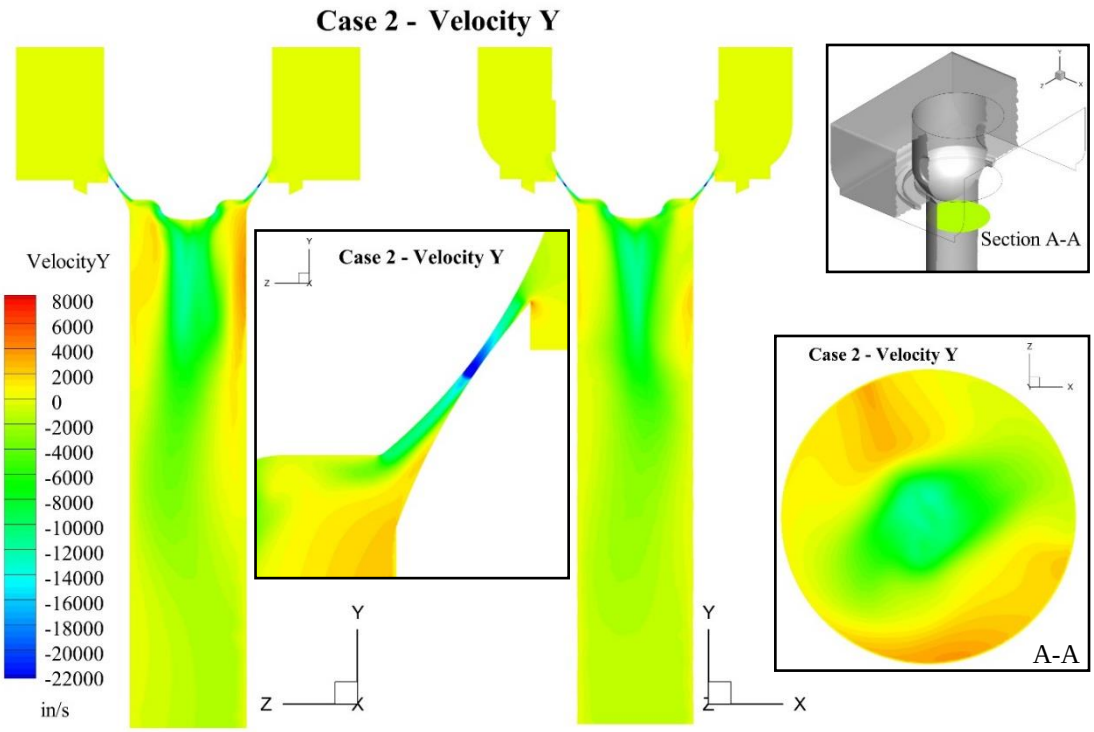

Figure 4.28. Vertical Velocity Contours at $OR = 0.018$, MPC Disc.

4.3.1.2. Modification 1 disc

4.3.1.2.1. Opening ratio = 0.007

The velocity streamlines and contours for the modification 1 disc at case 1, displayed in figures 4.29 and 4.30, reveal mostly stable annular flow with small asymmetry in the downstream wall flow. The reverse flow region is not symmetric, which indicates that an indentation placed on the underside of the disc to prevent the flow from moving laterally may improve on the flow pattern. This is a more stable condition than the original disc, with no vortex shedding.

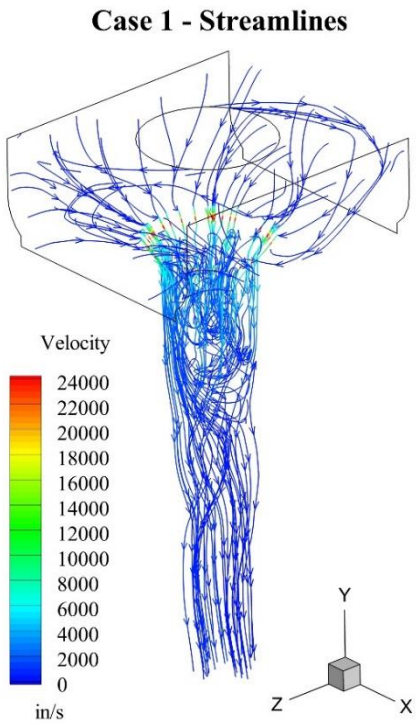

Figure 4.29. Velocity Streamlines at $OR = 0.007$, Modification 1 Disc.

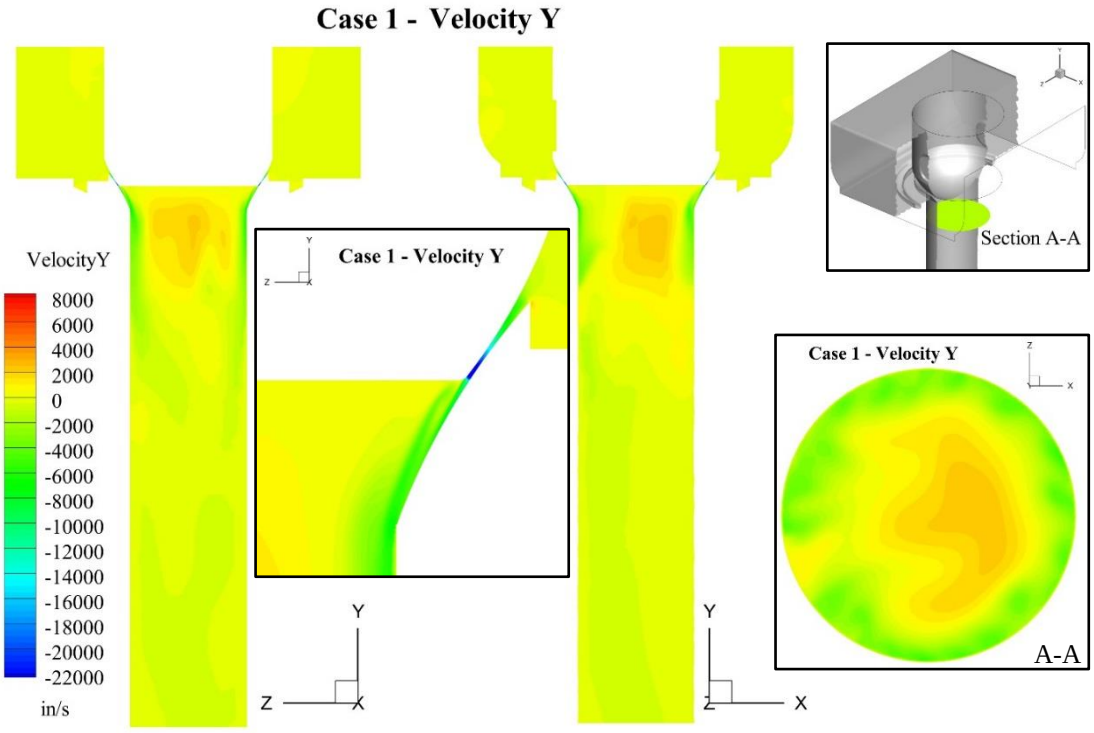

Figure 4.30. Vertical Velocity Contours at $OR = 0.007$, Modification 1 Disc.

4.3.1.2.2. Opening ratio = 0.018

With the valve opening ratio increased to 0.018, the annular flow condition becomes stable and symmetric, as shown in figures 4.31 and 4.32. This is flow pattern A, as defined by D. Zhang et al. [18], and is the desired flow pattern to obtain at all opening ratios within the vibration region.

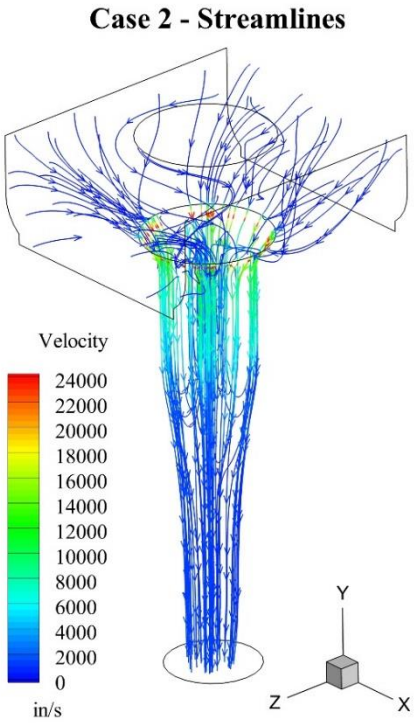

Figure 4.31. Velocity Streamlines at $OR = 0.018$, Modification 1 Disc.

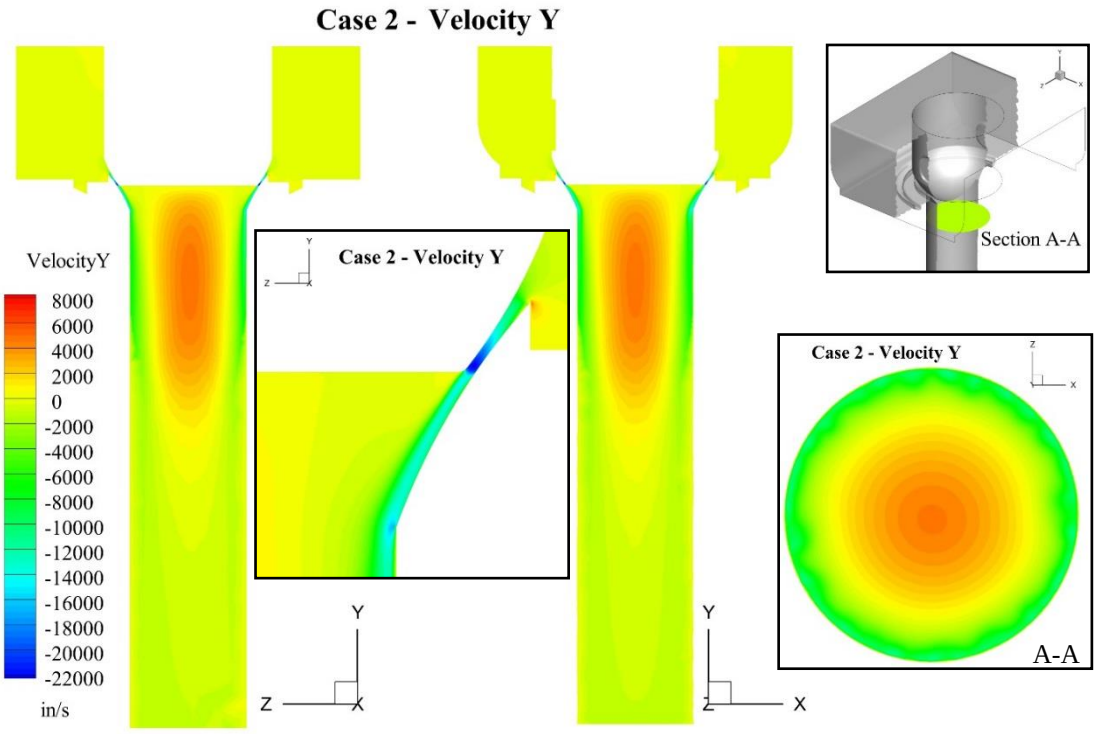

Figure 4.32. Vertical Velocity Contours at $OR = 0.018$, Modification 1 Disc.

4.3.1.3. Modification 2 disc

At an opening ratio of 0.018 the asymmetry of the flow leaving the modification 2 disc is slightly improved over the original disc and the flow tail maintains more lateral stability, as shown in figures 4.33 and 4.34. However, the downstream flow pattern is still strongly irregular; the erratic reverse flow region moves the flow tail, causing unstable flow.

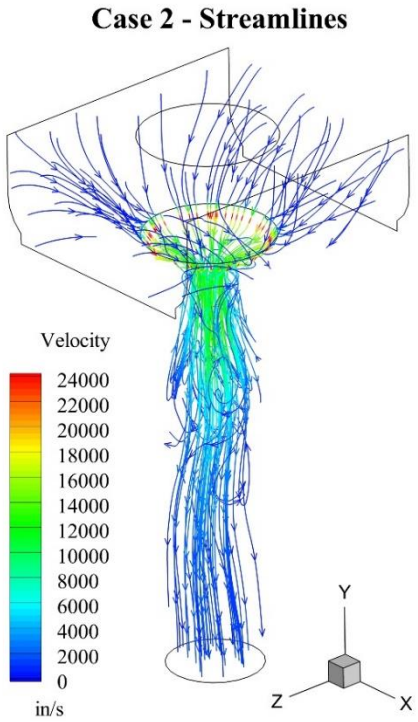

Figure 4.33. Velocity Streamlines at $OR = 0.018$, Modification 2 Disc.

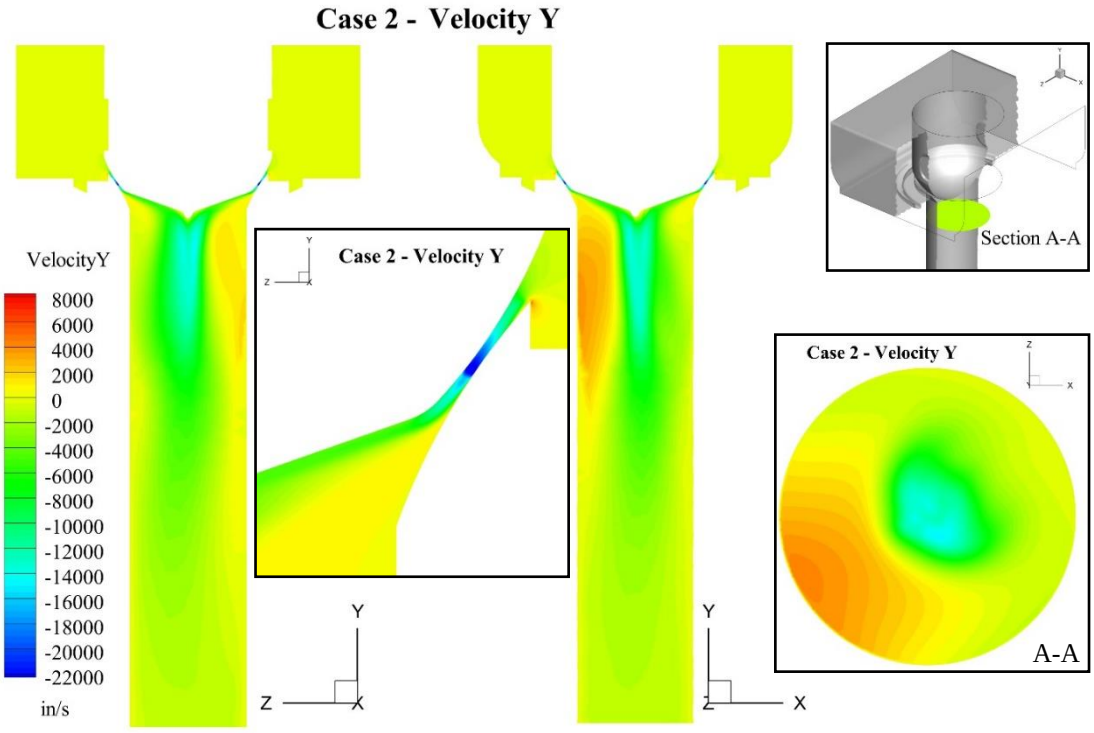

Figure 4.34. Vertical Velocity Contours at $OR = 0.018$, Modification 2 Disc.

4.3.1.4. Modification 3 disc

The velocity plots for the modification 3 disc at an opening ratio of 0.018, given below in figures 4.35 and 4.36, indicate a flow improvement over the original disc, but a less stable flow pattern than the modification 1 disc. A strong reverse core flow region exists, but it is not as symmetric as that found in the modification 1 disc results. There are also separation bubbles on seat wall directly downstream of the throat, causing irregular jet flow out of throat.

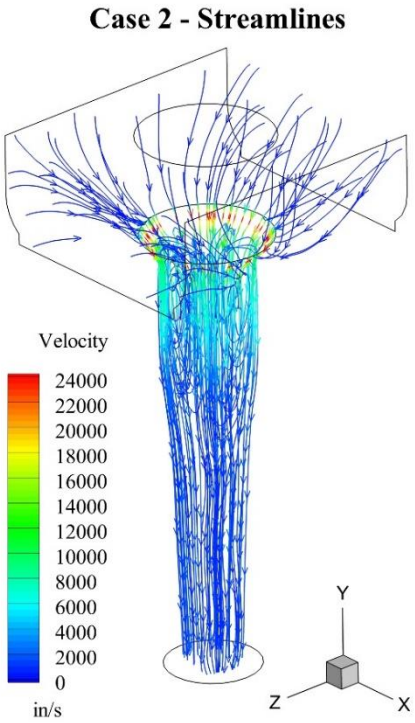

Figure 4.35. Velocity Streamlines at $OR = 0.018$, Modification 3 Disc.

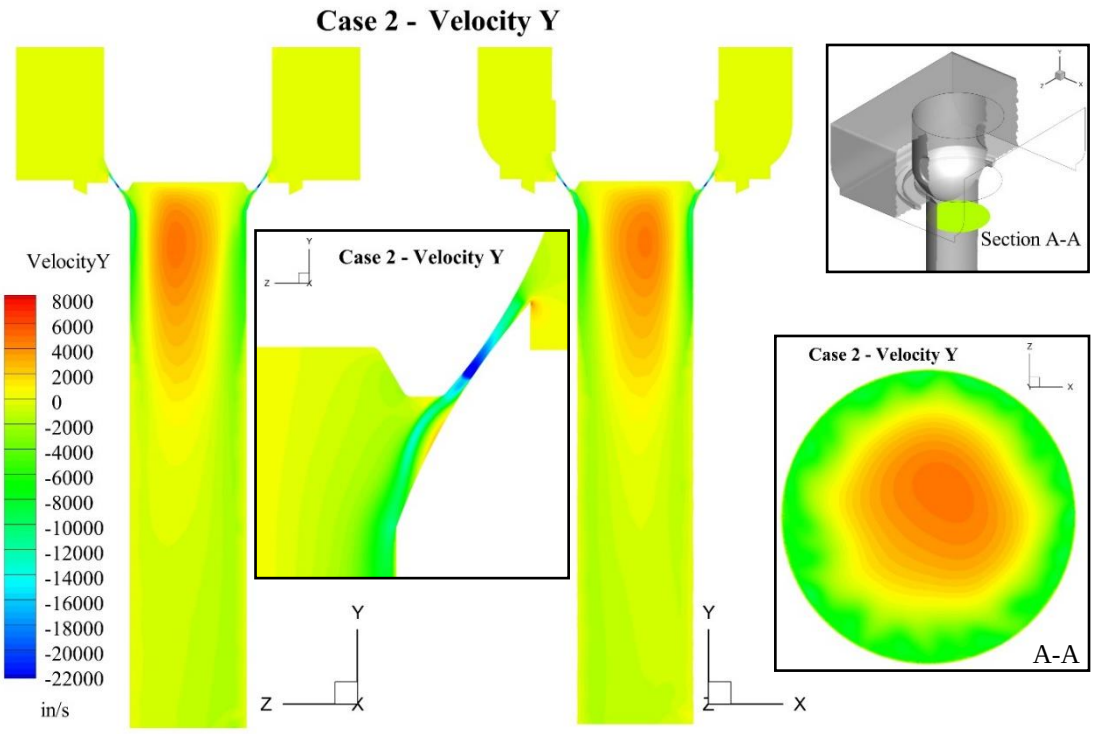

Figure 4.36. Vertical Velocity Contours at $OR = 0.018$, Modification 3 Disc.

4.3.1.5. Modification 4 disc

The flow at an opening ratio of 0.018 adheres to the modification 4 disc through the throat and then separates downstream, as shown in figures 4.37 and 4.38. It then immediately reattaches to the seat wall, causing an asymmetric region of reverse flow directly below the throat. The wall attachment is also irregular. There is a stable core flow region, however. Further investigation into this design could yield a pressure fluctuation reduction.

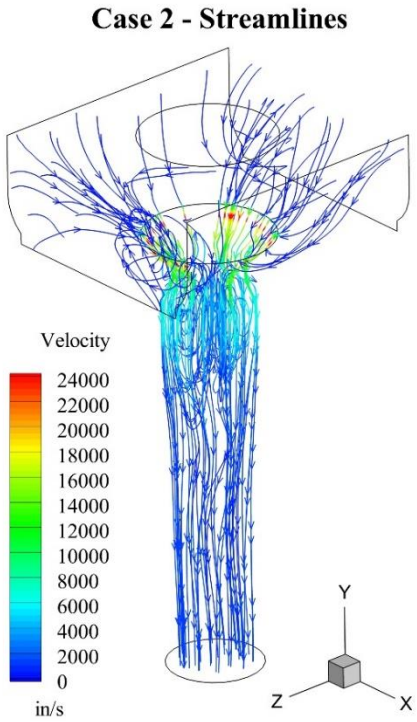

Figure 4.37. Velocity Streamlines at $OR = 0.018$, Modification 4 Disc.

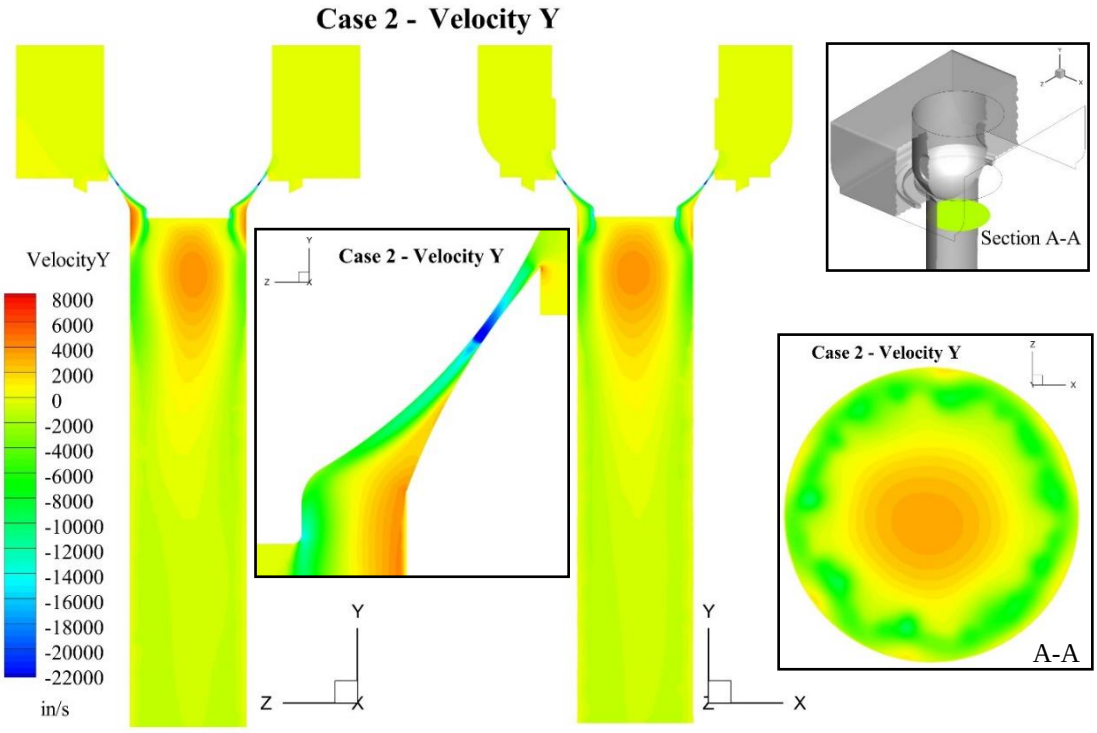

Figure 4.38. Vertical Velocity Contours at $OR = 0.018$, Modification 4 Disc.

4.3.1.6. Modification 5 disc

When the opening ratio is 0.018, the cutoff point of the modification 5 disc causes the flow to expand rapidly upon exiting the throat, as displayed in figures 4.39 and 4.40. This causes flow separation due to an adverse pressure gradient. The separation destabilizes the jets, causing an asymmetric reverse core flow region. The adverse flow region is not present in the modification 1 disc flow pattern because the cutoff occurs before the disc curvature causes expansion in the valve throat.

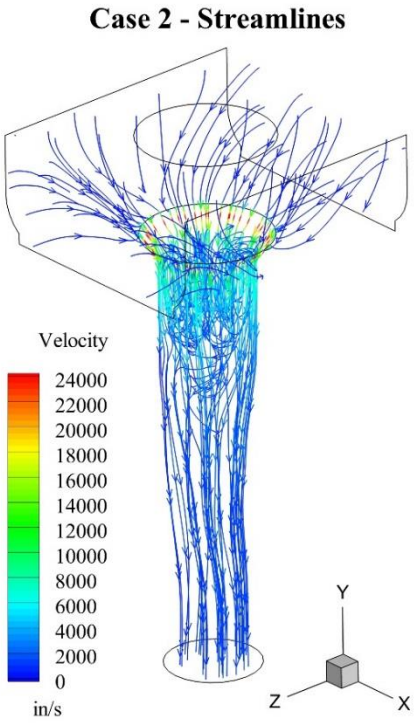

Figure 4.39. Velocity Streamlines at $OR = 0.018$, Modification 5 Disc.

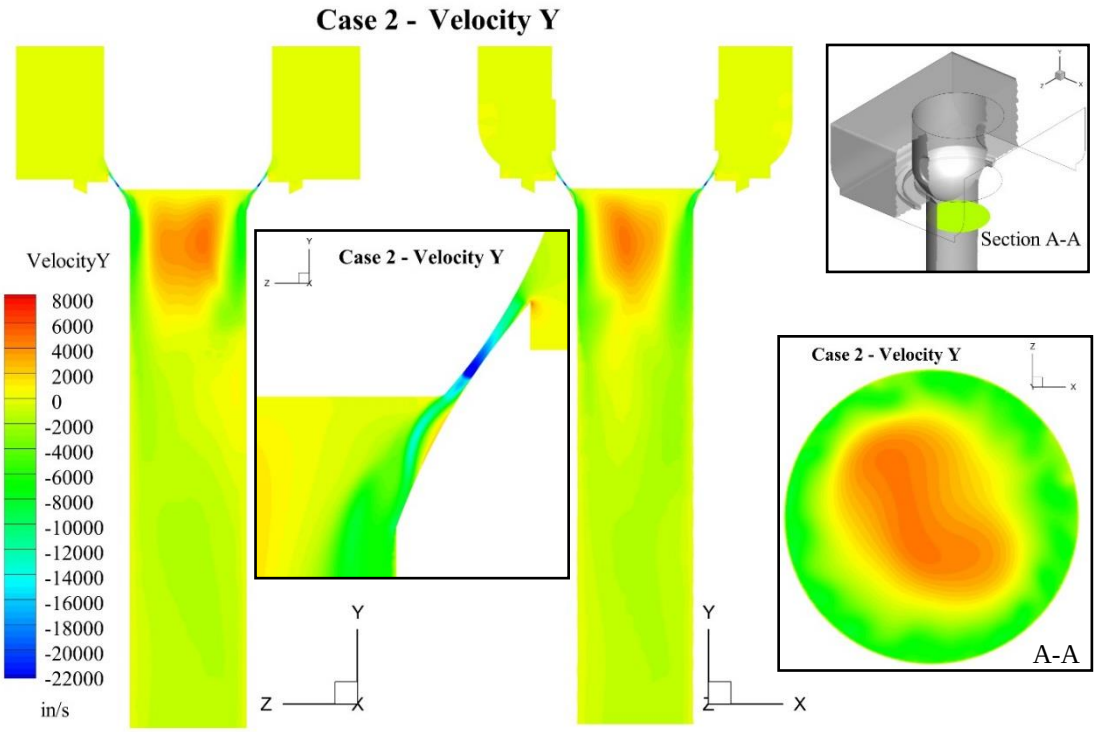

Figure 4.40. Vertical Velocity Contours at $OR = 0.018$, Modification 5 Disc.

4.3.1.7. Modification 6 disc

At an opening ratio of 0.018, the downstream flow pattern, given in figures 4.41 and 4.42, is an improvement over that for the modification 4 disc. The flow adheres to the seat wall better. However, the reverse flow regions directly downstream from the throat are more unstable; there is not a gradual stable flow expansion.

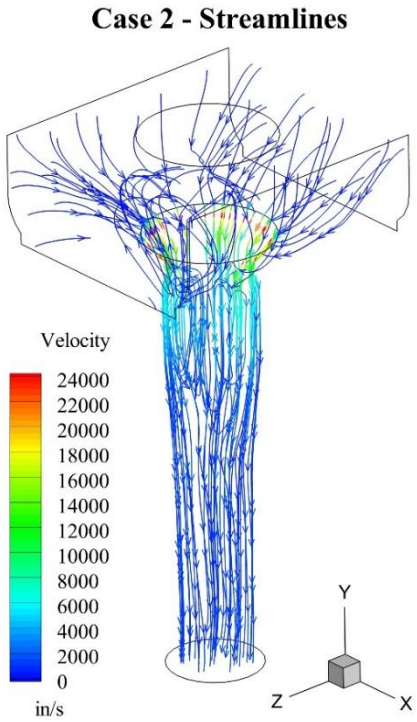

Figure 4.41. Velocity Streamlines at $OR = 0.018$, Modification 6 Disc.

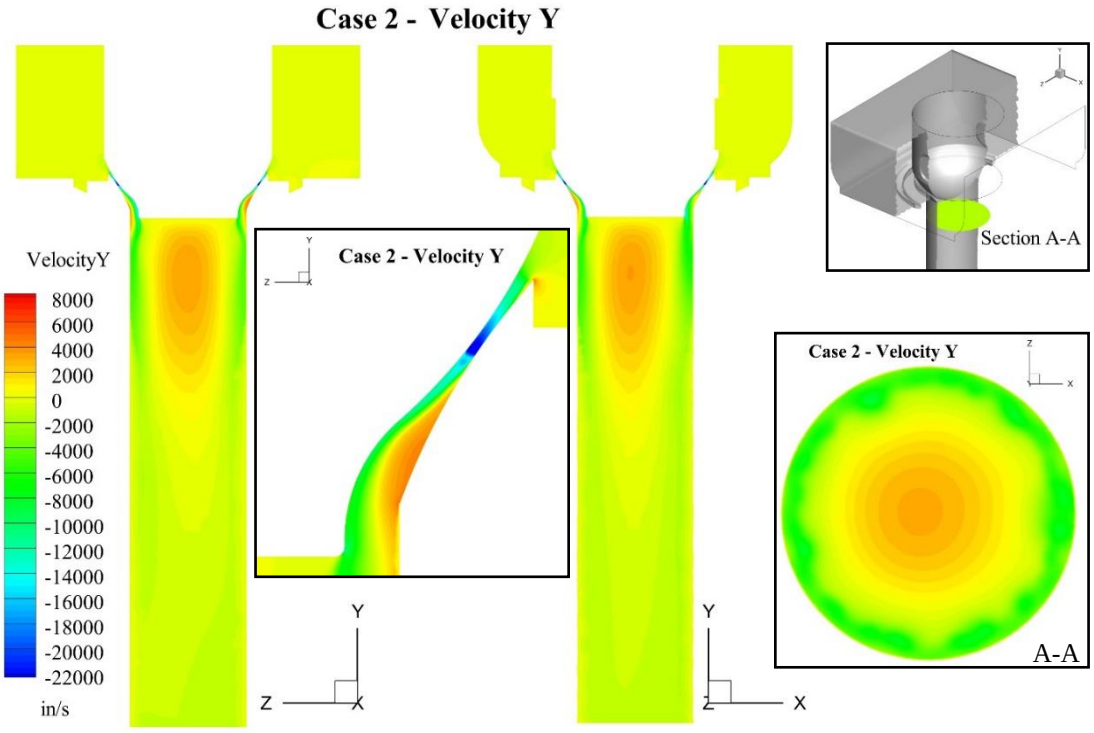

Figure 4.42. Vertical Velocity Contours at $OR = 0.018$, Modification 6 Disc.

4.3.1.8. Modification 7 disc

The flow pattern for the modification 7 disc at an opening ratio of 0.018 is very unstable. This can be seen in figures 4.43 and 4.44 and is due to the large radius cutoff corners on the disc allowing the flow to travel to the underside of the disc and form a flow tail. Based on this modification, corners on further cutoff discs are kept at a sharp radius.

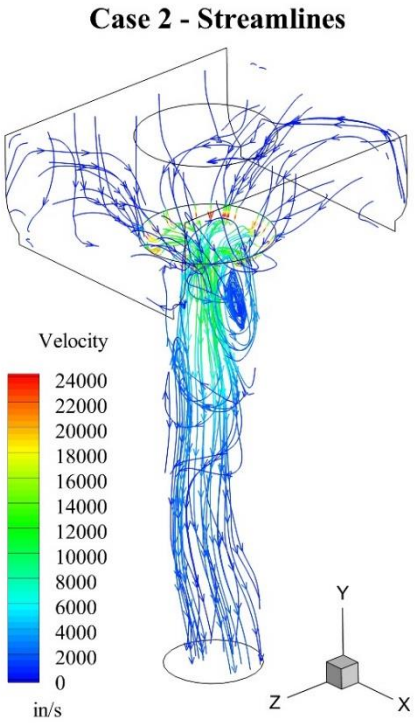

Figure 4.43. Velocity Streamlines at $OR = 0.018$, Modification 7 Disc.

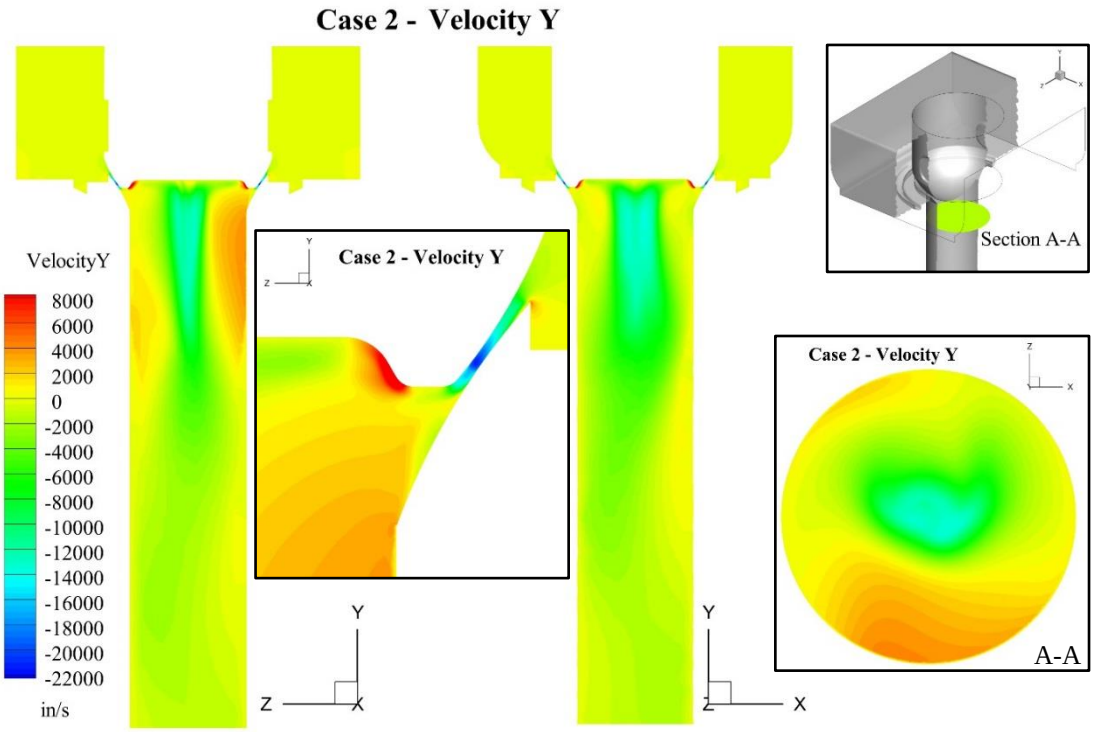

Figure 4.44. Vertical Velocity Contours at $OR = 0.018$, Modification 7 Disc.

4.3.1.9. Modification 8 disc

The modification 8 disc velocity plots, shown at an opening ratio of 0.018 in figures 4.45 and 4.46, are similar to those for the modification 1 disc. The cutoff occurs high enough on the disc to remove the effects of expansion due to the curvature of the disc. The downstream flow pattern is slightly asymmetric, as are the flow jets coming out of the throat. This is suspected to be due to the indentation geometry. The reverse flow region may be interacting with the flow jets. Further indented disc geometries are studied as revision discs in the following sections after the unsuccessful implementation of the modification 1 disc.

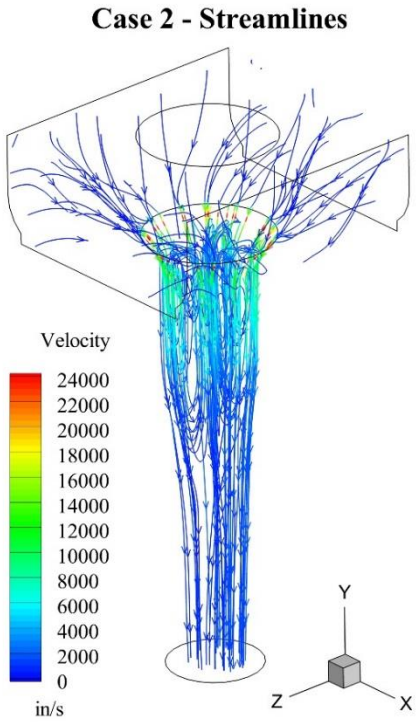

Figure 4.45. Velocity Streamlines at $OR = 0.018$, Modification 8 Disc.

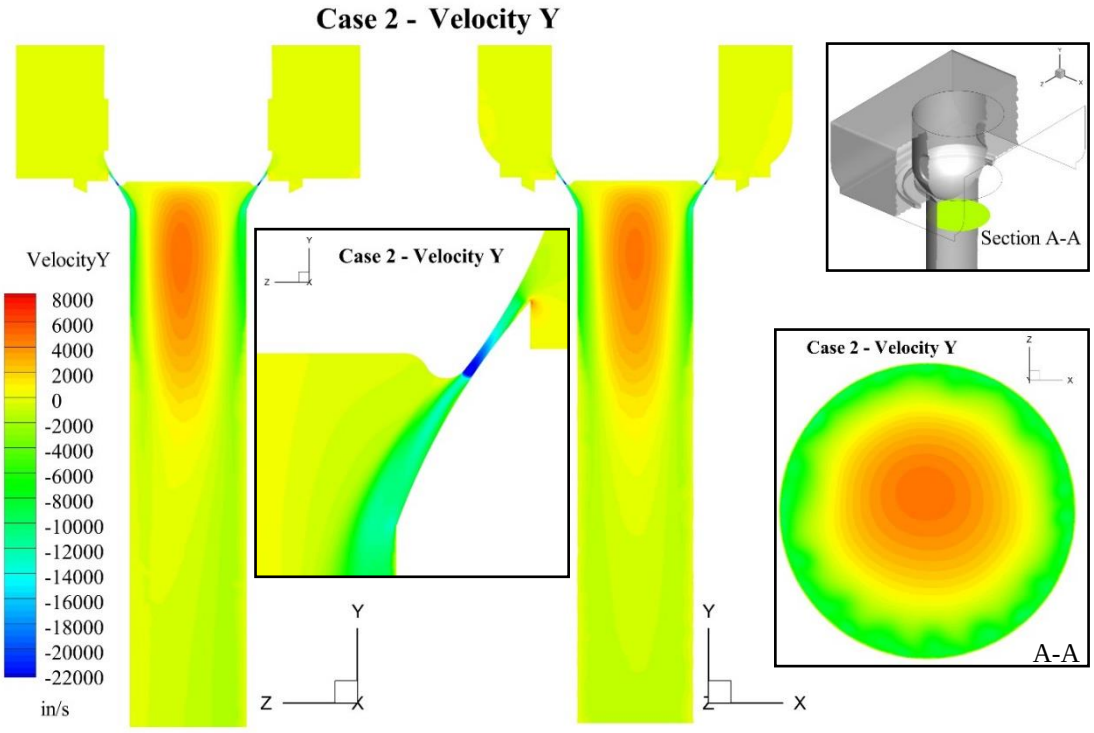

Figure 4.46. Vertical Velocity Contours at $OR = 0.018$, Modification 8 Disc.

4.4. Further Design Modifications

As the modification discs were being studied, the Minnkota Power Cooperative turbine control valves were undergoing periodic maintenance. Although a final design that would stabilize the flow pattern had not been completed and verified yet, the cutoff design of modification 1 was recommended based on preliminary results. This design was then modified slightly for implementation by lowering the cutoff point, allowing stellite to be placed on the sealing surface of the valve disc. The discs were then installed in valves 7 and 8.

Testing was performed approximately 2 months after the discs had been installed, and no vibrations were present. However, the vibrations reappeared one month later, although the magnitude of the vibrations seemed to be less than those that occurred with the original disc. Another testing session was completed and the testing data from this vibration test was used to refine the vibration initiation opening ratio. Operation points 5 through 8 were the result of this testing.

Due to the recurrence of vibrations in control valves 7 and 8 after the implementation of the revision 1 disc, further disc and seat modifications were investigated. These are detailed below.

4.4.1. Disc Revisions

The disc revisions are described in table 4.3 and shown in figures 4.47 through 4.49. The revision discs utilize even numbers for indented discs and odd numbers for extended discs.

Table 4.3. Revised Disc Designs.

Revision	Description
1	Same design as modification 1; adjusted to match disc put into MPC control valves 7 & 8. Cutoff moved lower on disc to allow for stellite facing of sealing surface.
1-1	Extended cutoff disc modeled after onion design. Designed to keep flow attached to seat, through the throat region and prevent the reverse flow region from disrupting the throat jet flow.
1-2	Indented cutoff disc with sharp indentation edge and very wide indentation.
1-3	Extended cutoff disc modeled after onion design with a gradual diverging nozzle at the valve throat. Designed to keep flow attached to disc through throat then force stable detachment.
1-4	Indented cutoff disc similar to revision 1-2, with deeper indentation and rounded to cutoff face.
1-6	Indented cutoff disc with medium width indentation. Recessed oval indentation perpendicular to cutoff face.
1-8	Indented cutoff disc with wider indentation than revision 1-6 but same depth. Recessed oval indentation perpendicular to cutoff face.
1-10	Indented cutoff disc with same width indentation as revision 1-6. Non-recessed oval indentation beginning at cutoff face.
1-12	Indented cutoff disc with same depth as revision 1-2, but a much smaller width. Intended to immobilize flow at lower opening ratios by decreasing indentation size.
1-14	Indented cutoff disc with same width as revision 1-12, but much deeper. Used to test the effectiveness of the revision 1-6 and 1-12 disc indentation depth.
1-16	Indented cutoff disc with same indentation design as revision 1-12. Flare added at bottom of disc sealing surface to reduce valve throat exit expansion at low opening ratios.
2	Indented cutoff disc with medium width flat indentation. Designed to seal at cutoff radius to ensure flow attachment to the seat.

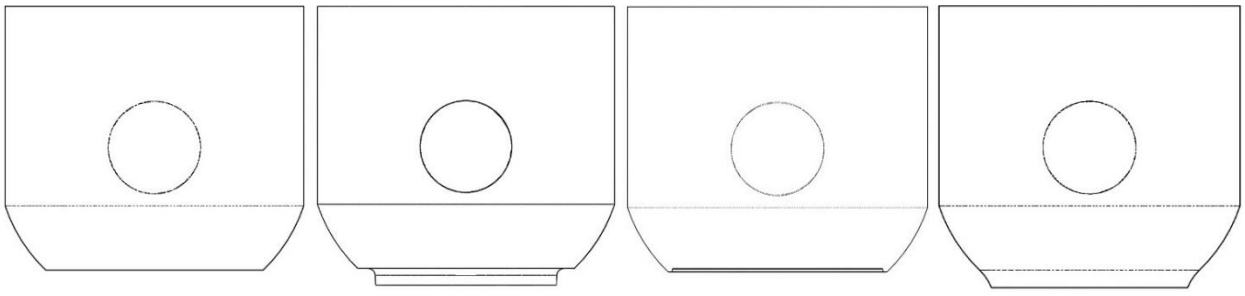

Figure 4.47. From Left to Right: Revision Discs 1, 1-1, 1-2, and 1-3.

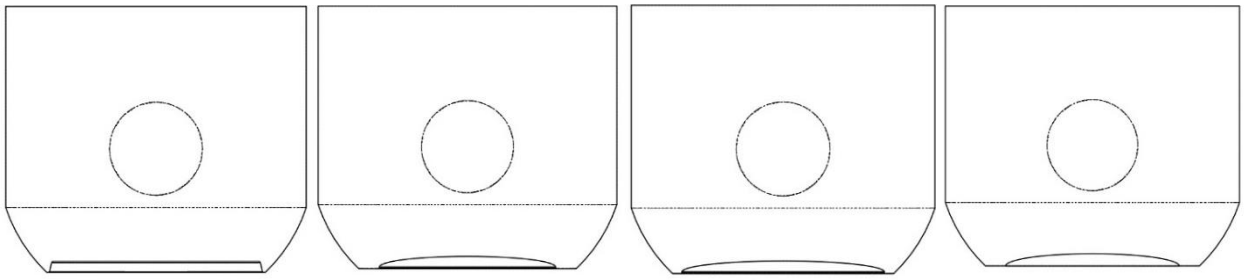

Figure 4.48. From Left to Right: Revision Discs 1-4, 1-6, 1-8, and 1-10.

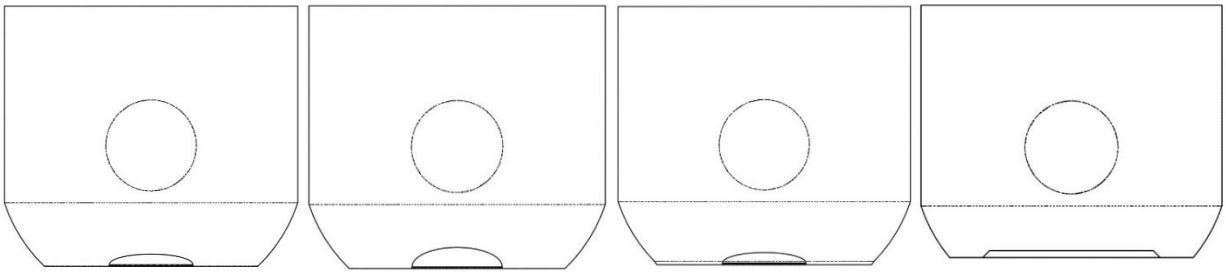

Figure 4.49. From Left to Right: Revision Discs 1-12, 1-14, 1-16, and 2.

4.4.1. Seat Revisions

Four different seat geometries were tested to determine if increasing the radii of the abrupt edge between the valve throat and the downstream region of the valve nozzle would improve flow the adhesion to the nozzle wall. The work of C. Domnick et al. [14] and others showed that valve flow leaving the throat stays attached to the surface with less curvature. Therefore, the abrupt angle between the sealing and downstream faces of the nozzle was rounded with varying radii. The seat sealing face curvature was not altered to maintain the current sealing condition. The revised seats are described further in table 4.4 and shown in figure 4.50.

Table 4.4. Revised Seat Designs.

Revision	Description
1	Incorporated a radius of 0.125 inches between the sealing face and the downstream face to increase flow adherence to seat.
2	Same as revision 1, with radius increased to 0.75 inches.
3	Same as revision 1, with radius increased to 0.5 inches.
4	Same as revision 1, with radius increased to 1 inch and top edge rounded to 0.0625 inches to remove flow separation from seat upstream of valve throat.

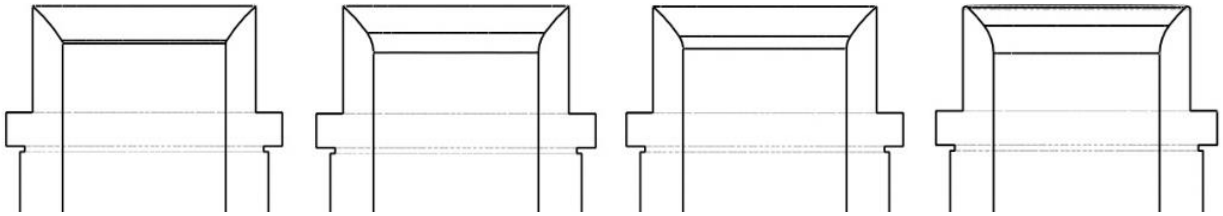

Figure 4.50. From Left to Right: Seat Revisions 1 through 4.

4.5. Additional Steady State Numerical Results

4.5.1. Revision 1 Disc

The revision 1 disc is the same disc that is currently installed in valves 7 and 8 of the MPC turbine. Valve vibrations are known to occur with this valve installed, so it is used as a baseline disc in addition to the original hemispherical disc.

4.5.1.1. Opening ratio = 0.007

Comparing the streamlines for the revision 1 disc, displayed in figure 4.51, to those of the modification 1 disc, there is no early annular flow development. Instead, there are asymmetric vortices. The velocity contours, given in figure 4.52, show a flow pattern in between that of modification disc 1 and 5. An unstable separation point is visible beneath the jets coming out of the throat as a result of flow expansion prior to the disc cutoff point. The downstream flow pattern is also irregular, but does not show any strong flow pattern because of the irregular separation region interfering with the throat flow jets.

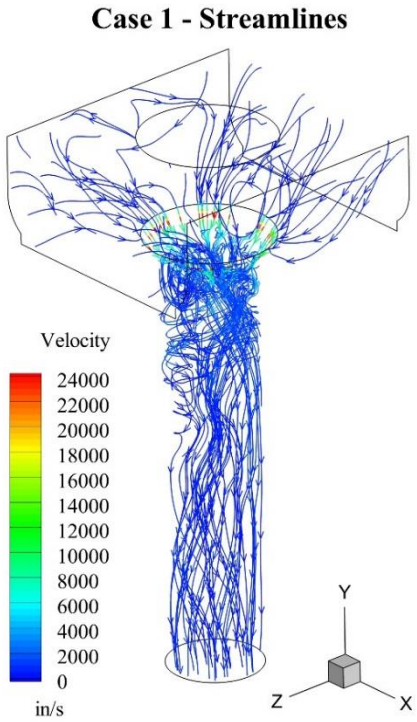

Figure 4.51. Velocity Streamlines at $OR = 0.007$, Revision 1 Disc.

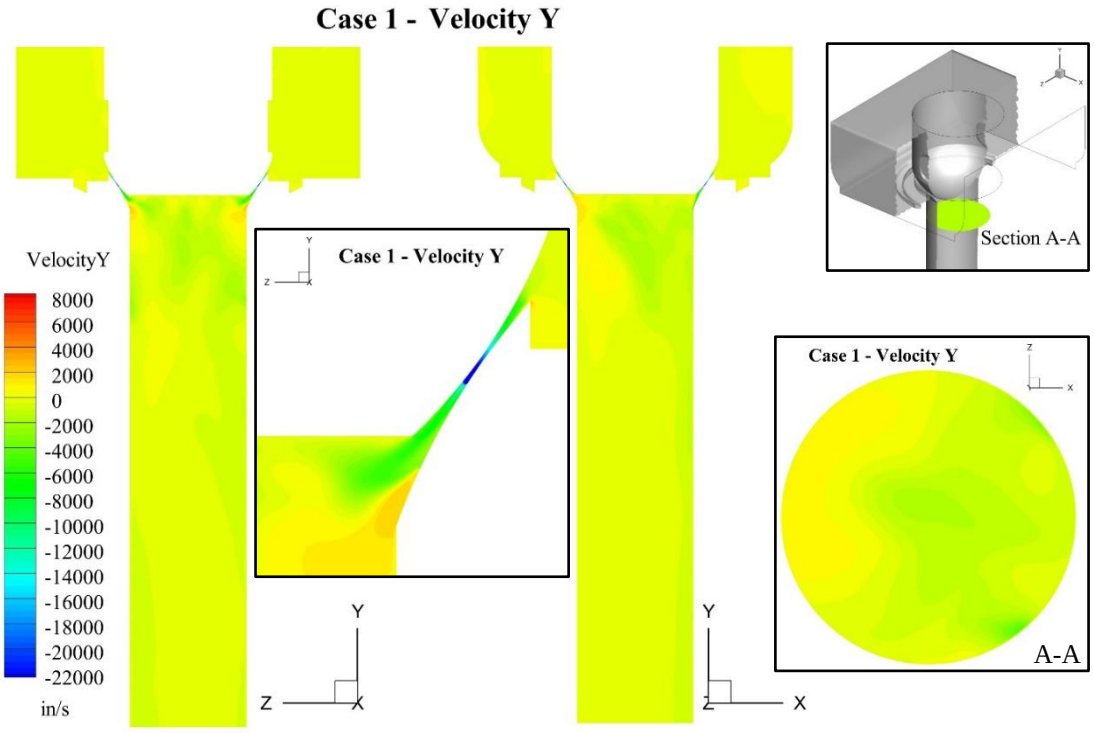

Figure 4.52. Vertical Velocity Contours at $OR = 0.007$, Revision 1 Disc.

Figures 4.53 and 4.54 show the change in the velocity pattern from correcting the seat geometry. Changing the seat sealing angle decreases the downward throat expansion, creating an irregular annular flow pattern with an intermittent separation bubble on the seat at the end of the throat in place of angled flow jets above an unstable separation point. The throat expansion caused by the convex disc curvature at the cutoff point continues to draw the flow jets to the center of the nozzle. After traveling upward, the flow from the jet on one side moves across the disc. As it leaves the disc surface, it disrupts the flow jet coming out of the throat on the opposing side. This causes a low pressure region on the disc side of the throat exit on the opposing side, reversing the flow pattern. The result is periodic vortex shedding off of the disc.

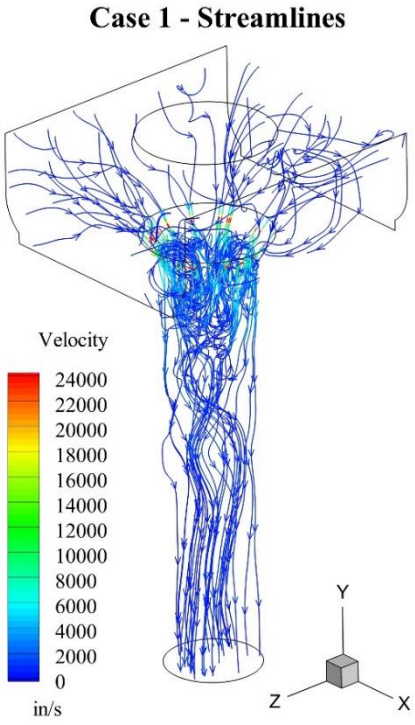

Figure 4.53. Velocity Streamlines at $OR = 0.007$, Revision 1 Disc, Corrected Seat Shape.

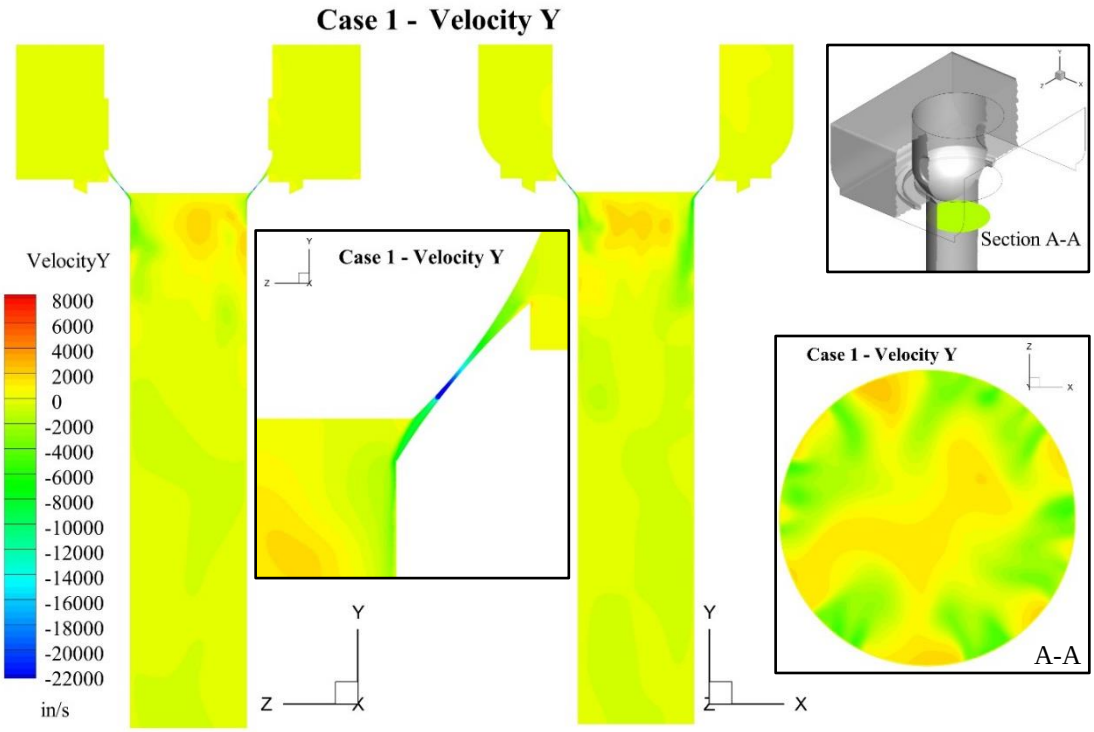

Figure 4.54. Vertical Velocity Contours at $OR = 0.007$, Revision 1 Disc, Corrected Seat Shape.

4.5.1.2. Opening ratio = 0.012

At case 8, the flow pattern is developing into a stable annular flow, as shown in figures 4.55 and 4.56. It is in an unstable transition region in between cases 1 and 2. Both the reverse core flow and annular wall flow are asymmetric, and the unsteady separation bubble at the throat exit is still present. However, the flow directly downstream of the disc appears to be more stable than the original disc, indicating a moderate improvement in flow stability.

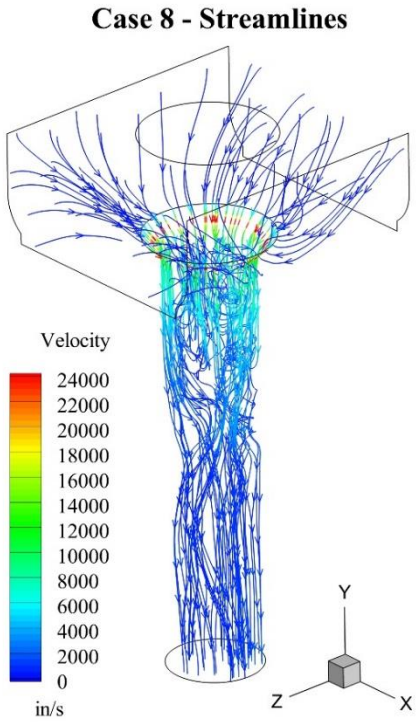

Figure 4.55. Velocity Streamlines at $OR = 0.012$, Revision 1 Disc.

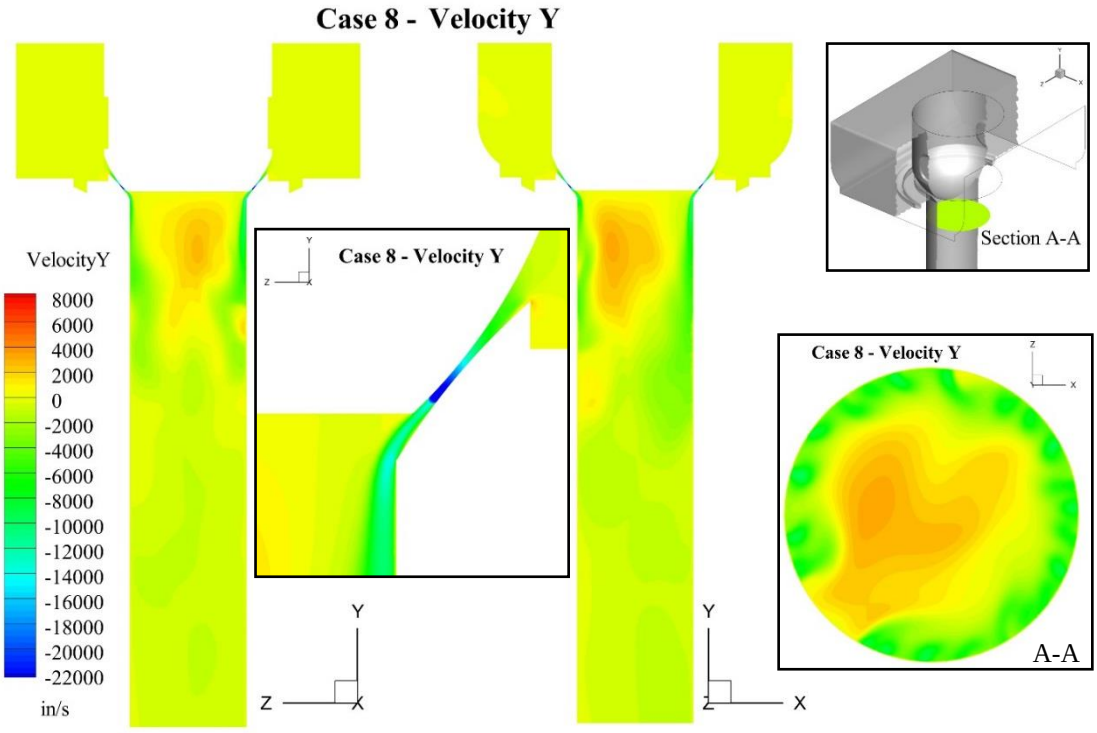

Figure 4.56. Vertical Velocity Contours at $OR = 0.012$, Revision 1 Disc.

4.5.1.3. Opening ratio = 0.014

By an opening ratio of 0.014, the flow reaches a stable annular pattern, displayed in figures 4.57 and 4.58. The sharp corner where the seat sealing and downstream surfaces meet causes a high velocity flow region to form due to the increased pressure gradient. Placing a radius at this corner would smooth out the seat attached flow profile; this is examined in a later section.

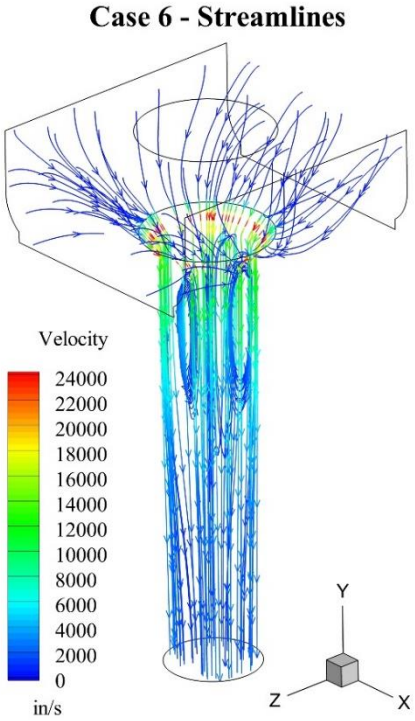

Figure 4.57. Velocity Streamlines at $OR = 0.014$, Revision 1 Disc.

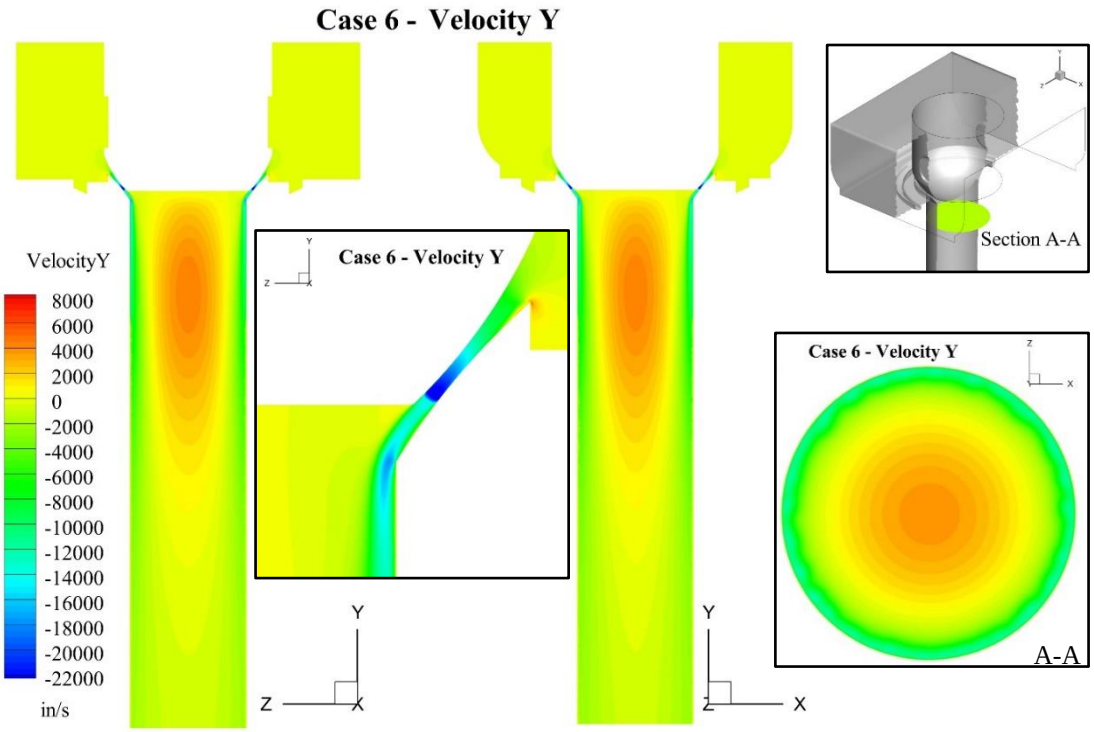

Figure 4.58. Vertical Velocity Contours at $OR = 0.014$, Revision 1 Disc.

4.5.1.4. Opening ratio = 0.018

The velocity plots for the revision 1 disc at an opening ratio of 0.018 initially indicated very unstable flow due to jet expansion causing separation bubbles directly beneath the throat. This is displayed in figures 4.59 and 4.60. After the seat geometry was corrected, the stable annular flow found in an opening ratio of 0.014 for the revision 1 disc was found to continue.

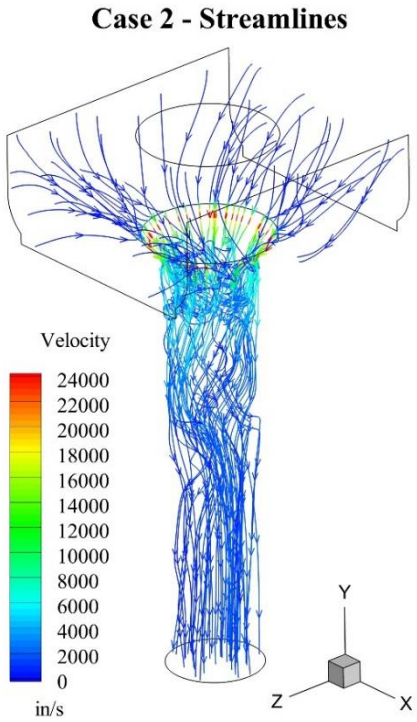

Figure 4.59. Velocity Streamlines at $OR = 0.018$, Revision 1 Disc.

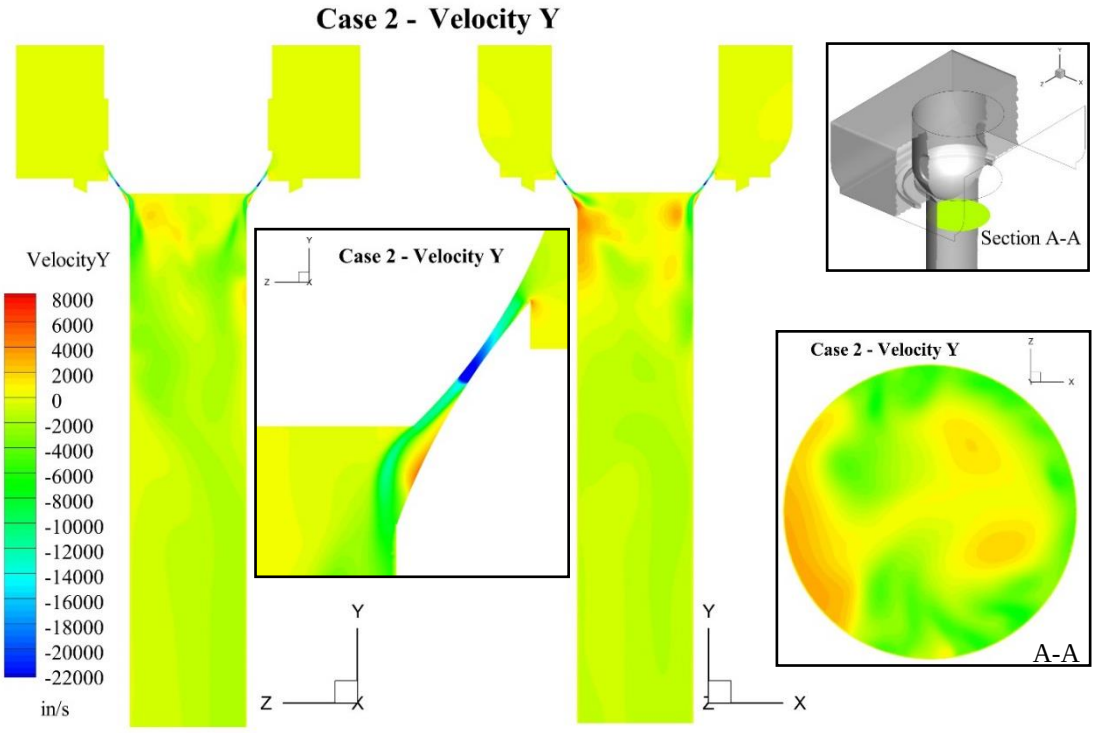

Figure 4.60. Vertical Velocity Contours at $OR = 0.018$, Revision 1 Disc.

Figures 4.61 and 4.62 show a similar flow pattern to the 0.014 opening ratio. A small separation bubble at the throat exit still exists, but the opening ratio is large enough to prevent it from adversely affecting the flow pattern. There a decrease in flow velocity around the abrupt downstream seat edge. The annular flow is more segmented than at an opening ratio of 0.014, with low velocity spikes moving from the reverse flow region to the seat wall.

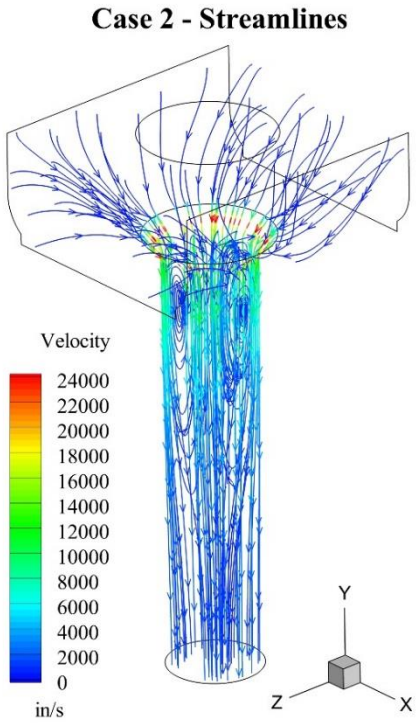

Figure 4.61. Velocity Streamlines at $OR = 0.018$, Revision 1 Disc, Corrected Seat Geometry.

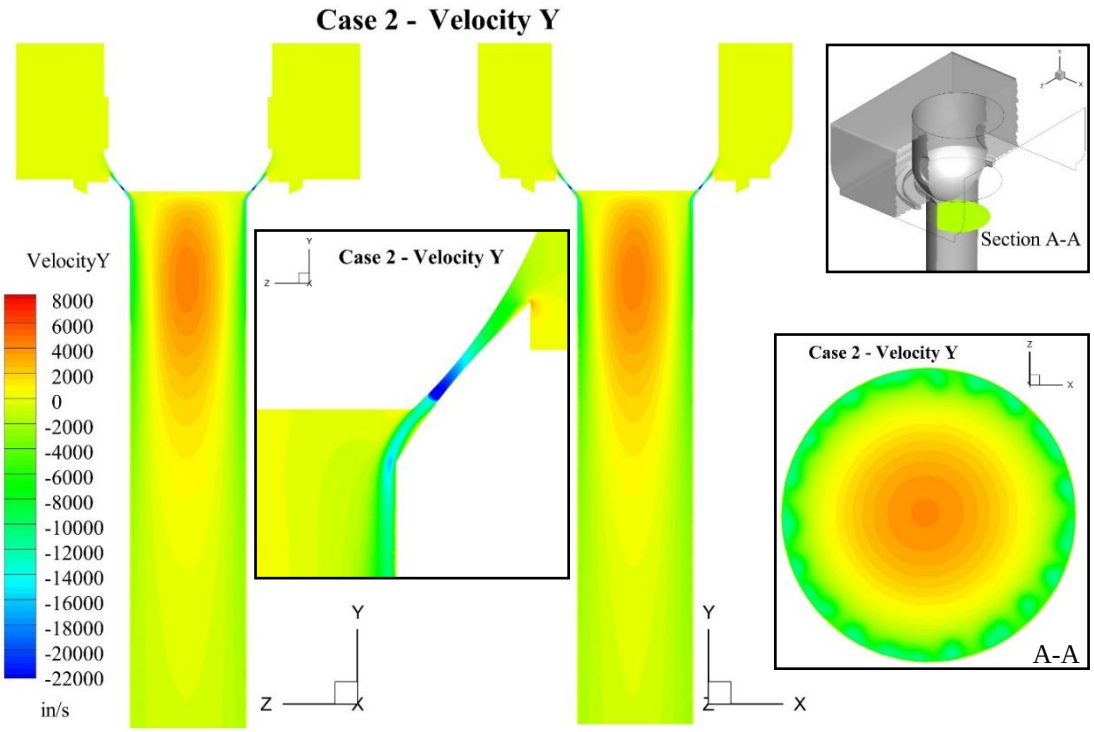

Figure 4.62. Vertical Velocity Contours at $OR = 0.018$, Revision 1 Disc, Corrected Seat Shape.

4.5.1.5. Opening ratio = 0.024

The flow pattern for case 7, given in figures 4.63 and 4.64, is comparable to an opening ratio of 0.018, with stable annular flow present. There is still a separation bubble at the throat exit, but it does not disturb the flow pattern at larger opening ratios. There is a larger high velocity section across the abrupt seat edge.

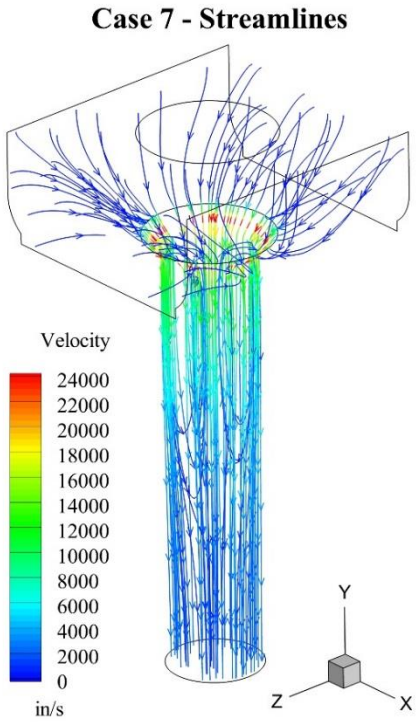

Figure 4.63. Velocity Streamlines at $OR = 0.024$, Revision 1 Disc.

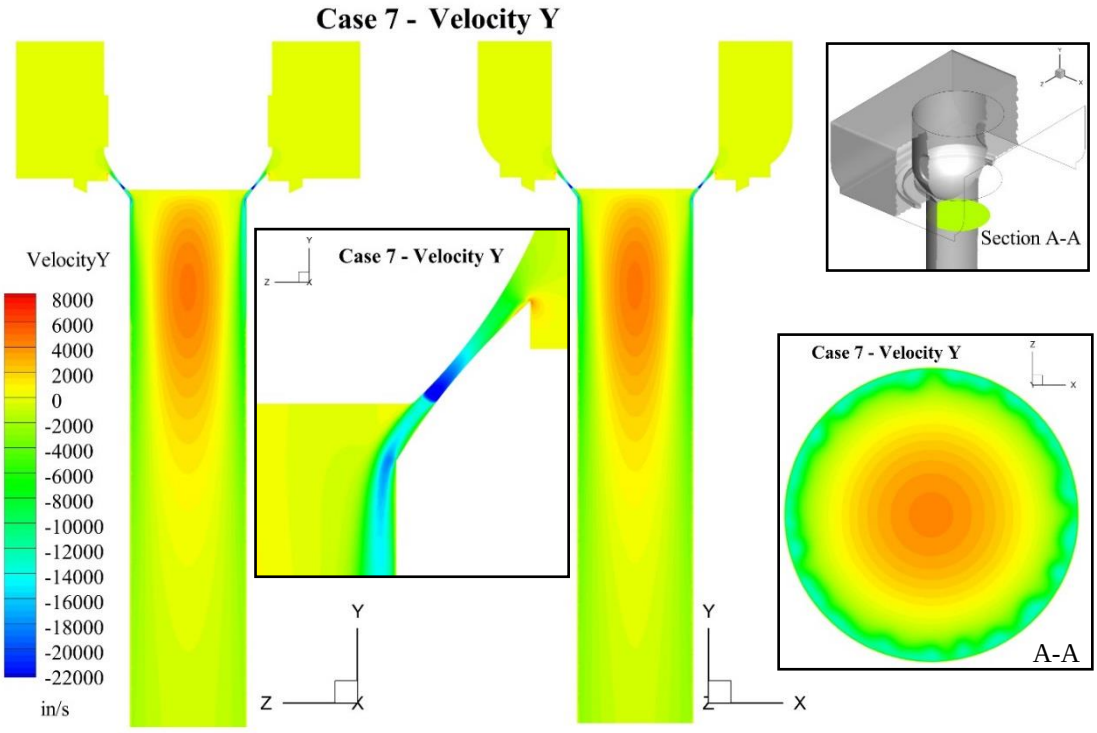

Figure 4.64. Vertical Velocity Contours at $OR = 0.024$, Revision 1 Disc.

4.5.1.6. Opening ratio = 0.028

The flow pattern established for the revision 1 disc at 0.024 continues up to an opening ratio of 0.035 and 0.028, both before (figures 4.65 and 4.66) and after (figures 4.67 and 4.68) the change in the opening ratio due to the stem/disc lift correction. There is strong, stable annular flow with increased velocity around the abrupt seat edge.

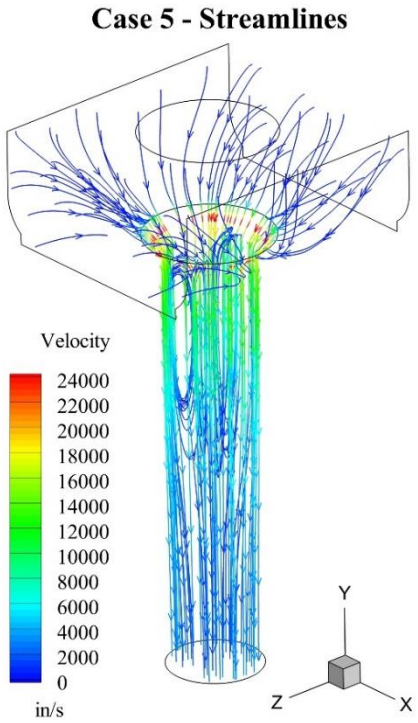

Figure 4.65. Velocity Streamlines at $OR = 0.035$, Revision 1 Disc.

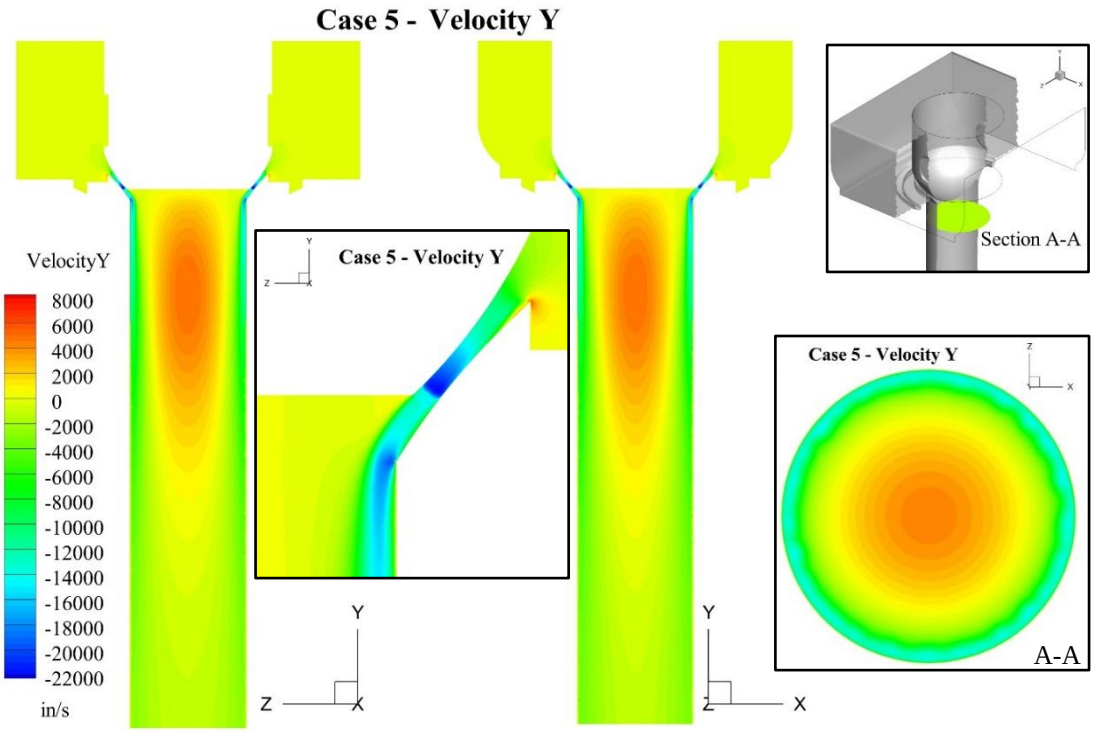

Figure 4.66. Vertical Velocity Contours at $OR = 0.035$, Revision 1 Disc.

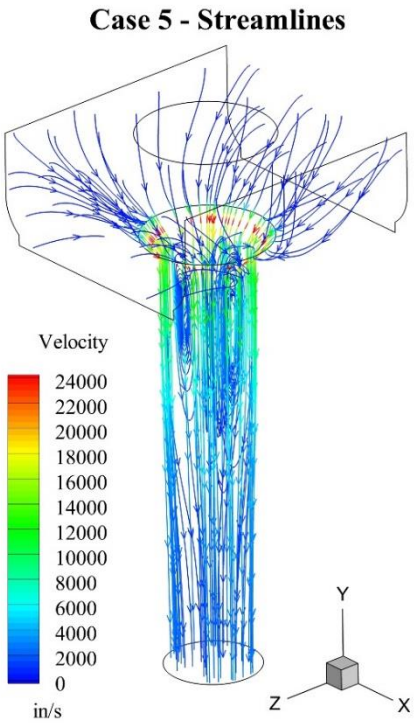

Figure 4.67. Velocity Streamlines at $OR = 0.028$, Revision 1 Disc.

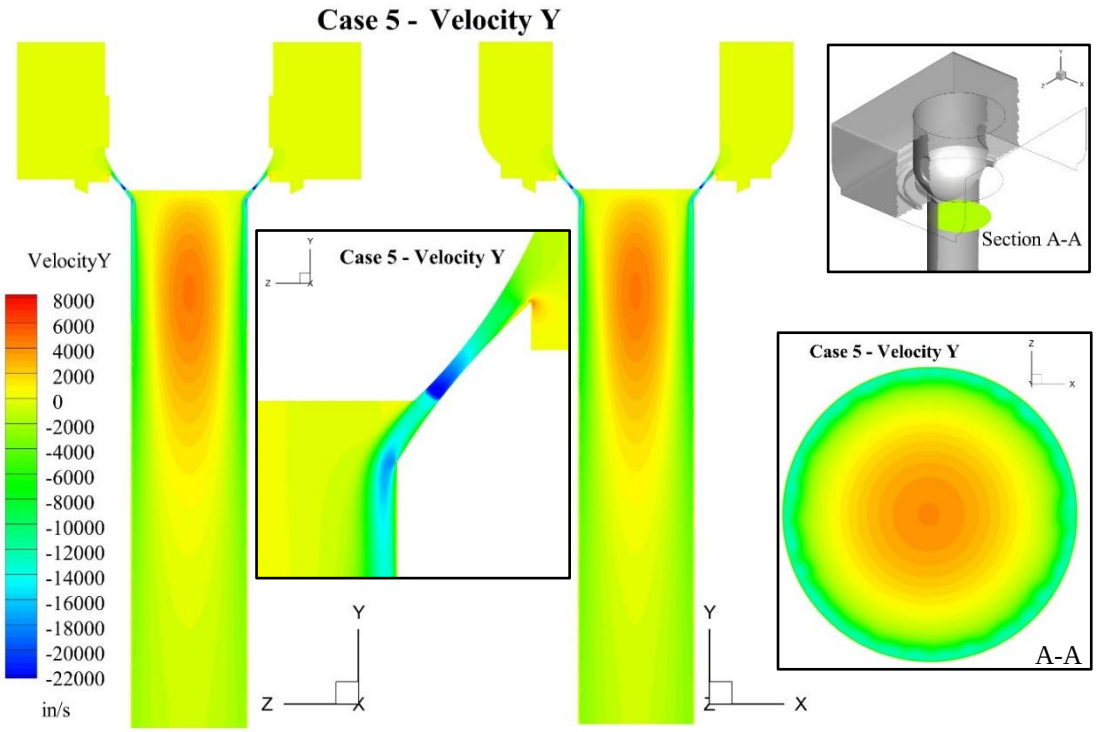

Figure 4.68. Vertical Velocity Contours at $OR = 0.028$, Revision 1 Disc, Corrected Disc Lift.

4.5.2. Further Disc Design Revisions

4.5.2.1. Revision 1-1 disc

Figures 4.69 and 4.70 show that the flow jets remain attached to the seat for the revision 1-1 disc at an opening ratio of 0.007. However, fluctuating stagnant flow regions directly downstream of the disc cause throat jet flow irregularity. In addition, the extended portion is so wide that it disrupts the jet flow downstream. This design is not an improvement over revision 1.

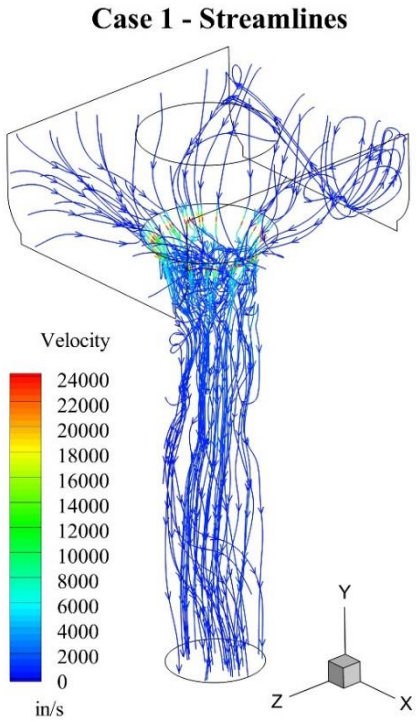

Figure 4.69. Velocity Streamlines at $OR = 0.007$, Revision 1-1 Disc.

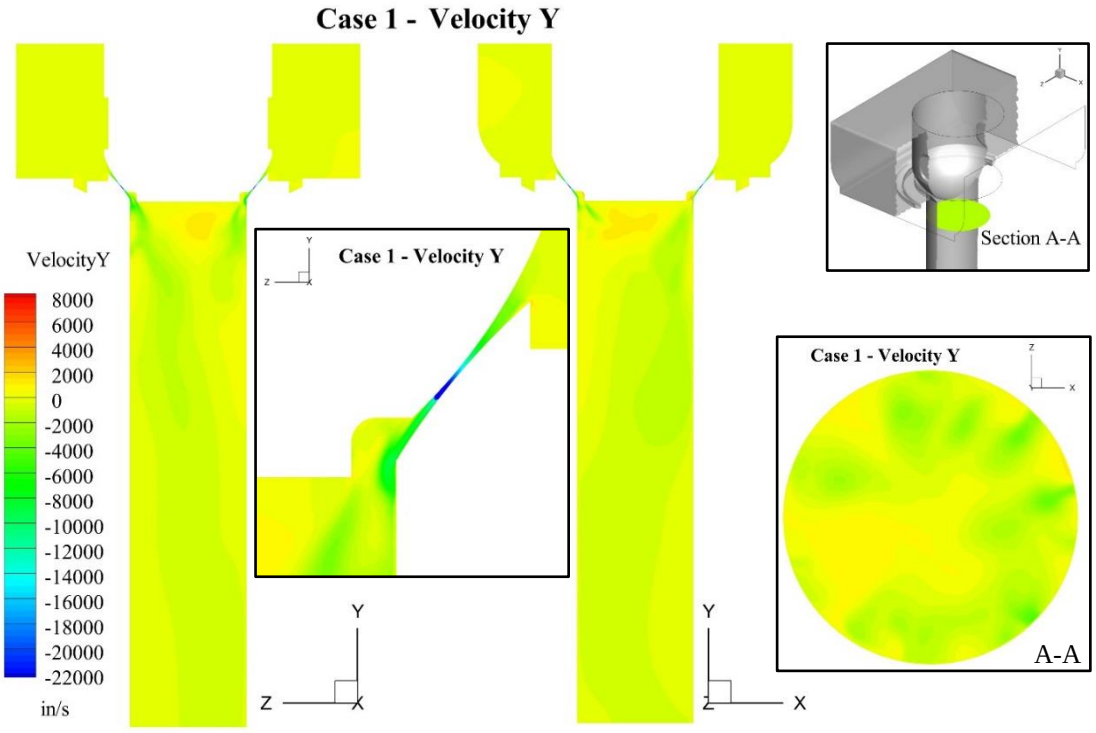

Figure 4.70. Vertical Velocity Contours at $OR = 0.007$, Revision 1-1 Disc.

4.5.2.2. Revision 1-2 disc

At an opening ratio of 0.007, the flow pattern for the revision 1-2 disc is the same as for the revision 1 disc; the indentation does not make a difference. This is shown in figures 4.71 and 4.72. The indentation appears to be too wide and shallow to effectively immobilize the reverse flow region. The separation bubble at the throat exit still exists.

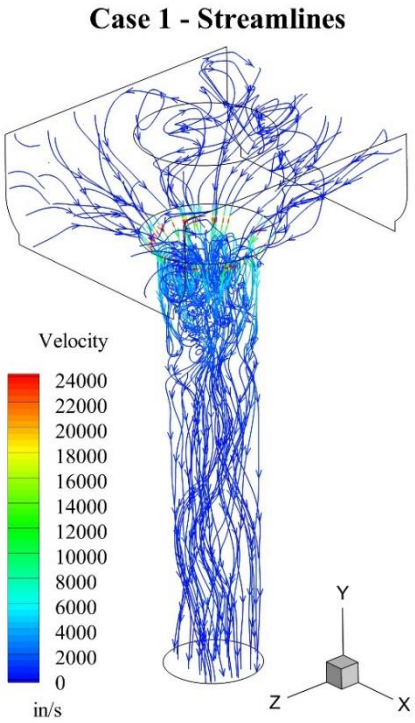

Figure 4.71. Velocity Streamlines at $OR = 0.007$, Revision 1-2 Disc.

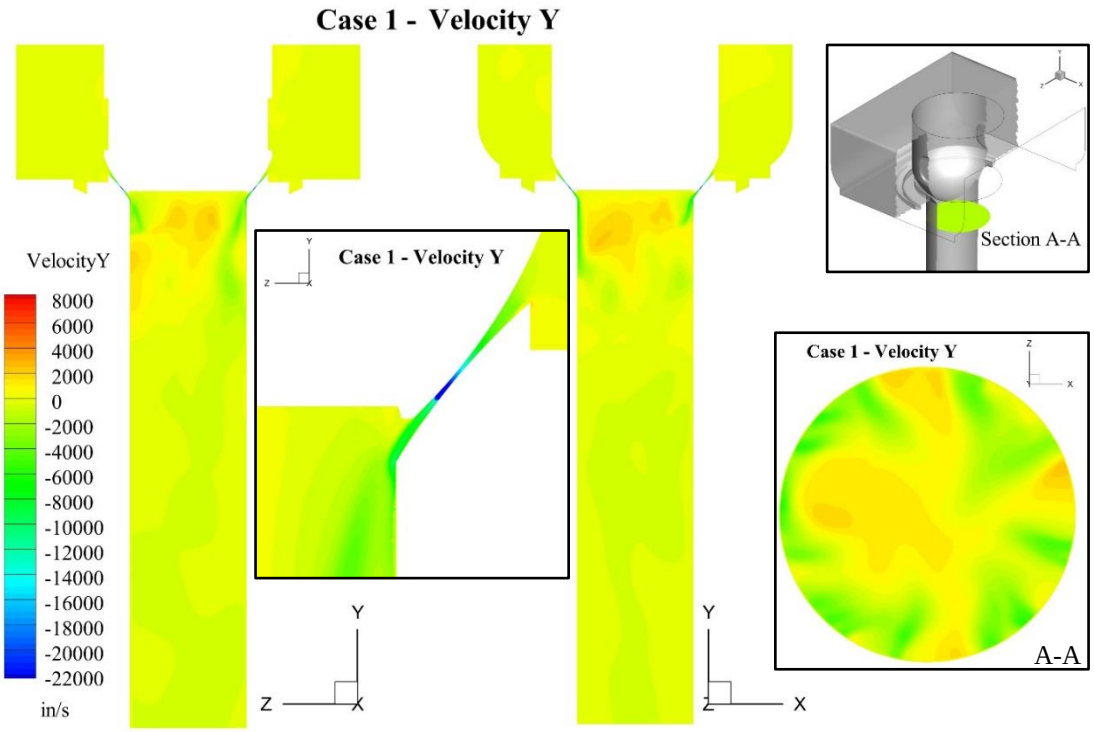

Figure 4.72. Vertical Velocity Contours at $OR = 0.007$, Revision 1-2 Disc.

4.5.2.3. Revision 1-3 disc

The revision 1-3 disc was intended to expand the throat flow jets slowly into the downstream region of the seat. The expansion is too rapid for an opening ratio of 0.007, however. As displayed in figures 4.73 and 4.74, the disc the flow alternates between attaching to the seat and disc. The downstream region maintains the unstable vortex shedding found with the revision 1 disc. An indentation could potentially correct this, but the extended geometry does not provide the flow improvement to justify continued investigation into this design.

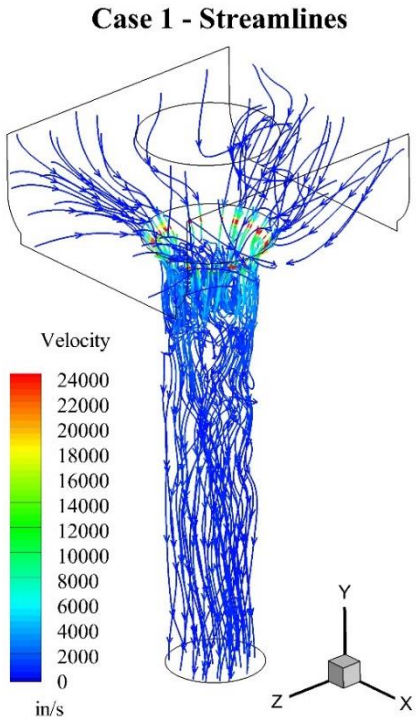

Figure 4.73. Velocity Streamlines at $OR = 0.007$, Revision 1-3 Disc.

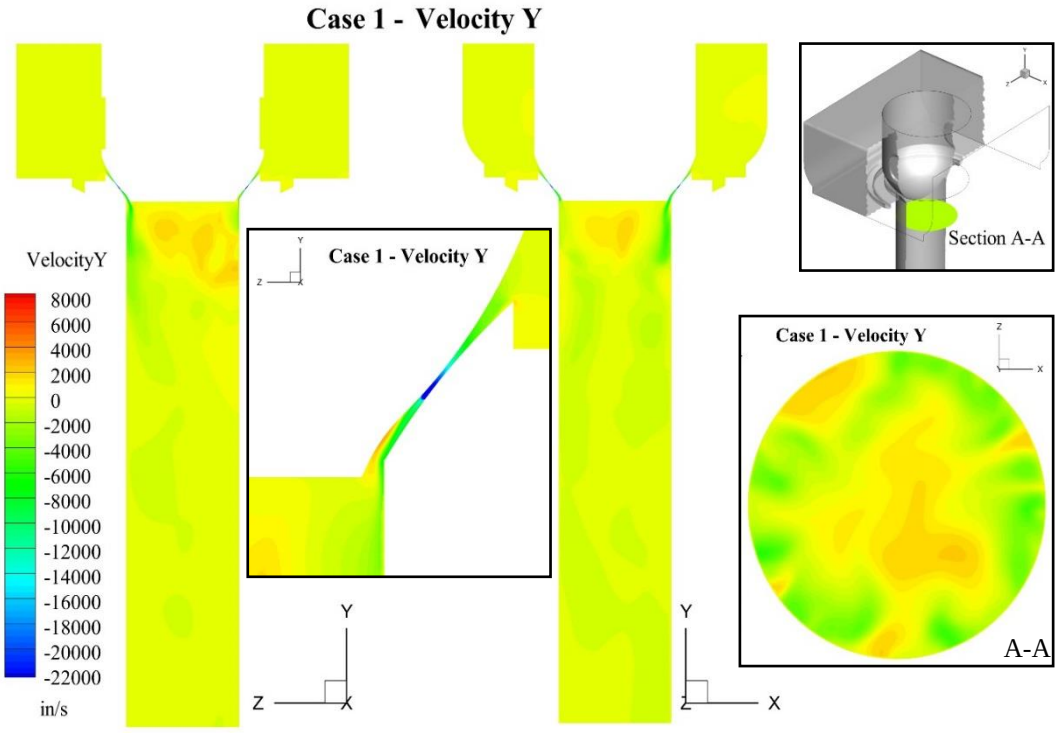

Figure 4.74. Vertical Velocity Contours at $OR = 0.007$, Revision 1-3 Disc.

4.5.2.4. Revision 1-4 disc

The indentation in the revision 1-4 disc is slightly wider and twice as deep as that in the revision 1-2 disc. The flow pattern, shown in figures 4.75 and 4.76 using velocity plots, is more symmetric. Hence, the depth of the revision 1-2 disc is not sufficient to stabilize the core flow. Further indented disc modifications are warranted because the flow jets are still asymmetric for the revision 1-4 disc. A decreased indentation radius may improve effectiveness at low lift and prevent flow coming out of the indentation from disrupting the throat jet flow.

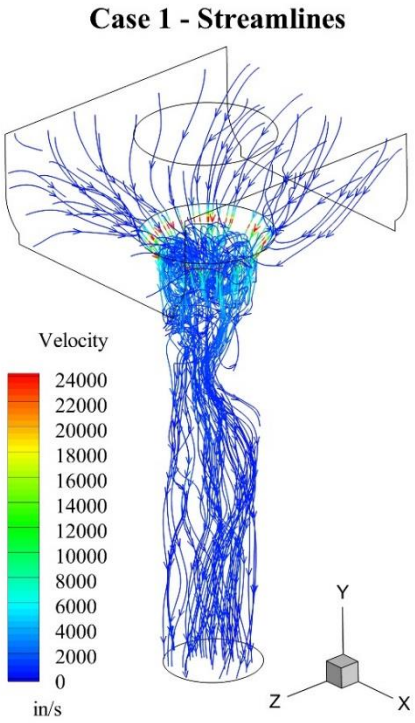

Figure 4.75. Velocity Streamlines at $OR = 0.007$, Revision 1-4 Disc.

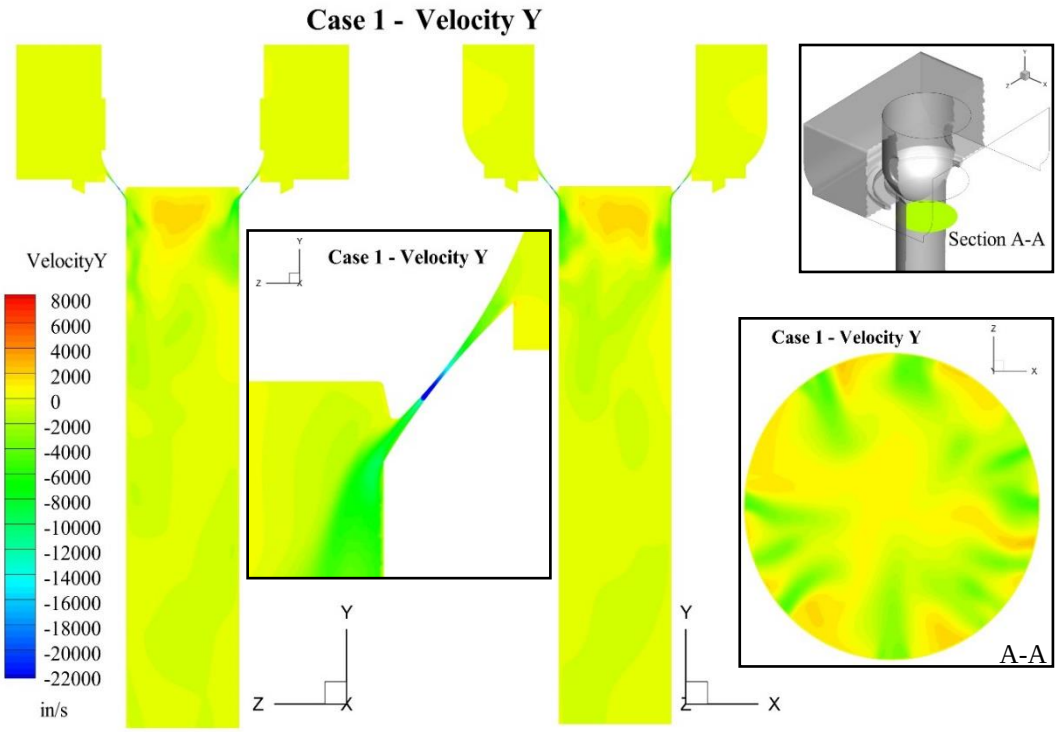

Figure 4.76. Vertical Velocity Contours at $OR = 0.007$, Revision 1-4 Disc.

4.5.2.5. Revision 1-6 disc

The revision 1-6 disc replaced the flat bottomed indentation with a domed indentation to improve reverse flow region immobilization. The width of the indentation was also narrowed and the domed surface was recessed into the disc, making the indentation perpendicular to the cutoff face.

4.5.2.5.1. Opening ratio = 0.007

The flow pattern at an opening ratio of 0.007, shown for velocity in figures 4.77 and 4.78, is a slight improvement over the revision 1 disc. The throat jets are less disturbed by the reverse flow region, but there are no significant improvements. The core reverse flow region at the disc indentation is narrower than the indentation; this indicates that the indentation is too wide to capture only the high pressure region underneath the disc. This disc is comparable to the revision

1-4 disc for an opening ratio of 0.007. Because the domed indentation bottom should provide a more stable core flow region than the flat bottom according to D. Zhang [8], it is kept for further modifications.

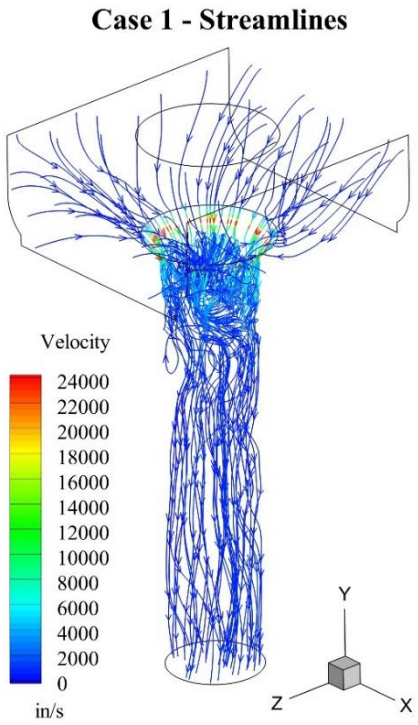

Figure 4.77. Velocity Streamlines at $OR = 0.007$, Revision 1-6 Disc.

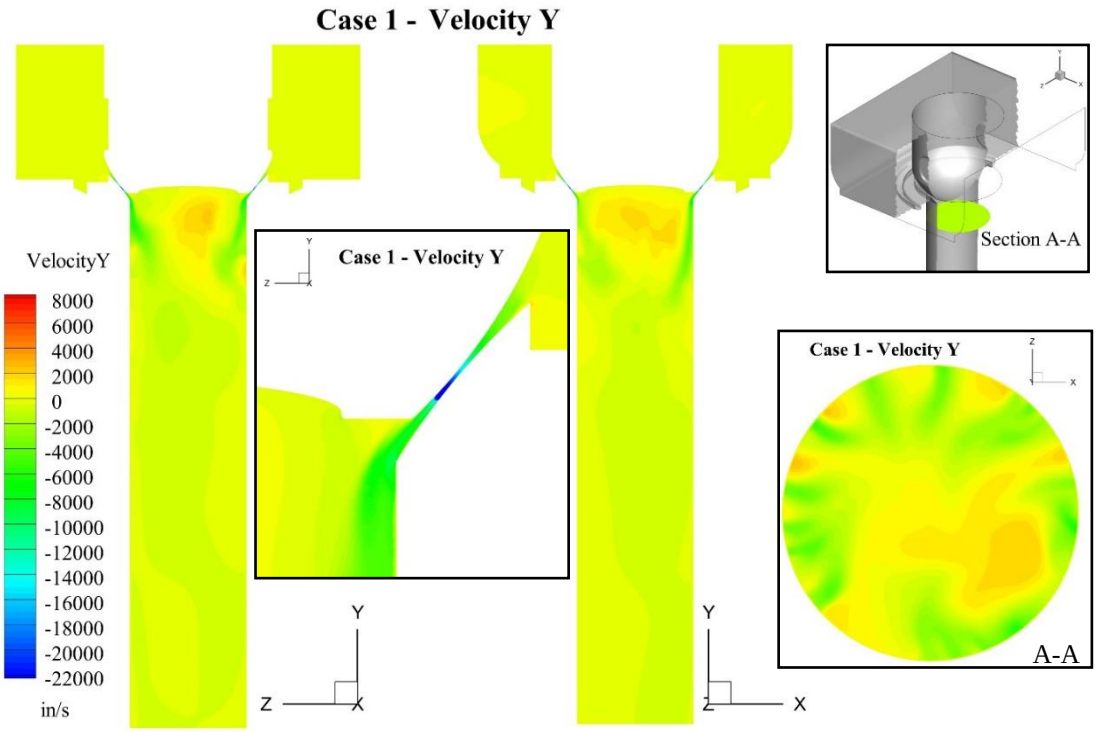

Figure 4.78. Vertical Velocity Contours at $OR = 0.007$, Revision 1-6 Disc.

4.5.2.5.2. Opening ratio = 0.012

At an opening ratio of 0.012, the flow pattern for the revision 1-6 disc, given in figures 4.79 and 4.80, is similar to the revision 1 disc. A stable reverse flow region is not yet established. The reverse flow region is more centered than the revision 1 disc, however. The unstable separation bubble beneath the valve throat is still present.

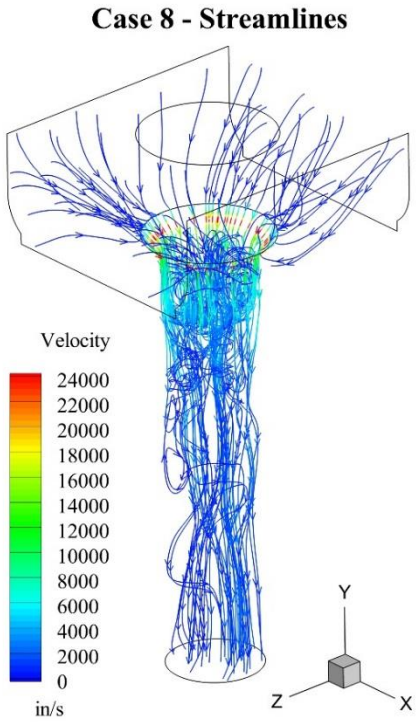

Figure 4.79. Velocity Streamlines at $OR = 0.012$, Revision 1-6 Disc.

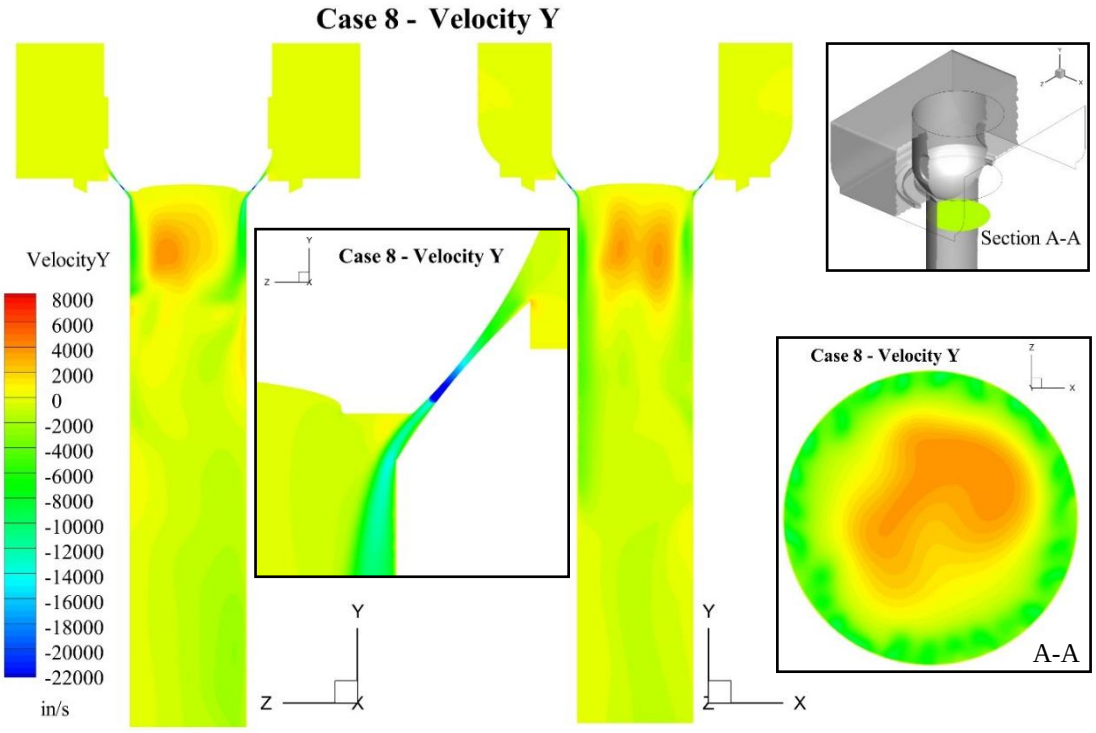

Figure 4.80. Vertical Velocity Contours at $OR = 0.012$, Revision 1-6 Disc.

4.5.2.5.3. Opening ratios 0.024 and 0.028

The higher opening ratio cases for the revision 1-6 disc show strong stable annular flow. The velocity contours for cases 7 and 5 are shown in figures 4.81 and 4.82; the flow patterns correlates well with those of the revision 1 disc.

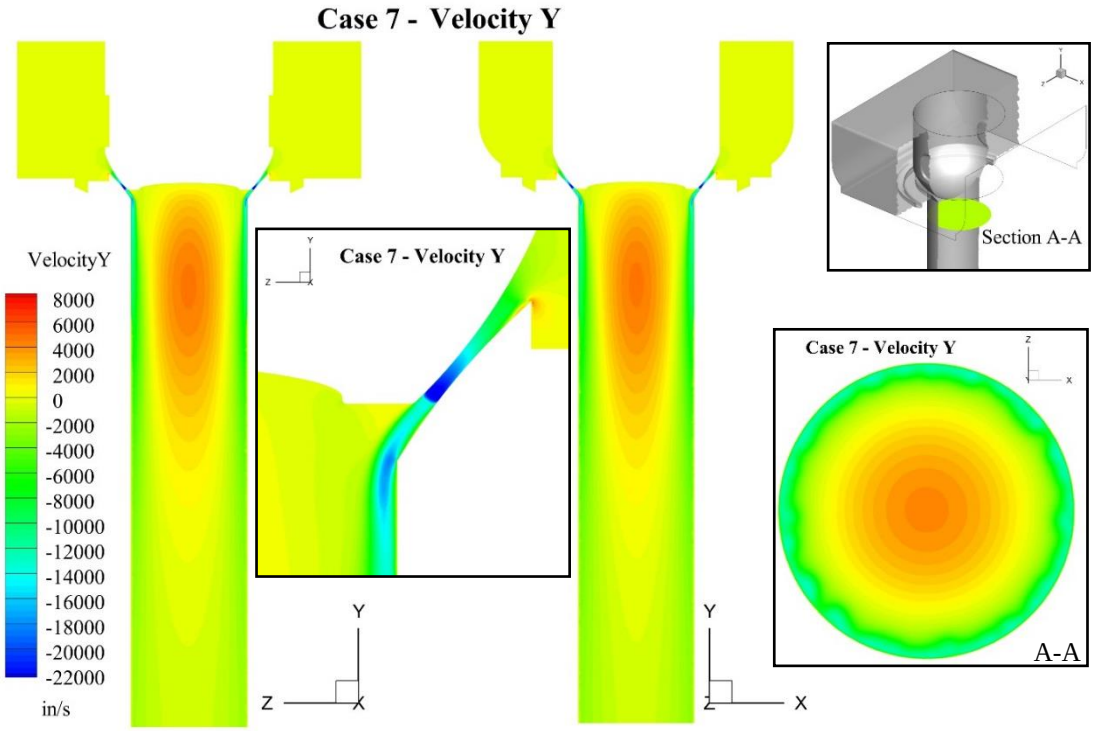

Figure 4.81. Vertical Velocity Contours at $OR = 0.024$, Revision 1-6 Disc.

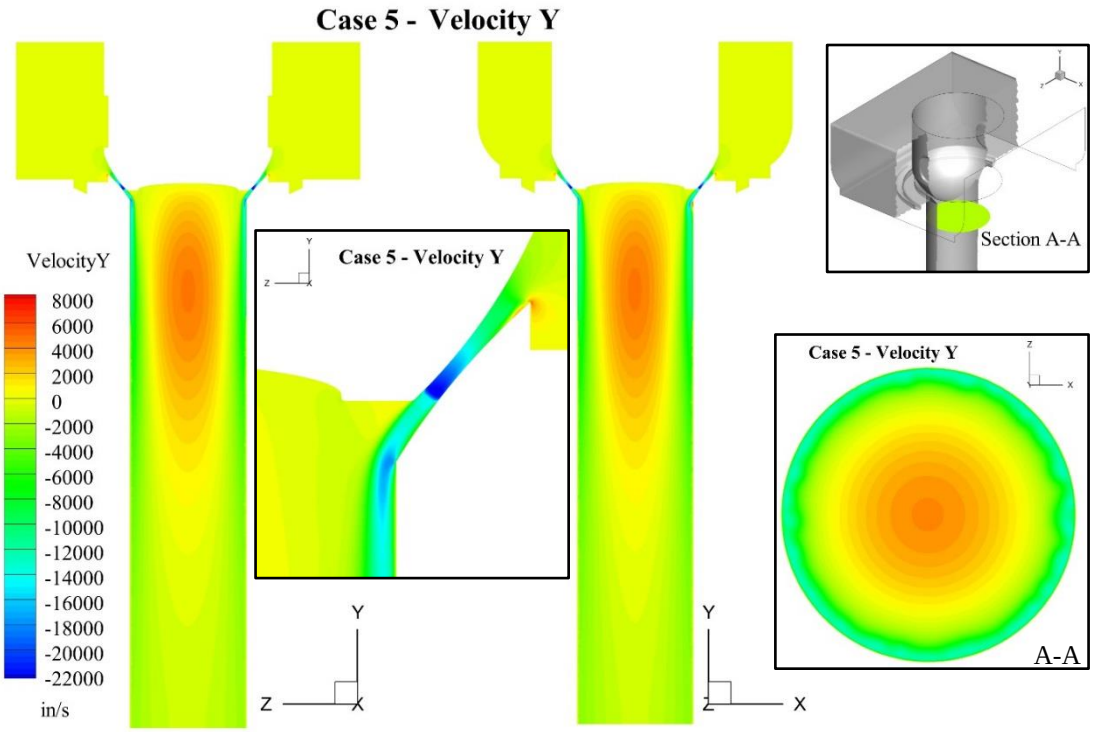

Figure 4.82. Vertical Velocity Contours at $OR = 0.028$, Revision 1-6 Disc.

4.5.2.6. Revision 1-8 disc

The revision 1-6 and 1-8 discs are identical except for a wider indentation on the revision 1-8 disc. With an increase in the indentation width, the flow pattern changes dramatically. Highly unstable flow is present downstream at an opening ratio of 0.028, as displayed in figures 4.83 and 4.84. The wider indentation expands the jet cross-sectional passage rapidly, causing the throat jet flow to expand upward after leaving the throat instead of remaining attached to the seat. The flow then attaches to the disc inside the indentation and travels downward on the opposite side, disrupting the opposing flow jet. A wide indentation, therefore, destabilizes the flow pattern.

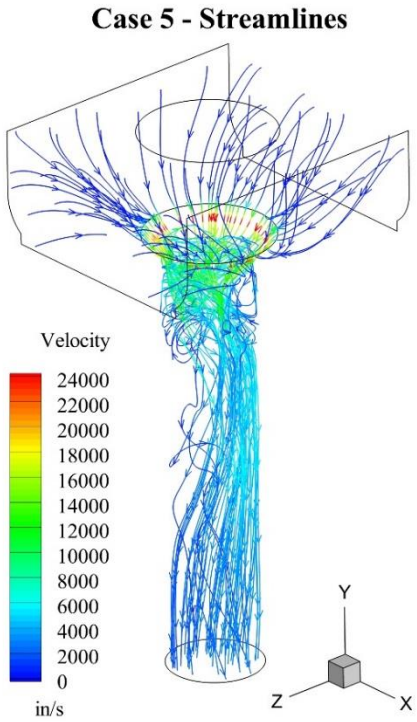

Figure 4.83. Velocity Streamlines at $OR = 0.035$, Revision 1-8 Disc.

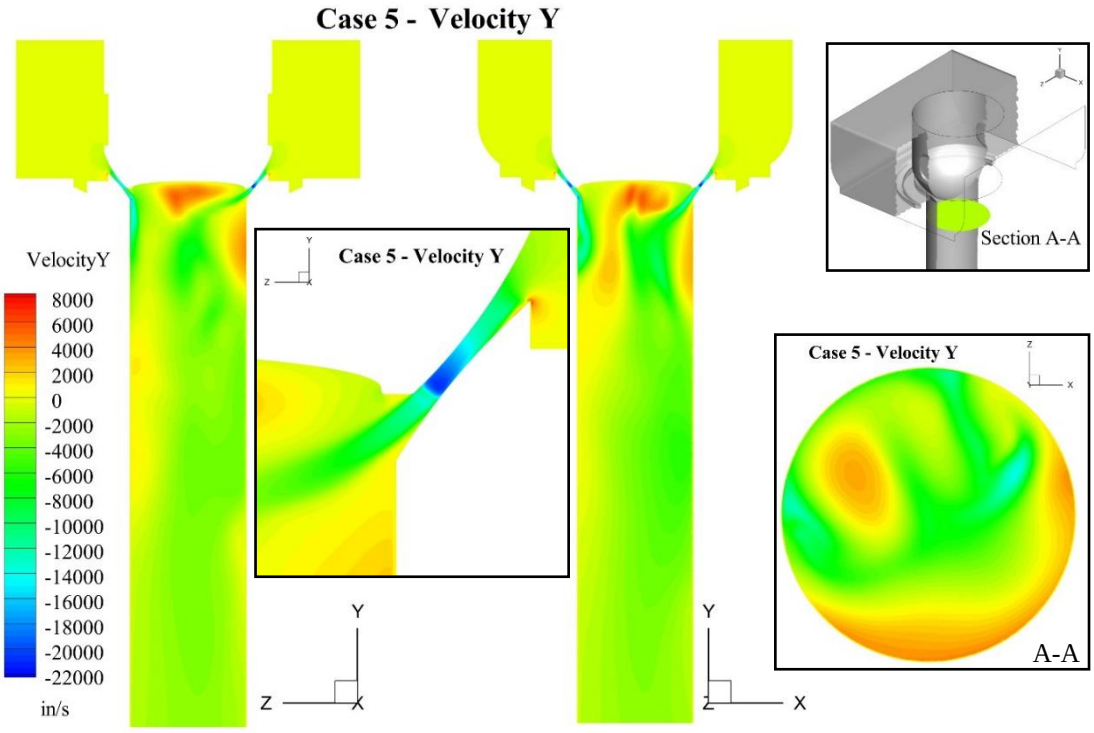

Figure 4.84. Vertical Velocity Contours at $OR = 0.035$, Revision 1-8 Disc.

4.5.2.7. Revision 1-10 disc

The revision 1-10 disc contains an indentation that is the same width as the revision 1-6 disc, but does not recess the curved indentation surface. Therefore, the revision 1-10 disc indentation does not constrain as much flow as the revision 1-6 disc indentation and the pressure in the indentation is lower. At an opening ratio of 0.035, this causes the flow jet to expand upward into the disc as the jet cross-sectional passage expands at the indentation. Figures 4.85 and 4.86 show that the jet then attaches to the disc indentation near the center and travels to the opposite side, detaching from the disc as it leaves the indentation. Upon separating from the disc, the flow disrupts the opposing throat flow jet, creating a very unstable flow pattern.

The highly unstable velocity pattern for the revision 1-10 disc is the same as that found for the revision 1-8 disc. Designing a deeper indentation with a perpendicular edge resolves the flow instability. A further adjustment to improve indentation efficiency is to reduce the width of the revision 1-6 and 1-10 disc indentation. This is examined in the revision 1-12 through 1-16 discs.

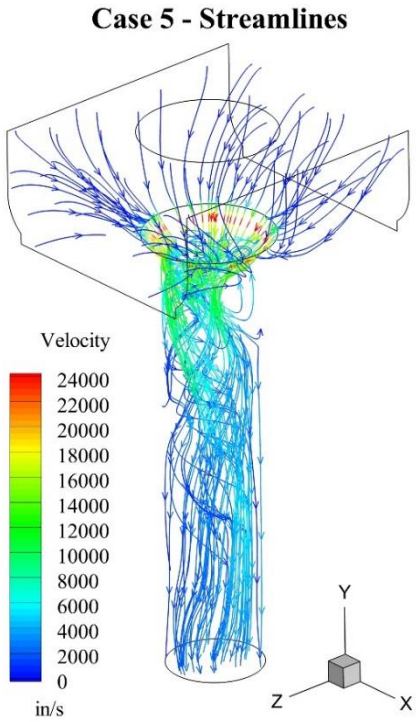

Figure 4.85. Velocity Streamlines at $OR = 0.035$, Revision 1-10 Disc.

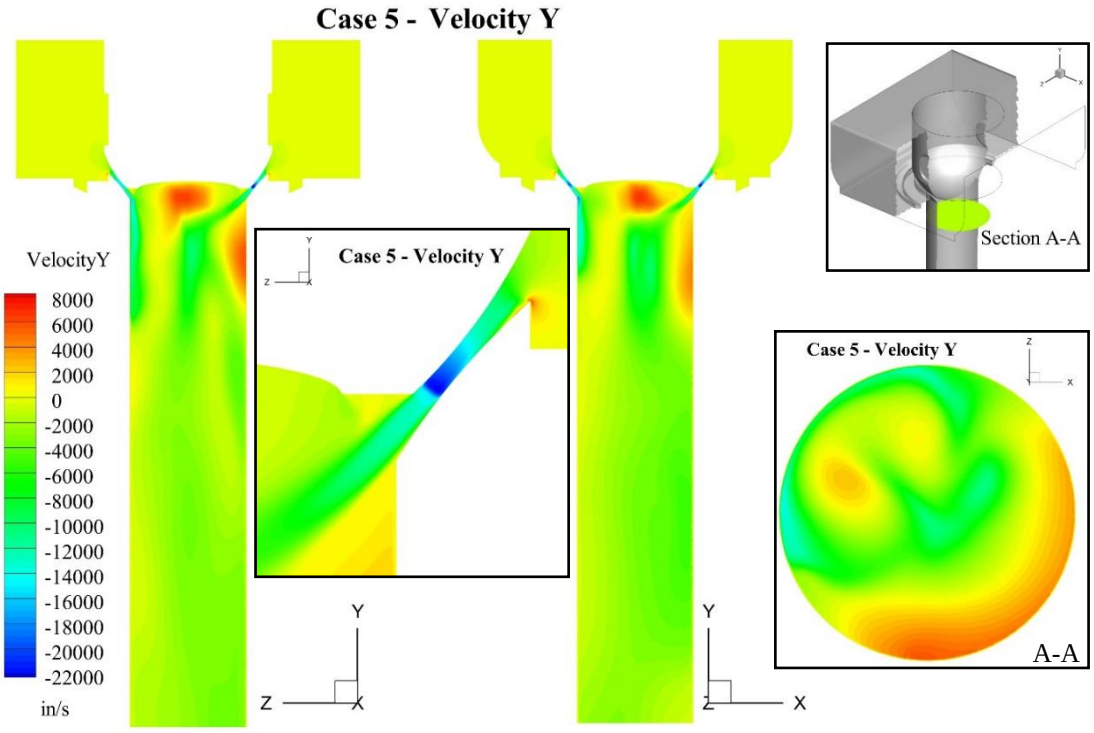

Figure 4.86. Vertical Velocity Contours at $OR = 0.035$, Revision 1-10 Disc.

4.5.2.8. Revision 1-12 disc

The indentation in the revision 1-12 disc is the same depth as that in the revision 1-6 disc, but much narrower. The separation bubble at the throat exit is present at an opening ratio of 0.012 for the revision 1-12 disc. Shown in figures 4.87 and 4.88, the resultant vortex shedding is more unstable than that on the revision 1-6 disc due to the indentation width reduction. The narrower indentation traps a high pressure region, pushing the reverse core flow to the cutoff face where it interacts with the throat flow jets more rapidly.

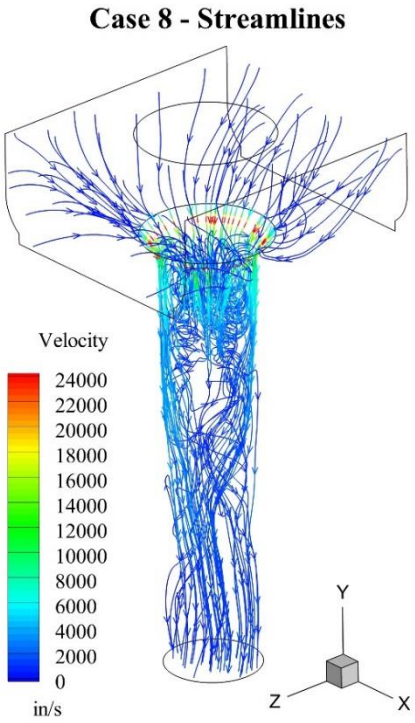

Figure 4.87. Velocity Streamlines at $OR = 0.012$, Revision 1-12 Disc.

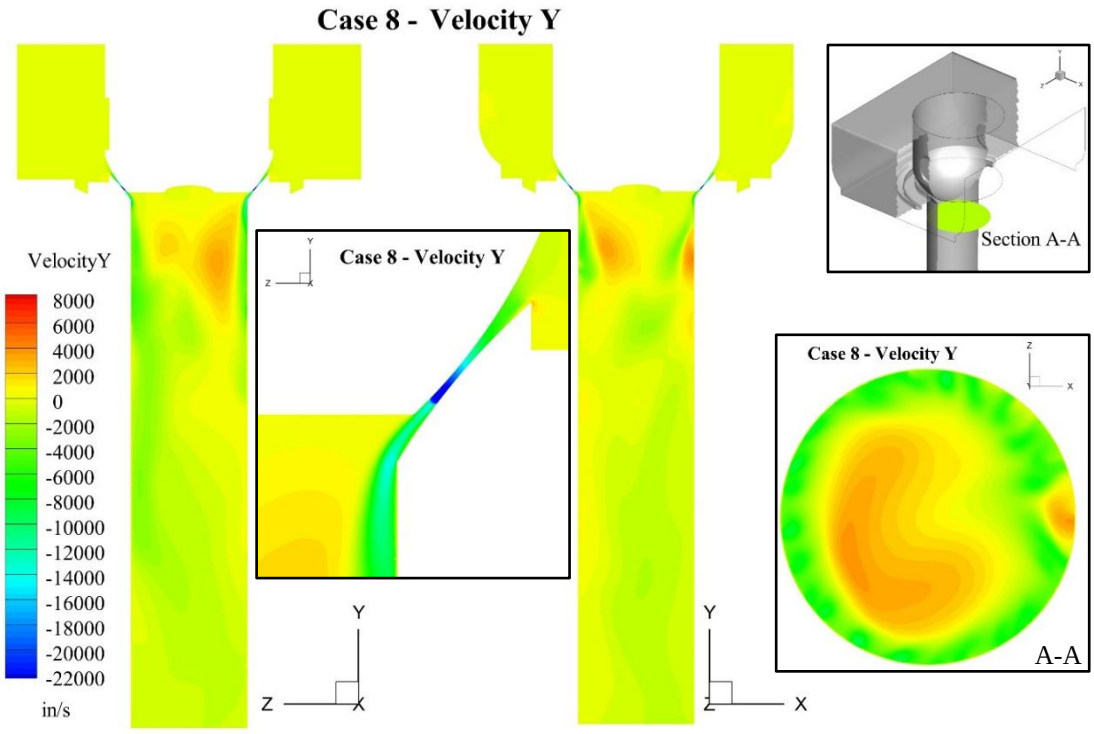

Figure 4.88. Vertical Velocity Contours at $OR = 0.012$, Revision 1-12 Disc.

In an attempt to remove the separation bubble from the throat exit, the turbulence level of the flow in the throat was increased. A surface roughness of approximately 250 Ra was added to the seat sealing surface.

The flow pattern, given in figures 4.89 and 4.90, is highly improved. Strong annular flow and a slightly asymmetric reverse core flow region are present. The core flow region is wider than the disc indentation, indicating that the high pressure region in the indentation is fixed.

A separation bubble persists at the throat exit. The flow separation and reattachment points are the same as that for the revision 1-12 disc without a rough seat, but the separation bubble for the rough seat is much thinner. This causes the flow pattern to look similar to those found at higher opening ratios with stable flow, where a separation bubble was still present. The thinner unsteady separation bubble has a reduced effect on the throat flow jet.

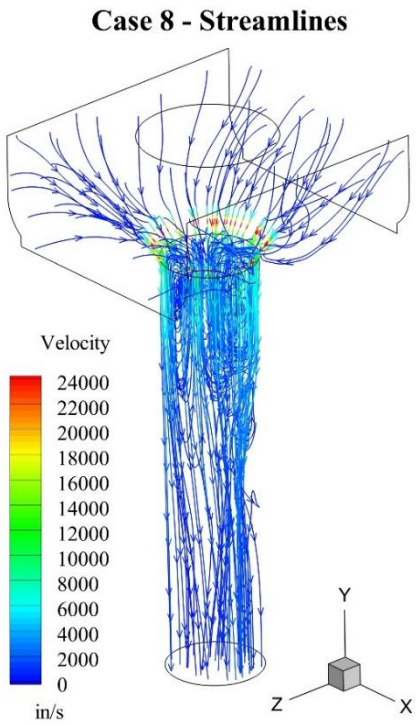

Figure 4.89. Velocity Streamlines at $OR = 0.012$, Revision 1-12 Disc, Rough Seat.

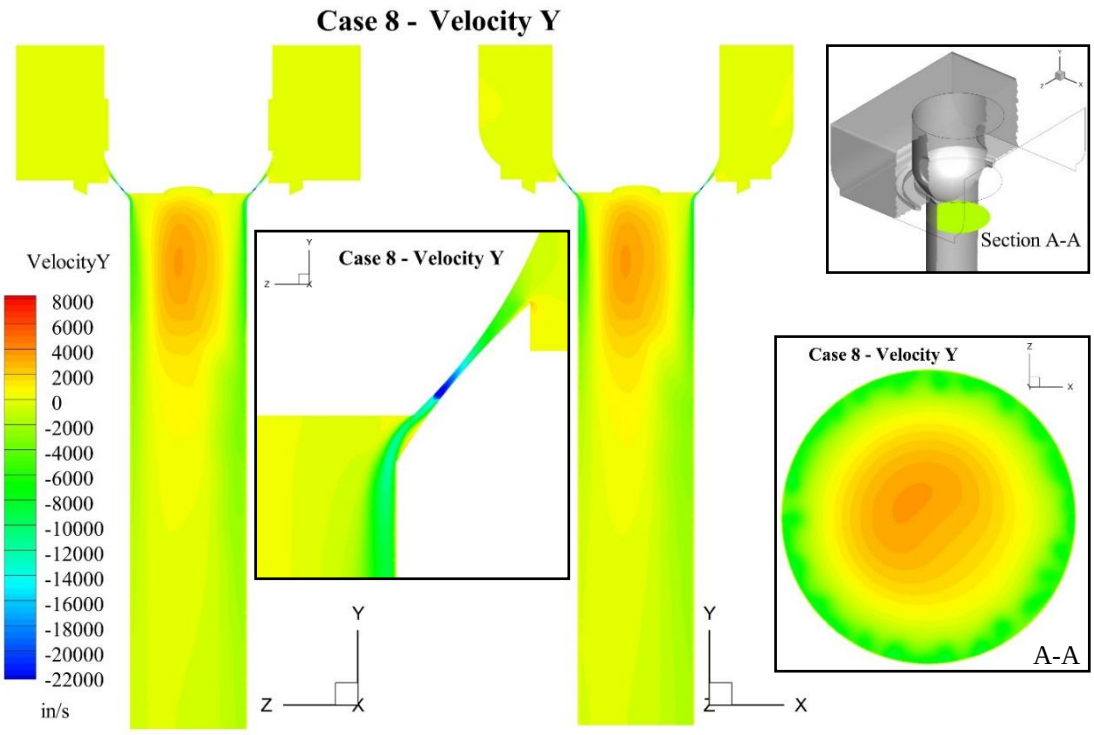

Figure 4.90. Vertical Velocity Contours at $OR = 0.012$, Revision 1-12 Disc, Rough Seat.

4.5.2.9. Revision 1-14 disc

The revision 1-14 disc has the same width indentation as the revision 1-12 disc, but deeper. Comparing the velocity plots for the revision 1-14 disc at an opening ratio of 0.012 (figures 4.91 and 4.92) to the revision 1-12 disc (figures 4.113 and 4.114), both in combination with the revision 4 seat, there is little difference. The high pressure region in the indentation is somewhat larger and, therefore, stabilizes the disc better.

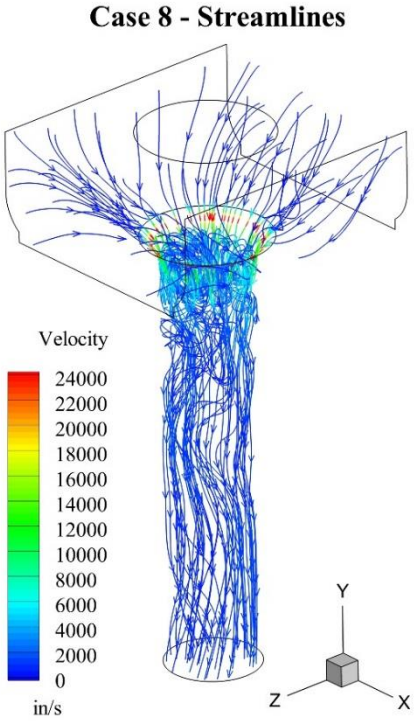

Figure 4.91. Velocity Streamlines at $OR = 0.012$, Revision 1-14 Disc, Revision 4 Seat.

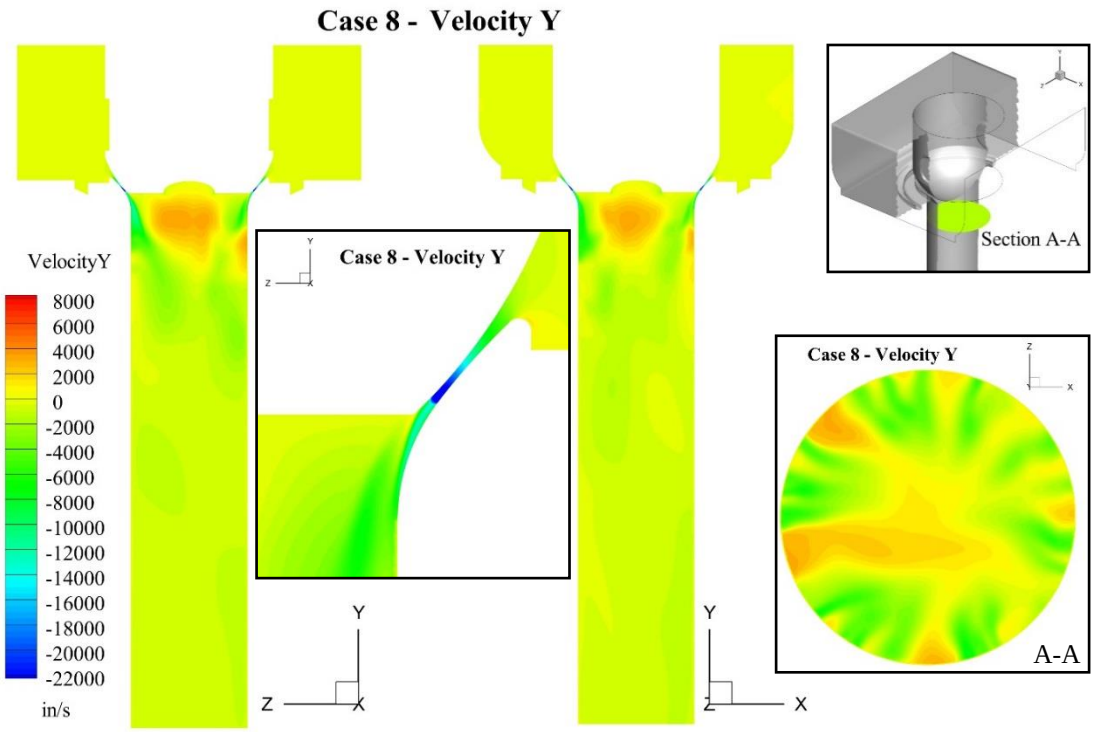

Figure 4.92. Vertical Velocity Contours at $OR = 0.012$, Revision 1-14 Disc, Revision 4 Seat.

4.5.2.10. Revision 1-16 disc

The throat expansion at the end of the revision 1 disc domain causes an adverse pressure gradient to form on the disc wall and is responsible for the separation bubble at the throat exit. The revision 1-16 disc utilizes a concave section at the bottom of the sealing surface, directly prior to the cutoff edge, to remove it. The indentation in the revision 1-16 disc is the same as that of the revision 1-12 disc.

By contracting the end of the throat to form a converging nozzle, the unsteady separation bubble at the throat exit is removed. The flow patterns, given in figures 4.93 through 4.97 at opening ratios 0.007, 0.012, and 0.018, respectively, all show stable, annular flow.

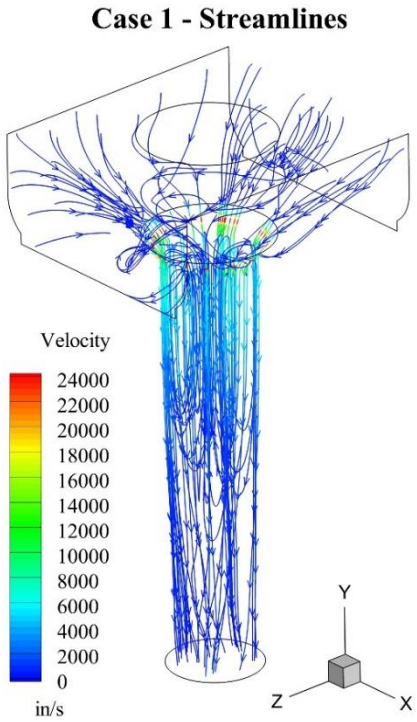

Figure 4.93. Velocity Streamlines at $OR = 0.007$, Revision 1-16 Disc.

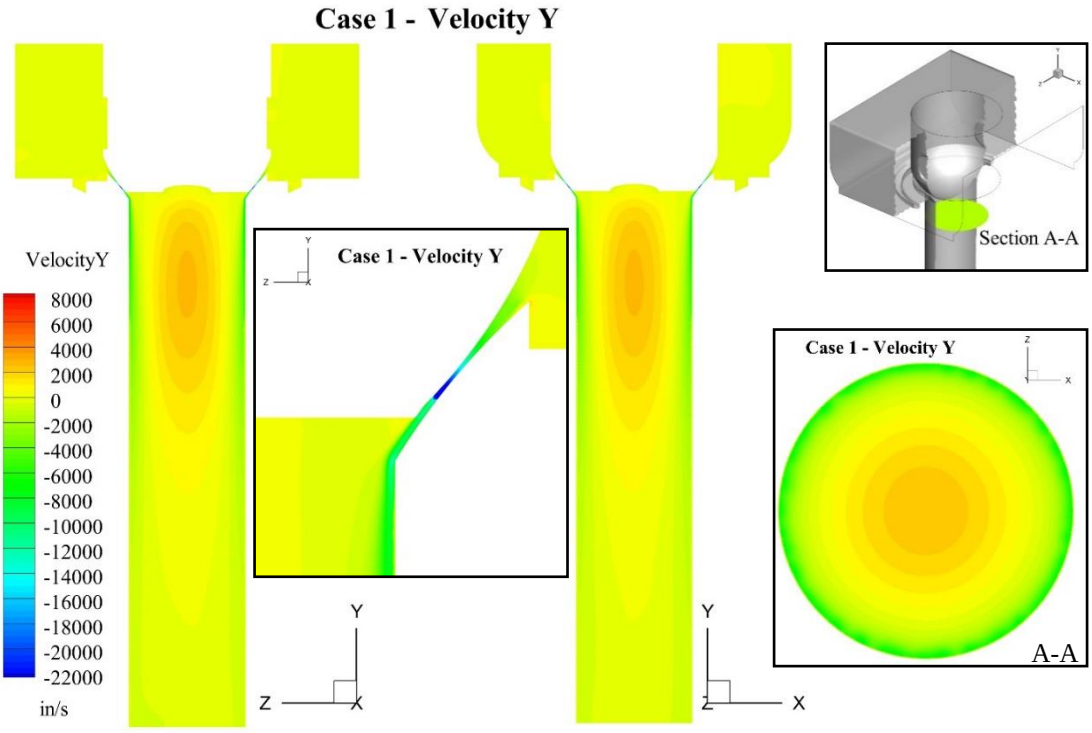

Figure 4.94. Vertical Velocity Contours at $OR = 0.007$, Revision 1-16 Disc.

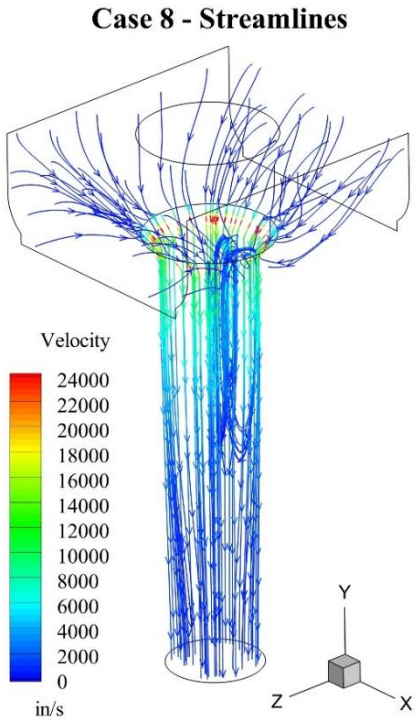

Figure 4.95. Velocity Streamlines at $OR = 0.012$, Revision 1-16 Disc.

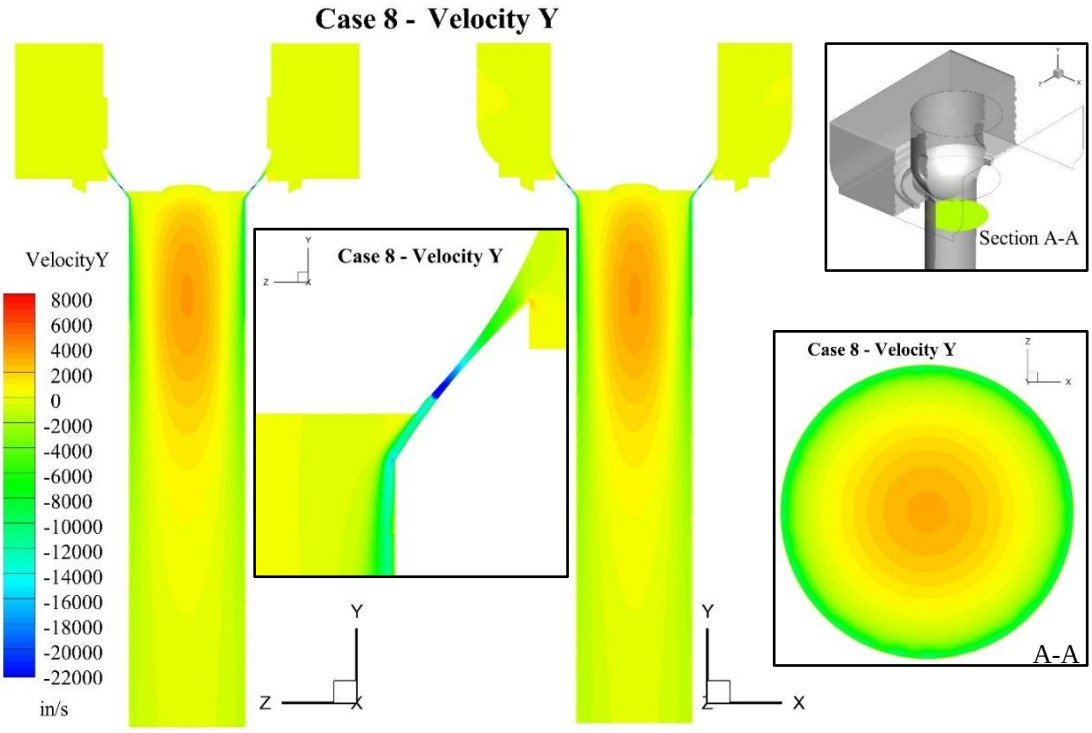

Figure 4.96. Vertical Velocity Contours at $OR = 0.012$, Revision 1-16 Disc.

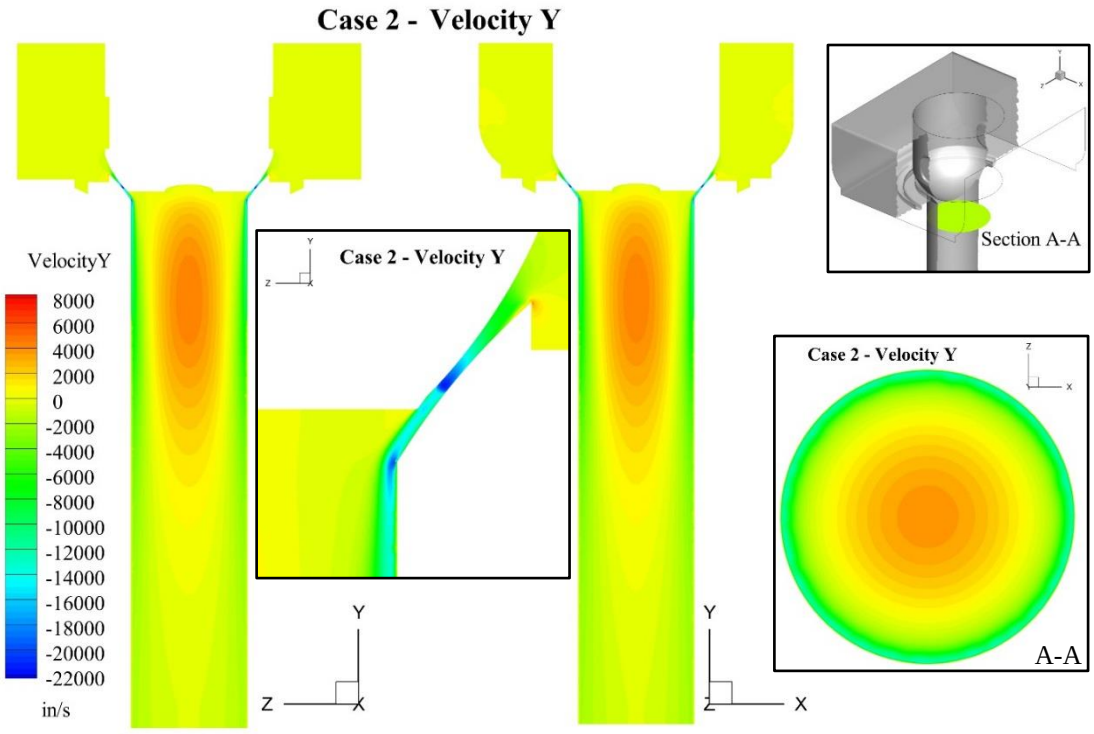

Figure 4.97. Vertical Velocity Contours at $OR = 0.018$, Revision 1-16 Disc.

4.5.2.11. Revision 2 disc

After encountering separation bubbles downstream of the throat on many of the altered discs, the revision 2 disc was designed to ensure flow attachment to the seat. By using the cutoff edge as the sealing surface, the flow cannot expand due to throat expansion; the narrowest part of the throat will always be at the cutoff edge. A flat indentation was also used to restrain reverse flow from moving on the backside of the disc.

The revision 2 disc displayed a stable flow pattern at opening ratios 0.024 and 0.028, shown in figures 4.98 and 4.99, respectively. The flow velocity in the converging-only revision 2 disc throat is decreased in comparison to the discs with a converging-diverging throat. This would alter the mass flow rate passing through the valve, potentially requiring extensive testing by MPC. As a result, keeping the design modifications closer to the original disc geometry is

desirable. The revision 1-16 disc requires less modification, so it is preferred over the revision 2 disc.

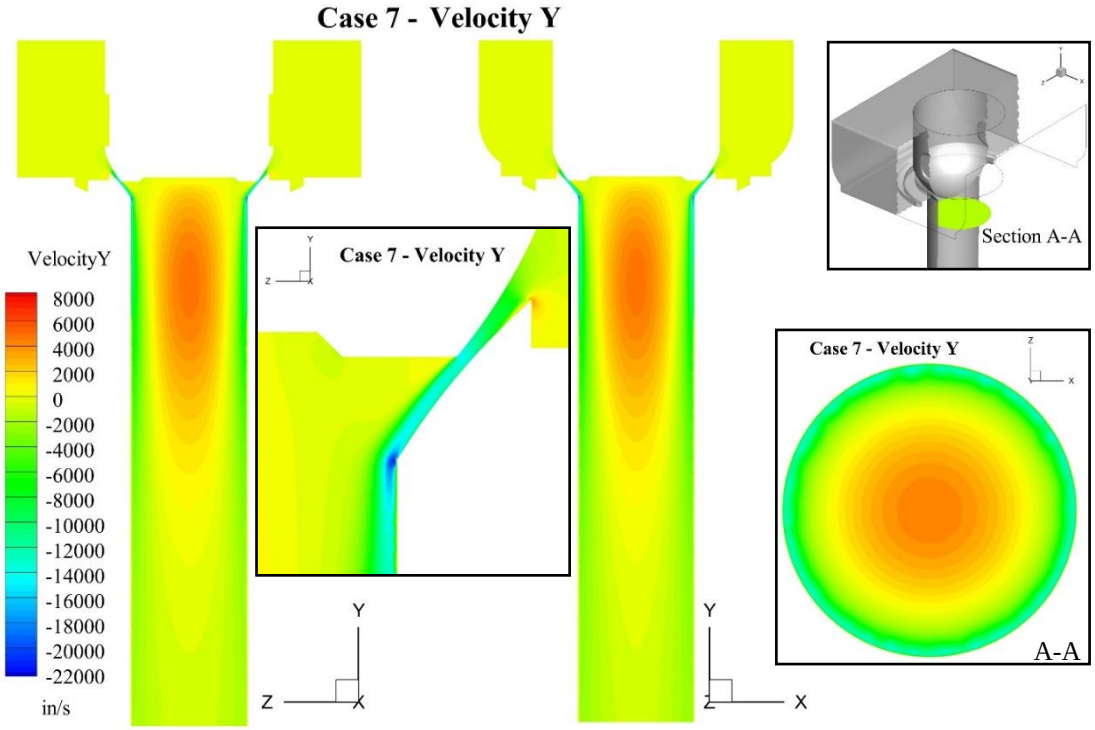

Figure 4.98. Vertical Velocity Contours at $OR = 0.024$, Revision 2 Disc.

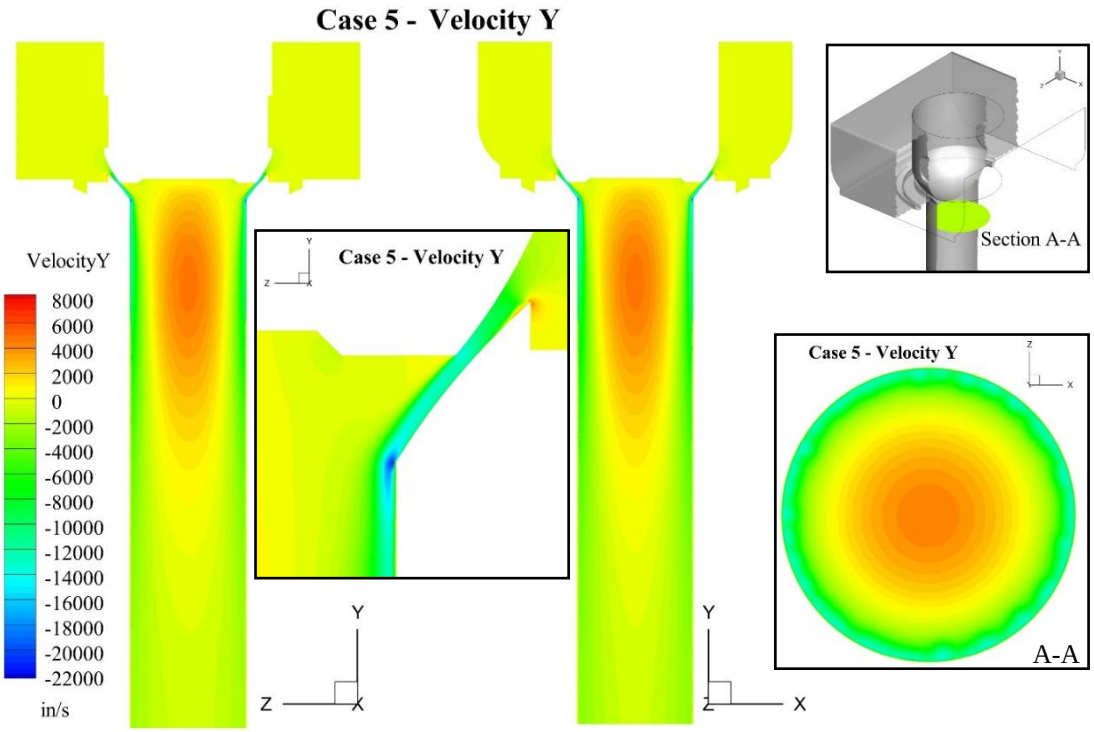

Figure 4.99. Vertical Velocity Contours at $OR = 0.028$, Revision 2 Disc.

4.5.3. Seat Design Revisions

4.5.3.1. Revision 1 seat

The revision 1 seat employs a small radius at the edge between the seat sealing and downstream surfaces. The overall flow pattern, displayed in figures 4.100 and 4.101, indicates an annularity improvement over the unmodified seat, shown in figures 4.53 and 4.54. The separation bubble on the seat at the end of the throat is still present. A further increase in the seat edge radius may move the flow expansion closer to the wall; this is investigated in the other seat revisions.

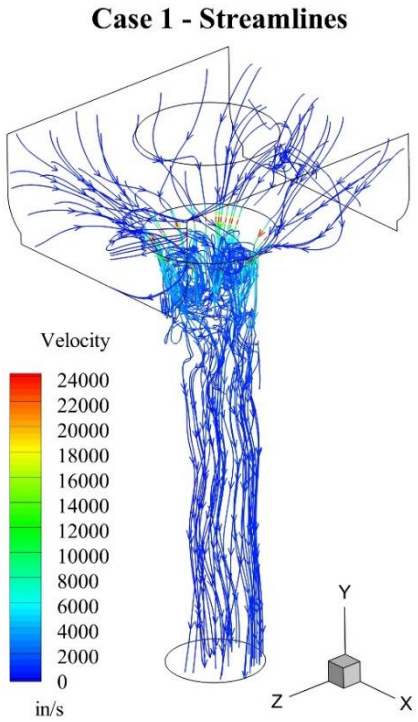

Figure 4.100. Velocity Streamlines at $OR = 0.007$, Revision 1 Disc, Revision 1 Seat.

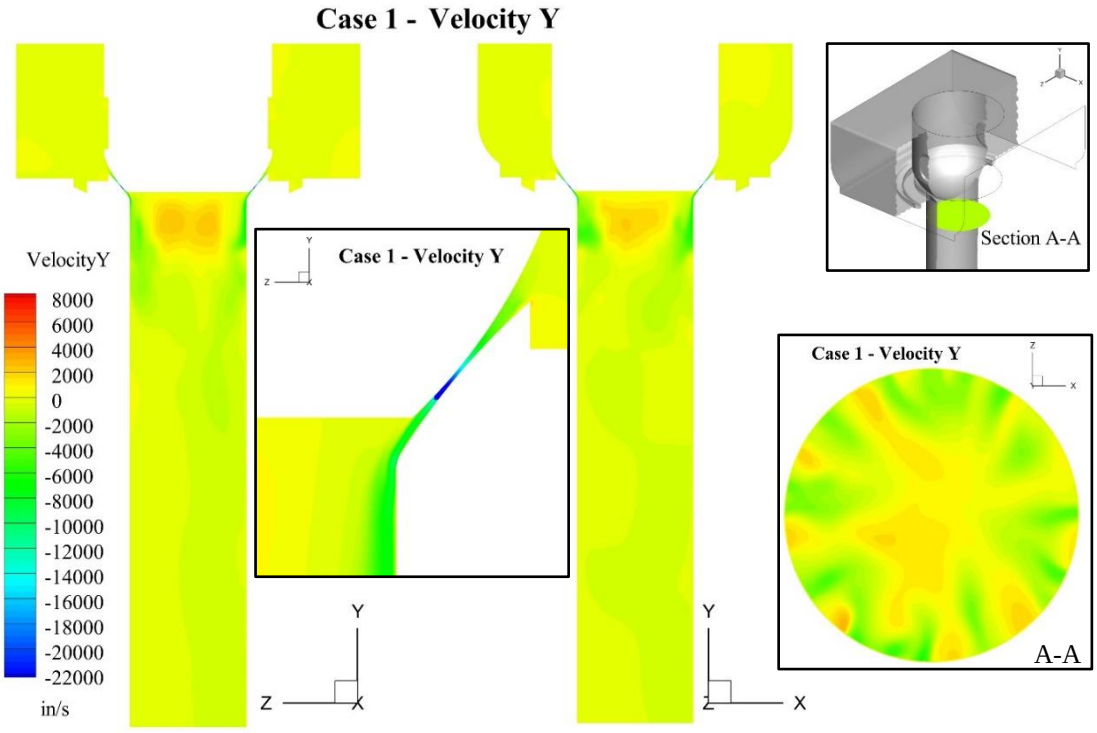

Figure 4.101. Vertical Velocity Contours at $OR = 0.007$, Revision 1 Disc, Revision 1 Seat.

4.5.3.2. Revision 2 seat

Increasing the abrupt seat edge radius removes the throat separation bubble, but the vortex shedding remains. The velocity plots, figures 4.102 and 4.103, show that a large seat edge radius does not enhance the flow pattern at an opening ratio of 0.007 for the revision 1 disc. When combined with the revision 1-3 disc, the revision 2 seat reduces the flow jet instability and improves core flow, but does not remove the alternating seat-disc flow attachment at the throat exit. This is displayed in figure 4.104. There is not enough flow stabilization to justify the use of this combination.

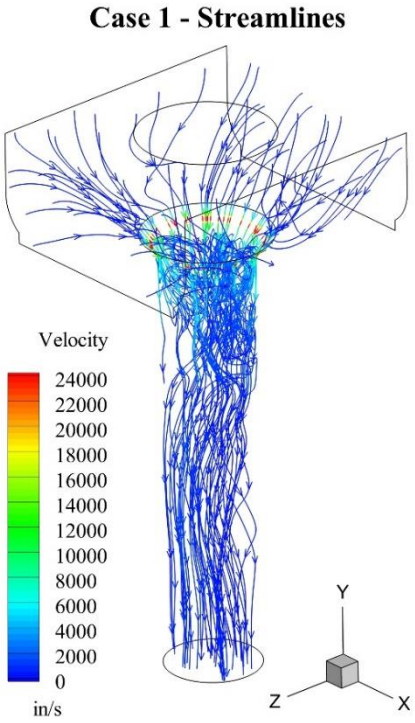

Figure 4.102. Velocity Streamlines at $OR = 0.007$, Revision 1 Disc, Revision 2 Seat.

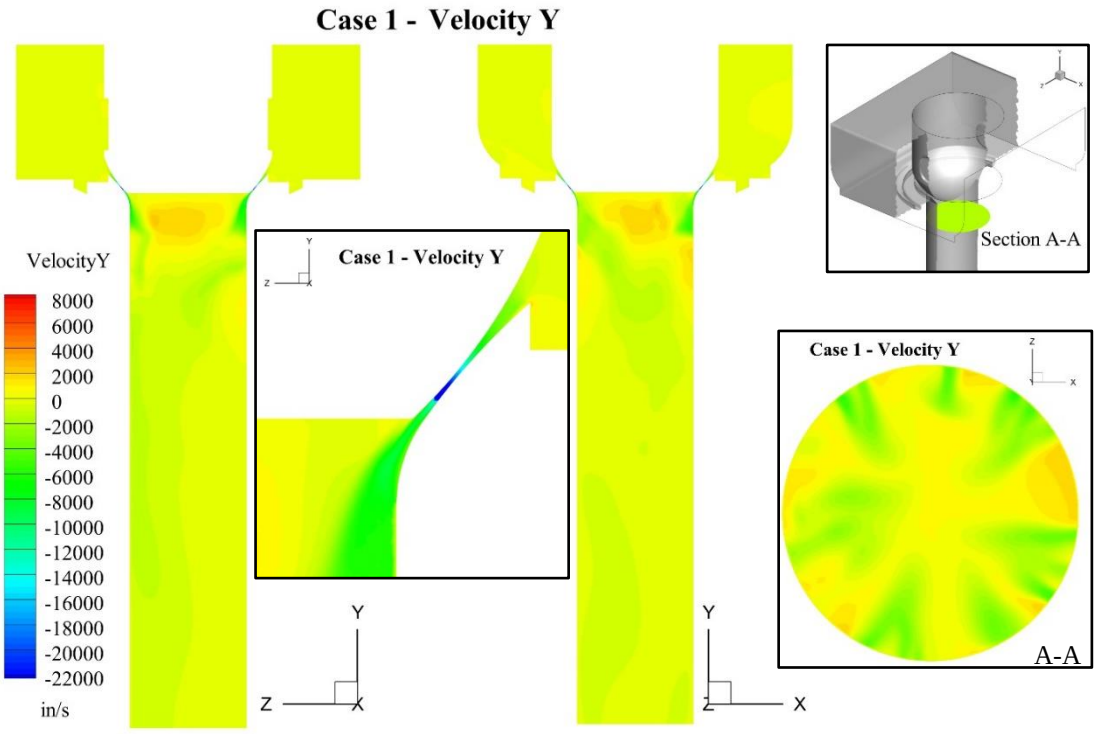

Figure 4.103. Vertical Velocity Contours at $OR = 0.007$, Revision 1 Disc, Revision 2 Seat.

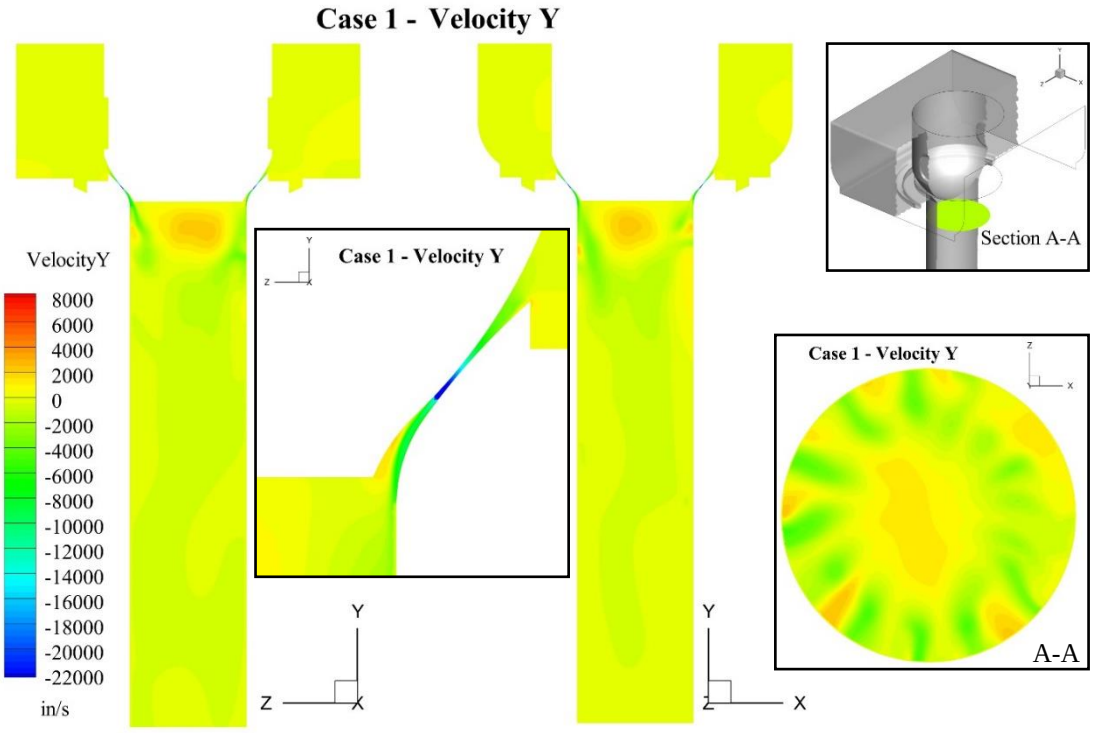

Figure 4.104. Vertical Velocity Contours at $OR = 0.007$, Revision 1-3 Disc, Revision 2 Seat.

4.5.3.3. Revision 3 seat

The revision 3 seat was tested for the revision 1-6 disc at an opening ratio of 0.028. Modification of the seat design did not alter the stable flow, shown in figures 4.105 and 4.106.

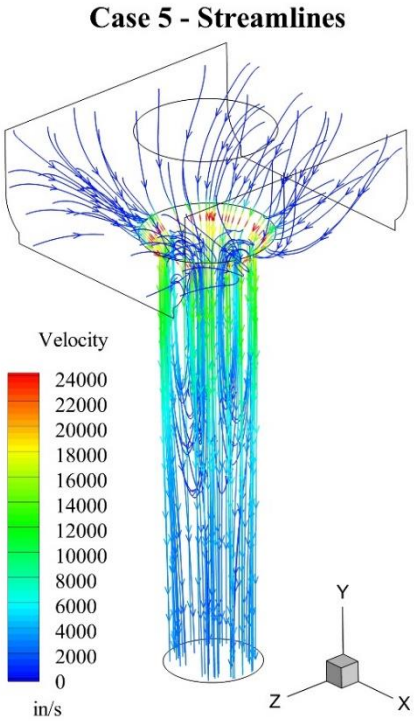

Figure 4.105. Velocity Streamlines at $OR = 0.035$, Revision 1-6 Disc, Revision 3 Seat.

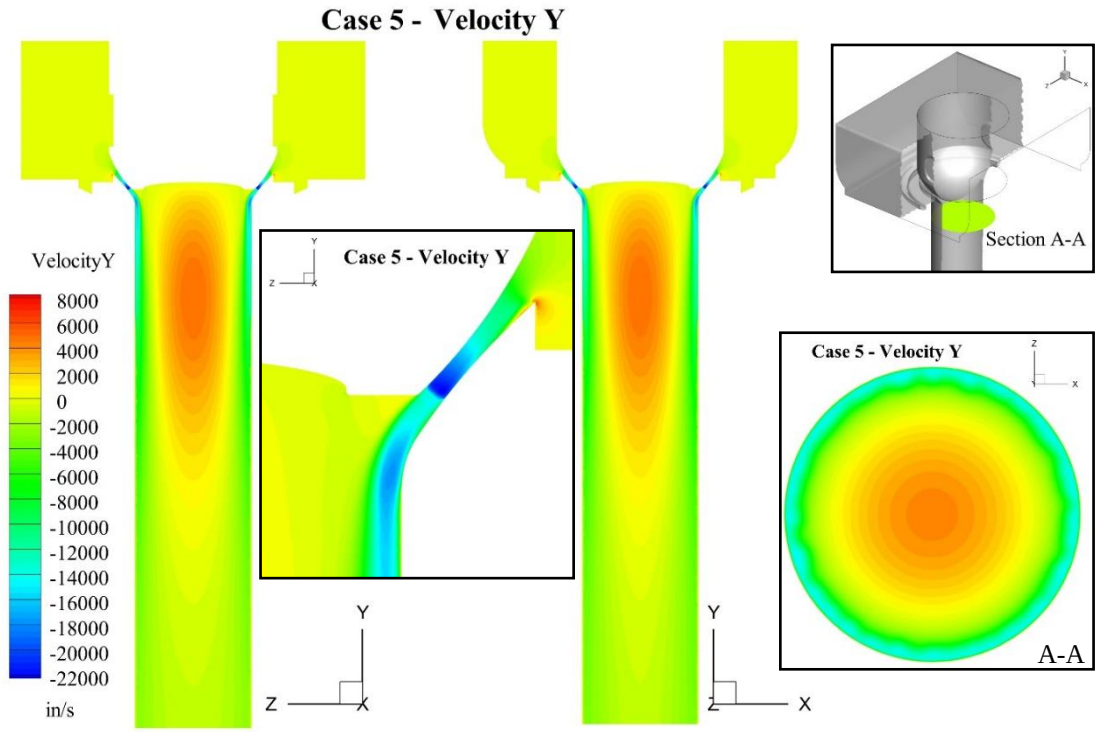

Figure 4.106. Vertical Velocity Contours at $OR = 0.035$, Revision 1-6 Disc, Revision 3 Seat.

4.5.3.4. Revision 4 seat

The revision 4 seat combines a large radius on the abrupt seat edge with a radius on the top edge of the seat. The lower radius is intended to improve flow adhesion to the seat downstream of the throat and the upper radius is used to remove the flow separation from the seat at the beginning of the throat.

4.5.3.4.1. Opening ratio = 0.012

The flow pattern for the original hemispherical disc in combination with the revision 4 disc at an opening ratio of 0.012 is displayed in figures 4.107 and 4.108. The upper radius performs as designed, removing the upstream flow separation on the seat. Below the throat, the flow is no longer attached to the seat, but does not detach at a set location either, causing instability in the flow jets. The flow has a random asymmetric pattern downstream.

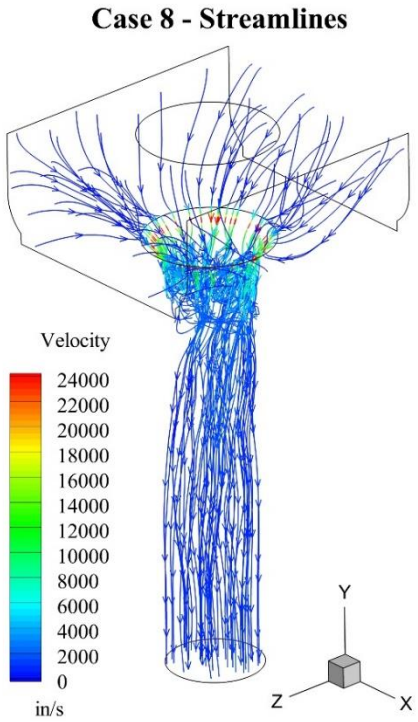

Figure 4.107. Velocity Streamlines at $OR = 0.012$, Original Disc, Revision 4 Seat.

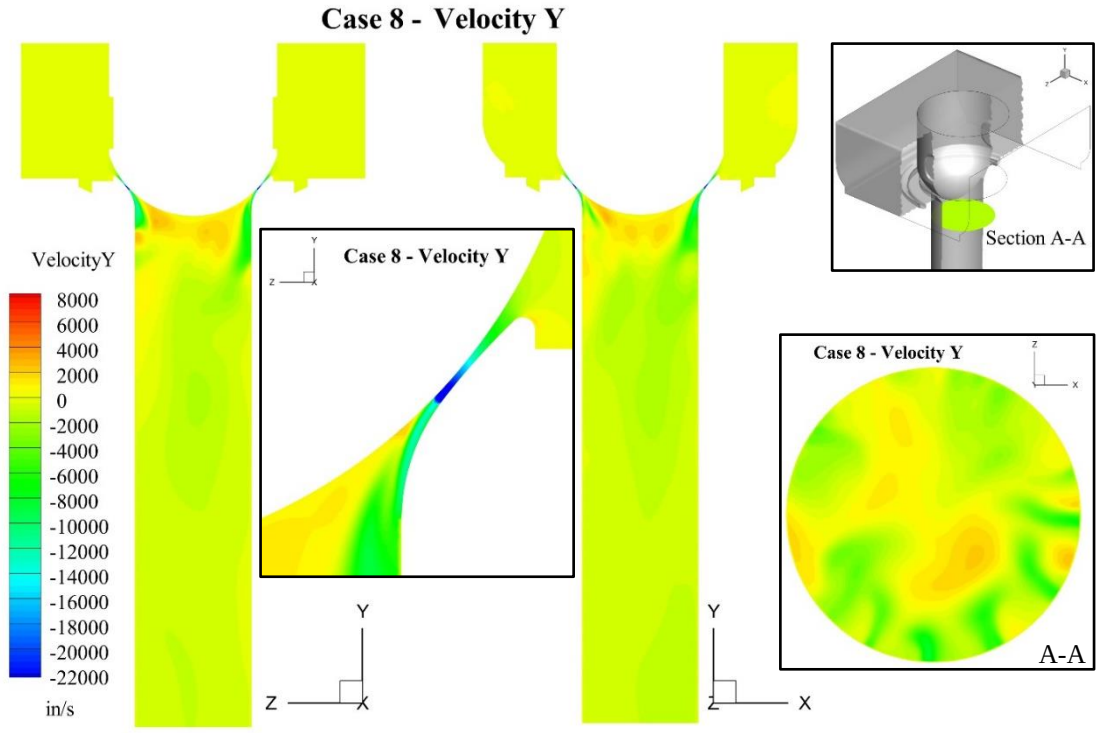

Figure 4.108. Vertical Velocity Contours at $OR = 0.012$, Original Disc, Revision 4 Seat.

With the revision 1 disc, the velocity plots, given in figures 4.109 and 4.110, show the throat flow jets to remain unstable. The only changes in the flow pattern are in the reverse flow regions; the core reverse flow region is more stable due to the flat bottom on the disc and the annular reverse flow region beneath the flow jets is more symmetric. Although there is no separation bubble beneath the throat, the convex curvature of the disc at the cutoff continues to expand the flow to the center of the nozzle. The vortex shedding is still present.

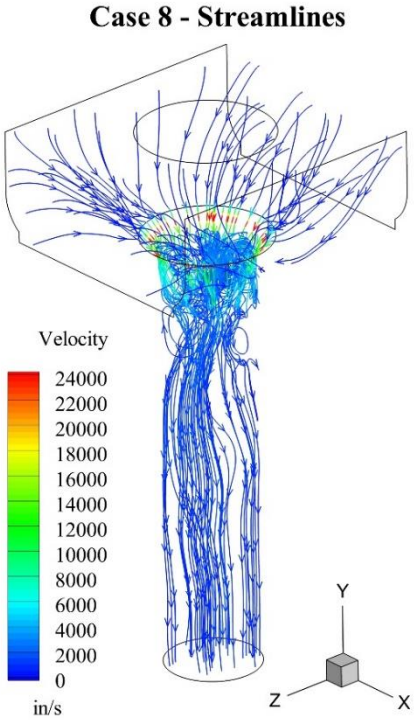

Figure 4.109. Velocity Streamlines at $OR = 0.012$, Revision 1 Disc, Revision 4 Seat.

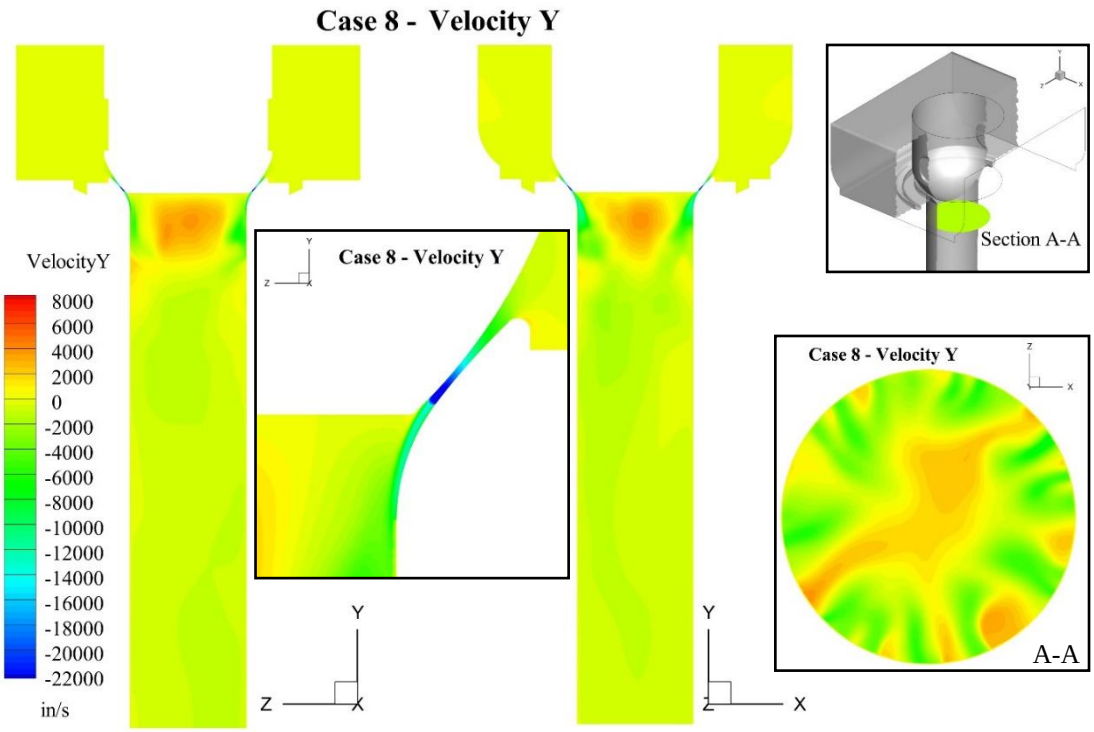

Figure 4.110. Vertical Velocity Contours at $OR = 0.012$, Revision 1 Disc, Revision 4 Seat.

The upstream seat flow attachment is still present for the indented revision 1-6 disc with the revision 4 seat, displayed in figures 4.111 and 4.112. The unstable separation bubble at the throat exit is gone. However, the throat flow jets are still strongly asymmetric from continued vortex shedding. Compared to the unrevised seat velocity plots in figures 4.79 and 4.80, this is a less stable condition.

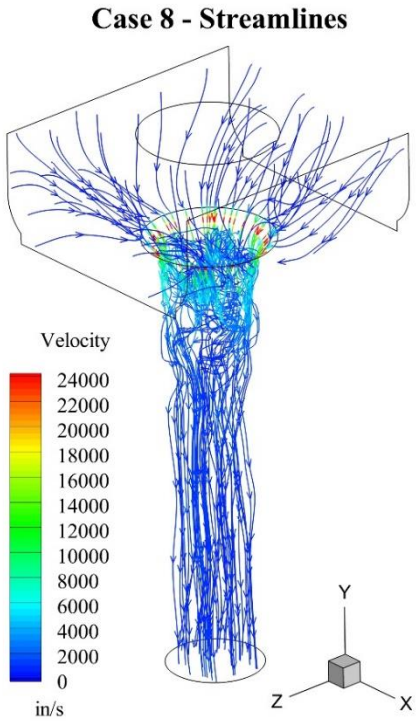

Figure 4.111. Velocity Streamlines at $OR = 0.012$, Revision 1-6 Disc, Revision 4 Seat.

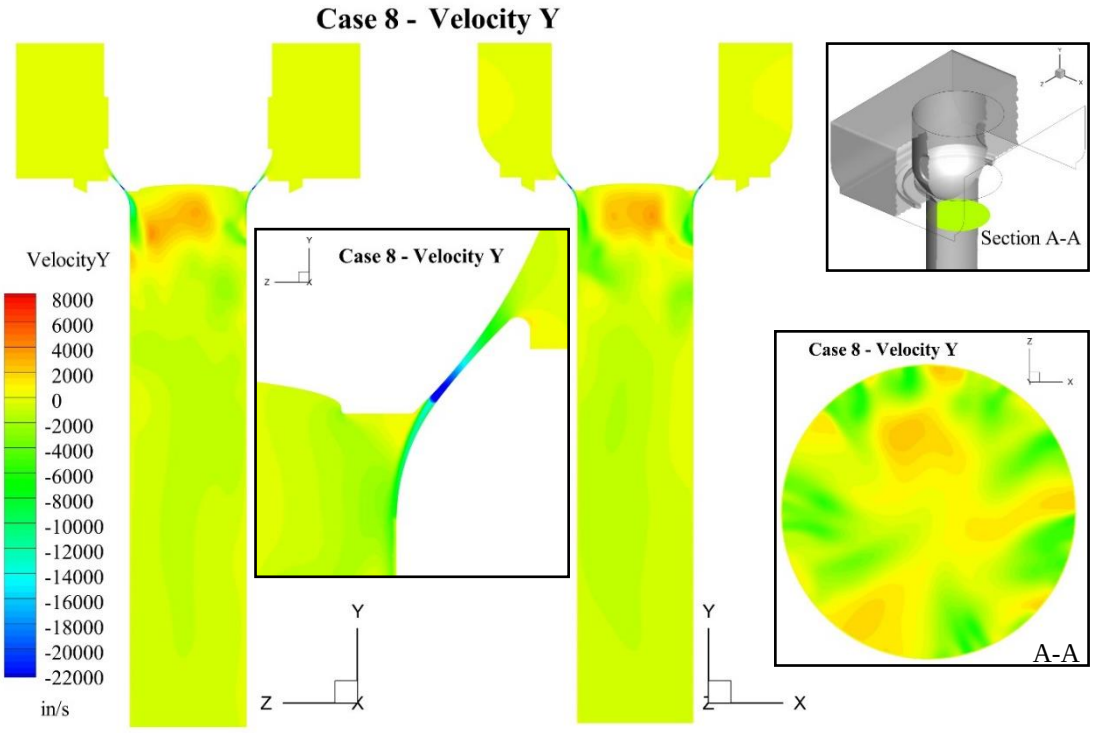

Figure 4.112. Vertical Velocity Contours at $OR = 0.012$, Revision 1-6 Disc, Revision 4 Seat.

The core reverse flow region for the revision 1-12 disc paired with the revision 4 seat at an opening ratio of 0.012, given in figures 4.113 and 4.114, is more stabilized than the revision 1-12 disc with the unrevised seat. There is no longer an unsteady separation bubble at the throat exit, and the vortex shedding is less severe.

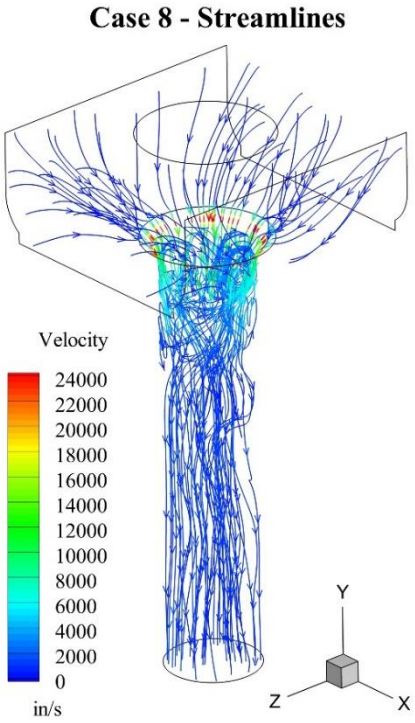

Figure 4.113. Velocity Streamlines at $OR = 0.012$, Revision 1-12 Disc, Revision 4 Seat.

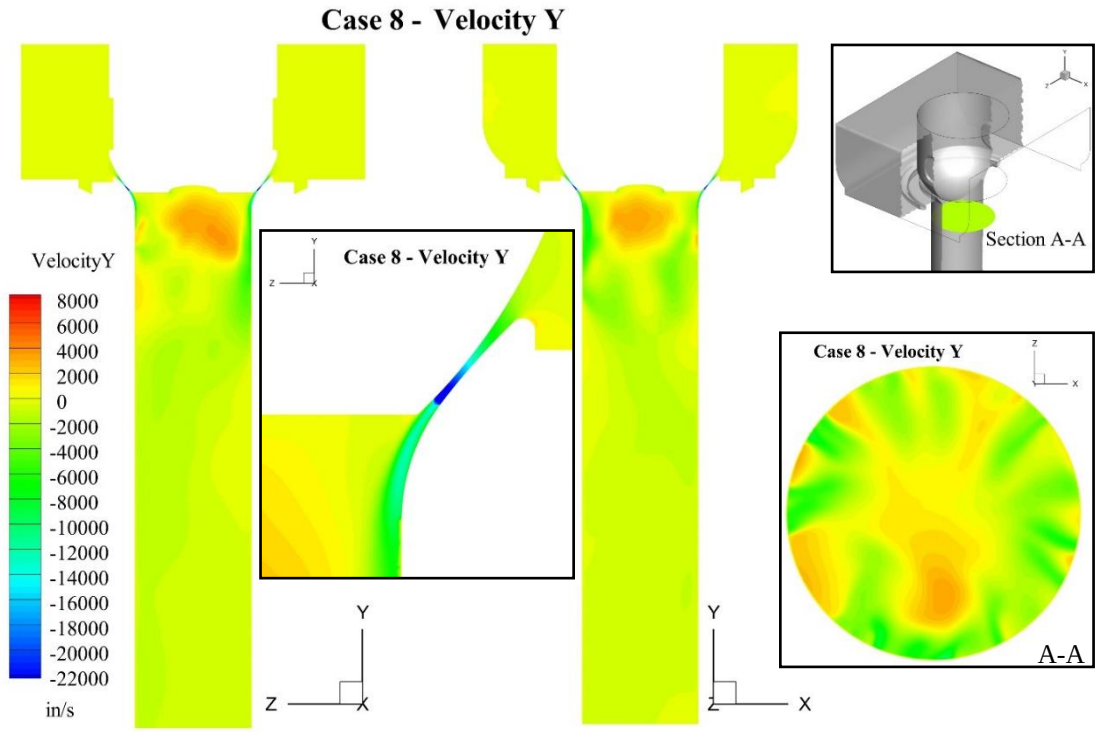

Figure 4.114. Vertical Velocity Contours at $OR = 0.012$, Revision 1-12 Disc, Revision 4 Seat.

4.5.3.4.2. Opening ratio = 0.024

When the opening ratio increases to 0.024, the disc flow separation observed in figure 4.108 disappears and is replaced by a flow tail attached to the disc, shown in figures 4.115 and 4.116. Compared to the unrevised seat, displayed in figure 4.19, the flow tail is stronger and slightly less violent. The reverse annular flow is more symmetric, and there is no upstream flow separation.

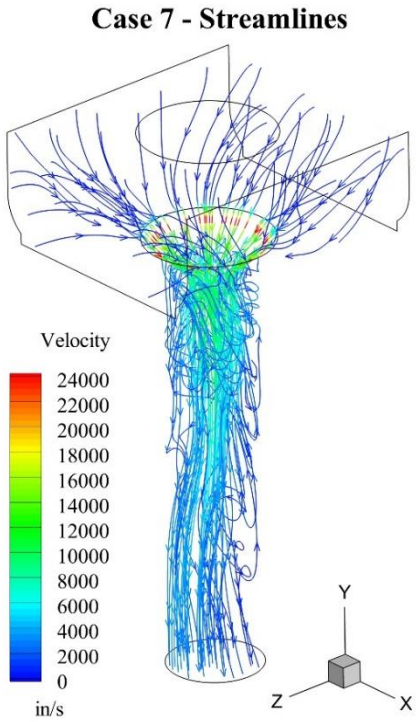

Figure 4.115. Velocity Streamlines at $OR = 0.024$, Original Disc, Revision 4 Seat.

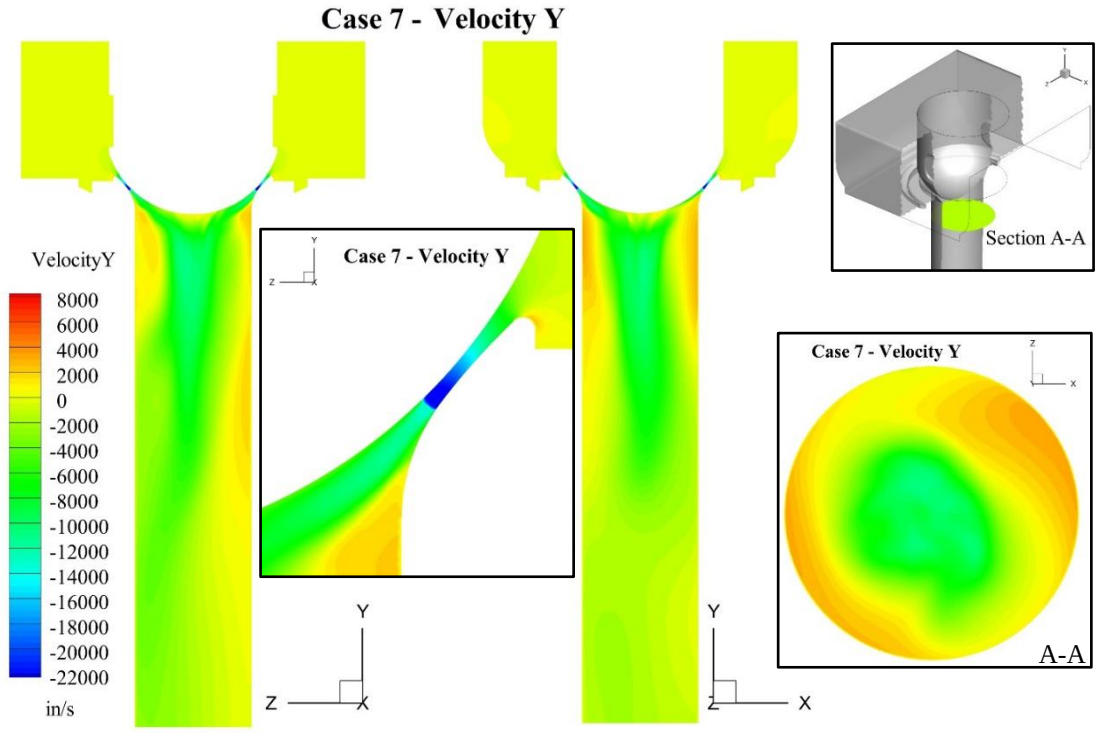

Figure 4.116. Vertical Velocity Contours at $OR = 0.024$, Original Disc, Revision 4 Seat.

The revision 1 disc flow pattern with the revision 4 seat, shown in figures 4.117 and 4.118, does not change significantly from the unrevised seat when the opening ratio increases to 0.024. The upstream throat flow remains attached and the flow velocity does not increase as much when traveling around the downstream edge.

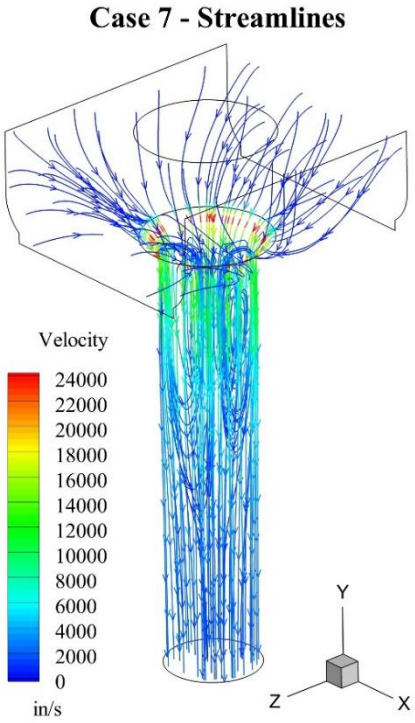

Figure 4.117. Velocity Streamlines at $OR = 0.024$, Revision 1 Disc, Revision 4 Seat.

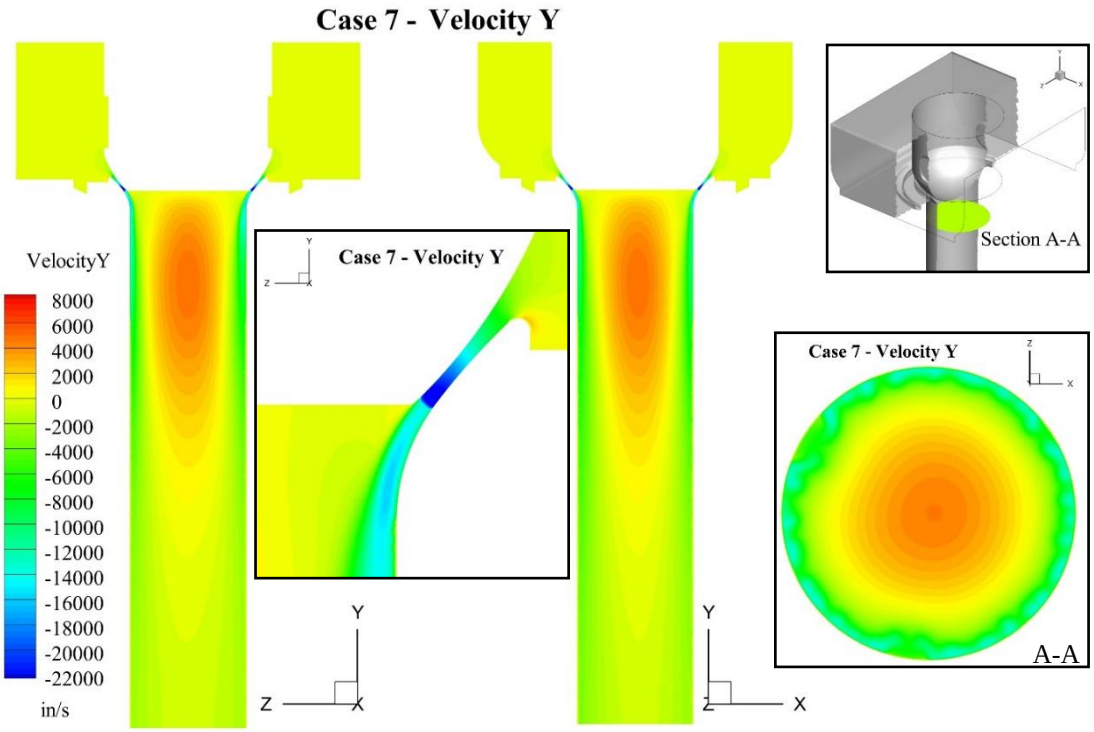

Figure 4.118. Vertical Velocity Contours at $OR = 0.024$, Revision 1 Disc, Revision 4 Seat.

4.6. Steady State Pressure Forces

The lower portion of the disc, shown in figure 4.2, was used as the surface for obtaining all pressure force measurements. An area integral of the pressure over the selected surface was calculated in each coordinate direction. Due to disc axisymmetry in the lateral direction, a zero *x*-*z* force magnitude indicates a stable flow pattern void of pressure fluctuations to excite valve vibration. Detailed force analysis including the time parameter is completed in section 4.7 for baseline valve designs and those with low lateral forces.

The results are given in order of increasing opening ratio. The original and revision 1 discs, which were used as the baseline discs, were simulated first for all cases. Some discs did not show enough of a flow pattern improvement at the initial case they were simulated at so they were not used at all operating points. Opening ratios 0.014 and 0.028 were intermediate cases;

only a few valve configurations were simulated at them before they were adjusted, as discussed in section 3.3.3. Because the forces are steady state, and the flow problem is unstable, there is some variation in the data obtained. The force values are only taken as an indication of force reduction because complete convergence to 1×10^{-6} was not obtained.

4.6.1.1. Opening ratio = 0.007

In table 4.5, the two designs that incorporated an extension, revisions 1-1 and 1-3, show a greater lateral force magnitude than the original geometry. This concurs with the plots for these designs. The seat revisions all have high lateral forces; the force increases with the seat edge radius. The cutoff designs all have similar lateral forces. The revision 1, 1-2, and 1-6 discs all have low forces, and were some of the designs that had the most promising flow patterns. As expected, the revision 1-16 disc, which has the only stable flow pattern at an opening ratio of 0.007, has practically no lateral force on the disc surface in the throat. It is also the only design that has a vertical force comparable to the original disc. All of the other vertical forces are very similar, but at a higher level.

Table 4.5. Steady State Pressure Forces on Throat Region of Disc at *OR* = 0.007.

***OR* = 0.007**	**Pressure Force X (lbf)**	**Pressure Force Y (lbf)**	**Pressure Force Z (lbf)**	**X-Z Force Magnitude**
Original Disc	-4.13	30732.40	1.82	4.52
Revision 1 Disc	2.47	31302.50	3.27	4.10
Revision 1 Disc, Revision 1 Seat	2.37	31304.30	-3.57	4.29
Revision 1 Disc, Revision 2 Seat	4.69	31310.70	1.45	4.91
Revision 1-1 Disc	11.08	31282.60	-6.57	12.88
Revision 1-2 Disc	2.21	31259.20	3.12	3.82
Revision 1-3 Disc	-14.84	31217.50	3.35	15.22
Revision 1-3 Disc, Revision 2 Seat	1.81	31252.50	5.74	6.02
Revision 1-4 Disc	-4.51	31313.80	1.43	4.73
Revision 1-6 Disc	-0.65	31302.20	0.59	0.88
Revision 1-16 Disc	0.11	30793.70	0.04	0.12

4.6.1.2. Opening ratio = 0.012

The seat revision steady-state pressure forces at case 8, listed in table 4.6, still indicate significantly higher lateral disc forces than the original disc. The revision 1-16 disc has very low lateral forces, as does the revision 1-12 disc with a rough seat. All force data correlates well with the flow pattern analysis.

Table 4.6. Steady State Pressure Forces on Throat Region of Disc at *OR* = 0.012.

***OR* = 0.012**	**Pressure Force X (lbf)**	**Pressure Force Y (lbf)**	**Pressure Force Z (lbf)**	**X-Z Force Magnitude**
Original Disc	-9.03	30586.10	12.28	15.24
Original Disc, Revision 4 Seat	-5.10	30571.60	39.88	40.20
Revision 1 Disc	3.10	30503.40	-2.80	4.18
Revision 1 Disc, Revision 4 Seat	-2.42	30600.80	-5.26	5.79
Revision 1-6 Disc	-4.27	30499.40	3.04	5.25
Revision 1-6 Disc, Revision 4 Seat	2.79	30583.00	-4.05	4.92
Revision 1-12 Disc	-3.44	30502.30	0.62	3.50
Revision 1-12 Disc, Revision 4 Seat	-7.03	30580.40	7.15	10.03
Revision 1-12 Disc, Rough Seat	-2.32	30747.20	-1.89	2.99
Revision 1-14 Disc, Revision 4 Seat	-3.54	30585.80	2.91	4.58
Revision 1-16 Disc	-0.22	30705.20	-0.04	0.22

4.6.1.3. Opening ratio = 0.014

Only the revision 1 design was run at operation point 6 before it was cancelled. The low lateral force for this case, shown in table 4.7, corresponds well to the other revision 1 disc cases.

Table 4.7. Steady State Pressure Forces on Throat Region of Disc at *OR* = 0.014.

***OR* = 0.014**	**Pressure Force X (lbf)**	**Pressure Force Y (lbf)**	**Pressure Force Z (lbf)**	**X-Z Force Magnitude**
Revision 1 Disc	-1.09	30696.20	0.68	1.29

4.6.1.4. Opening ratio = 0.018

The original valve design has a very large lateral force, as listed in table 4.8. All design modifications are an improvement over it. As with an opening ratio of 0.007, most of the

extended design discs have a higher lateral force. The cutoff designs again show the smallest lateral forces.

Table 4.8. Steady State Pressure Forces on Throat Region of Disc at *OR* = 0.018.

***OR* = 0.018**	**Pressure Force X (lbf)**	**Pressure Force Y (lbf)**	**Pressure Force Z (lbf)**	**X-Z Force Magnitude**
Original Disc	15.46	30592.30	-29.14	32.99
MPC Modification Disc	-11.16	30083.38	10.66	15.43
Modification 1 Disc	0.61	30306.31	0.03	0.61
Modification 2 Disc	20.27	30109.71	8.32	21.91
Modification 3 Disc	-0.41	29926.51	5.03	5.05
Modification 4 Disc	-6.74	29974.86	-10.00	12.06
Modification 5 Disc	10.28	29942.11	0.09	10.28
Modification 6 Disc	-7.89	29772.86	-5.55	9.65
Modification 7 Disc	1.92	30364.40	2.03	2.79
Modification 8 Disc	-0.03	30492.75	0.21	0.21
Revision 1 Disc	-2.89	30850.20	1.48	3.25
Revision 1-16 Disc	1.71	30829.70	-1.94	2.59

4.6.1.5. Opening ratio = 0.024

All revised designs, listed in table 4.9, show a substantial reduction in lateral forces on the disc throat over the original at case 7. As with an opening ratio of 0.007, all seat revisions perform worse than their unmodified counterparts.

Table 4.9. Steady State Pressure Forces on Throat Region of Disc at *OR* = 0.024.

***OR* = 0.024**	**Pressure Force X (lbf)**	**Pressure Force Y (lbf)**	**Pressure Force Z (lbf)**	**X-Z Force Magnitude**
Original Disc	-16.20	30477.30	-8.31	18.21
Original Disc, Revision 4 Seat	8.96	30360.00	-14.05	16.66
Revision 1 Disc	-1.85	30271.60	2.10	2.80
Revision 1 Disc, Revision 4 Seat	3.24	30324.80	-1.31	3.49
Revision 1-6 Disc	0.06	30264.40	0.11	0.13
Revision 2 Disc	-0.76	31457.70	1.17	1.40

4.6.1.6. Opening ratio = 0.028

At an opening ratio of 0.028, the revision 1-8 and 1-10 discs have extremely large lateral forces, as displayed in table 4.10. These discs showed the most unstable velocity pattern. The other revision discs are all improvements over the original.

Table 4.10. Steady State Pressure Forces on Throat Region of Disc at *OR* = 0.028.

***OR* = 0.028**	**Pressure Force X (lbf)**	**Pressure Force Y (lbf)**	**Pressure Force Z (lbf)**	**X-Z Force Magnitude**
Original Disc	-5.96	30979.10	5.37	8.02
Revision 1 Disc	0.18	30837.70	-1.19	1.20
Revision 1-6 Disc	-0.64	30833.30	-2.16	2.25
Revision 1-8 Disc	37.06	31145.00	-187.61	191.24
Revision 1-10 Disc	66.75	30984.90	-202.10	212.84
Revision 2 Disc	-0.31	32146.30	1.51	1.54

4.7. Transient Numerical Results

After the steady state analysis was complete, time-dependent simulations were used to determine the characteristics of the pressure forces on the disc surface in the throat region (figure 4.2). The original valve configuration and the revision 1 disc, the baseline designs, were investigated first. Designs that performed well in the steady-state analysis were then compared to these results. The revision 1-6, 1-12, 1-14, and 1-16 discs were used. The revision 4 seat was also paired with the revision 1 and 1-14 discs to examine the accuracy of the steady state forces.

As with the steady state forces, the area integral of the pressure on the disc in the throat section was used to determine the pressure forces. This was calculated at each timestep and plotted against time. The timestep was initially set at 5×10^{-4} seconds; this was refined to 5×10^{-5} seconds to capture the vortex shedding off of the original hemispherical disc. The total time for each simulation was set to 0.01 seconds. All simulations showed consistent behavior by this time. The results are compared by case.

The revision 2 disc was studied in the time-dependent analysis, but did not show promising results. Investigation on it was stopped before the final timestep was selected, so the results are not included.

4.7.1. Opening Ratio = 0.028

4.7.1.1. Original hemispherical disc

The transient force magnitude and frequency on the original disc wall at case 8 are very unsteady in the lateral direction, as shown in figure 4.119. In the vertical direction, the force magnitude given in figure 4.120 is large, but develops a consistent frequency. The force characteristics correspond well with the reports from MPC concerning severe valve vibrations with the original disc.

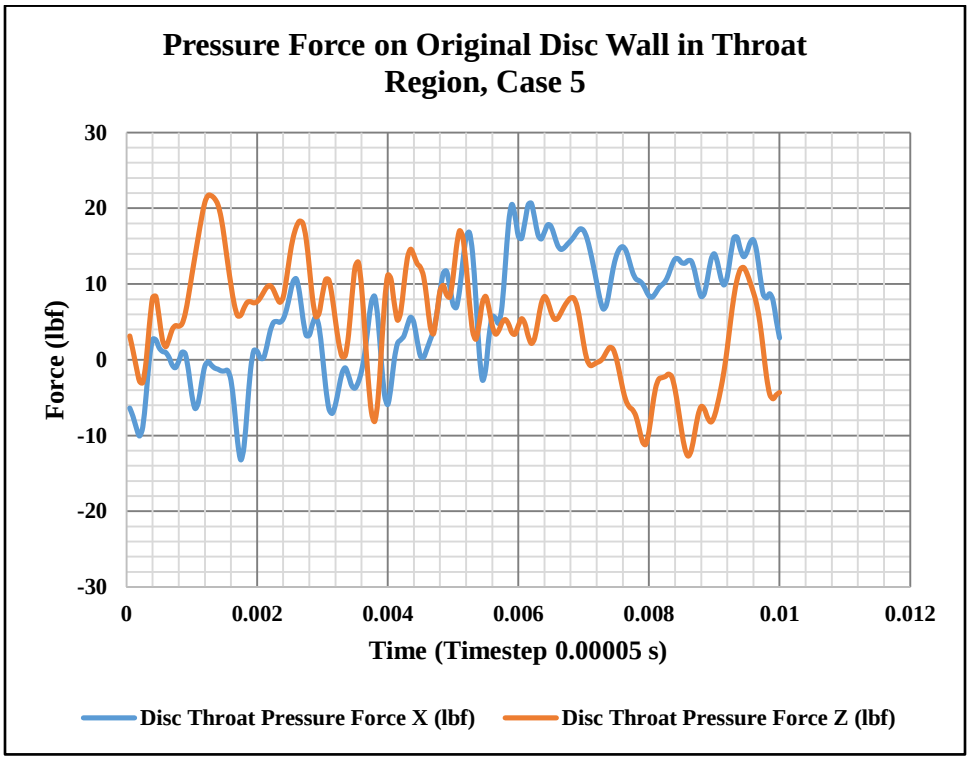

Figure 4.119. Transient Lateral Forces on Original Disc at $OR = 0.028$.

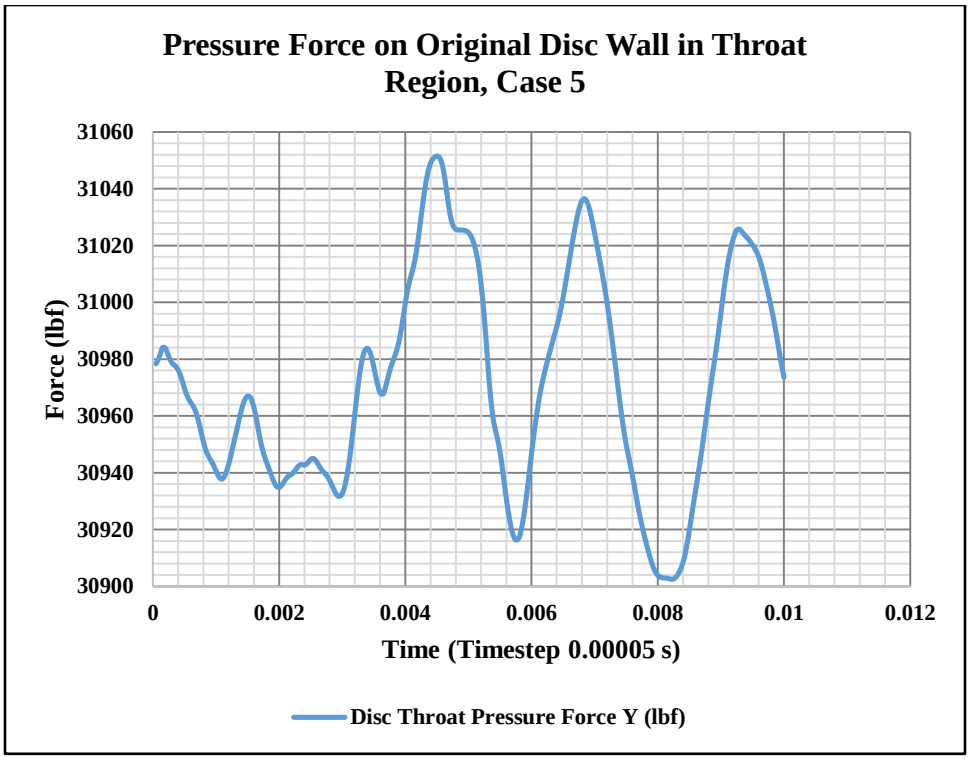

Figure 4.120. Transient Vertical Forces on Original Disc at $OR = 0.028$.

4.7.1.2. Revision 1 disc

At an opening ratio of 0.028, the revision 1 disc reduces the pressure forces to a steady low force in the lateral direction, as given in figure 4.121. In the vertical direction, figure 4.122 shows a constant force. The flow pattern for the revision 1 disc shows stable annular flow; the transient force analysis verifies the stability.

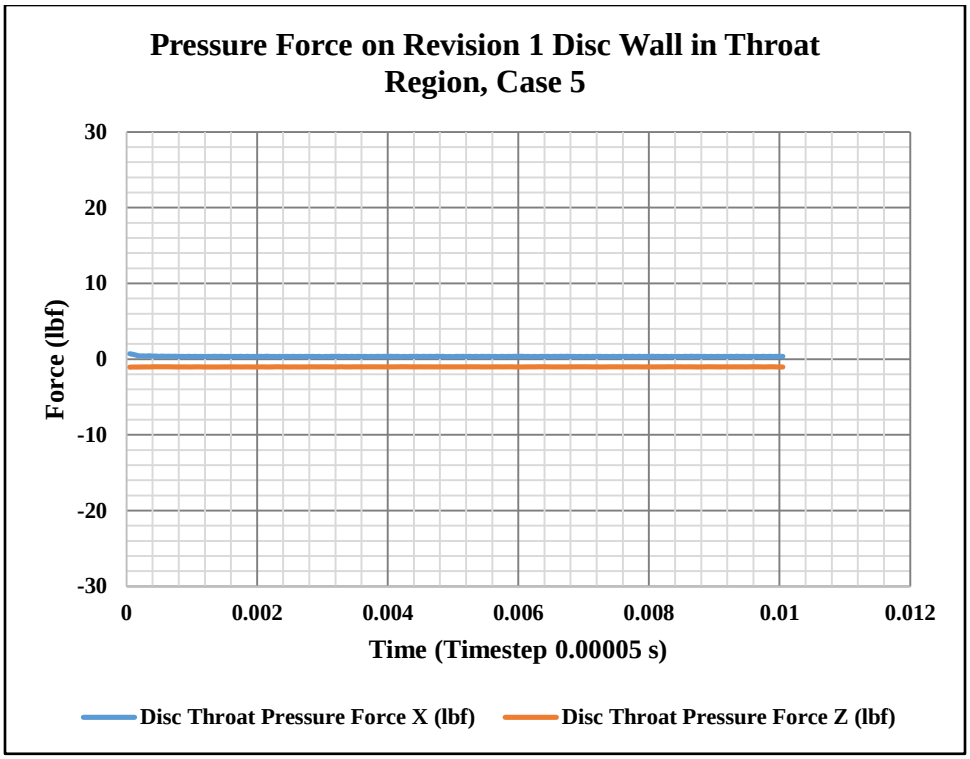

Figure 4.121. Transient Lateral Forces on Revision 1 Disc at $OR = 0.028$.

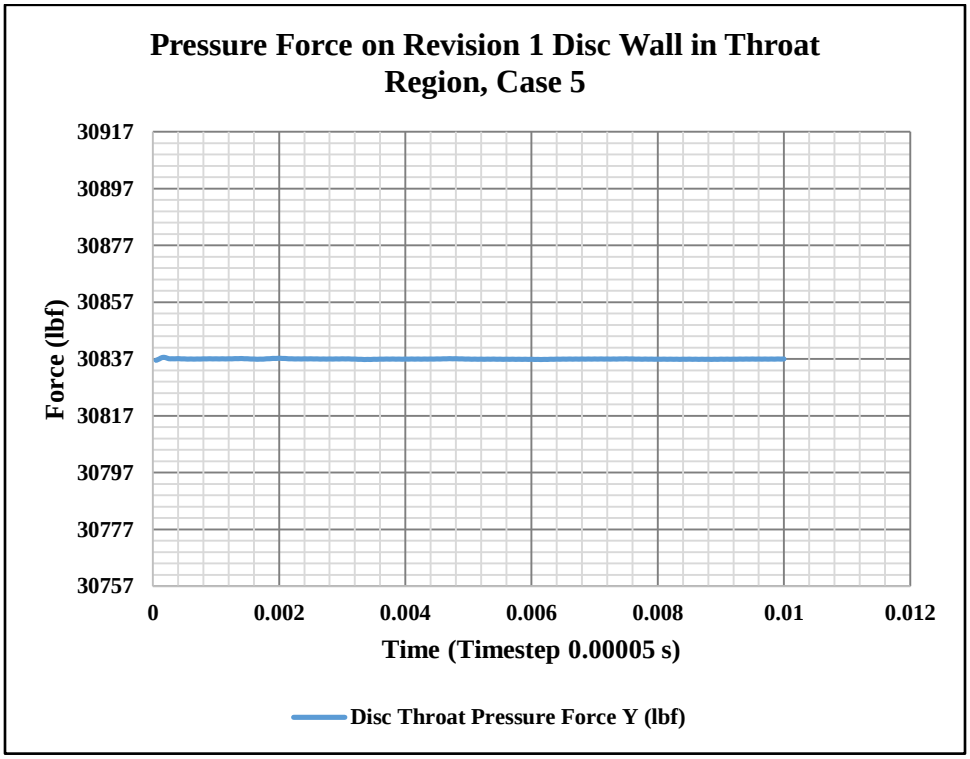

Figure 4.122. Transient Vertical Forces on Revision 1 Disc at $OR = 0.028$.

4.7.1.3. Revision 1-6 disc

The lateral forces on the throat surface of the revision 1-6 disc, displayed in figure 4.123, are slightly greater and more unstable than the revision 1 disc. The vertical force magnitude, given in figure 4.124, is less than the revision 1 disc. Both the flow patterns and transient plots for these discs are very similar.

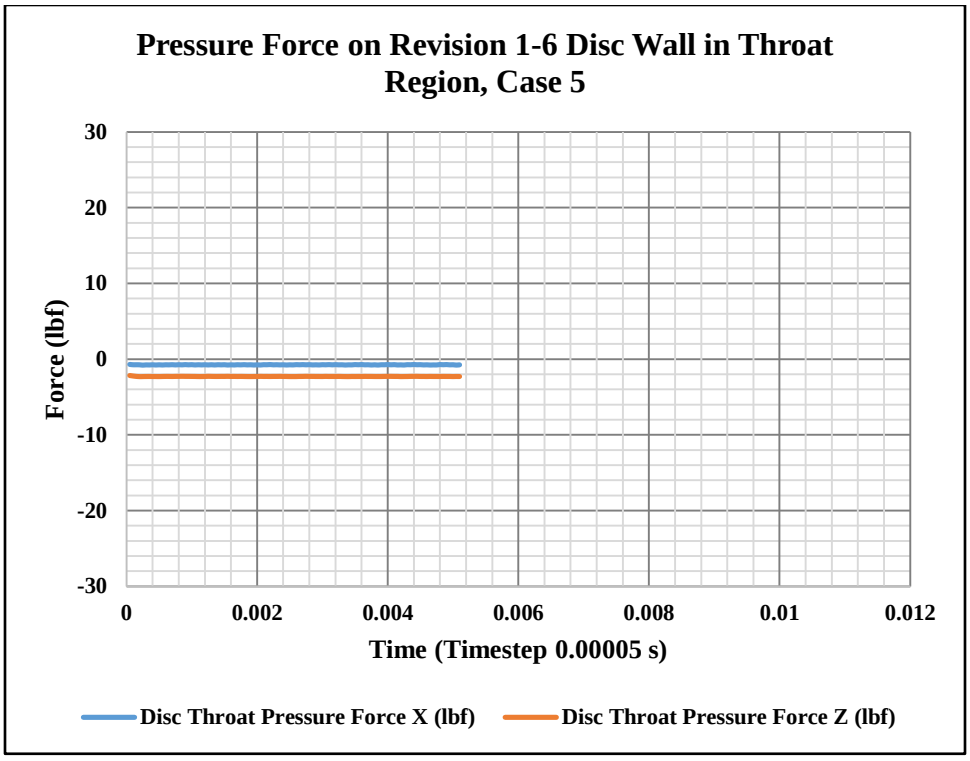

Figure 4.123. Transient Lateral Forces on Revision 1-6 Disc at $OR = 0.028$.

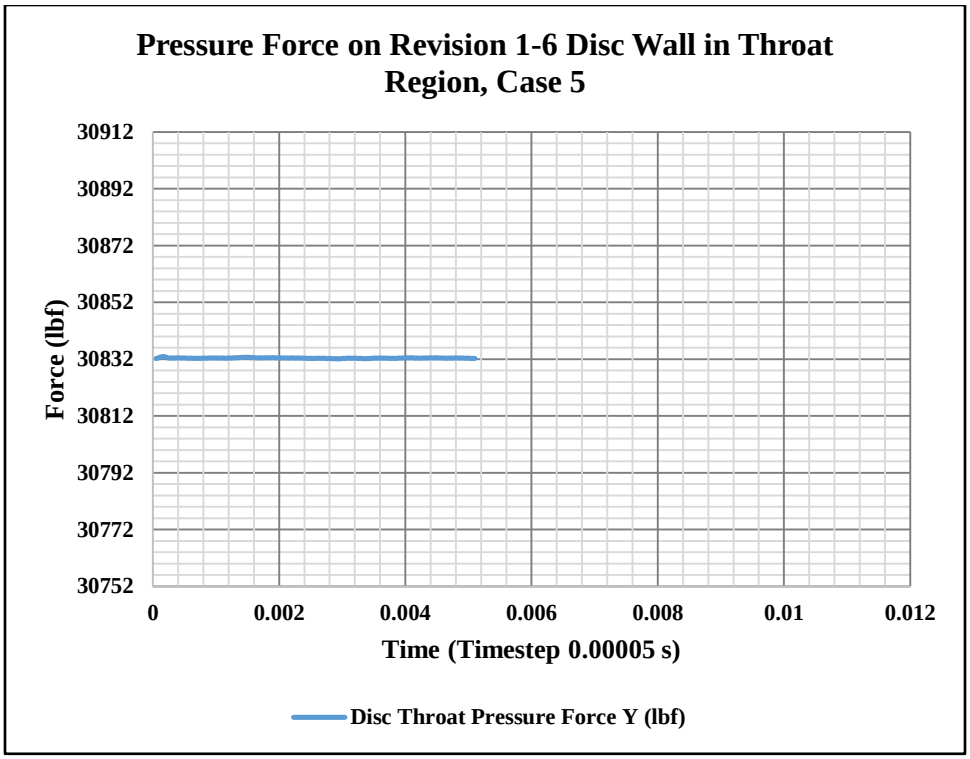

Figure 4.124. Transient Vertical Forces on Revision 1-6 Disc at $OR = 0.028$.

4.7.2. Opening Ratio = 0.024

4.7.2.1. Original hemispherical disc

The original disc shows the same transient instability at case 7, plotted in figures 4.125 and 4.126, that is present at an opening ratio of 0.028. The lateral force magnitude and frequency are more severe, but the vertical force does not fluctuate as intensely.

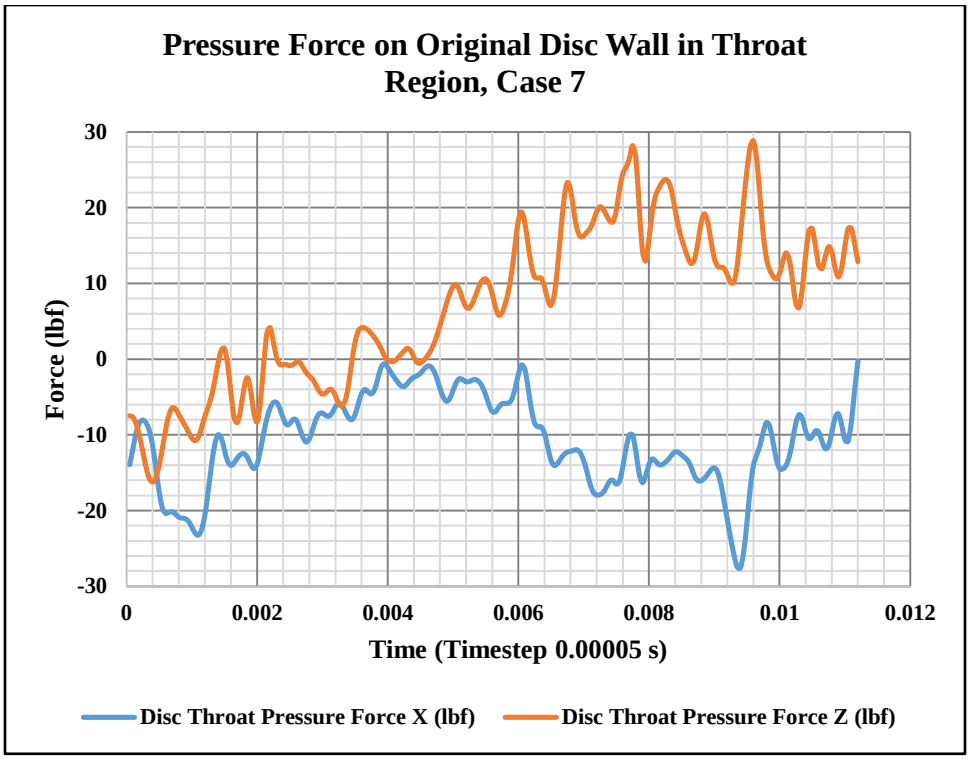

Figure 4.125. Transient Lateral Forces on Original Disc at $OR = 0.024$.

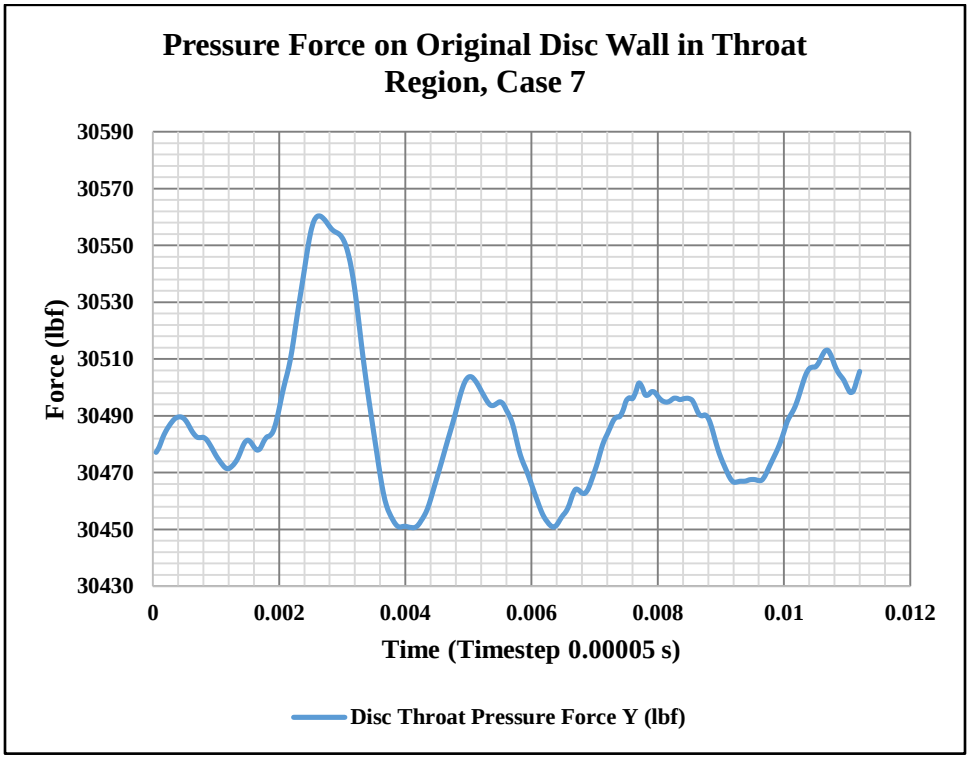

Figure 4.126. Transient Vertical Forces on Original Disc at $OR = 0.024$.

4.7.2.2. Revision 1 disc

As with an opening ratio of 0.028, the lateral forces on the revision 1 disc are reduced to a very low, stable value, as shown in figure 4.127. The vertical force, given in figure 4.128, is also mostly steady.

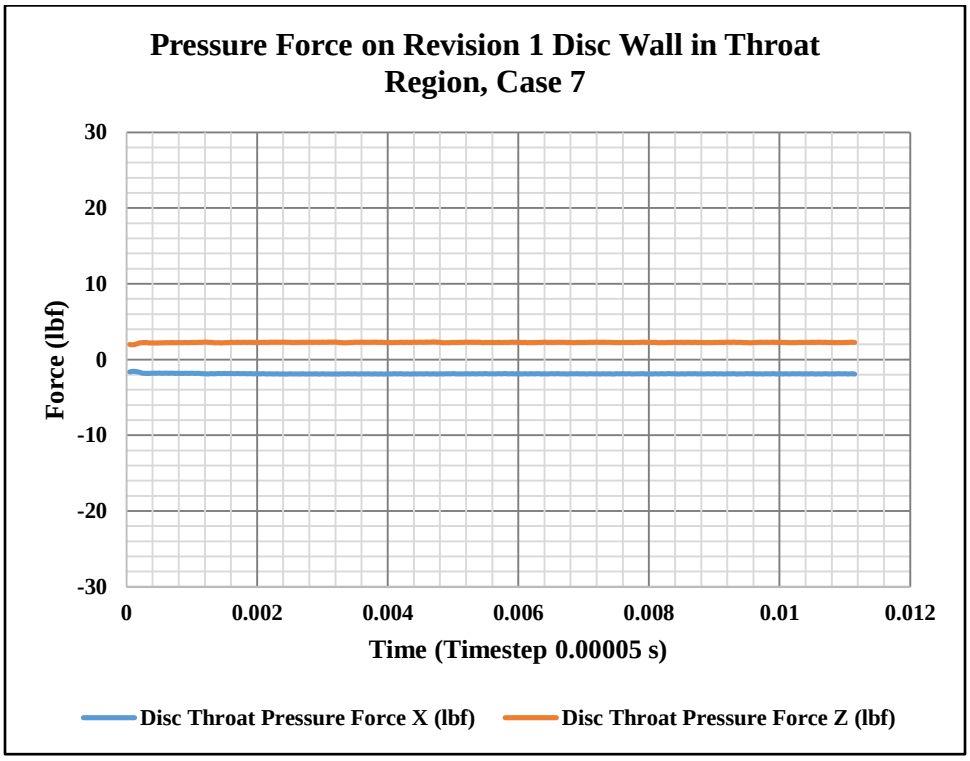

Figure 4.127. Transient Lateral Forces on Revision 1 Disc at $OR = 0.024$.

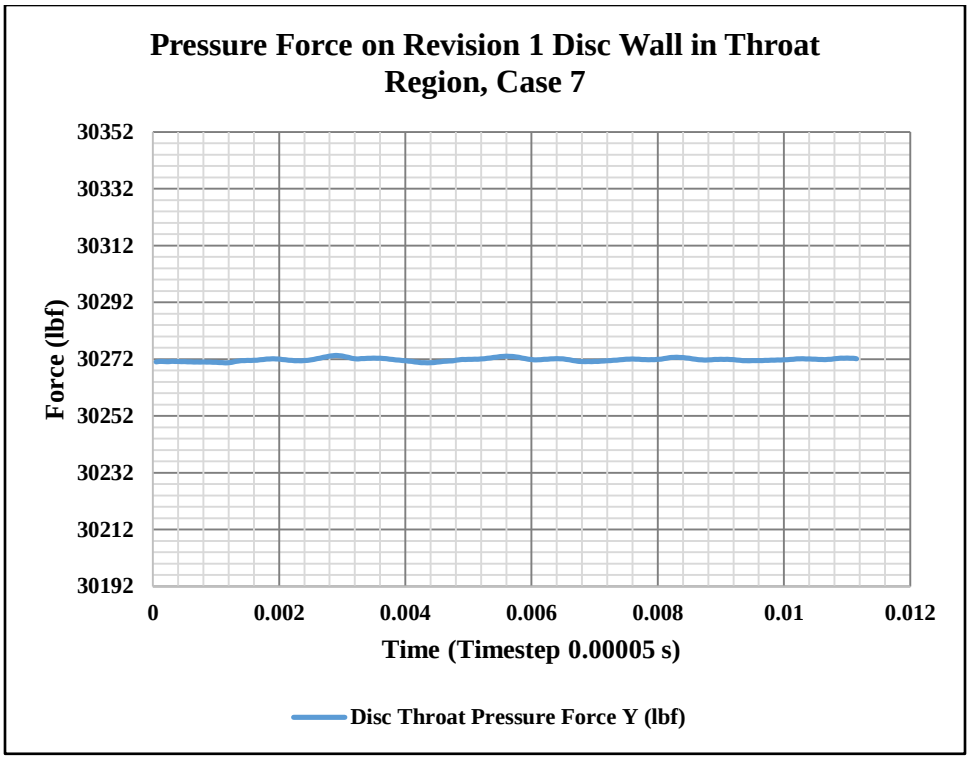

Figure 4.128. Transient Vertical Forces on Revision 1 Disc at $OR = 0.024$.

4.7.2.3. Revision 1-6 disc

The revision 1-6 disc is an improvement over the revision 1 disc at an opening ratio of 0.024, reducing the slight lateral forces, displayed in figure 4.129, to near zero. The vertical forces, shown in figure 4.130, are further stabilized.

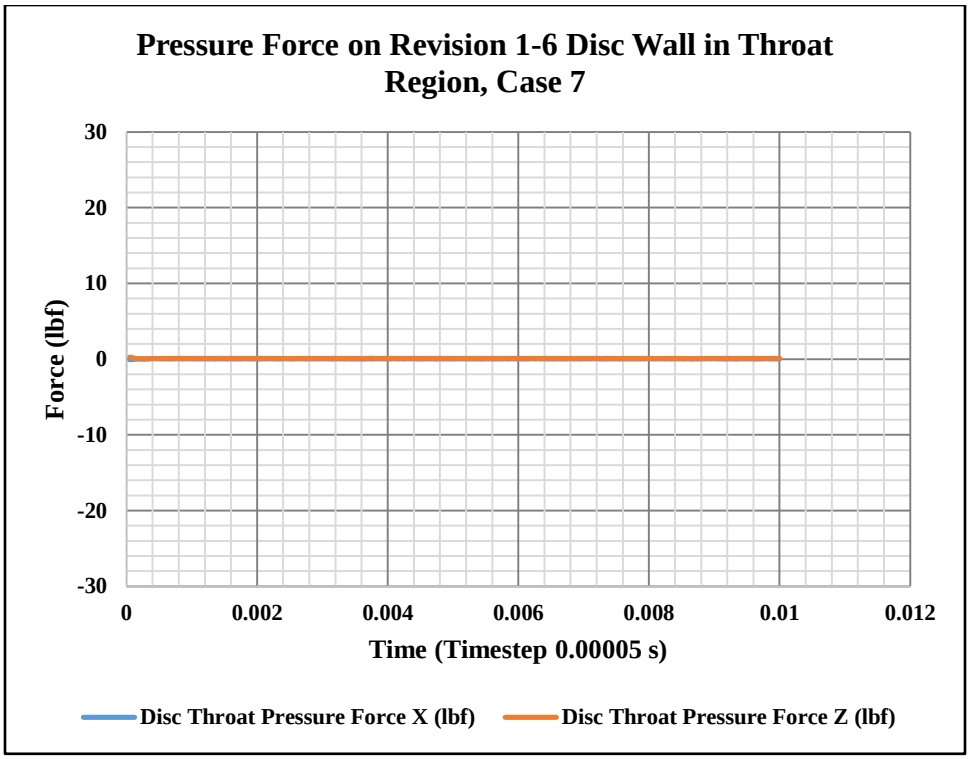

Figure 4.129. Transient Lateral Forces on Revision 1-6 Disc at $OR = 0.024$.

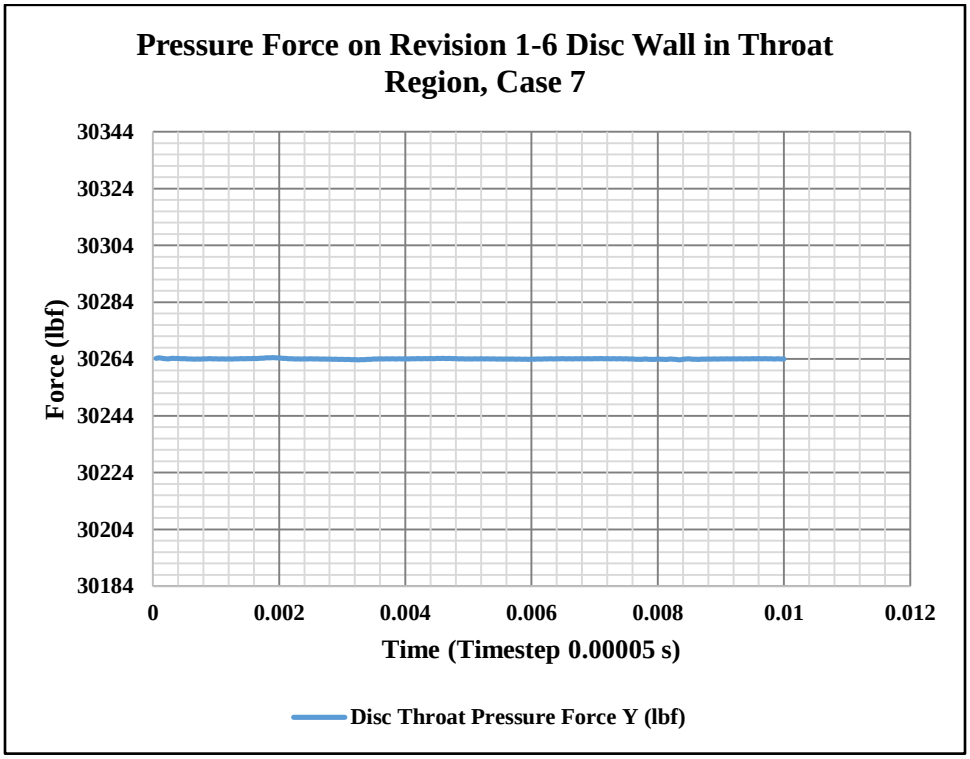

Figure 4.130. Transient Vertical Forces on Revision 1-6 Disc at $OR = 0.024$.

4.7.3. Opening Ratio = 0.012

4.7.3.1. Original hemispherical disc

Unlike the higher opening ratio cases, the frequency of the lateral forces on the disc throat surface, shown in figure 4.131, is steady at case 8. The magnitude of the forces is comparable to the other cases. The vertical force frequency, given in figure 4.132, is more stable and the magnitude is lower.

The velocity flow patterns in figure 4.133 show that the flow separating off of the back of the disc fluctuates from side to side. As the throat flow jets fight each other for attachment to the disc, the flow tail moves back and forth, shedding vortices and applying uneven pressure fluctuations to the disc surface.

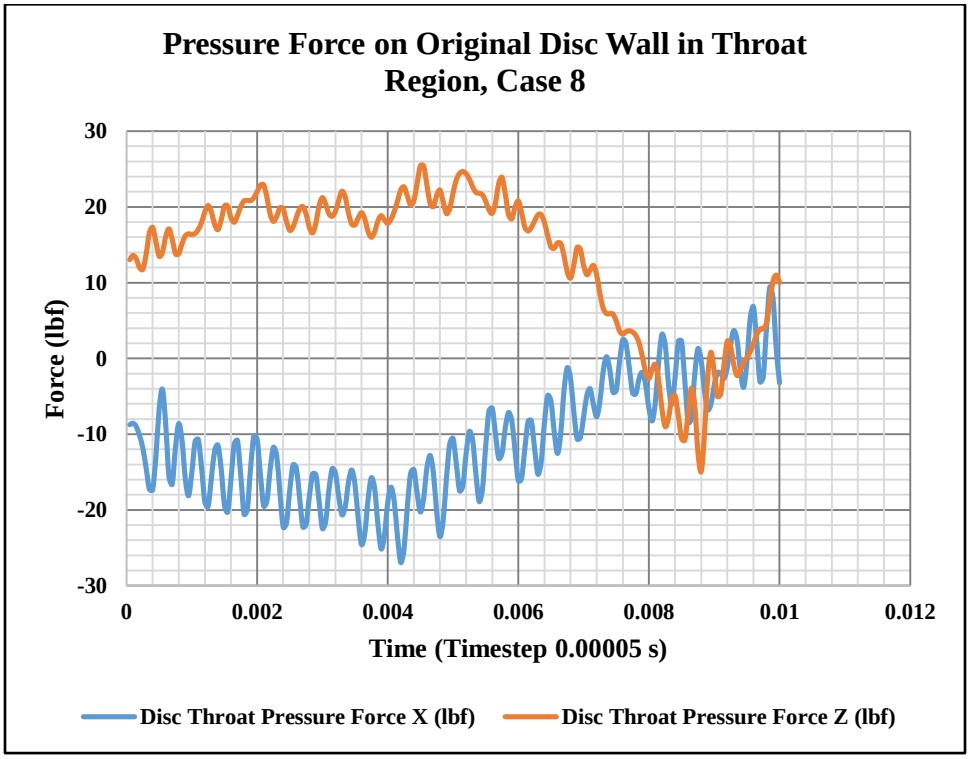

Figure 4.131. Transient Lateral Forces on Original Disc at $OR = 0.012$.

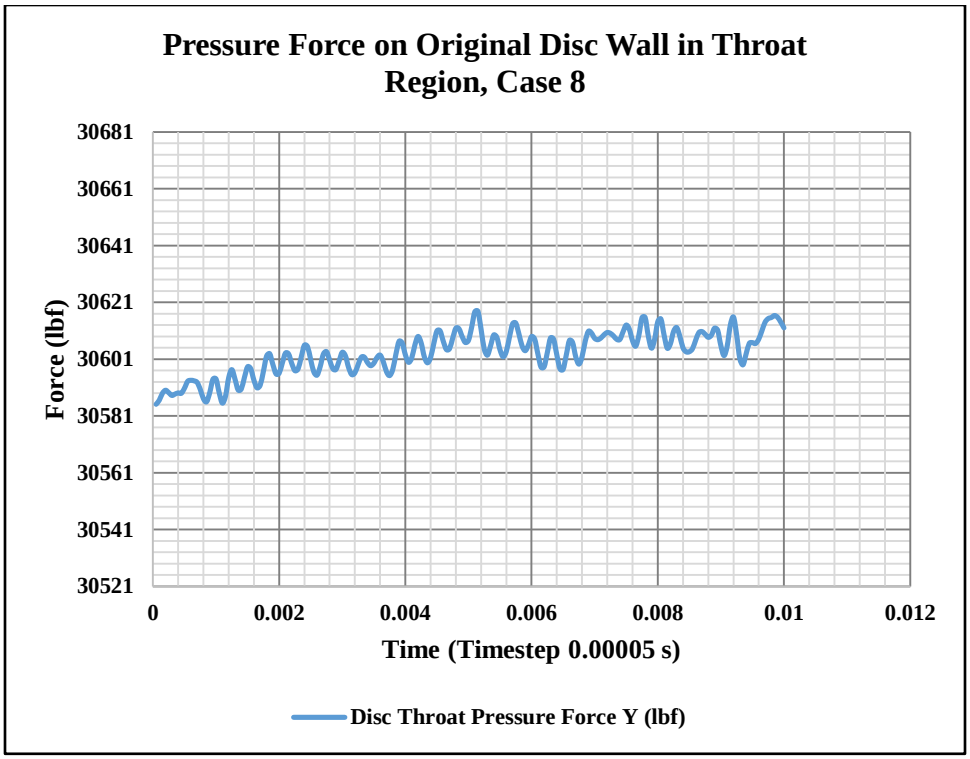

Figure 4.132. Transient Vertical Forces on Original Disc at $OR = 0.012$.

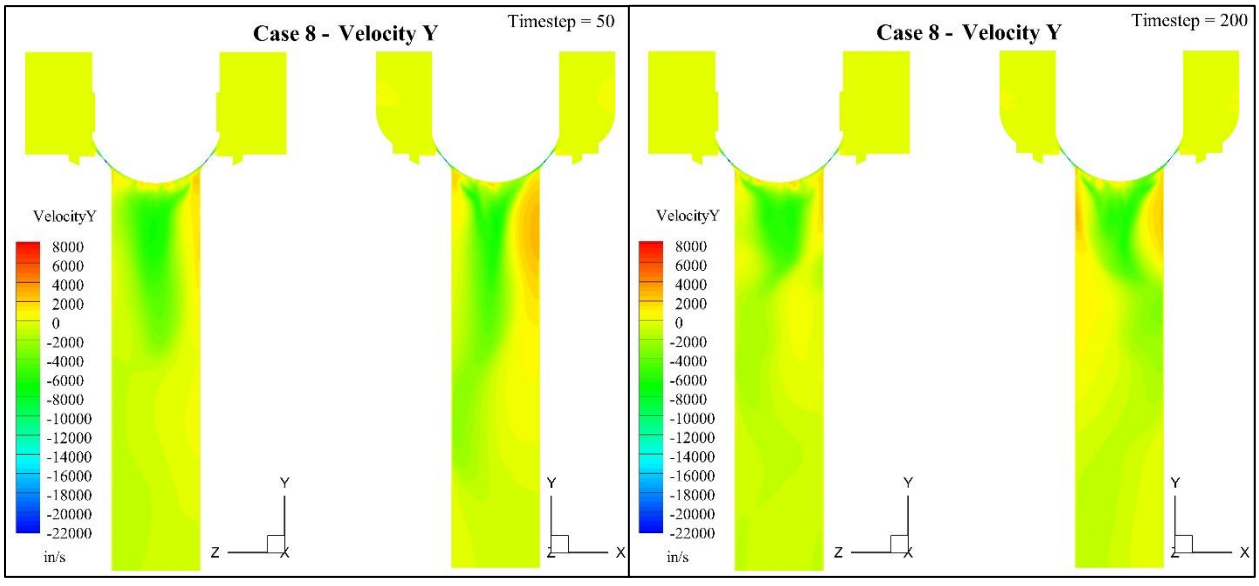

Figure 4.133. Comparison of Original Disc Flow Patterns at 0.0025 (L) and 0.01 (R) Seconds.

4.7.3.2. Revision 1 disc

The revision 1 disc does not provide nearly as much lateral force reduction at an opening ratio of 0.012, shown in figure 4.134, as at an opening ratio of 0.024 or 0.028. This aligns with the MPC report that the revision 1 disc was unable to remove the valve vibrations, but did seem to reduce their intensity. The vertical forces, given in figure 4.135, are also lower than the original disc, but higher than the larger opening ratios.

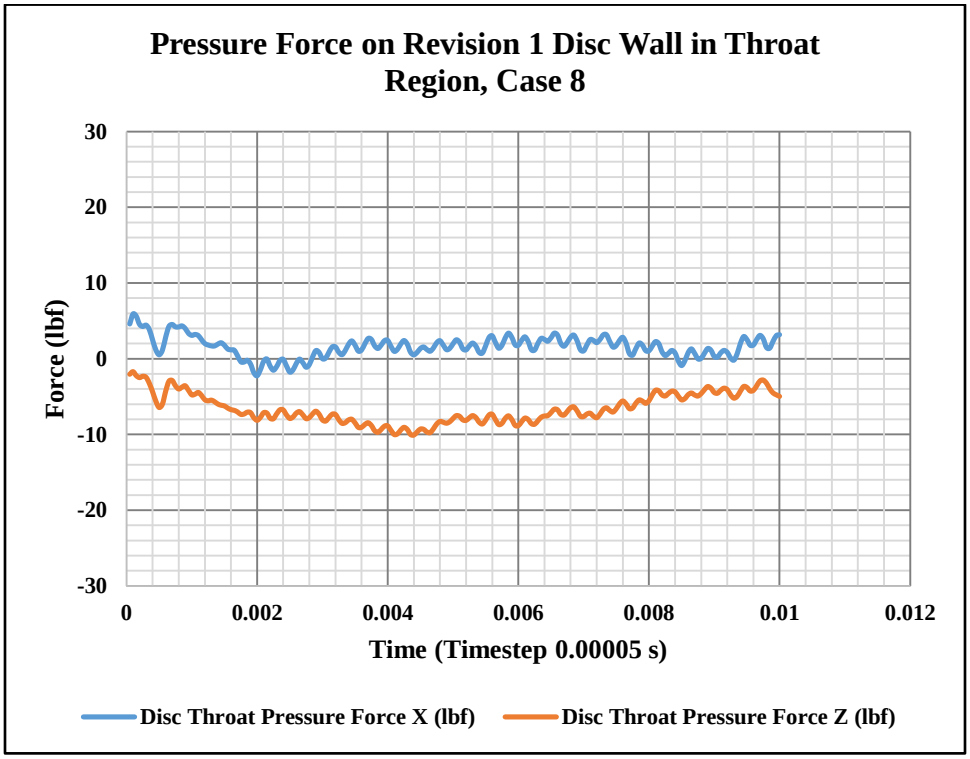

Figure 4.134. Transient Lateral Forces on Revision 1 Disc at $OR = 0.012$.

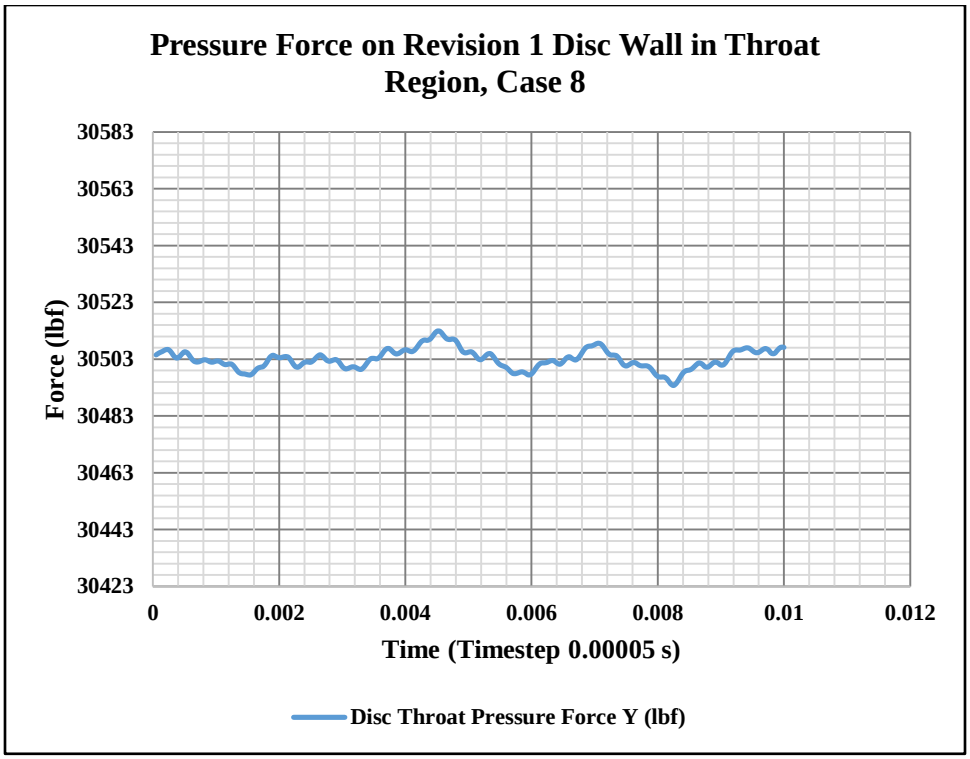

Figure 4.135. Transient Vertical Forces on Revision 1 Disc at $OR = 0.012$.

4.7.3.3. Revision 1-12 disc

With the addition of an indentation to the revision 1 disc, the pressure forces decrease considerably. Figure 4.136 shows reduced force oscillation in the lateral direction. The vertical force, displayed in figure 4.137, is unchanged.

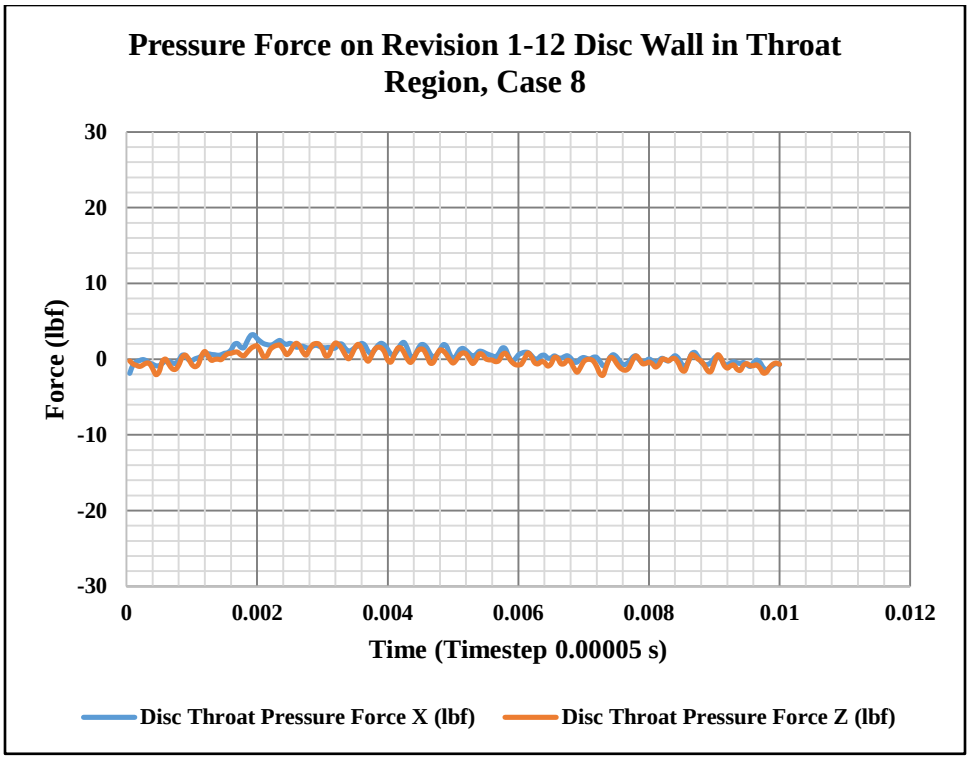

Figure 4.136. Transient Lateral Forces on Revision 1-12 Disc at $OR = 0.012$.

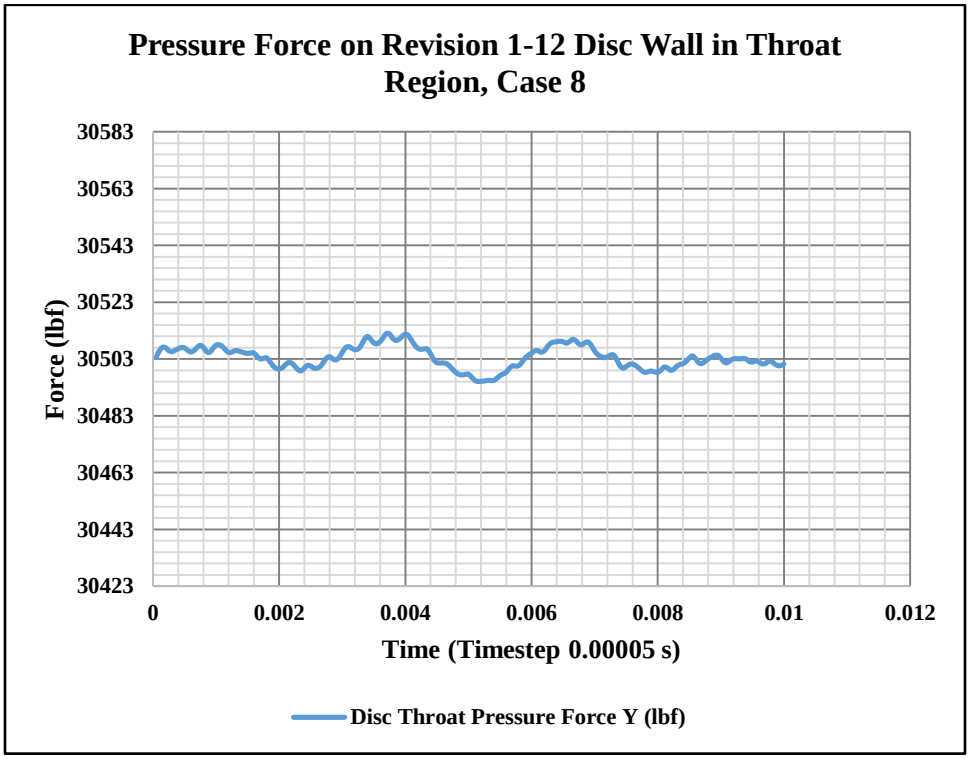

Figure 4.137. Transient Vertical Forces on Revision 1-12 Disc at $OR = 0.012$.

4.7.3.4. Revision 1-16 disc

Changing the throat to a converging nozzle decreases the lateral pressure forces to zero; this is shown in figure 4.138 for the revision 1-16 disc at case 8. The vertical pressure force, given in figure 4.139, is increased, but stabilized. As with the steady state analysis, the revision 1-16 disc generates the only stable flow pattern at an opening ratio of 0.012.

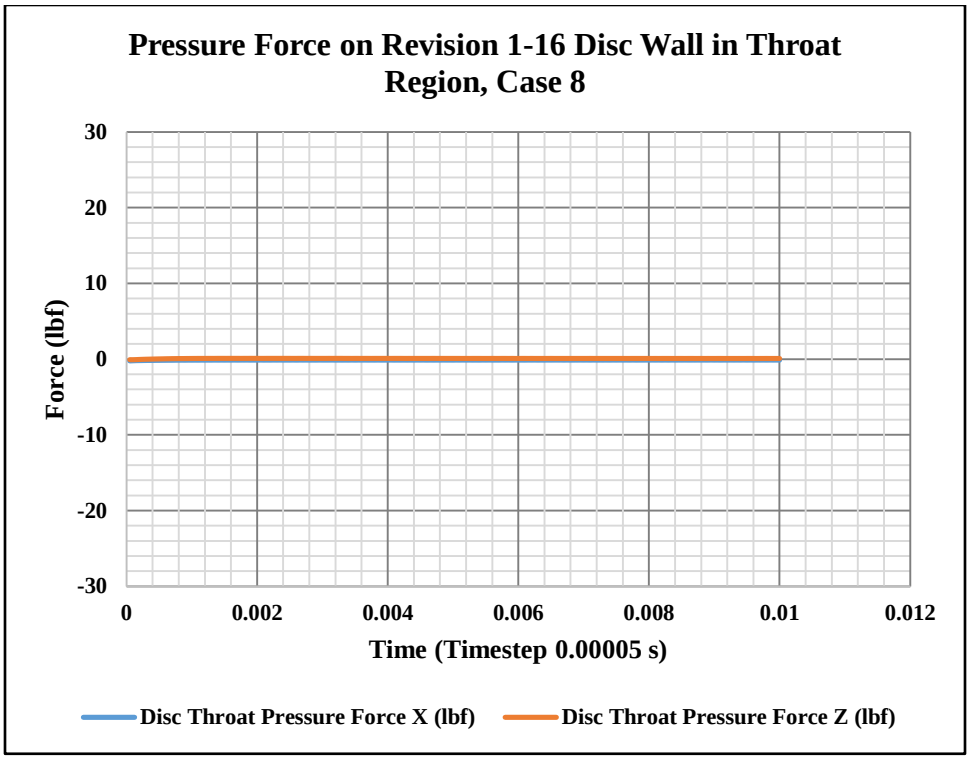

Figure 4.138. Transient Lateral Forces on Revision 1-16 Disc at $OR = 0.012$.

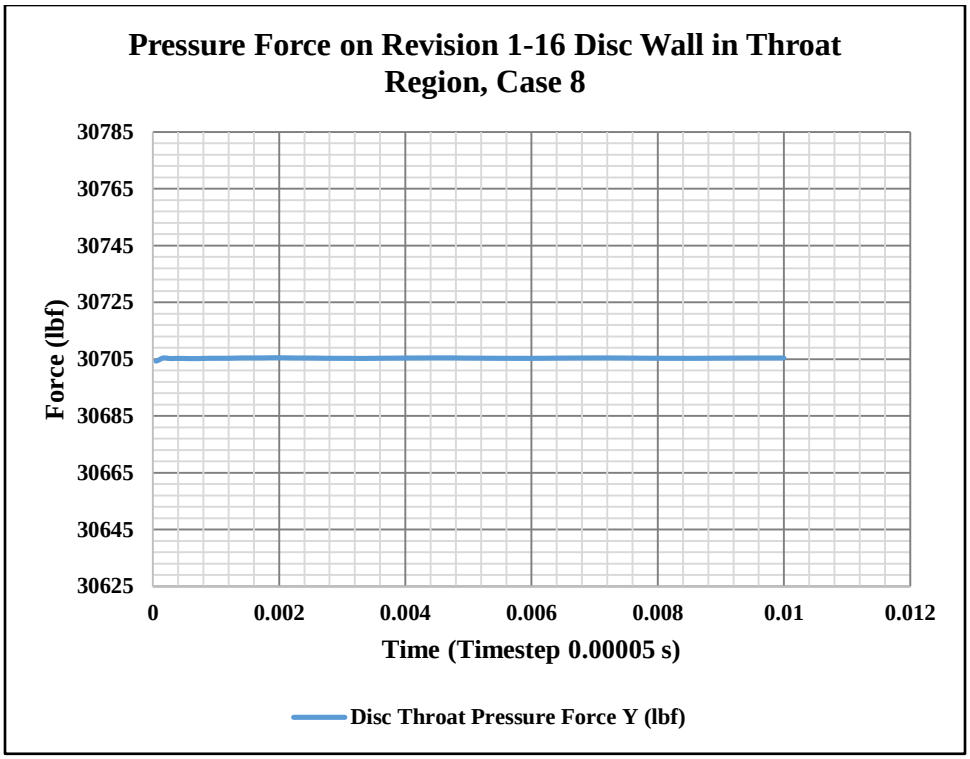

Figure 4.139. Transient Vertical Forces on Revision 1-16 Disc at $OR = 0.012$.

4.7.3.5. Revision 4 seat

Verification of the steady state results for the revision 4 seat was completed using the transient numerical analysis. The revision 1 disc was paired with the revision 4 seat at an opening ratio of 0.012. Placing a radius on the seat edge equalizes the forces *x* and *z* lateral directions, but greatly increases the force amplitude, as shown in figure 4.140. The same effect is present with the vertical force in figure 4.141.

The revision 1-14 disc was also used with the revision 4 seat for transient force investigation. The lateral and vertical forces, displayed in figures 4.142 and 4.143, respectively, resemble the revision 1-12 disc forces with increased amplitude.

Based on the revision 4 seat results for both the revision 1 and 1-14 discs, the pressure force amplitude increase seems to be linked to the revised seat. Without the amplitude increase,

there is not a noticeable difference between the revision 1-12 and 1-14 discs. The transient study does not show a noticeable force reduction from increasing the revision 1-12 disc indentation depth.

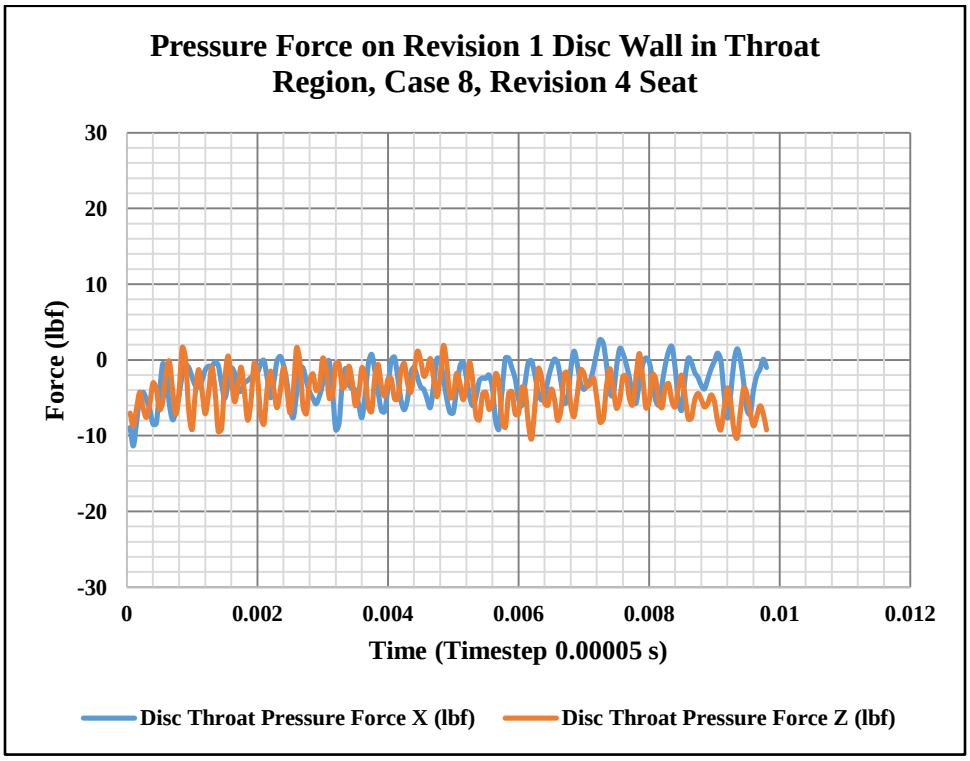

Figure 4.140. Transient Lateral Forces on Revision 1 Disc, Revision 4 Seat at $OR = 0.012$.

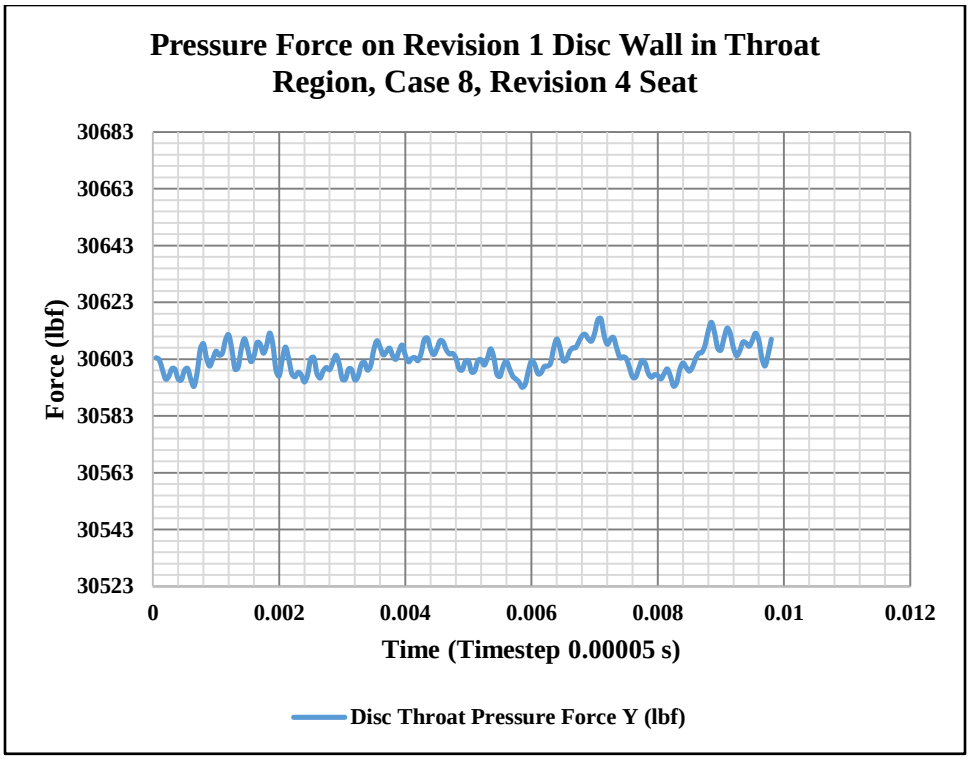

Figure 4.141. Transient Vertical Forces on Revision 1 Disc, Revision 4 Seat at $OR = 0.012$.

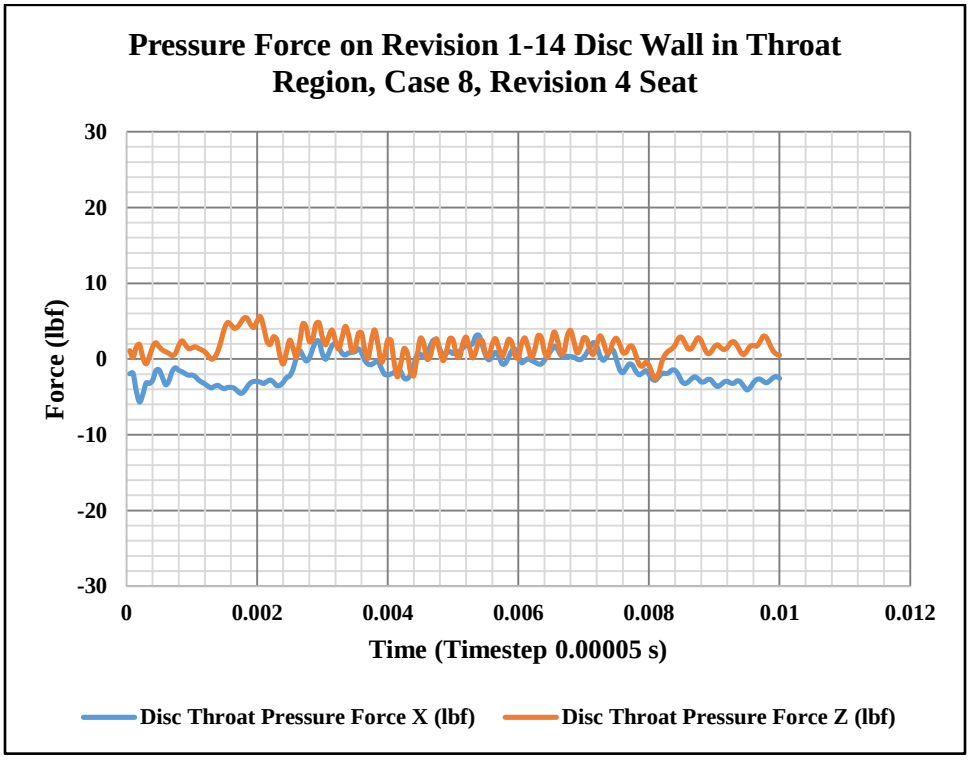

Figure 4.142. Transient Lateral Forces on Revision 1-14 Disc, Revision 4 Seat at $OR = 0.012$.

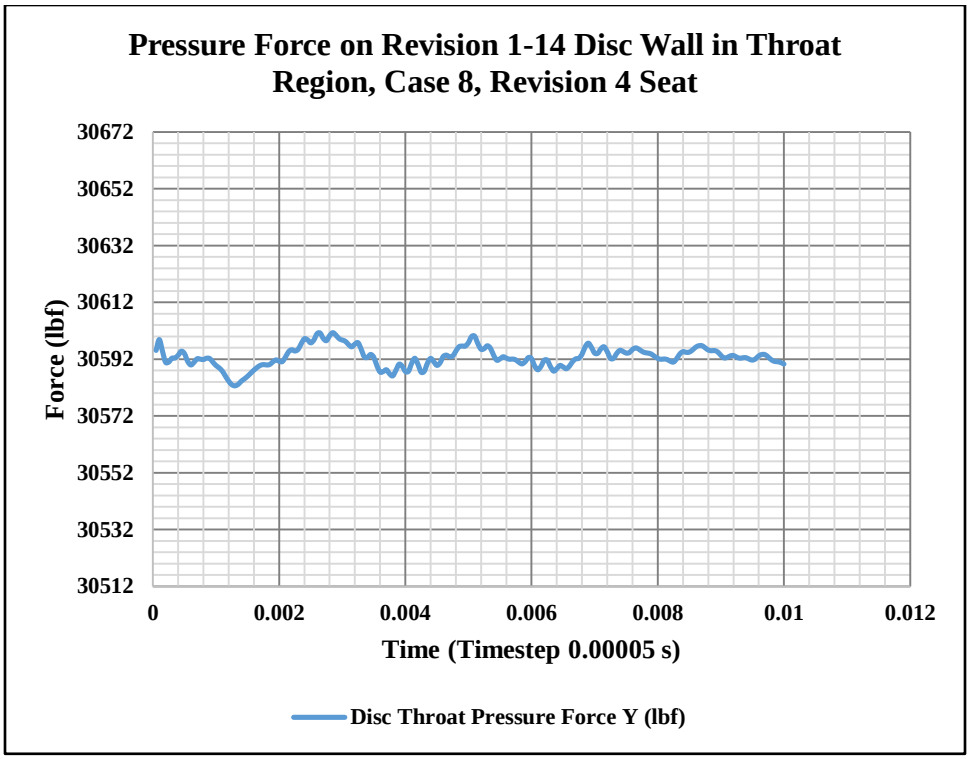

Figure 4.143. Transient Vertical Forces on Revision 1-14 Disc, Revision 4 Seat at $OR = 0.012$.

5. SUMMARY AND CONCLUSIONS

In 2006, the Unit 1 main steam turbine at the Minnkota Power Cooperative MR Young station was retrofitted. The opening sequence for the control valves was altered, changing the number of steam admissions from eight to three. After being returned to service for three years, the system was inspected and valves 7 and 8 were found to be severely damaged by valve vibration.

Based on past research completed on steam control valve vibrations, the vibrations are most likely induced by unsteady pressure fluctuations on the disc surface. These are generated by flow instability. Numerical and experimental results from other researchers indicate that vortex shedding off the disc, unstable jet flow, and transonic flow can lead to strong flow instability. Modifying the shape of the valve disc and seat can stabilize the flow pattern, equalizing the pressure forces on the disc.

The MPC valve components were not modified during the retrofit, but modifying the opening sequence changed the pressure ratio across the valves. Hence, the change in the pressure ratio and its relationship with the opening ratio is the most suspect reason for valves 7 and 8 to begin vibrating. A modification to the opening and pressure ratio correlation would change the flow pattern in the valves. The flow structure variation is easily identifiable using a numerical analysis, and valve seat and disc design alterations can be rapidly implemented to create and verify a stable flow pattern at multiple valve operation points.

Multiple operation points were established in the valve operating region where the vibrations occur. Simulation point 8 is based on the average pressure ratio at the vibration initiation point from MPC testing data; it identifies the critical operating condition for

stabilization. The others are used to ensure that the flow pattern for a successful design modification is stable over a range of operating conditions.

An analytical solution for the valve was completed at all of the operation points where choked flow was present using standard flow equations. The resultant mass flow rates were compared to the calculated values that MPC found from measured turbine data and the numerical simulation values to verify their accuracy. All of the numerical and analytical results matched very closely, but were much greater than those found from the MPC calculations. This is most likely due to the assumptions required for the MPC calculations.

The simulation inlet was placed in the steam chest, where the pressure was known. The outlet was placed well downstream of the valve throat so any flow instabilities would be resolved before reaching it. The first numerical simulations were run using an axisymmetric section of the valve; the use of a partial geometry expedited the simulation setup. After this was complete, a full-scale model was implemented for the steady-state and transient simulations to capture the three-dimensional flow phenomena. To maintain a close relation to the physical problem, steam was used as the working fluid.

Steady state simulations were completed for all of the disc designs created. The valve configuration with the original hemispherical disc was used as a reference at all operation points. An unstable flow pattern with vortex shedding off of the back of the disc was present at all operation points. A series of modified discs were then run. The disc with a simple cutoff design stabilized the flow pattern the most. Cutoff discs with an indentation on the bottom improved the flow pattern but not as effectively. Other disc designs did not provide any stability improvements.

After the initial steady state simulations were complete, MPC installed a cutoff disc into valves 7 and 8 based on the preliminary results, but moved the cutoff diameter lower on the disc to allow for the installation of stellite facing at the sealing diameter. The valves operated for a few months with this disc installed before the vibrations reappeared, but at a lower perceived vibration level.

Further disc revisions were studied with the steady state analysis after the vibrations reappeared. Simulation point 8 was established from the testing data completed with the currently installed revised disc, and an unstable flow pattern was found to persist there. The steady state results show an unsteady separation bubble present at the throat exit on the seat wall; the bubble occurs at all simulation points, but does not affect the stable flow pattern at larger opening ratios.

The disc design changes focused mostly on adjusting the cutoff disc indentation to stabilize the flow pattern with a high pressure region present in the disc indentation. This reduced the lateral pressure forces on the disc, but did not remove them. Seat modifications that increased the radius of the abrupt edges were also tested. These removed the separation bubble, but destabilized the overall flow pattern.

Two final configuration modifications were successful in stabilizing the flow pattern at low opening ratio operation points. The first introduced a surface roughness to the valve seat upstream of the throat to trigger turbulent flow prior to the separation bubble at the throat exit. The revision 1-12 disc was used. The resulting flow pattern reduced the thickness of the separation bubble at an opening ratio of 0.012; this reduced the effect it had on the throat jets and pressure fluctuations on the disc. For the second modification, the throat was changed from a converging-diverging nozzle to a purely converging nozzle. The revision 1-16 disc shape used is

an indented cutoff disc with a flare on the sealing surface, directly before the cutoff edge. This disc was combined with the unrevised seat. The resulting flow pattern shows stable annular flow at opening ratios 0.007, 0.012, and 0.018. The separation bubble is not present at the throat exit for any case and the steady state lateral pressure forces on the disc surface are minimal.

After the steady-state analysis was completed, a time-dependent investigation was used with the baseline designs and a few indented designs that had low steady-state lateral pressure forces. The original disc showed strong lateral pressure fluctuations in all cases. The revision 1 disc showed improvement at all cases, but still had significant lateral forces at an opening ratio of 0.012. Other discs agreed with the revision 1 disc results or improved on them; the revision 1-16 disc showed no lateral pressure forces at the 0.012 opening ratio.

Based on the combined investigation of all design modifications, the revision 1-16 disc will remove the flow instability in valves 7 and 8. This in turn eliminates the asymmetric flow-induced pressure fluctuations on the disc. A stable flow pattern was found at multiple points and minimal lateral pressure forces were found on the disc surface at cases opening ratios of 0.007, 0.012, and 0.018.

6. FURTHER WORK

Although the revision 1-16 disc resolves the flow instability, there is additional work that could be completed to verify and improve the results. The mass flow rate discrepancy could be resolved and the disc indentation depth could be optimized. A structural vibration analysis should also be performed to verify that the vibrations are due to flow instability and not interaction of any structural components of the valve.

The difference between the mass flow rate found with the MPC data and the analytical/numerical data needs to be fully investigated. Adding the instrumentation necessary to obtain the mass flow rate for valves 7 and 8 to the steam turbine will provide more accurate data, allowing the disc designs to be validated across the entire range of valve operation.

The results indicated that the deeper indentation of the revision 1-14 disc in comparison to the revision 1-12 disc increased the stable high pressure region inside the indentation. This was not used with the revision 1-16 disc because making the indentation deeper could necessitate redesigning the stem/disc attachment mechanism. The disc is hollow, and removing too much material from the bottom could affect the integrity of the disc. The intent was to find a realistic solution with little modification required. More investigation into the indentation depth would show if the increase in stability would warrant the extensive disc redesign.

7. REFERENCES

[1] D. S. Weaver, S. Ziada, M. K. Au-Yang, S. S. Chen, M. P. Païdoussis and M. J. Pettigrew, "Flow-Induced Vibrations in Power and Process Plant Components - Progress and Reports," *Journal of Pressure Vessel Technology,* vol. 122, pp. 339-348, 2000.

[2] D. Zhang and A. Engeda, "Venturi Valves for Steam Turbines and Improved Design Considerations," *Proceedings of the Institution of Mechanical Engineers,* vol. 217, no. 2, pp. 219-230, 2003.

[3] D. Kim, "Experimental Study on a Venturi Valve Application for Steam Turbines," ProQuest LLC, Ann Arbor, MI, 2010.

[4] J. Hardin, F. Kushner and S. Koester, "Elimination of Flow-Induced Instability from Steam Turbine Control Valves," in *Proceedings of the Thirty-Second Turbomachinery Symposium*, Houston, 2003.

[5] R. Gazur, "MR Young Unit No 1 Main Turbine Control Valve Damage Discussion," Minnkota Power Cooperative, Grand Forks, 2015.

[6] Minnkota Power Cooperative, "Unit 1 Turbine-Generator Control Valve Computerized Fluid Dynamics Evaluation," Minnkota Power Cooperative, MR Young Station, Center, ND, 2015.

[7] R. Gazur, "Unit 1 Turbine Control Valve 'Flutter' Testing," Minnkota Power Cooperative, Center, 2013.

[8] D. Zhang, "Theoretical, Numerical and Experimental Study on Venturi Valves for Steam Turbine Inflow Control," ProQuest Information and Learning Company, Ann Arbor, MI, 2004.

[9] H. R. Graf, S. Ziada, R. Rohner and R. Kälin, "Verification of Scaling Rules for Control Valve by Means of Model Tests," *Fluid-Structure Interaction, Aeroelasticity, Flow-Induced Vibration and Noise,* vol. 2, no. AD-Vol. 53-2, pp. 45-462, 1997.

[10] M. Hajšman, D. Kovandová and R. Matas, "Some Aspects of Numerical Simulations of Control Valves for Steam Turbines," *EPJ Web of Conferences,* vol. 25, no. 01052, pp. 1-12, 2012.

[11] R. Morita and F. Inada, "Pressure Fluctuations Around Steam Control Valve - Steam Experiments and CFD Calculations," in *Proceedings of PVP2007,* San Antonio, 2007.

[12] P. D. Iredale, "Investigation Into Unsteady Valve Flow in Steam Turbine Inlet Governing Valves," ProQuest LLC, Ann Arbor, 2013.

[13] L.-f. Zeng, G.-w. Liu, J.-r. Mao, S.-s. Wang, Q. Yuan, H. Yuan, K.-g. Wang, J.-j. Zhang and Y.-t. Xu, "Flow-Induced Vibration and Noise in Control Valve," *Journal of Mechanical Engineering Science,* vol. 229, no. 18, pp. 3368-3377, 2015.

[14] C. B. Domnick, F. K. Benra, D. Brillert, H. J. Dohmen and C. Musch, "Improving the Design of Steam Turbine Inlet Valves by Numerical Methods for Enhanced Part Load Operation," in *11th European Conference on Turbomachinery Fluid Dynamics and Thermodynamics 2015*, Madrid, Spain, 2015.

[15] H. K. Sam, "Study of Steam Chest Control Valves in Steam Turbines," Bell & Howell Information and Learning Company, Ann Arbor, MI, 2001.

[16] T. Araki, Y. Okamoto and F. Ootomo, "Fluid-Induced Vibration of Steam Control Valves," *Toshiba Review,* vol. 36, no. 7, pp. 648-656, 1981.

[17] C. Bolin and A. Engeda, "Analysis of Flow-Induced Instability in a Redesigned Steam Control Valve," *Applied Thermal Engineering*, vol. 83, pp. 40-47, 2015.

[18] D. Zhang, A. Engeda, J. R. Hardin and R. H. Aungier, "Experimental Study of Steam Turbine Control Valves," *Proceedings of the Institution of Mechanical Engineers, Part C: Journal of Mechanical Engineering Science*, vol. 218, no. 5, pp. 493-507, 2004.

[19] G. Liu, S. Wang, H. Guo, J. Mao, Z. Feng and X. Xiang, "Investigation on Flow Characteristics and Stability of Control Valves for Steam Turbines," in *Proceedings of ASME Turbo Expo 2008: Power for Land, Sea, and Air*, Berlin, Germany, 2008.

[20] K.-E. Widell, "Governing Valve Vibrations in a Large Steam Turbine," in *IAHR Symposium Proceedings*, Karlsruhe, 1979.

[21] K. Yonezawa, R. Ogawa, K. Ogi, T. Takino, Y. Tsujimoto, T. Endo, K. Tezuka and R. Morita, "Flow-Induced Vibration of a Steam Control Valve," *Journal of Fluids and Structures*, vol. 2012, no. 35, pp. 76-88, 2012.

[22] R. Morita, F. Inada, M. Mori, K. Tezuka and Y. Tsujimoto, "CFD Calculation and Experiments of Unsteady Flow on Control Valve," in *Proceedings of HT-FED04*, Charlotte, 2004.

[23] G. Zanazzi, O. Schaefer, M. Sell and C. Ridoutt, "Unsteady CFD Simulation of Control Valve in Throttling Conditions and Comparison With Experiments," in *Proceedings of ASME Turbo Expo 2013: Turbine Technical Conference and Exposition*, San Antonio, 2013.

[24] S. Ziada, E. T. Bühlmann and U. Bolleter, "Flow Impingement as an Excitation Source in Control Valves," *Journal of Fluids and Structures*, vol. 3, pp. 529-549, 1989.

[25] R. Morita, F. Inada, M. Mori, K. Tezuka and Y. Tsujimoto, "CFD Simulations and Experiments of Flow Fluctuations Around a Steam Control Valve," *Journal of Fluids Engineering*, vol. 129, pp. 48-54, 2007.

[26] R. Morita, F. Inada, M. Mori, K. Tezuka and Y. Tsujimoto, "Flow Induced Vibration of a Steam Control Valve in Middle-Opening Condition," in *Proceedings of PVP2005*, Denver, 2005.

[27] K. Yonezawa, Y. Toyohira, T. Nagashima, Y. Tsujimoto, K. Tezuka, M. Mori, R. Morita and F. Inada, "An Experimental Study of Unsteady Transonic Flow in a Steam Control Valve With Simple Model," *Journal of Environment and Engineering,* vol. 5, no. 1, pp. 134-143, 2010.

[28] D. A. Johns, D. Rasmussen and J. Beverly, "Turbine Remanufacture - One Option for Reliability and Efficiency Improvement," in *Proceedings of the 26th Turbomachinery Symposium*, Houston, 1997.

[29] ANSYS, Inc., ANSYS CFX-Solver Theory Guide, Canonsburg: ANSYS Inc., 2012.